5-2018

Bioconjugation Techniques to construct Spontaneously assembling DNA-Enzyme Macromolecules

Malithi Wickramathilaka
Purdue University

BIOCONJUGATION TECHNIQUES TO CONSTRUCT SPONTANEOUSLY ASSEMBLING DNA-ENZYME MACROMOLECULES

by

Malithi Wickramathilaka

A Dissertation

Submitted to the Faculty of Purdue University

In Partial Fulfillment of the Requirements for the degree of

Doctor of Philosophy

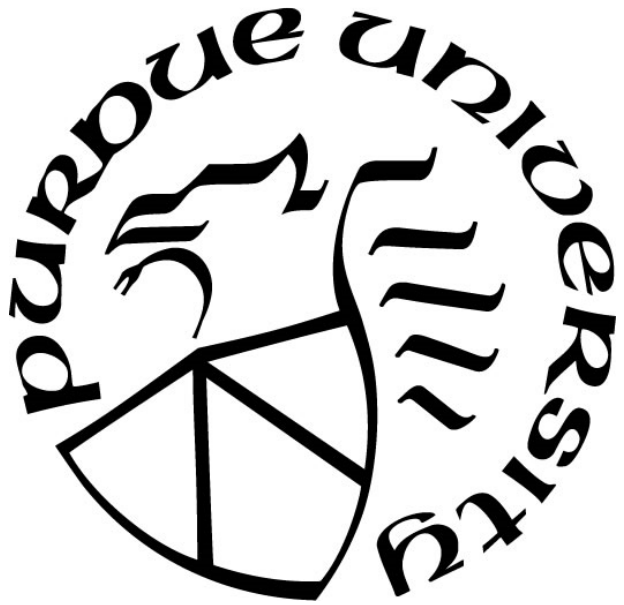

School of Agricultural & Biological Engineering

West Lafayette, Indiana

May 2018

THE PURDUE UNIVERSITY GRADUATE SCHOOL
STATEMENT OF COMMITTEE APPROVAL

Dr. Bernard Y. Tao

Dept. of Agricultural and Biological Engineering

Dr. Frederick S. Gimble

Dept. of Biochemistry

Dr. Jenna L. Rickus

Dept. of Agricultural and Biological Engineering

Dr. Kari L. Clase

Dept. of Agricultural and Biological Engineering

Dr. Nathan S. Mosier

Dept. of Agricultural and Biological Engineering

Approved by:

Dr. Nathan S. Mosier

Head of the Graduate Program

I dedicate this dissertation to my beloved parents and all my teachers!

ACKNOWLEDGMENTS

First, I thank the Agricultural and Biological Engineering department at Purdue University for accepting me into their prestigious program. I also thank the College of Agriculture, and College of Engineering for inducting me with the prestigious Ross Fellowship.

I thank all the funding sources for my graduate work, including the Purdue Agricultural and Biological Engineering (ABE) department, Indiana Soybean Alliance, and the USDA National Institute of Food and Agriculture.

It is not an overstatement if I say that I wouldn't be here today if it weren't for Rachel Watson, Dr. William Jacoby, and Dr. Bernard Tao, who have been acting as my academic mentors and advisers throughout my eleven years in academia. I wish to extend my heartfelt gratitude to all my teachers in Sri Lanka, as well as in USA. The tenacious, curious and creative scientist and mentor I am today is wholeheartedly devoted to these brilliant teachers and professors. If not for the opportunities and feedback they have provided me with, I would not have been able to accomplish my research, or teaching goals.

I also wish to thank Dr. Nathan Mosier, Dr. Lisa Mauer, Dr. Andrea Liceaga, Dr. Frederick Gimble, Dr. Kari Clase, Dr. David Umulis, and Dr. Jenna Rickus for their invaluable mentoring and advising. They were always willing to assist me utilizing their technical expertise, connecting me to the correct resources/facilities.

I also wish to thank Dr. Bernard Engel as well as the entire ABE staff who has always assisted me promptly whether it be placing a purchase order, printing out a poster, reserving locations for my office hours, or sorting out immigration paperwork. Without Pamela Hancock, Nikki Zimmerman, Barbara Davies, Rebecca Peer, Gail Bilberstine, Carol Weaver, Katie Maish, or Stan Harlow, my workloads would have been impossible to bear.

I also wish to extend my gratitude to Seda Arioglu, Sunantha Ketnawa, Darwin and Ingrid Ortiz, Felicia Hall, Dinara Gunasekara, Anton Terekhov, Bhavesh Patel, Dr. Jia Ma, Dr. Karl Wood,

Connie Bonham, Dharshini Munashinghe, CB Gamlath and Udeni Dharmawansa for their instrumentation support, technical support, professional assistance, and expertise.

I also greatly appreciate my office mates Leah Liston, Jeff de Kozlowski, Jinsha Li, Junli Liu, and Shelly Xu for creating a wonderful work space, because of which, I looked forward to coming to work every day.

Furthermore, I wish to mention my closest friends Chanika Kahandawala, Manisha Fernando, Anirudh Patel, Aditya Kaul, Puja Banerjee, Dinushi Samarasekara, Jinsha Li, Nevandika Seneviratne, Achint Sanghi, Lakshmi Yaddanapudi, Anand Kunda, and Pushpak Bhandari for their unending love and friendship throughout my PhD journey. I also extend my warm gratitude to the Sri Lankan community at Purdue, and my badminton coaches (Hiroko and Mark) for constantly lifting up my spirits during my extracurricular activities.

I also thank all the wonderful employees of Cook Biotech Incorporated who facilitated a great learning environment for me throughout my two term internships there.

I wished to save the best for last – My family! If it were not for my beloved parents (Upali Wickramathilaka and Udeni Dharmawansa), my sister (Siluni Gamage), and my brother-in-law, (Pubudu Gamage), it is needless to say that I would not have made it to the end of this marathon. Their constant emotional support, unconditional love, encouragement and advices were a large driving force for me. Thank you for always being there for me, and for blessing me with the biggest joy I have had the honor of filling my heart with – My baby nephew.

I wish I could find better words to express my sincere gratitude to everyone who has assisted me in numerous technical, and non-technical ways throughout my stay at Purdue. Now on the verge of graduation, I recognize that I would not have travelled my journey in any other way, and I wouldn't have chosen any other college to pursue my PhD. Thank you Purdue!

TABLE OF CONTENTS

LIST OF TABLES

LIST OF FIGURES

ABSTRACT

Author: Wickramathilaka, Malithi P. PhD
Institution: Purdue University
Degree Received: May 2018
Title: Bioconjugation Techniques to construct Spontaneously assembling DNA-Enzyme Macromolecules
Committee Chair: Bernard Y. Tao

In the past two decades, crosslinking has been a popular choice in synthesizing bioconjugates in the fields of biotechnology, medical diagnostics, and genetic screening. However, their efficacy in synthesizing the desired bioconjugates is scarcely analyzed and documented. The scope of this investigation encompassed studying covalent bioconjugation techniques, and determining the structural characteristics of the bioconjugates formed via several crosslinking strategies. The major goal of the study was to determine relatively inexpensive, less complex, and universal bioconjugation techniques with the flexibility to control the distance between wild-type enzymes. In this investigation, three different crosslinkers were studied to determine the efficacy of crosslinking biological molecules.

In the first aim of the study, an adapted strategy from the conventional 1-ethyl-3-(3-dimethylaminopropyl) carbodiimide hydrochloride (EDC) was developed to form a novel phosphoramidated single stranded DNA (ssDNA) bioconjugate. Matrix-assisted laser desorption/ionization time-of-flight (MALDI-TOF) was used to determine the molecular weights, and the stability of the bioconjugates formed. A reversed phase high performance liquid chromatography (RP-HPLC) analytical method was developed to determine the conjugate product yields. The analytical procedure's accuracy, precision, linearity, limit of detection (LOD), and limit of quantitation (LOQ) were determined. Afterwards, the yield of the phosphoramidated ssDNA bioconjugate was determined using the developed analytical procedure. In our attempts to determine suitable crosslinkers, another crosslinker (BS3) was also investigated to accomplish bioconjugation between ssDNA, and a small peptide. However, mass spectrometry results indicated conjugate molecular weights evidencing only partial bioconjugate formation.

In the next aim, the successful adapted EDC crosslinking technique was applied to two wild-type enzymes to synthesize enzyme-single stranded DNA (enzyme-ssDNA) bioconjugates, in an aqueous system. Like so, glucose oxidase-ssDNA$_4$ (GOD-ssDNA$_4$), and horseradish peroxidase-ssDNA$_3$ (HRP-ssDNA$_3$) conjugates were synthesized separately. These enzyme-ssDNA conjugates were analyzed, and purified using size exclusion chromatography (SEC). Fluorescence spectroscopy was used to determine the presence of ssDNA in the GOD-ssDNA$_4$ bioconjugates, while MALDI-TOF spectrometry was used to determine the molecular weights of the HRP-ssDNA$_3$ bioconjugates. Altogether, size exclusion chromatography, fluorescence spectroscopy, and MALDI-TOF results suggest that the adapted EDC crosslinking method was successful in producing the expected enzyme-ssDNA conjugates.

In order to spontaneously assemble the GOD-ssDNA$_4$, and HRP-ssDNA$_3$ bioconjugates, DNA hybridization was utilized. However, high annealing temperatures used in the general heating-cooling protocols has the potential to degenerate these enzyme conjugates. Therefore, possibilities of accomplishing DNA hybridization at lowered annealing temperatures was investigated as well. After facilitating DNA hybridization between GOD-ssDNA$_4$ and HRP-ssDNA$_3$, the final enzymatic macromolecule was analyzed on size exclusion chromatography. Based on the structural evidence obtained from mass spectrometry, UV-Vis spectrophotometry, reversed phase chromatography, size exclusion chromatography, and fluorescence spectroscopy, we analyzed the desired bioconjugates at each successive stage in this bottom-up-synthesis.

CHAPTER 1. BACKGROUND AND INTRODUCTION

1.1 Background

1.1.1 Bioconjugation

Any strategy of covalent or non-covalent bond formation between two or more molecules, where at least one molecule is a biomolecule, is referred to as bioconjugation. Researchers use bioconjugation techniques to manipulate a few or several diverse biological molecules with unique properties, to deliver criteria required in a final biomolecule design or system. Biological molecules are quite diverse and they exhibit unique properties. By bioconjugation, we have the capability of manipulating a few or several biological molecules to cater certain criteria we require for a certain system or a device. Bioconjugation is generally accomplished by a bottom-up approach, where each building block of a final structure is synthesized successively to obtain the final structure. Assembly of these building blocks could be via covalent attachments, electrostatic interactions, or ionic reactions. However, in the field of bio-nanotechnology, top-down approaches are also heavily used to synthesize nano-structured materials. In a top-down approach, bulk material is broken down to obtain nano-sized elementary building blocks. These are then assembled as desired, to obtain the final nanostructure [1].

It is important and relevant to study, and optimize bioconjugation techniques because these techniques govern the ultimate molecular nanotechnology, i.e., synthesis of supramolecular assemblies, micro-arrays, and molecular detection probes. In the past, scientists have exploited both covalent and noncovalent coupling chemistries to synthesize bioconjugates. They have been used in a variety of biotechnology and translational medicine applications such as diagnostics, biosensors, detection probes, affinity chromatography, and assays such as ELISA (enzyme-linked immunosorbent assay). On the exterior, bioconjugation may appear quite straight forward, and their design possibilities may only be limited by the imagination of the scientist. However, even with the vast knowledge on bioconjugation techniques, given a new application, these construction methods have to be optimized from the very beginning. For an example, attaching a fluorescent label to an antibody is as well-known step in the study/development of binding assays[2]. Although the steps are to simply attach a fluorescent dye to a purified antibody, the methodology is much

more intricate. Before labeling an antibody (Fig.1b), an appropriate fluorescent dye should be selected based on intrinsic spectral properties (e.g. excitation, emission wavelengths). Next, a variety of factors such as hydrophilicity of the dye, relative ratio of molecules, buffer systems, and other reaction conditions should be considered prior to carrying out the bioconjugation between the fluorescent dye and the antibody. The selected dye should be hydrophilic in order to prevent antibody aggregation. As many dyes have highly aromatic, hydrophobic regions, they can form non-specific interactions with the hydrophobic regions of the antibody. This leads to antibody aggregation, as well as non-specific (electrostatic interactions) interactions between the dye and the antibody. Such electrostatic interactions are contrary to the desired, stronger covalent bonds. The selected buffer system should be compatible for both the molecules, and should not lead to degradation of either. The selected linking reagent (e.g. crosslinker) should also form specific interactions (covalent) only between the antibody and the dye. If the linking reagent forms antibody-antibody links, or dye-dye crosslinking, that defeats the purpose of fluorescent tagging. Another largely important consideration is the relative ratio of dyes: antibody. It is important to attach more than one dye per antibody molecule in order to facilitate adequate fluorescence emission in the detection ranges of the instruments use. However, oversaturating one antibody molecule with too many dye molecules would lead to antibody precipitation, or quench the potential fluorescence emission output due to dye-dye interactions and energy transfer. Therefore, for a given antibody-dye complex, there is an optimal level of fluorescence dye conjugation which will provide the maximum signal in the detection assay. This is attained by controlling the stoichiometry of the antibody, and dye molecules. Synthesis of an optimal antibody-dye bioconjugate is only achievable via a carefully structured design of experiments which accounts for solution stability, fluorescence intensity levels, and assay performance.

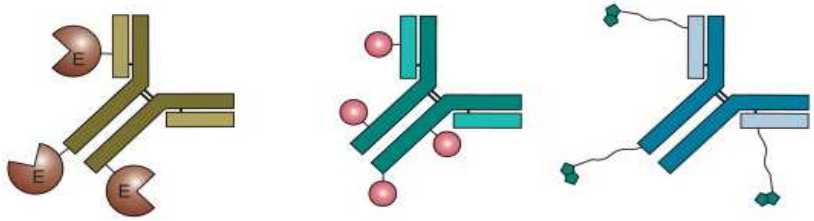

Figure 1: Common antibody conjugates used in bioassays [2].

1.1.2 Bioconjugate techniques

Bioconjugation is carried out by utilizing functional groups present on biomolecules (e.g. proteins, enzymes, antibodies), with the aid of external reagents and/or reactants. Methods of protein bioconjugation includes reacting amines with aldehydes via a Schiff-base, cross-linking amine groups to an amine surface with gluteraldehyde to form peptide bonds, cross-linking carboxylic acid groups present on the protein via cross-linking, attaching proteins to proteins based on disulfide bridge formation between two thiol groups, and the formation of thiol-Au nanoparticles. Amine groups in proteins are widely used for protein covalent immobilization via crosslinking, which is a widely used method of accomplishing covalently bounded bioconjugates[2]. The 1^0 amine group of lysine, the thiol group in cysteine, and the hydroxyl groups in serine, threonine, and tyrosine have been identified as appropriate candidates for modifications. Most proteins contain lysine and arginine groups at the surface. Although naturally occurring peptides, proteins, and enzymes may or may not always contain these functional groups, every protein will contain an N-terminal primary amine, and a C-terminal carboxyl. However, the concern is that the terminal ends of a protein or enzyme tend to be conserved during their natural 3-D structure (due to protein folding). Therefore, bioconjugation utilizing surface exposed amino acid residues remain the best hope for wild-type proteins.

Prior to carrying out any bioconjugation, a thorough review should be conducted on the physicochemical characteristics (structural and chemical stability) of each biomolecule in the selected buffer media. Furthermore, careful attention should also be given so that the selected bioconjugation reaction does not affect the ultimate functionality of the final macromolecules. For example, if the intended design was to design an enzyme-antibody conjugate as depicted in Fig.1a, it is imperative that any of the chosen bioconjugation chemistries do not harm the ultimate reactivity of the enzyme, or the functionality of the antibody.

Over the past few decades, researchers have utilized a vast number of chemistries, and methods to form bioconjugates. Such bioconjugate techniques can be divided into site-specific bioconjugation methods and random bioconjugate methods. For a conclusive discussion, they are further sub-divided into covalent bond forming methods, and non-covalent bond forming methods. Covalent bonds are stronger than non-covalent bonds, and hence cater higher conjugate product

stabilities (i.e., they do not dissociate easily over time). They can also withstand buffer condition alterations and changes in temperature [3]. When attempting to control bioconjugation and the extent of conjugate product formation, many variables such as solvent pH, temperatures, reaction times and reactant amounts could be tweaked.

1.1.3 Site-specific bioconjugation: Chemoselective

Chemoselectivity refers to coupling one reactive group in one molecule with another specific reactive group on another molecule, without any side reactions. Therefore, chemoselective ligation can be carried out in cells, cell extracts, or *in vivo* models, without cross-reactivity with other ubiquitous functional groups in the reaction system. Reagents which take part in chemoselective reactions are also called biorthogonal to each other. An important requirement of bioorthogonal reagents is their stability in aqueous systems (i.e., resist hydrolysis, or oxidation). Diels–Alder cycloadditions, hydrazine–aldehyde, aminooxy–aldehyde, boronic acid–salicylhydroxamate, Cu^{I}-catalyzed azide–alkyne [3+2] cycloadditions, Huisgen 1,3,-dipolar cycloaddition, Staudinger ligation, native chemical ligation, and expressed protein ligation are examples of chemoselective reactions. Bioconjugates obtained from all chemoselective reactions are formed via strong, covalent bonds.

1.1.3.1 Covalent strategies

(i) "Click chemistry"

A famous method of synthesizing covalently bound bioconjugates is via "click chemistry". Since its inception in 2001, click chemistry has been used widely to construct covalently bound bioconjugates regioselectively. Regioselectivity refers to the preference of one direction (i.e., one isomer) in a reaction, and hence enables producing a homogenous bioconjugate product. There are four major click chemistry reactions which have been identified so far; (1) Nucleophilic ring opening reactions of epoxides and aziridine, (2) Non-aldol type carbonyl reactions (e.g. formation of hydrazones and heterocycles), (3) Additions to carbon-carbon multiple bonds (e.g. oxidative formation of epoxides), (4) Cycloaddition reactions.

The latter mentioned cycloaddition reaction has been recognized as one of the best click reactions due to its high yield[2]. Generally, "click" chemistries are conducted at elevated

temperatures and pressures. However, it has been shown that in the presence of a catalyst (Cu^{I}), the reaction kinetics are dramatically accelerated[4] (Fig.2). The Cu^{I} -catalyzed azide-alkyne [3+2] cycloaddition (CuAAC) reaction is one example of a DNA click-chemistry that has shown much potential [5]. Azides and unactivated alkynes are not reactive with other functional groups found in the nature. Therefore, their reactions are highly regiospecific. The product formed from the reaction of an azide and the alkyne is a triazole, which is extremely stable and non-toxic.

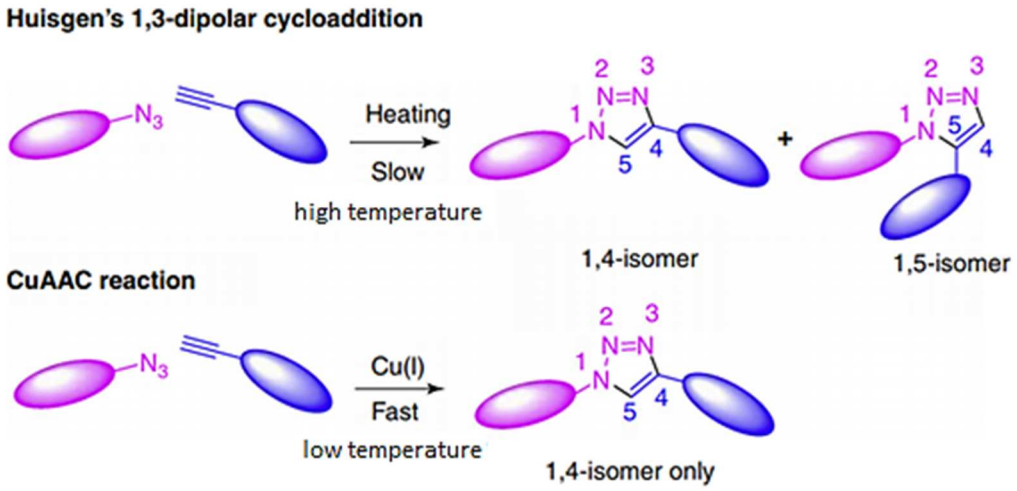

Figure 2: Schematic of the Huisgen 1,3,-dipolar cycloaddition, and the CuAAC reaction [6].

A study conducted by Duckworth and his team used the very selective enzyme (PFTase) to enzymatically tag a protein-CVIA to an azide modified isoprenoid diphosphate. This azide was then reacted with an alkyne modified DNA using the Huisgen cycloaddition click reaction (Duckworth et al., 2007). Alkyne functional groups can be attached to DNA without perturbing the biophysical characteristics of the naturally occurring DNA. While this is a fascinating approach to create spontaneously assembling chimeras of proteins, it lacks universal application due to several reasons; the selectivity of the enzyme, the extremely long lengths of the tagging chains, the large number of chemical modification steps, and the high amounts of chemicals/catalysts used in the click reactions. When developing multi-functional enzymes or antibodies, deviations from physiological conditions poses a risk of deactivating the molecules.

In the recent history, copper-free "click" reactions have also been investigated to synthesize bioconjugates in *in vivo* [7], as well as *in vitro* [8] systems. In the first study, they used the strain-promoted azide-alkyne [3+2] cycloaddition (SPAAC) to create a bioconjugate probe in a living cell (Fig.3). In the SPAAC method, instead of an alkyne, a cyclooctyne is used to carry out the "click" reaction. As the cyclic triple bond is activated, the kinetics in the 3+2 cycloaddition reaction is enhanced (Fig.3). In the latter, SPAAC was used to synthesize protein-oligodeoxynucleotide (protein-ODN) conjugates to demonstrate reaction efficiencies of the method. Here, they first synthesized azide-functionalized proteins prepared by enzymatic prenylation of C-terminal CVIA tags with synthetic azidoprenyl diphosphates. Next, they were "clicked" to ODNs which were pre-modified with a strained dibenzoclyclooctyne [8]. Using size exclusion chromatography, and gel electrophoresis, they reported that the yields, and the reaction times of the SPAAC bioconjugation reaction are comparable to previously reported copper-catalyzed azide-alkyne [3+2] cycloaddition (CuAAC) reactions. However, since the SPAAC technique does not utilize any catalyst (Cu^{I}), it does not pose a threat of deactivating the functionality of the biological molecules involved in the bioconjugation (e.g. proteins, enzymes, antibodies, DNA).

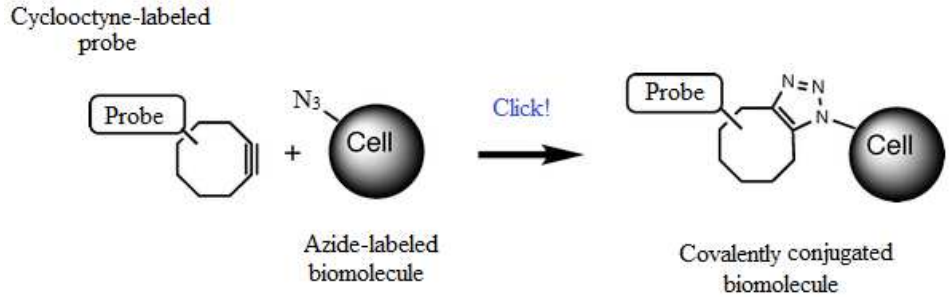

Figure 3: Illustration of the copper-free, strain-promoted [3+2] Azide-Alkyne cycloaddition (SPAAC), reproduced from [7].

(ii) Staudinger ligation

In the 1920's, Hermann Staudinger discovered a reaction where phenylphosphine (PPh_2) reacts with azides (N_3) to form a phenylphosphine oxide and a primary amine. Later, Saxon and Bertozzi developed an adapted technique which was termed the Staudinger ligation. In Staudinger ligation, a modified PPh_2-derivative reacts with an N_3-derivative, ultimately forming an amide bond between the two derivatives (Fig.4). The product is essentially a covalently bound

bioconjugate. Soon after their discovery, they investigated a potential application of their method. In that investigation, Bertozzi and team used N_3-modified mannose derivatives to visualize their behavior in a biosynthetic pathway. They first created thiazide-modified mannose derivatives, i.e., *N*-azidooacetylmannosamine. Next, they incubated these with Jurkat cells, which are an immortalized line of human T lymphocyte cells. This facilitated the uptake of the modified compound into the glycans produced through the sialic acid biosynthetic pathway. Next, using a PPh_2-biotin, they conjugated the azidosaccharides with the PPh_2-biotins. This was the Staudinger ligation step. Afterwards, they used a fluorescein-labeled avidin, facilitating the famous avidin-biotin interaction (discussed in the next section). The fluorescence detection of the final glycan-avidin-biotin-fluorescein glycoconjugate was used to detect the amount of glycan output produced via the pathway [9].

Staudinger ligation is highly amenable to bioconjugation needs in *in vivo* models, because azido analogs can be incorporated in biopolymers (e.g. polysaccharides), and also because this highly bioorthogonal reaction does not contain any cytotoxic catalysts, or byproducts.

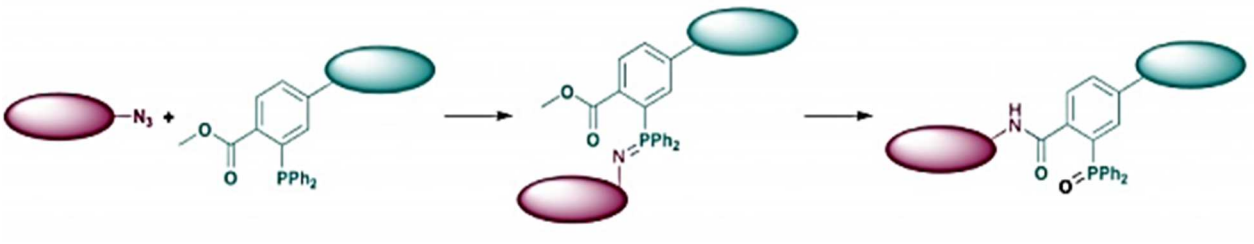

Figure 4: Schematic of a Staudinger ligation between an azide-derivative, and a phosphine-derivative.

(iii) Native chemical ligation

In native chemical ligation (NCL), a peptide containing a C-terminal thioester reacts with an N-terminal cysteine residue in another peptide, undergoing a transthioesterification reaction. The resulting product is a peptide-peptide bioconjugate linked via a strong amide bond (Fig.5). Although a very useful bioorthogonal ligation, the applications of this method are not broad because it can not be extended to wild-type peptides. NCL has mostly been used in peptide chemistry, as opposed to synthesizing bioconjugates in the field of biotechnology. NCL helps

overcome the shortcomings of Solid Phase Peptide Synthesis (SPPS) by allowing researchers to synthesize peptides that are greater than 50 amino acids in length [10].

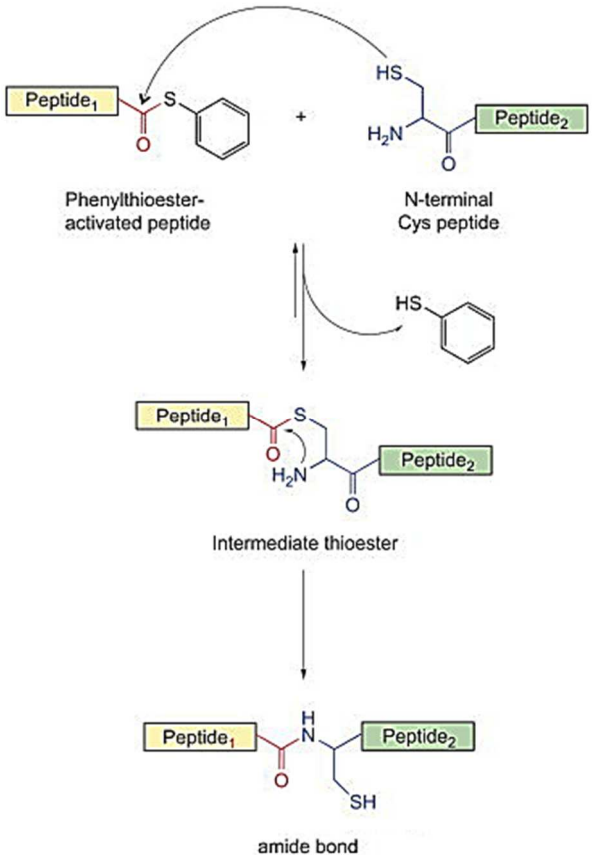

Figure 5: Native chemical ligation [2].

1.1.3.2 Non-covalent strategies

Avidin-biotin interaction

This is perhaps one of the most exploited interactions in the field of bio-nanotechnology, as biotin-streptavidin bonding is the strongest non-covalent biological interaction known (dissociation constant, $K_d = 10^{-15}$ M). Biotin and avidin has molecular weights of 244.3 Da, and 67,000 – 68,000 Da respectively [11]. The biotin-avidin binding is kinetically favorable, highly specific, and is resistant to extremes of heat, pH and proteolysis. This reaction also occurs very rapidly, and the avidin-biotin complex is very stable (Fig.6).

Biotinylation is the process of covalently attaching biotin (also known as vitamin H) to a protein, nucleic acid or any other molecule of interest (Fig.6, step 2). Afterwards, previously immobilized avidin (Fig.6, step 1) is used to bind the biotin, ultimately forming the desired final complex (Fig.6, step 3). Streptavidin is avidin with tetrameric binding sites, and has an iso-electric point very close to neutral. This renders streptavidin-biotin based bioconjugates amenable for biological assays [12]. The avidin-biotin detection systems allows an almost unlimited number of primary detection reagents (i.e., antibodies, nucleic acids probes and ligands) to be easily captured, recovered, immobilized or detected. Although the avidin-biotin system is simple to set up and use, it does have certain limitations. Because any biotinylated molecule will bind to any biotin binding protein, biotinylated molecules must be used in combination with other detection-probe systems (i.e., primary-secondary antibodies) for multiplex experiments [11].

Also, because biotin is a biological molecule, endogenous biotin can cause background noise, and raise specificity issues in assay development on certain biotin-rich tissues and extracts (i.e., brain, liver, milk, eggs, corn). In capture-and-release bioconjugate applications (e.g. purification methods), the strength of the binding interaction between biotin and avidin is a factor that limits its utility. In order to dissociate the interaction between avidin and biotin, harsh conditions are required. Such harsh buffer conditions could easily denature the proteins in the bioconjugates. To overcome this limitation, modified versions of avidin resins, and modified forms of biotin labeling reagents are commercially available which make the interaction readily reversible. These include monomeric avidin, cleavable disulfide biotin reagents, and iminobiotin and desthiobiotin derivatives [11]. Regardless, avidin-biotin remains extremely useful in applications without product purification necessities, and in *in vitro* bioconjugate applications, which does not involve biological molecules that naturally contain biotin.

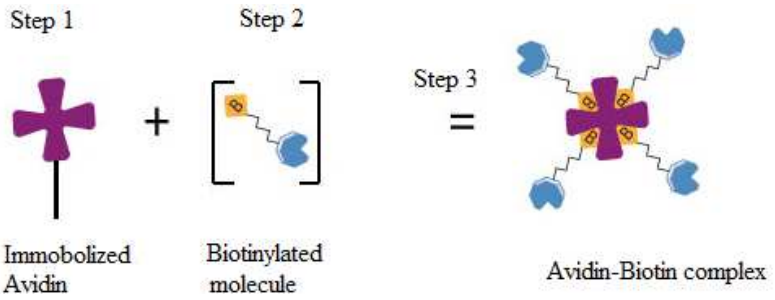

Figure 6: Formation of bioconjugates using the avidin-biotin interactions [10].

1.1.4 Random bioconjugation

One of the biggest drawbacks in site-specific bioconjugation techniques discussed above is the necessity for modifying each biomolecule with the desired functional groups. As such derivatization is time consuming, and are not universal methods to be used on wild-type peptides, proteins, enzymes, and antibodies, random bioconjugation techniques such as crosslinkers are perhaps the better choice. However, the trade-off in random bioconjugation techniques is poor product yield, and lack of control over the chemoselectivity.

1.1.4.1 Non-covalent strategies

(i) Ni^{2+}- Histidine

A common non-covalent, random bioconjugation strategy is binding His-tagged proteins to Ni^{2+}-chelating supports. A previous study has demonstrated a one-step protocol to remove toxic impurities from biological assays, by utilizing affinity chromatography principles [13]. Generally, purification of recombinant proteins expressed in a bacterial system (such as *E.coli*) is based on physicochemical characteristics of the proteins such as charge, size and hydrophobicity. These authors recognized such purification steps laborious, and hence investigated an alternate route to accomplish purification of His-tagged proteins by using Ni-NTA (Nickel-nitrilotriacetic acid) beads. After the His-tagged proteins were recovered from the isopropanol washing step, they stated that the proteins were able to refold into their native structures, ensuring protein functionality. Their method had succeeded in removing the *E.coli* bacterial endotoxin debris, as well as detergents used to lyse the bacterial cell.

(ii) Physical adsorption

It is known that colloidal particles of metals serve as highly useful tools in the magnetic, plasmonic and optoelectronic fields. Previous work in the nanoparticle fields prove that they could be used as signal enhancers. One very early study conducted in 1979 used gold and silver nanoparticle absorbed pyridine molecules to obtain Raman signals. The degree of signal intensity is strongly dependent on the excitation wavelength. These metal particles are polarizable, and the

collective excitation resonance oscillations of the electrons on the surface of these colloidal particles are the reason for the enhanced Raman scattering [14]. Furthermore, metal nanoparticles have many applications in the field of chemical sensors. Biological macromolecules could be successfully attached to nanoparticles with a high affinity. The adsorption of metal nanoparticles to biological molecules occurs via electrochemical interactions, as opposed to covalent cross linking. Therefore, the functionalities of the biological molecule remain unchanged, upon binding to such metal particles [15]. In the past, colloidal gold has been adsorbed to many biological molecules in the nature, such as enzymes, hormones, streptavidin, toxins, glycoproteins, and immunoglobulins. After an antigen is labelled with colloidal gold particles, their relative densities could be determined because of our ability to quantitate the gold particles. These gold nanoparticles have high electron densities compared to ferritin, and can be easily detected by TEM (transmission electron microscopy), even under low magnification. They can be visualized easily even in thick layers of biological components [15]. Furthermore, gold nanoparticles adsorption is highly specific and is feasible to be used in affinity cytochemistry. The above mentioned, and many other advantages of colloidal gold particles, make it a suitable candidate for chemical sensors and nanostructure fabrication.

1.1.4.2 Covalent strategies

(i) Crosslinkers

The principles of crosslinkers have been used to create covalent bioconjugates in many bioconjugation studies. Crosslinkers generally have a hydrocarbon chain (i.e., spacer arm) with one or two functional groups at the terminal ends which are reactive with other functional groups (Fig.7). The spacer arm refers to the portion of the crosslinker which becomes a part of the final bioconjugate. The spacer arm dictates the distance between two molecules in a final bioconjugate. Crosslinkers should be carefully selected based on their water solubility, spacer arm length, and if applicable, cell-membrane permeability as well.

The main crosslinker classifications are zero-length, bifunctional (heterobifunctional, and homobifunctional), and trifunctional crosslinkers. The most popular crosslinker functional groups are NHS-esters, imidoesters, and diazirines. Regardless of the crosslinker used, crosslinker chemistry optimization is extremely important. Using low molar amounts of crosslinkers would

result in low bioconjugate yields. Molar amounts which are too high could lead to undesired adducts, and byproducts. Zero-length crosslinkers contain spacer arms which do not become a part of the final bioconjugate (e.g. carbodiimide). Homobifunctional, and heterobifunctional crosslinkers are those which have the same functional groups, and different functional groups at the two ends of their spacer arm respectively. Trifunctional crosslinkers are those which carry three functional groups, which are susceptible for reaction with three other biomolecules.

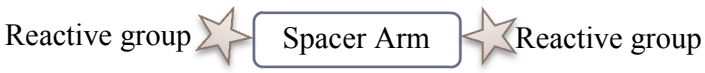

Figure 7: The molecular structure of a crosslinker.
The reactive groups undergo reaction with respective functional groups. The spacer arm generally becomes a part of the final bioconjugate, unless it is a zero-length crosslinker.

The three crosslinkers studied in this investigation (BS3, EDC, and NHS-diazirine) are discussed in greater detail in chapters 2 and 3.

Homobifunctional crosslinkers: Bis(sulfosuccinimidyl)suberate (BS3) is a homobifunctional crosslinker which has two NHS-ester functional groups at the two ends of a 11Å carbon spacer arm. The two NHS-esters are reactive towards primary amines. The advantages of using crosslinkers owe to their ability to be used with functional groups in naturally occurring biomolecules. Although NHS-esters have good stability in aqueous conditions, it should be noted that amide bond formation and hydrolysis of the NHS-ester both occur competitively. Several studies have reported that both hydrolysis and amination increases with increasing buffer pH. At a pH 8.6, and 4 °C the half-life of BS3 was only 10 mins [16].

Heterobifunctional crosslinkers: Sulfosuccinimidyl 4-(N-maleimidomethyl)cyclohexane-1-carboxylate (sulfo-SMCC), *N*-(β-maleimidopropyloxy)succinimide ester (BMPS), and succinimidyl 3-(2-pyridyldithio)propionate (SPDP) are examples of commonly used heterobifunctional crosslinkers. In a previous study, sulfo-SMCC and SPDP were used to crosslink amine modified single stranded DNA to form a tetrahedron of DNA, which was then used to cage a single cytochrome c molecules [17]. In another study, BMPS was used to bring two fluorescence proteins together, and studied their proximity effects [18].

Zero-length crosslinkers: 1-ethyl-3-(3-dimethylaminopropyl)carbodiimide (EDC) is a water soluble zero-length crosslinker which is convenient to use, and is relatively inexpensive. It has therefore been used in a variety of conjugation techniques to couple carboxyl groups to primary amines [2]. EDC first forms an active ester intermediate with a negatively charged functional group, which then undergoes nucleophilic substitution in the presence of a strong nucleophile, such as a primary amine.

Table 1 illustrates a list of the types of reaction, and the functional group in the crosslinker responsible for the corresponding reaction, modified from [2].

Table 1: Summary of commonly used crosslinkers in bioconjugation studies.

Reactivity	Reactive group in the crosslinker
Carboxyl/phosphoryl-to-amine	Carbodiimide
Amine-reactive	NHS-ester Imidoester Pentaflurophenyl ester Hydroxymethyl phosphine
Suldhydry-reactive	Maleimide Haloacetyl (bromo- or, iodo-) Pyridyldisulfide Thiosulfonate Vinylsulfonate
Aldehyde-reactive	Hydrazide Alkoxyamine
Photo-reactive	Diazirine Aryl azide
Hydroxyl-reactive	Isocyanate

1.1.5 DNA nanotechnology

From the inception of DNA nanotechnology in the 1980's, synthetic DNA-bioconjugates have been used in an enormous amount of studies across various fields. Although this field was initiated by Nadrian Seeman in the early 1980's, its widespread interest blossomed only about a decade ago. In DNA nanotechnology, rather than using DNA as the carrier of genetic information, other chemical and physical properties of DNA is exploited to create stable biological structures.

Single stranded DNA (ssDNA) has numerous attractive features for the bottom-up design of diverse supramolecular building blocks for the production of nanostructures, namely, rigidity, predictable structure, and re-assembly through complimentarity. In molecular biology, complimentarity is referred to as the lock-and-key relationship followed by two separate biomolecules. In DNA complimentarity (i.e., complimentary hybridization) when the nucleotides of one strand are aligned anti-parallel to the complimentary strand, they form very specific base pairs. The conceptual foundation of DNA nanotechnology is based on the strict base-pairing rules exhibited by the four building blocks, i.e., nucleotides of DNA (adenine, thymine, cytosine and guanine). Such strict base pairing of nucleotides allows a scientist to bind desired pieces of ssDNA to a variety of other molecules, and ultimately facilitate precisely controlled final complex structures. DNA hybridization is further discussed in chapter 4.

DNA-bioconjugates generated either by covalent, or non-covalent coupling chemistries have been utilized in nano-biotechnology, bioanalytical chemistry, therapeutics, molecular diagnostics, biosensors and many other fields. In the past, researchers have exploited these unique features of DNA in order to create nano-assemblies in the shapes of cubes, tetradehrals, octahedrals, 2D arrays and fascinatingly complex DNA origami scaffolds [19-21]. Furthermore, researchers have also succeeded in utilizing DNA as a diagnostic tool to create ultra-sensitive antibody-DNA conjugates [3,22] producing protein chips through DNA-directed immobilization [23], constructing supramolecules of DNA-streptavidin conjugates for high detection immuno-PCR [24], and also oligonucleotide-enzyme conjugates using natural enzymes such as horseradish peroxidase [25].

1.1.5.1 DNA-mediated self-assembly of biomolecules and particles

A disadvantage of random molecular self-assembly methods is their inability to maintain the engineered intermolecular/interparticle distances. On the contrary, many previous studies demonstrate that DNA mediated nanoparticle assembly has more flexibility in tuning these distances [26,27]. In a pioneering work conducted by Mirkin and coworkers, a model to assemble macroscopic aggregates was discovered. They first attached two sets of non-complementary DNA oligonucleotides to 13 nm gold particles. These oligonucleotides were capped with thiol groups, which attached to the gold colloidal particles. Then they added the complementary DNA sequence with sticky ends to this solution, which caused complementary nucleotides to bind. The result was

nanoparticle aggregation [28]. Since DNA can be denatured under high temperatures, this self-aggregation procedure could be thermally reversed [28].

Some studies have also probed the possibility of creating DNA based nano-assemblies in the shapes of cubes, tetradehrals, octahedrals, 2D arrays, and fascinating DNA origami scaffolds [19-21]. A study conducted in early 2006 informs the ability of DNA to form complex nanoscale shapes and patterns [21]. This probably is the most fascinating work conducted on DNA scaffolding, where the assemblies were termed DNA origami. The assembly consisted of six different shapes, namely squares, triangles and five-pointed stars [21]. While the creation of arbitrary patterns were concluded successfully in this study, the use of such scaffolds of long DNA have limitations brough upon factors such as strand invasion and undesired cooperative effects [21].

In a recent study, nanoparticles coated with small DNA chains were assembled with other particles to produce a desired nanoparticle aggregate. The nanoparticle assembly involved 3 main steps; carboxylic group grafting, streptavidin conjugation, and the attachment of the biotinylated DNA (from step 2) to the nanoparticles (Fig.8). Short mercapto acid ligands, and amphiphilic polymers (lipid-PEG carboxylic acid) were used on hydrophilic and hydrophobic nanoparticles respectively. The subsequent two steps relied on the 1-ethyl-3-(3-dimethylaminopropyl)carbodiimide (EDC) chemistry and on the specific and strong streptavidin-biotin binding (association constant; $K_d = 2.5\times10^{15}$ M^{-1}).

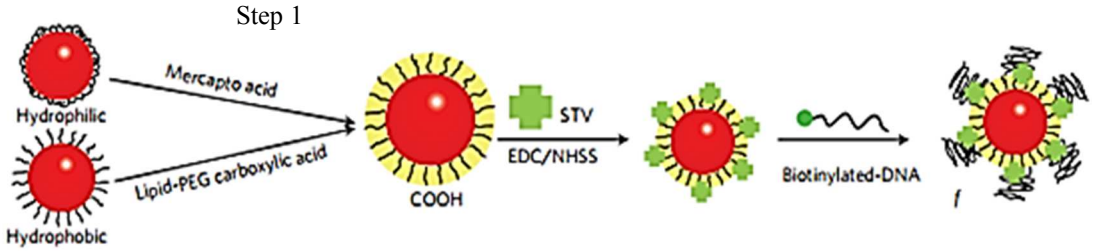

Figure 8: The three-step strategy for DNA functionalization onto hydrophilic and hydrophobic nanoparticles [29].

After functionalizing the desired particles with DNA, they investigated the possibility of incorporating fluorescent dyes, proteins, and quantum dots into nanoparticle lattices and clusters. As such, Zhang and his team investigated assembling catalytic/plasmonic nanoparticles, systems of magnetic/plasmonic nanoparticles, and systems of luminescent/plasmonic nanoparticles. The catalytic-plasmonic nanoparticles were made with spherical Au, and Pd with three different shapes (cube, octahedron, and dodecahedron). Magnetic-plasmonic nanoparticles were constructed with FeO and Au. The quantum dots were constructed with Cd, Se, Te, and ZnS. This mix-and-match investigation of nanoparticles and DNA opens doors to various opportunities for material fabrication. The control of the interparticle distance is very important for system functionality, and their models have been successful in attaining this by controlling factors such as the particle radii, and ssDNA lengths.

Therefore, as illustrated above DNA-based bioconjugates could be synthesized by either site-specific methods, or random crosslinking methods. However, to carry out "click reactions" with DNA, the DNA building blocks must carry either an alkyne or an azide functional group. One should note that the synthesis of azide-modified synthetic DNA by solid-phase synthesis is intrinsically difficult, as azides are reduced by the P^{III} atom of the phosphoramidites (Staudinger reaction) [30]. This is a large limitation of the CuAAC approach to DNA labeling, as azide-modified DNA is not directly accessible by solid-phase DNA synthesis. However, this can still be overcome by functionalizing the DNA with the alkyne group, as opposed to the azide group.

1.1.5.2 Bioconjugates of DNA and proteins or enzymes

Previously, covalent attachments between DNA and proteins have been accomplished by methods such as chemical cross-linking using a surface modified lysine or cysteine residue [18], expressed protein-ligation [31], chemoenzymatic methods [32,33], and via photoaptamers [34]. Photoaptamers are ssDNA molecules capable of forming covalent bonds with their cognate proteins, upon electronic excitation. All of the above methods have formed covalently bound protein-DNA bioconjugates. While a vast number of studies have been conducted on synthesizing protein-DNA conjugates covalently, there have also been a number of studies on noncovalent protein-DNA interactions. The majority of such studies on non-covalent methods exploited the well-known streptavidin-biotin interaction [24].

A recent study utilized a chemoenzymatic method to regioselectively, and covalently link proteins and DNA. The enzyme, protein farnesyl transferase, was used to label an engineered substrate protein containing a C-terminal tetrapeptide (SVIA) with an azide-modified isoprenoid diphosphate. Alkyne-modified DNA was added to it subsequently. The site specific DNA conjugation was achieved by a click reaction of the protein-azide with the alkyne-DNA. These protein–oligonucleotide chimeras were then spontaneously assembled into nano-architectures by complementary hybridization of the DNA. This strategy yielded a short and compact protein-DNA linkage that allowed precise control over protein spacing and orientation in the assembled nanostructure [33].

Attaching single stranded DNA (ssDNA) to enzymes enables synthesis of multifunctional moieties. For example, by attaching an enzyme to ssDNA, and attaching its complimentary ssDNA to another enzyme, we could co-localize two enzymes. If the two enzymes could participate in a continuous reaction, such a co-localized system would enable an enzyme cascade. Glucose oxidase and horseradish peroxidase are two such enzymes which are already in use to study enzyme kinetics. This technique of self-assembly of molecules is essentially extendable to other molecules with different functionalities as well. The attachment of proteins to DNA might also allow us to artificially model complex wild-type protein assemblies, which are hard to isolate using currently known protein extraction methods.

Proteins and enzymes offer exposed amino acid functional groups that can be used for crosslinking with commercially available reagents, to generate protein-DNA conjugates. These methods are acceptable as long as they do not functionally inactivate the protein, i.e., perturb the enzymatic activity (in enzymes), or the antigen binding capabilities (in antibodies). If the active site of enzymes and antibodies are utilized in the bioconjugation step, the enzymatic activities and efficiencies will be diminished drastically. As many hydrophilic residues such as lysine are present at protein surfaces the primary amine in these lysine groups renders a very useful functional group exploitable in creating DNA-enzyme bioconjugates.

1.1.5.3 Bioconjugates of DNA and other small molecules

Gene transfer and drug delivery are also other intriguing applications of DNA mediated assembly of multifunctional molecules or bioconjugates. Curiel led one such study on gene transfer,

where they derived virion particle complexes (adenovirus-polylysine-DNA complexes) to which foreign DNA attached. This was a successful effort to eliminate the limitations on the gene transfer vectors due to constraints on the size and the functional design of the genetic material that is desired to be transferred [35]. They accomplished this conjugate linkage by using an antibody bridge, where a monoclonal competent antibody was constructed to carry DNA after a polylysine residue was attached. This antibody-polylysine binding to the virus was possible because of the antibody's specificity to the virion.

In another novel study, site-specific caged plasmid DNA were transfected into cells by lipofection [36]. The conventional caging processes involves random reactions between a photolabile protecting groups and the phosphate backbone of the DNA [37]. Yamagucchi and his team first created, a site-specific amino-modification by overlap extension PCR, using a 5'amino DNA primer. Second, the amine group incorporated within the PCR product was reacted with the amine-reactive group of a biotinylated caging agent. Lastly, streptavidin was bound to the biotin group of the site-specifically caged plasmid DNA, as a steric regulator to block transcription factors binding to the promoter sequence [36].

In a pioneering work in DNA bioconjugation, Corey and Schultz synthesized a covalently attached enzyme-ssDNA with catalytic functionality. Staphylococcal nuclease hydrolyzes the phosphodiester bonds in single stranded DNA (ssDNA), RNA, as well as double stranded DNA (dsDNA). Wild-type staphylococcal nuclease does not have any site-specificity when cleaving phosphodiester bonds, which are the backbone of DNA and RNA. However, this team synthesized a hybrid-staphylococcal nuclease which could cleave phosphodiester bonds site-specifically. They accomplished this by selectively fusing a staphylococcal nuclease to an ssDNA, to create a hybrid DNase enzyme which cleaves DNA site-specifically [32]. Staphylococcal nuclease was covalently attached to a 3'-thiol containing ssDNA through a disulfide link. The unique cysteine was pre-derivatized onto the enzyme. Cysteine is a relatively rare amino acid and hence, derivatization of the staphylococcal nuclease was important. Ultimately, they demonstrated that their hybrid enzyme was able to selectively cleave incoming single stranded DNA (substrates), in comparison with the wild-type enzyme, which cleaved DNA nonspecifically. In 2007, Gianneschi and his team used a similar method to construct a semisynthetic enzyme, with programmable capacity. They employed an intricate mechanism where two orthogonal DNA-directed processes established

programmed allosteric activation/deactivation of an enzyme, by a trigger signal provided by sequence specific binding of ssDNA. Here, they conjugated a ssDNA to an allosteric enzyme, creating a semisynthetic enzyme-ssDNA. Next, they attached its complimentary ssDNA to the specific inhibitor of that enzyme. [38]. They were able to intrasterically activate, or inactivate the enzyme by hybridizing (annealing the two strands) the two ssDNA together, or denaturing (separating the two strands).

In another study related to DNA bioconjugation, Erben and his team encapsulated a cytochrome *c* molecule within a rigid tetrahedral structure constructed from DNA [17]. In this novel architecture, they first constructed the DNA cage by facilitating self-assembly (via complimentary nucleotide base pairing) of four 20 base paired ssDNA. In one of the ssDNA strands, they conjugated a model globular protein (cytochrome *c*). When the final spontaneous assembly of DNA was facilitated, they were able to position the small cytochrome molecule on the interior of the DNA tetrahedral cage. Their method was adopted from a DNA cage development strategy from one of their own previous works [17,19].

1.1.5.4 Applications of DNA-based bioconjugates

DNA based bioconjugation is often a random process that leads to heterogeneous conjugates with variable stoichiometry and no regiospecificity. Regiospecific conjugation of proteins and DNA is a requirement for bottom-up design of supramolecular architectures. Albeit the lack of regiospecificity, DNA directed immobilization is reversible, and could be manipulated to yield high conjugation efficiencies [23]. These characteristics are invaluable for fabrication and reconfiguration in the fields of biotechnology, medical diagnostics, and translation medicine, and hence have been utilized in a wide variety of applications.

One of the earliest studies used site-specific DNA bioconjugations to yield fluorophore-tagged-DNA as sequencing primers [38]. They utilized the widely employed Huisgen's 1,3-dipolar cycloaddition chemistry to react alkynyl 6-carboxyfluorescein (FAM) with single stranded DNA (ssDNA) which have been functionalized with azide. These fluorescein labelled oligonucleotides were used as the primers in DNA sequencing [39]. This process was lengthy and required high temperatures (90 °C). However, since their study, attention was diverted to reverse the order of derivatization. As discussed previously, derivatizing DNA with azide groups is problematic due

to its potential of undergoing Staudinger reaction with the phosphoramidites [40]. Therefore, successive studies with fluorescent labeling of DNA using "click reactions" have been centered on alkyne-functionalizing the DNA, while azide-functionalizing the tagging dye/fluorescent protein. Many site-specific, as well as random crosslinking reactions have yielded successful labelled DNA which were used in fluorescent *in situ* hybridization (FISH) applications [41], high through-put DNA sequencing [42], chromosome and genetic analysis [43], and direct visualization of microorganism communities [44].

In an early study, scientist followed an expressed protein ligation procedure to synthesize protein-nucleic acid conjugates [23]. This is a perfect example of utilizing immobilized DNA to capture other biomolecules such as proteins. In their expressed protein ligation procedure, they first expressed the target proteins in *E.coli*. This target protein contained a chitin binding domain, which was utilized to bind the protein to a chitin matrix column. Next, the protein was liberated from the column by a mercaptoethansulfonic acid wash. As a result, the target protein was derivatized with a C-terminal thioester. This C-terminal thioester was utilized to carry out native chemical ligation with a polyamide nucleic acid (PNA) containing an N-terminal cysteine, as well as a Cy5 labeled peptide. PNAs are non-ionic analogs of DNA where the entire sugar-phosphate backbone is replaced by an N-aminoethylglycine-based polyamide structure. In their final step, these protein-PNA conjugates and protein-Cy5 conjugates were successfully annealed onto their complimentary strands which had been previously immobilized onto glass slides. As such, their protein chip (i.e., protein microarray) was developed via DNA-directed immobilization [23]. A common concern of protein biochips is that when multiple proteins are immobilized on chemically activated surfaces, their intrinsic instabilities could lead to loss of protein functionalities. However, DNA microarray matrices involve very few steps involving strong chemical agents, and hence allows for unique parallel attachment of multiple proteins to the surface of the matrix.

Niemeyer has reviewed another area of application of protein-DNA conjugates in the field of immunological detection assays and biosensors [24]. The devices reviewed in this article indicates the high potential of DNA-labelled antibodies for immunodiagnostics. Immunoassays are widely used for the detection of drugs of abuse. The most commonly used counterpart methods for detection are PCR and GC-MS techniques. These methods are labor intensive, time consuming, and require usage of many reagents [21,24]. However, immunoassays could prove extremely useful

in overcoming many of the above mentioned problems, without trading off the sensitivity of the detection assays as well. They can be developed to be highly specific, sensitive, relatively rapid, require no extraction steps, and they usually require little or no preparative clean up steps too. The following are types of immunoassays that are used for detection of drugs, analytes and precursors: enzyme-linked immunosorbent assay (ELISA), enzyme-multiplied immunoassay techniques (EMIT), fluorescence polarization immunoassays (FPIA) and up-converting phosphor technology (UCP). While there are many other sub divisions of immunoassays, the basis of all enzyme immunoassays is the binding of the antibody to the antigen of interest. This binding is detected using an enzyme, with the enzyme acting on a substrate producing a colored product which is subsequently measured via colorimetric analysis. Capabilities and future directions of DNA based nanostructures in sensing and detection of drugs, would be extremely useful for on-site drug detection in fields such as athletics, law enforcement, and medicine (point-of-care). One advancement that could be implemented on current immunoassay techniques, is multiplexing using protein-DNA bioconjugates (simultaneous detection of multiple analytes using different protein-DNA conjugates). These methods have been successfully used to produce antibody-DNA conjugates, utilized in ultrasensitive diagnostics such as immuno-PCR [3].

A recent study exemplified the ability of using DNA bioconjugation onto enzymes, as a new class of protein transfection material. In the last decade, spherical nucleic acid (SNA)-nanoparticles have been recognized as new architectures with diverse applications in immunology and intracellular detection. These SNAs are simply nanoparticles with dense shells of ssDNA. Brodin and his team applied this concept to create a proSNA (protein-SNA) where β-galactosidase enzyme was covered with a dense shell of ssDNA. They report that the pro-SNA resulted in increased cellular uptake while maintaining the enzymes catalytic activity of the where β-galactosidase enzyme [45]. Another study which developed an influenza A vaccine utilized the BS^3 homobifunctional crosslinker to fuse the extracellular domain of a transmembrane protein (M2e), to a Leucine zipper domain from the yeast transcription factor (tGCN4), and created a fusion protein synthetically, which elicited antibodies specific to the influenza antigen [46]. This is an example of utilizing random crosslinking techniques to construct DNA-enzyme bioconjugates.

As demonstrated all of these previous studies have used random bioconjugation techniques (e.g.crosslinkers such as BS^3, and BMPS), and site-specific bioconjugation techniques (“click

reactions", Staudinger ligation) to synthesize a variety of diagnostic tools, detection systems, novel transfection materials, and many more.

1.1.6 Enzymatic studies

1.1.6.1 Overview of Enzymes

Approximately 200 enzymes have been discovered up to date, and most of these enzymes come from a limited number of fungi, yeast, and bacteria [47]. Enzymes are considered as a potential biocatalyst for a large number of reactions. Microbial enzymes have widespread uses in industries and medicine. The microbial enzymes are also more active and stable than plant and animal enzymes. In addition, microorganisms provide an attractive source for enzymes because they can be cultured in large quantities in a short time by fermentation and owing to their biochemical diversity and susceptibility to gene manipulation. Industries are looking for new microbial strains in order to produce different enzymes to fulfil the current enzyme requirements [48]. While animal and plant sources require careful and planned collection and storage of raw material, microbes are convenient and can be grown in fermenters easily. Microbes can also be experimented with mutagens, to yield alterations in naturally occurring enzymes. Most of the enzymes used in industrial applications are extracellular enzymes. These extracellular proteins are mainly obtained from fungal or bacterial sources (ex: *Aspergillus*, *Bacillus*, *Streptomyces*, *Escherichia* species). Examples of such enzymes in commercial use are; α-amylase, cellulose, dextranase, protease, and amyloglucosidase. Other enzymes which are not used in industrial applications are also produced in small quantities, and they are mostly enzymes produced in intracellular spaces. Examples of such proteins are asparaginase, catalase, cholesterol oxidase, glucose dehydrogenase, and glucose 6-phosphate dehydrogenase.

1.1.6.2 Methods of Enzyme immobilization

The method of adsorbing enzymes to solid supports, or crosslinking enzymes to solid surfaces is referred to as enzyme immobilization. If performed carefully, using only the enzyme surface, this technique could be utilized in the development of a variety of biosensors and biological assays. Since the active sites of enzymes are generally conserved, there is little risk of

tampering with the catalytic activity. However, once immobilized, the enzyme has less rotational freedom, which is not necessarily an advantage for catalytic activity for all enzymes. The two techniques of enzyme immobilization are entrapment, and surface immobilization (Fig.9). Enzyme immobilization could be accomplished passively via electrostatic interactions, or covalently by reacting the functional groups present on the surfaces of the protein.

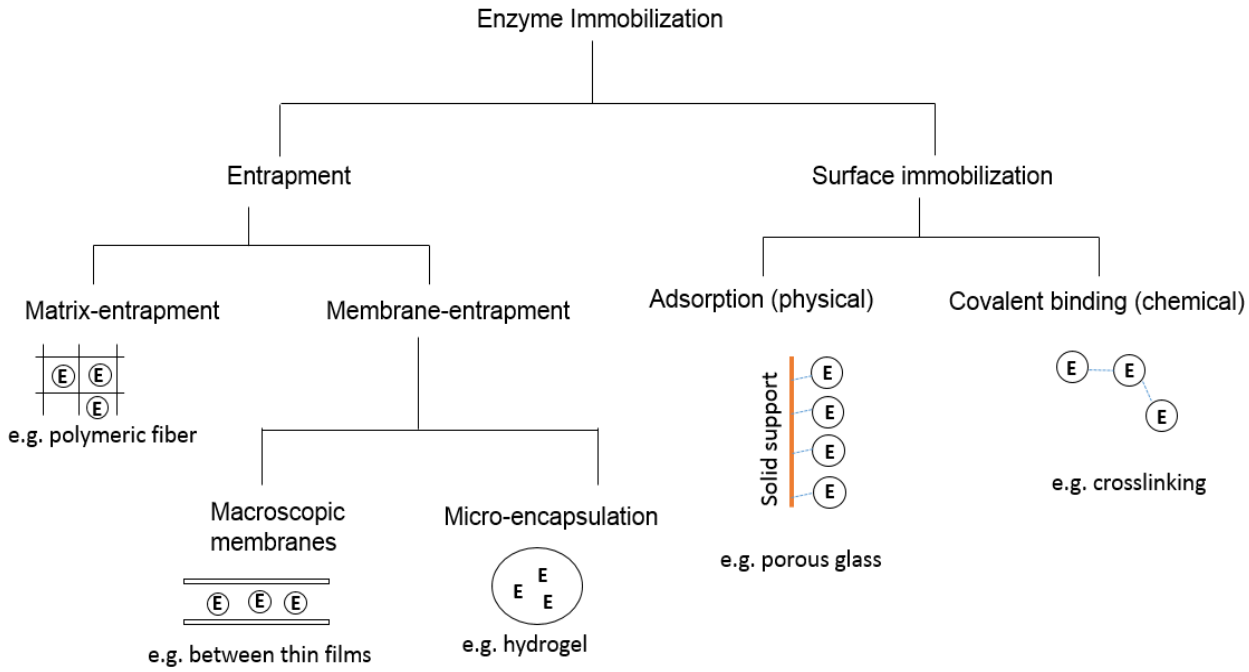

Figure 9: Enzyme immobilization techniques [49].

Enzyme entrapment and encapsulation are generally achieved by using polymeric networks and alginate solutions [50]. Surface immobilization has been accomplished on many matrices such as cellulose paper [51] , nanoparticles [52] and gel-silica [53]. Studies on surface immobilization have reported concerns regarding tortuosity, crosslinker cleavage, spacer arm disorientation/cleavage, spacer length issues, flexibility, loss of peptide functionality, dissociation at the functional groups, restricted kinetics, and limited accessibility for the reactants [54,55]. These could interplay and result in a loss of functionality of the molecules.

However, enzymes in free solution have been speculated to form aggregates, making them less accessible for their substrates. This in return could lead to poor product formation. Immobilizing enzymes onto supports could accomplish high densities of enzymes in a localized environment, which could enhance the enzymatic activities by 100-folds [56]. In one previous study, celB and β-glucosidase were immobilized on to a polystyrene layer which was treated with plasma [54]. They immobilized the celB enzymes to a polymer binding surface pre-treated with plasma immersion ion implantation (PII). Afterwards, they studied the enzymatic activity of the immobilized system via analyzing the V_{max}, and K_m, values of the carboxymethyl cellulose hydrolysis activity [55]. Their studies showed that the immobilized celB enzyme's activity was enhanced, compared to that of the free enzyme during carboxymethyl cellulose hydrolysis. In another study, glucose isomerase (GI) from *Streptomyces rubiginosus* was immobilized covalently onto Eupergit® C 250 L made by copolymerization of *N*,*N*-methylene-*bis*-methacrylamide, glycidyl methacrylate, allyl glycidyl ether and methacrylamide [57]. GI facilitates isomerization of glucose to fructose. The catalytic efficiency of immobilized GI was found to be three-fold higher than that of free GI. They also discussed the similarities in the thermal stabilities of the free GI, and immobilized GI [57].

1.2 Introduction

1.2.1 Overview and objectives

This study explored programmable DNA hybridization in order to co-localize two wild-type enzymes. Single stranded DNA (ssDNA) attached to enzymes yields conjugate possibilities limited only by one's imagination. For example, by attaching an enzyme to ssDNA, and attaching the complimentary ssDNA to another enzyme, we would be able to program spontaneous association of the two enzymes. Previous bioconjugation techniques such as chemoenzymatic labeling methods, and other chemical strategies do not render a universal covalent bioconjugation method for wild-type proteins, enzymes, or peptides. Because such labeling/derivatization steps pose a risk of hindering enzyme functionality, our investigation was solely constructed around utilizing ubiquitous functional groups present on natural enzymes. Therefore, we have essentially removed the need for extensive modifications on the enzyme's surface, and immobilization steps.

The main objective in this study was to synthesize two separate bioconjugates with two complimentary single stranded DNA (ssDNA) covalently coupled to two separate enzymes, in an

aqueous system. The next objective was to exploit complimentary binding of ssDNA to co-localize those two enzymes in an aqueous system. The two enzymes chosen for the proof-of-concept were glucose oxidase (GOD), and horseradish peroxidase (HRP) (Fig.10).

There are several reasons for choosing GOD and HRP as the two enzymes for the proof-of-concept. GOD and HRP both have surface amine residues which we would utilize for covalent bond formation between phosphorylated ssDNA, using crosslinking strategies. This voids the necessity for performing prior surface modifications on these two wild type enzymes. The fewer the modifications introduced to any biological molecule, the better the process is. That is because fewer modifications leads to fewer chances of affecting enzyme activities, improved yields owing to the fewer steps, and lesser costs.

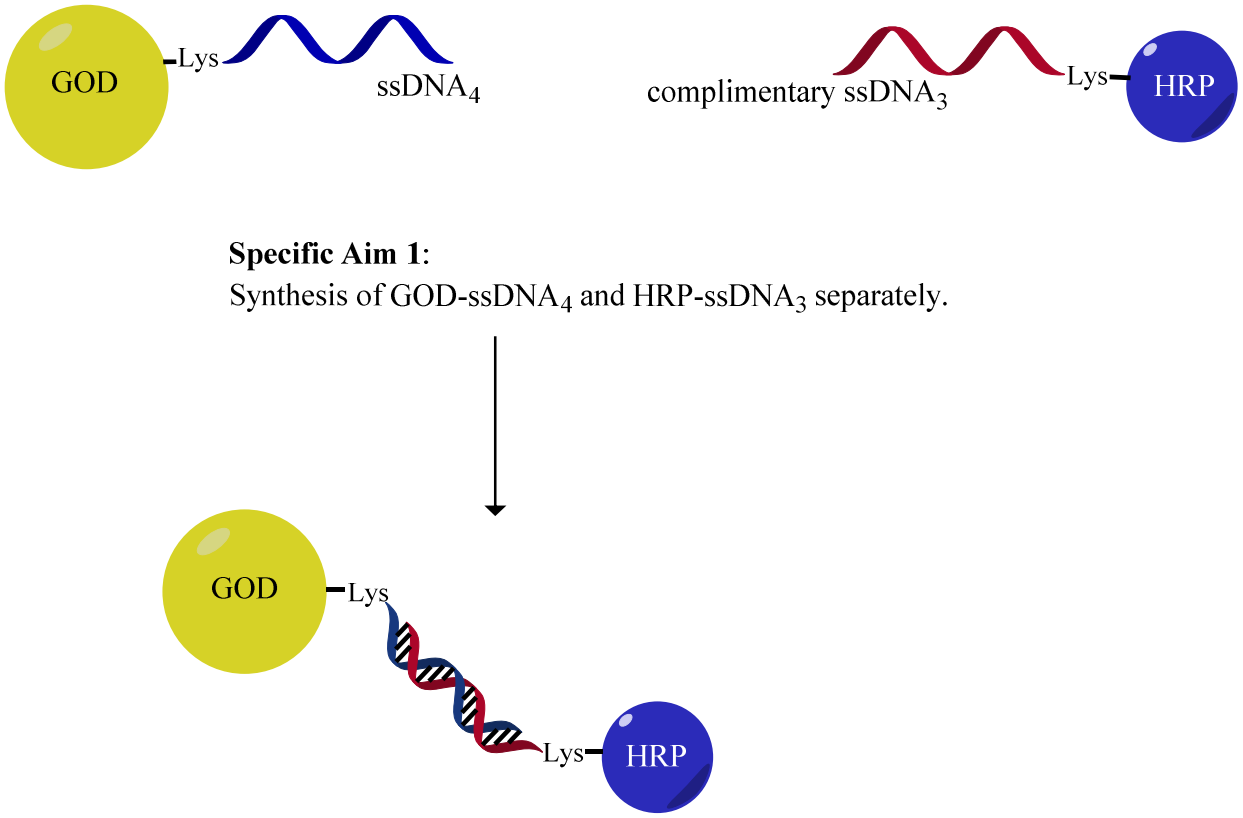

Figure 10: Illustration of the final assembly of a co-localized enzyme system.

1.2.2 Gaps in current state-of-art

Molecular immobilization: The major gaps we address in previously reported co-localized enzymatic designs are mainly molecule immobilization onto intricate DNA scaffolds, as well as direct enzyme-enzyme conjugation [58,59]. Enzyme immobilization techniques have numerous limitations such as loss of enzyme activity, cumbersome surface immobilization strategies, bond cleavage, enzyme leeching, restrictions of spacer flexibility, constricted enzyme orientation at interface, and poor robustness [54].

Quantitation of conjugated/immobilized enzymes: In an immobilized system, if the enzyme leeches from the support, the desired microenvironment around the concerted enzymes is no longer existential. In immobilized bioconjugation studies, in order to quantitate the amount of enzymes bound to a solid surface, scientists have usually taken an indirect route. First, the $enzyme_{bound}$ are indirectly quantitated by measuring the $enzyme_{unbound}$ leeched out into the wash solution [60]. Then, using the; $enzyme_{bound} = enzyme_{total} - enzyme_{unbound}$ equation, they have determined the amount of bound enzymes. The other method is using fluorescence imaging/spectroscopic analyses, which requires tagging or attaching fluorescent or dye molecules to the biomolecules [59]. Another direct method of quantitating enzymes on an immobilized support is via using spectrophotometers designed for solid samples. Agilent Cary 500 is an example of a specialized instrument which can detect in the UV-Vis-NIR (ultraviolet-visible-near infrared) region, specifically in the range of 175 – 3300 nm. A previous study which studied enzymatic activity of glucose oxidase (GOD) immobilized onto Whatman papers utilized the aforementioned spectrophotometer, and analyzed their samples at 280 nm, with Teflon used as the blank [51]. However, the instruments and materials involved in both of these techniques are expensive, and involves a large no. of steps in the analytical procedure.

Substrate diffusion limitations: In immobilization, even if a residue on the enzyme's active site is not utilized in crosslinking (the desired scenario), the active site could still be oriented in a position which cannot be accessed by the substrate. For example, if the immobilized enzyme's active site is facing towards the solid support, the substrate will have spatial hindrances to get to the reactive site of the enzyme. Therefore, this could pose as a kinetic limitation to the enzymes catalytic activity. We recognized that a bioconjugation scheme conducted in an aqueous scheme would not encounter these pitfalls.

The other concerted model for developing enzymatic cascades have been direct enzyme conjugation models where $enzyme_1$ is conjugated to $enzyme_2$ directly via any chosen crosslinking method [58]. The same concern with substrate diffusion limitations are applied to direct conjugations as well. For example, in a design where a crosslinker with a spacer arm of only 8.3Å (sulfo-SMCC) is used, the two enzyme molecules could be too close together [58]. Although C–C single bonds with 120° rotational freedom could be the best scenario for enzyme-enzyme rotational abilities, by incorporating DNA to link the two enzymes, we are not trading off the rotational abilities of the enzymes. All the six bonds in a DNA backbone (C–C, phosphodiesterase etc.) have rotational freedom compared to hydrocarbon chains as well (C–C single bonds) [61].

Controlling the distance between the enzymes in enzymatic bioconjugates: The optimal distance between two enzymes for enhanced catalytic activities is not well characterized yet. This is because the optimal distance of enzymes could easily differ based on the type of enzymes used in a concerted model. However, the underlying principle is that if the two enzymes in the cascade are too close, the enzymatic activities could easily undergo product inhibition. The proximity of the enzymes could be controlled by using crosslinkers with different spacer arm lengths (Å). The spacer arm of a crosslinker refers to the length of the hydrocarbon chain in between the one/two functional groups at the crosslinkers terminal ends. If a longer distance is desired between the two enzymes in the cascade, the choice is to use a longer spacer arm (e.g. BS3, DPDPB). However, the maximum spacer arm length of the crosslinkers discovered up-to-date is approx. 11 Å. Therefore, after a certain limit, researchers are unable to use crosslinkers to control the distance between two biomolecules. On the other hand, using crosslinkers with medium length, or short spacer arms result in the two enzymes being extremely close together. We recognize this as a potential pitfall, giving rise to kinetic limitations.

1.2.3 Scope of dissertation

In our design, the factor governing the distance between the two enzymes is the length of the DNA. The usage of DNA to control the distance between the two molecules is more promising because the distance will be based on how many base pairs there are in the ssDNA sequence. And this factor is easily controllable. In chapter 4 of this dissertation, we also report results from DNA hybridization analyses. The purpose of this experimentation was to validate that the ssDNA used

in the study could be thermally programmable, i.e., DNA hybridization facilitated by heating-and-cooling.

Additionally, this investigation utilizes cost-effective crosslinkers compared to many previous studies [18,45,59], enabling large throughputs. Previous studies have repeatedly used expensive crosslinkers such as BS^3, and BMPS to accomplish crosslinking. This study focused on accomplishing bioconjugation via three different crosslinkers, and discusses the importance of optimization of bioconjugation chemistries in order to obtain useful bioconjugates. The investigation reported herein demonstrates the ability of using a relatively inexpensive, and universal crosslinker such as carbodiimide to accomplish crosslinking of naturally occurring enzymes and ssDNA.

Our investigation attempts to address the above mentioned gaps by adapting current knowledge in the field, and attempts to evade the drawbacks of molecular immobilization, surface modifications, and direct enzyme-enzyme conjugation. To our knowledge, this is one of the first attempts to synthesize bioconjugates using wild-type enzymes and ssDNA, in a single-step crosslinking procedure. As our study only involved naturally occurring enzymes (wild-type proteins) a greater focus of this study has been devoted to creating a final enzyme macromolecule in solution, and characterizing the final macromolecule's structure. A heavy emphasis has been devoted to characterizing crosslinking strategies (i.e., comparison between EDC, EDC/Im), developing analytical methods which could be routinely used to separate and purify bioconjugates, and gathering structural information of the bioconjugates formed via the chosen crosslinking technique. The reaction schemes, optimized protocols developed in this study will be universally applicable to a wide variety of peptides, proteins, and enzymes. It is an innovative, improved, holistic study, and the conclusions drawn from the study could pave a path for simplified bioconjugation techniques in aqueous phase systems.

CHAPTER 2. CONJUGATING SSDNA AND ORGANIC COMPOUNDS VIA EDC CROSSLINKING

2.1 Abstract

An adapted strategy from the conventional 1-ethyl-3-(3-dimethylaminopropyl) carbodiimide hydrochloride (EDC) crosslinking method was developed to form a covalently coupled phosphoramidated single stranded DNA (ssDNA). The novel ssDNA bioconjugate was used to compare the conventional carbodiimide (EDC) reaction with the adapted strategy using EDC and imidazole (EDC/Im). Matrix assisted laser desorption ionization-time of flight (MALDI-TOF) results demonstrated that the phosphoramidated conjugate is stable for several days, and that phosphoramidation was exclusively at the 5' end of ssDNA. A reversed phase liquid chromatography (RP-HPLC) method with UV detection was developed to determine the yield of conjugates. The methods coefficients of variation (%CV) were less than 6%, and biases ranged from -5.1% – 1.2%. The conjugate yield via the conventional EDC method was 68.3±2.2%, while that of the adapted EDC/Imidazole method was 79.2±2.4% (n=10). This study demonstrates a convenient, one-pot strategy for crosslinking biological molecules, which is useful in diagnostics, biosensor development, and constructing self-assembling macromolecules where there is a lack of flexibility in adjusting reaction temperature or pH.

2.2 Introduction

2.2.1 EDC (1-ethyl-3-(3-dimethylaminopropyl) carbodiimide) crosslinking.

EDC is a water soluble zero-length crosslinker which is convenient to use and relatively inexpensive. It has been used in a variety of conjugation techniques to couple carboxyl groups to primary amines [2,25,62]. EDC first forms an active ester intermediate which then undergoes nucleophilic substitution in the presence of a strong nucleophile, such as a primary amine. EDC crosslinking is generally carried out in buffers devoid of extraneous carboxyls or primary amines, at physiological pH. Although EDC crosslinking chemistry is well known, reverse reactions can limit its utility [63,64]. The o-acylisourea product intermediate can be easily hydrolyzed, reverting to the original carboxylate molecule [2]. To overcome this limitation, sulfo N-Hydroxysuccinimide (sulfo-NHS ester) has been used to form a more stable second intermediate prior to amidation [64].

This enhanced EDC/NHS method has been used in a wide range of applications such as immobilizing carboxymethylated coatings on enzyme-linked immunosorbent assay wells [65], immobilizing proteins onto grafted solid surfaces [66,67], crosslinking antibodies to functionalized solid supports [68], peptide functionalized gold nanoparticles [69], antibody functionalized superparamagnetic nanoparticles [70], grafting polymers onto porous silicon [71], constructing DNA-cellulose nanocrystals [72], and creating nucleic acid functionalized carbon nanotubes [73]. Although EDC and EDC/NHS reactions have been extensively used before, their reaction efficiencies have only been quantified indirectly [68] or in semiquantative FTIR analyses [74].

In the final step of the EDC/NHS reaction mechanism, amidation is favored at pH 7.5 – 8. Therefore, when many researchers used the EDC/NHS method, researchers have approached a two-step protocol [2,63,75]. The initial EDC/NHS reaction had been performed at pH 4.5 – 7.5. Immediately afterwards, the pH of the reaction mixture had been raised to approx. 8.0 prior to adding the amine reactant, as amidation is facilitated at higher pH. This two-step process faces the risk of hydrolyzing the NHS intermediate, as it is has a half-life ranging from 10 min – 1 hr [75]. Not only is this two-step process cumbersome, it can also be prone to poor product yields with enzymes or immunoglobins due to loss of activity, as these molecules generally have an isoelectric point (pI) around 7.4. Lastly, NHS esters are expensive, and are highly water labile.

This chapter discusses the synthesis of a novel phosphoramidated single stranded DNA (ssDNA) conjugate via a convenient, inexpensive, time efficient EDC crosslinking method. A 5'phosphoryl single stranded DNA (phosphoryl ssDNA) was crosslinked to ethylenediamine using 1-ethyl-3-(3-dimethylaminopropyl) carbodiimide (EDC). To study the EDC crosslinking reaction, an ssDNA modality was chosen to address unique problems related to DNA and nucleic acid bioconjugation techniques. The largest setback of EDC in nucleic acid studies is due to the formation of non-specific, electrostatic interactions with the phosphate backbone, and open nucleotide base pairs [2,76]. Additionally, EDC crosslinking can also face additional problems due to self-dimerization of DNA, preventing covalent bond formation between the desired functional groups. Previous literature does not suggest practical approaches to circumvent such adduct formation, hence the development of an alternate protocol to address these drawbacks. Therefore, upon identifying the tedious multi-step reactions involved with EDC and EDC/NHS crosslinking,

the expenses related to it, and the problematic non-specific binding with DNA, we investigated an alternate route to address these drawbacks.

The possibility of adding an alkaloid to drive the forward reaction has been previously proposed and tested in binding DNA to microwells [77], and in immobilizing phosphoproteins onto collagen [78]. However, to our knowledge, there are no studies which have reported bioconjugate product characterization, product stability, and product quantitation obtained via an imidazole mediated EDC (EDC/Im) crosslinking strategy. We quantitatively compared the conventional EDC and the modified EDC/Im method to crosslink negatively charged functional groups with primary amines in a one-pot reaction scheme, without adjusting the temperature or pH (Fig.11). This study also reports chromatographic analytical methods suitable to assess DNA conjugates.

The theoretical reaction mechanism is depicted in Fig.11. At neutral pH, O^- in the free 5'phosphate group of the ssDNA attacks the $C^{\delta+}$ on the EDC molecule, which then forms an unstable isourea intermediate. Imidazole (Im) at pH 6.0 ensures that one N atom in the ring is always protonated, and ensures that the other N atom carries a lone pair of electrons which makes the molecule a strong nucleophile [79]. When imidazole is immediately introduced to the isourea intermediate, the $P^{\delta+}$ undergoes nucleophilic substitution by imidazole. The intermediate phosphorylimidazole is highly reactive, and will undergo a nucleophilic attack by the primary amine in ethylenediamine (EDA), in an S_N2 reaction, resulting in a stable, covalent, phosphoramidate bond.

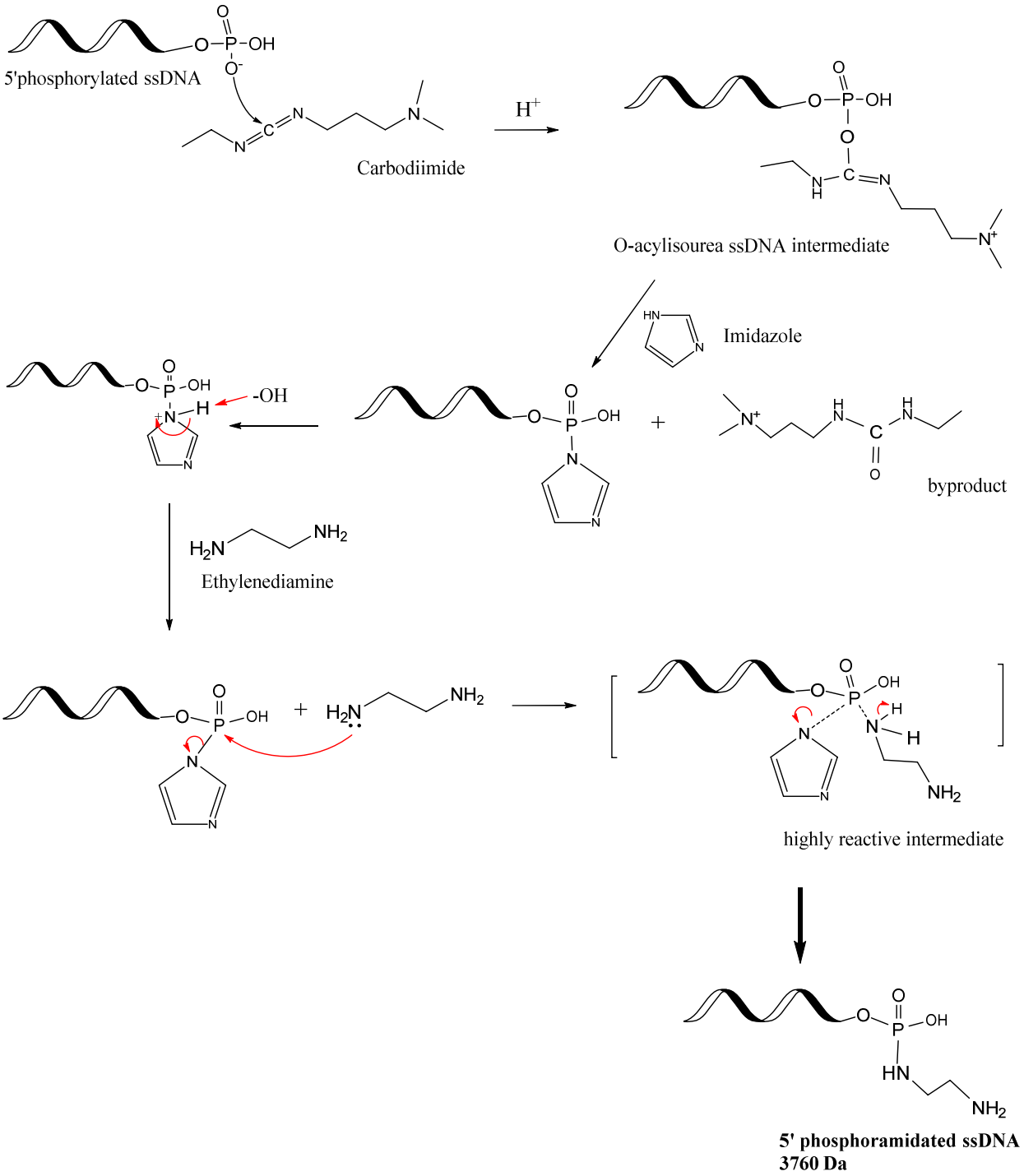

Figure 11: Schematic of the EDC/Im reaction.
– modified from [2].

2.2.2 Reversed phase high performance liquid chromatography (RP-HPLC).

Liquid chromatography (LC) is a separation technique that is widely used in many bioanalytical applications. Reversed phase is a famous choice in LC which separates molecules in an analytical sample based on their hydrophobicity. There are two major "phases" which are often used in RP-HPLC. The stationary phase is the solid surface which is generally silica particles functionalized with organic groups/ligands such as alkyl chains, alkane chains or amines. There are many stationary phases for RP-HPLC columns. The one used in this study was a C_{18} column, which has a ligand size of 18 carbons. These functionalized particles are ultimately packed into a column to create the stationary phase. Smaller particle sizes coupled with smaller column lengths, increase resolution, and decrease the overall experiment run times.

The mobile phase is the solution which is introduced to the packed beads (i.e., stationary phase) in the column. The mobile phase moves along the column due to a pressure gradient created. Optimizing the organic modifier (mobile phase) is one other key factors in chromatography. Mobile phase gradients could be profiled according to the decreasing polarity; water> methanol> acetonitrile> N-propanol> THF. Incorporation of ion paring agents is of great importance in RP-HPLC, because they impart hydrophobicity into the molecules in the analytical sample. This improves retention of the molecules in the column's stationary phase. Typically, TFA (trifluoroacetic acid) is used for protein and peptide separations, and TEAA is generally preferred for DNA quantification experiments.

In HPLC, a sample is injected to the column, and the mobile phase is introduced. Next, the separated constituents in the analytical sample are introduced to a UV spectrophotometer automatically. Here, the intensity of absorbance (AU) of each constituent in the sample are detected at the operator prescribed wavelength. The detection method determines the amount of each constituent in the analytical sample, along with their elution time from the column. Generally, HPLC instruments (a.k.a. separations module) are equipped with a software manager, which remotely controls the mobile phase ratios, column temperatures, flowrates, and sample injection volumes. There are several major HPLC separation techniques, namely, reversed phase, partition, normal phase, affinity, ion exchange, and size exclusion. Among these, reversed phase is a commonly used technique because it can be used for both nonpolar, and polar molecule separations.

2.3 Materials and Methods

2.3.1 Materials

A 12 base paired (bp) single stranded DNA (ssDNA) with the sequence; 5'phosphorylated-TGT GCA TTA TTT-3'; T_m 29.0 °C; molecular weight, 3721 Da, was purchased by IDT® DNA. The sequence was designed with a reduced no. of G, C, and a medium length, in order to minimize the ssDNA forming secondary structures. For the comparison study to determine if the bioconjugate formation is independent of the ssDNA sequence, we also conducted the EDC crosslinking experimentation with a 15 bp ssDNA with the sequence; 5'phosphorylated-TGT GCA TTA TTT GAT-3'; T_m 37.8 °C; molecular weight, 4665 Da.

Imidazole (Im), EDC and 99% v/v ethylenediamine (EDA) were purchased from ThermoFisher Scientific. 10 mM sodium phosphate ($NaH_2PO_4 \cdot H2O$), 0.15 M NaCl, buffer medium was freshly prepared, pH adjusted to 7.2±0.2, and filtered. 0.1 M Imidazole solutions were pH adjusted to 6.0±0.2.

2.3.2 Methods

2.3.2.1 Crosslinking phosphoryl ssDNA with ethylenediamine.

5' phosphorylated single stranded DNA (phosphoryl ssDNA) as received was dissolved in 50 µL of PBS (pH 7.2±0.2), and was added to EDC (carbodiimide) at a 150-fold molar excess amount to the ssDNA. In order to reduce non-specific EDC binding to the ssDNA phosphate backbone, the molar ratio of EDC: 5' phospho ssDNA was reduced to 150-fold excess, instead of the 430-fold molar excess suggested in literature [75]. Next, 0.025 M EDA dissolved in PBS (10mM, pH 6.0±0.2) was added in an equimolar amount to the ssDNA. In order to allow only one covalent bond per one phosphoryl group, the molar ratio of 5' phosphoryl ssDNA: EDA was maintained at 1:1. The reaction mixture was gently vortexed, and an additional 120 µL of PBS was added to the vial prior to incubation at r.t. (room temperature) for approx. 4 hrs. In the EDC/Im reaction, instead of PBS, Im (0.1 M, pH 6.0±0.2) was used to dissolve EDA in an equimolar amount to the ssDNA. The molar ratio of 5' phosphoryl ssDNA: EDA was maintained at 1:1. The reaction mixture was gently vortexed, and an additional 120 µL of Im was added to the vial prior to incubation at r.t. (room temperature) for approx. 4 hrs. The phosphate concentration of the PBS buffer was limited to 10mM so that the free phosphate groups did not bind with EDA (ethylenediamine).

After the 4 hrs incubation period, each sample was subjected to dialysis against deionized water for 2 hrs using 2000 MWCO (molecular weight cut-off) dialysis tubes to remove unreacted EDA, Im, and buffer salts.

2.3.2.2 Matrix-assisted laser desorption/ionization time-of-flight (MALDI-TOF).

MALDI-TOF spectrometric results were obtained using an Applied Biosystems (Framingham, MA) Voyager DE PRO mass spectrometer. This instrument utilizes a nitrogen laser (337 nm UV laser) for ionization with a time-of-flight mass analyzer. Prior to MALDI-TOF, each sample was purified using a C18 – ZipTip column (Millipore Corporation, Billerica, MA). The ZipTip columns were conditioned using two 10 µL of acetonitrile followed by two 10 µL of 0.1% trifluroroacetic acid (TFA). A negative linear mode was used (MH^-) to produce singly charged ssDNA species. In MALDI-TOF, the analyte sample is embedded in a mixture of weak organic acids, called the "matrix." The matrix is responsible for desorption of the sample. It also prevents the analytes in the sample from decomposing. Next, the molecules are ionized by a laser ablation, causing the molecules to ionize. The protonated/deprotonated molecules are then accelerated in an electric field, under a fixed kinetic energy, and detected using a time-of-flight mass spectrometer.

2.3.2.3 Confirming phosphoramidation exclusively at the 5'phosphate of ssDNA.

Since ssDNA is comprised of a phosphate backbone, any charged counter ions or species could interact with these groups, giving rise to weak, unstable electrostatic interactions. To investigate whether EDA is covalently bound exclusively at the 5' phosphate group of the ssDNA, an EDC/Im reaction with nonphosphorylated ssDNA (3641.4 Da) was conducted. In phosphorylated ssDNA, there is a phosphate group at the end of the strand, while in the nonphosphorylated ssDNA, it is an OH group. As nonphosphorylated ssDNA lacks an open phosphate group susceptible for conjugation, it was not expected to observe a mass signal during mass spectrometry at the otherwise expected conjugate mass region.

2.3.2.4 Stability of phosphoramidate bond.

To investigate the phosphoramidate bond over a prolonged time, MALDI-TOF analyses of the purified products was conducted after 7days, and 14days (n=4). These subsequent results for time point 0 (1day), time point 1 (7 day), and time point 2 (14 day) were obtained from the same product sample which were stored at -20 °C.

2.3.2.5 IP-RP-HPLC method development.

A C18 XTerra® (Waters, MA) column with 4.6 × 100 mm, 3.5 µm particle diameter, and a guard column was used for reverse phase separation of the conjugates. High-performance liquid chromatography (HPLC) was performed on an Alliance 2695 separation module, using Empower version 2.0 software (Waters Corp., Milford, MA), equipped with a Waters 2496 UV/Vis detector (Waters Corp., Milford, MA). Detection was carried out at $\lambda_{260\ nm}$. HPLC analysis was conducted in 0.1 M TEAA, pH 9.70±0.05 (triethylammonium acetate) buffer with 5% acetonitrile (ACN) and 30% ACN as the two mobile phases. 0.1 M TEAA buffer was prepared by adding 5.6 mL of glacier acetic acid to 950 mL of deionized water. To this, 13.8 mL of TEA was added gradually, and the solution was stirred. Afterwards, the pH of the solution was adjusted to 9.70±0.05, and the final volume was brought to 1000 mL by adding water. This solution was filtered using gravity filtration and qualitative-grade filter paper, and was stored at 4 °C. Mobile phases were prepared as follows; A: 5% acetonitrile in TEAA (v/v), B: 30% acetonitrile in TEAA (v/v). The gradient method incorporated was 90% – 60% A in 16 min, and 60% – 90% A in the next 14 min. A flow rate of 1.0 mL/min, an injection volume of 100 µL, sample and column temperatures of 33 °C, and 38 °C, were used respectively. The column was equilibrated for 50 mins prior to running samples, and for 30 mins in between the separate sample injections. The samples were diluted 50% (v/v) in TEAA buffer prior to HPLC experimentation. Each sample was filtered using a 0.45 µm PTFE syringe filter.

2.3.2.6 RP-HPLC standards preparation and calibration curve.

In order to validate the HPLC method, a calibration curve was generated using four concentration values of the starting material (5'phosphoryl ssDNA) in triplicates. 0.4 mg of 5' phosphoryl ssDNA as received was dissolved in 1 mL of TEAA buffer, and was used as the stock solution, from which the successive aliquots were used for the standards preparation. The dilutions yielded 0.57 mg, 0.285 mg, 0.1425 and 0.07125 mg/mL standard solutions respectively. Each level of concentration was run in triplicates to obtain a total of 12 determinations in the specified range. The precision of an analytical procedure entails the closeness of agreement between a series of measurements obtained by multiple sampling of a homogenous sample. This was assessed by the coefficient of variation (%CV) which was calculated by the following equation: %CV = (standard deviation of the triplicates/mean) ×100. The accuracy of the method was assessed by the %bias

from the theoretical concentration, which was calculated by the following equation: %bias= [(observed concentration – nominal concentration)/nominal concentration] ×100.

Linearity is the procedure's ability to obtain test results which are directly proportional to the concentration of the standard (5' phosphoryl ssDNA), and was assessed by fitting the data into a linear regression numerical model. The limit of detection (LOD) of a method is the lowest amount of analyte which can be detected by the method reliably, and was calculated according to the following equation: LOD = (3.3 × σ)/slope. Limit of quantitation (LOQ) is the lowest amount of analyte which can be quantitatively determined with suitable precision and accuracy, and was determined by the following equation: LOQ = (10 × σ)/slope. In both the LOD and LOQ equations, slope = slope of the average regression line. σ is the standard deviation of the y-intercepts of the three separate regression lines. Linearity, LOD, and LOQ were assessed according to the ICH Harmonized Tripartite Guidelines.

2.3.2.7 RP-HPLC product collection and purification.

Baseline separation was obtained allowing fractions corresponding to the conjugate to be collected. The collected fractions were left open overnight in the fume hood to evaporate the organics. The sample was then subjected to dialysis against deionized water for 2 hrs using 2000 MWCO dialysis tubes. Prior to usage, dialysis tubes were prewashed in deionized water thoroughly to remove any glycerin percent in the membranes. The recovered samples were freeze dried at -80 °C overnight and lyophilized the next day, and the conjugate masses were characterized on MALDI-TOF. The percentage yield of the conjugate is reported as; [ssDNA conjugate product (mg)/starting ssDNA (mg)] ×100.

2.4 Results and Discussion

2.4.1 Phosphoramidated ssDNA conjugate analysis; MALDI-TOF.

Conjugates formed via the conventional EDC, and the EDC/Im reaction mechanisms were characterized by MALDI-TOF. The expected conjugate molecular weight of 3758 Da was calculated by adding the individual molecular weights of ssDNA and EDA, and subtracting 17 Da to account for the loss of an -OH during conjugation. Fig.12 illustrates that the observed phosphoramidated ssDNA conjugate molecular weight was 3758.5±3.6 Da for the EDC/Im

mechanism (n=14) and 3758.4±3.6 for the EDC mechanism (n=7). The MALDI-TOF spectra of the starting material, and the conjugates are illustrated in Fig. 4a and 4b respectively. The average differences between the expected and observed conjugate molecular weights via the EDC/Im and EDC reaction mechanisms were 1.2 Da and 3.3 Da respectively, indicating successful conjugation.

Table 2: The calculated and experimentally observed molecular weights of bioconjugates.

Reactant or product	Average molecular weight (Da)	
	EDC/Im	EDC
12 bp ssDNA (reactant)	3714.9 ± 3.1	3714.4 ± 3.1
Expected conjugate (product)	3757.9 ± 3.1	3757.4 ± 3.1
Observed conjugate (product)	3758.5 ± 3.6	3758.4 ± 3.6
Reactant/product	Av. molecular weight of conjugate (Da), EDC/Im	
15 bp ssDNA	4660.1	
Expected conjugate	4703.1± 4.3	
Observed conjugate	4709.7± 3.5	

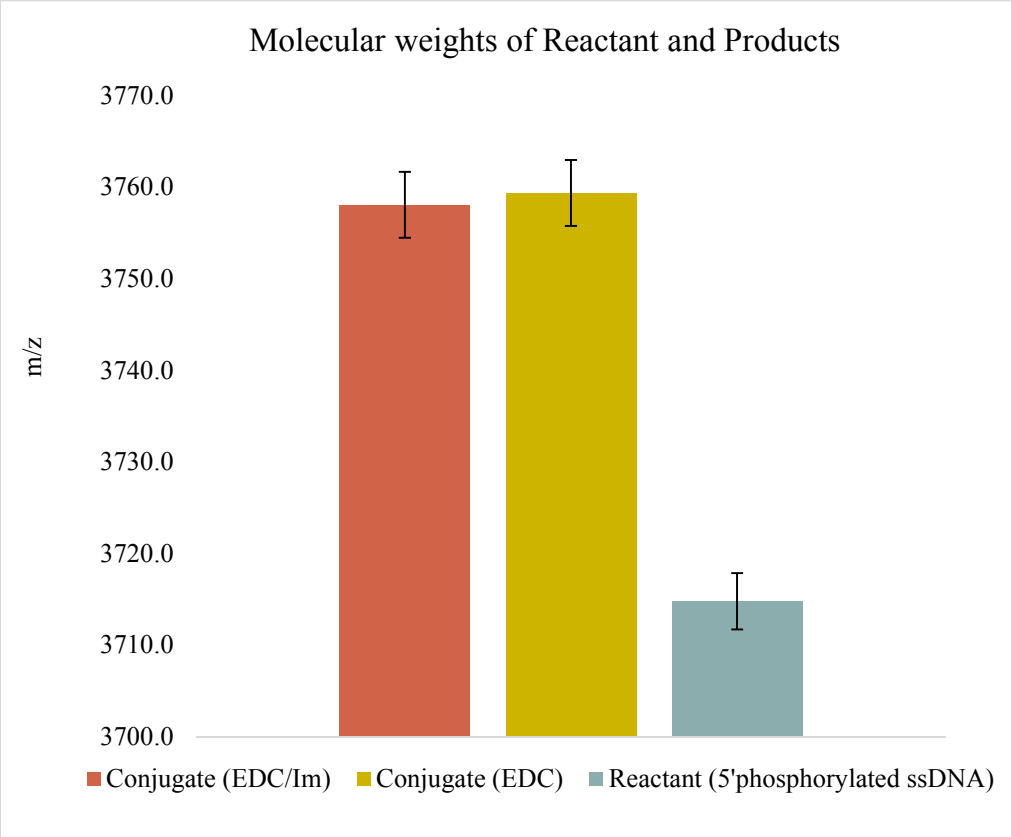

Figure 12: The observed molecular weights of the reactant, and conjugates. Error bars are represented by ±SD

The EDC/Im reaction scheme was also tested using 15 bp 5' phosphoryl ssDNA, and MALDI-TOF results indicated successful and repeatable phosphoramidation of 15 bp ssDNA (n=5). The expected molecular weight was 4703.1 ± 4.3, and the observed conjugate molecular weight was 4709.7±3.5 Da (Fig.13c, and Table 2). Given the high mass accuracy of the MALDI-TOF instrument (approx. ±3 atomic mass units (amu)), the high level of agreement between the expected, and observed conjugate molecular weights allowed us to conclude that the desired conjugate was produced. Fig.3b illustrates the MALDI-TOF mass spectra of ethylenediamine (EDA) dissolved in imidazole (Im) at a final concentration of 0.25 M. The major peak at 61 is that of EDA, while the major peak at 69 m/z is due to imidazole. The peaks at 212 and 379 are the matrices used during MALDI-TOF analysis sample preparation (i.e., α-Cyano-4-hydroxycinnamic acid).

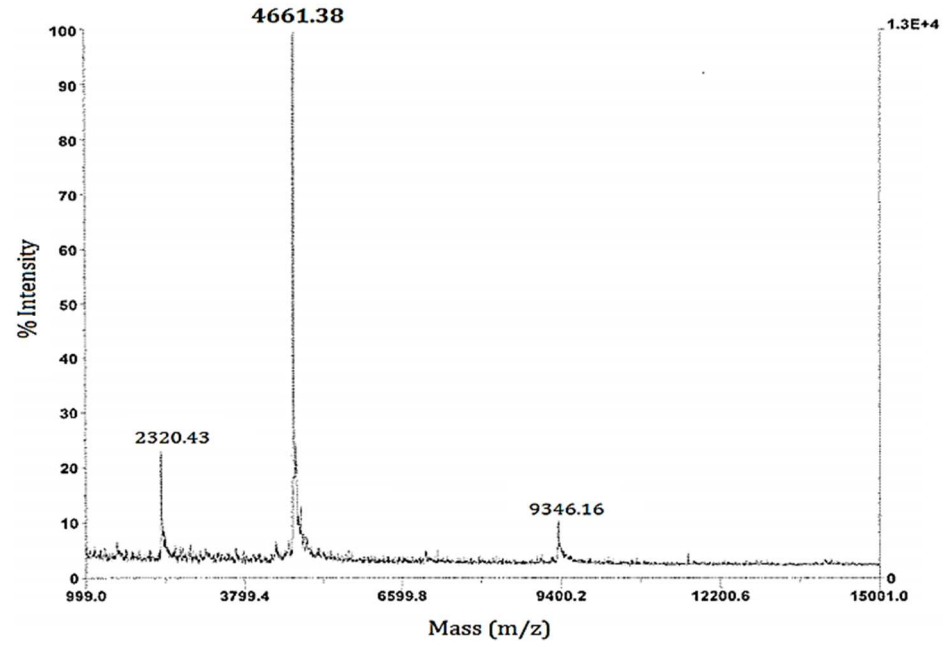

(a)

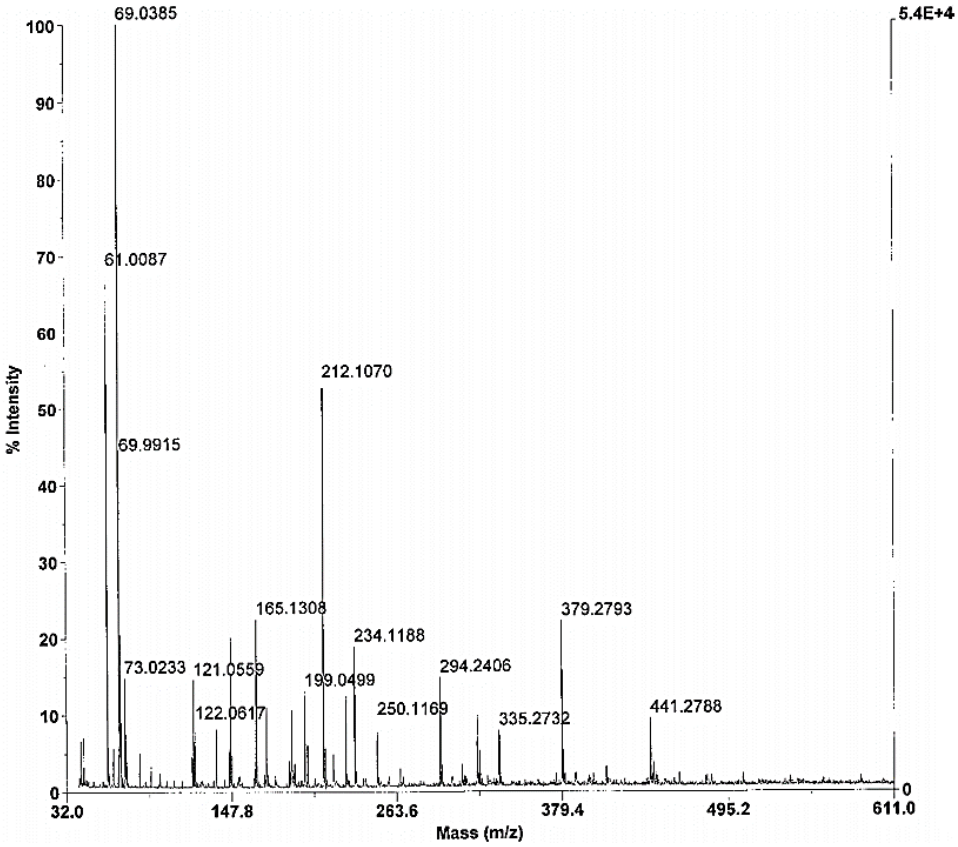

(b)

Figure 13: MALDI-TOF spectra of; 15 bp ssDNA (a), ethylenediamine, and imidazole (b), the phosphoramidated 15 bp ssDNA bioconjugate product after 7 days (c).

Figure 13 continued.

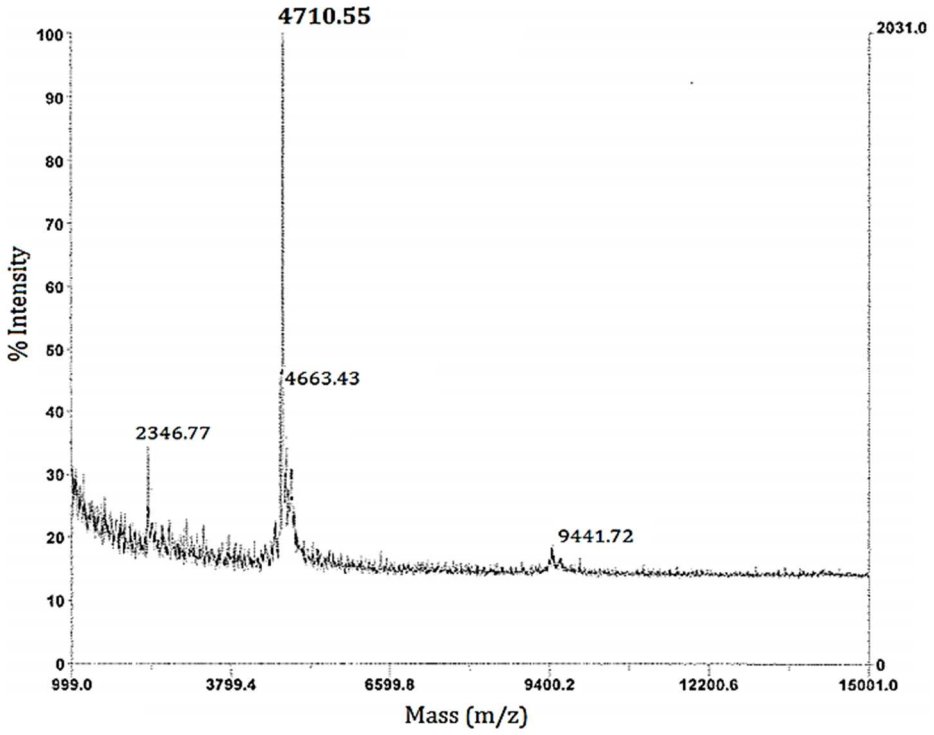

(c)

2.4.2 Stability of bioconjugate products.

MALDI-TOF indicated that a phosphoramidated conjugate is present, and it would have prolonged usage (n=5). The conjugate signal at 3758 m/z is observed upon storage at -20 °C (Fig.14 b,c,d). The major peak corresponding to the phosphoramidated ssDNA conjugate is still present even after 14 days, indicating that the product remains intact. As covalent bonds are stronger, these MALDI-TOF results suggest that the formed phosphoramidated ssDNA conjugate product consists of a stable covalent bond, as we observed its presence after longer term storage. However, a decrease in the signal intensity (i.e., increasing noise) is observed upon storage at -20 °C. The MALDI-TOF instrument's software normalizes the entire spectrum with respect to the most intense peak in the result. If we consider the magnitude of the major peak after 7 days we recognize that the major peak is weak compared to day 1. The observation is possibly due to hydrolysis of the product. Therefore, if this conjugate product is to be utilized for further research, it is recommended that the sample is lyophilized prior to storage at -20 °C.

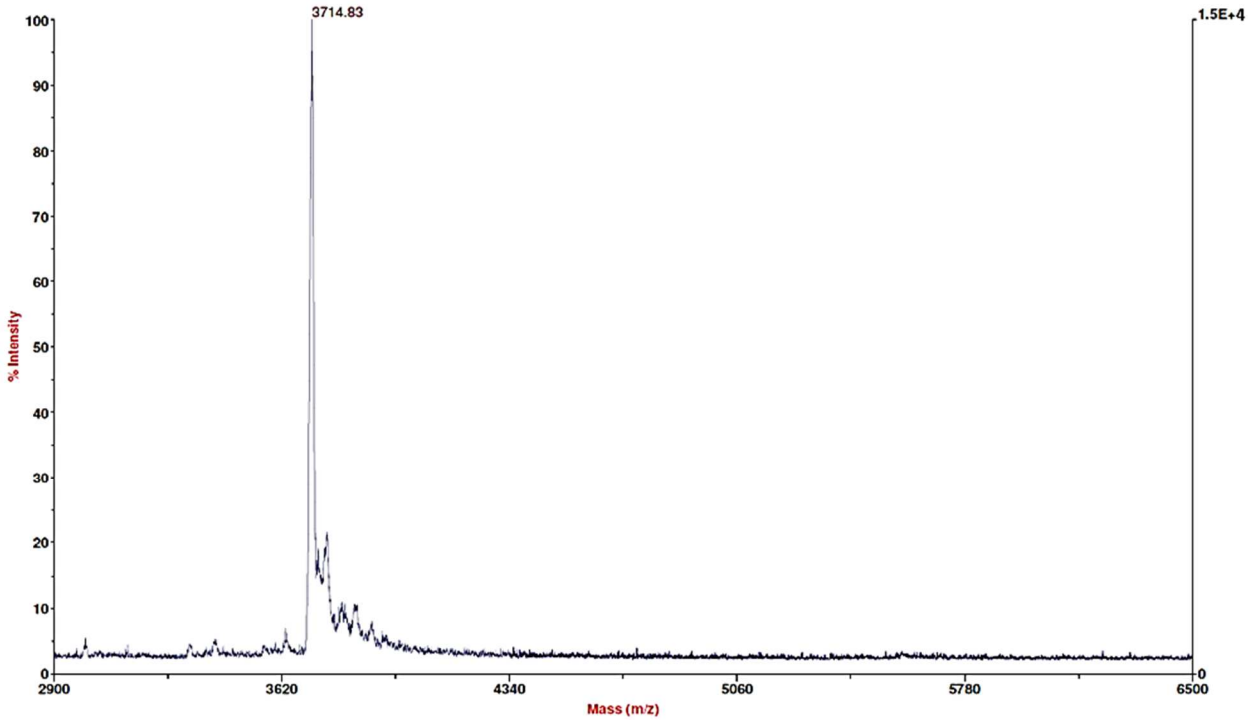

(a)

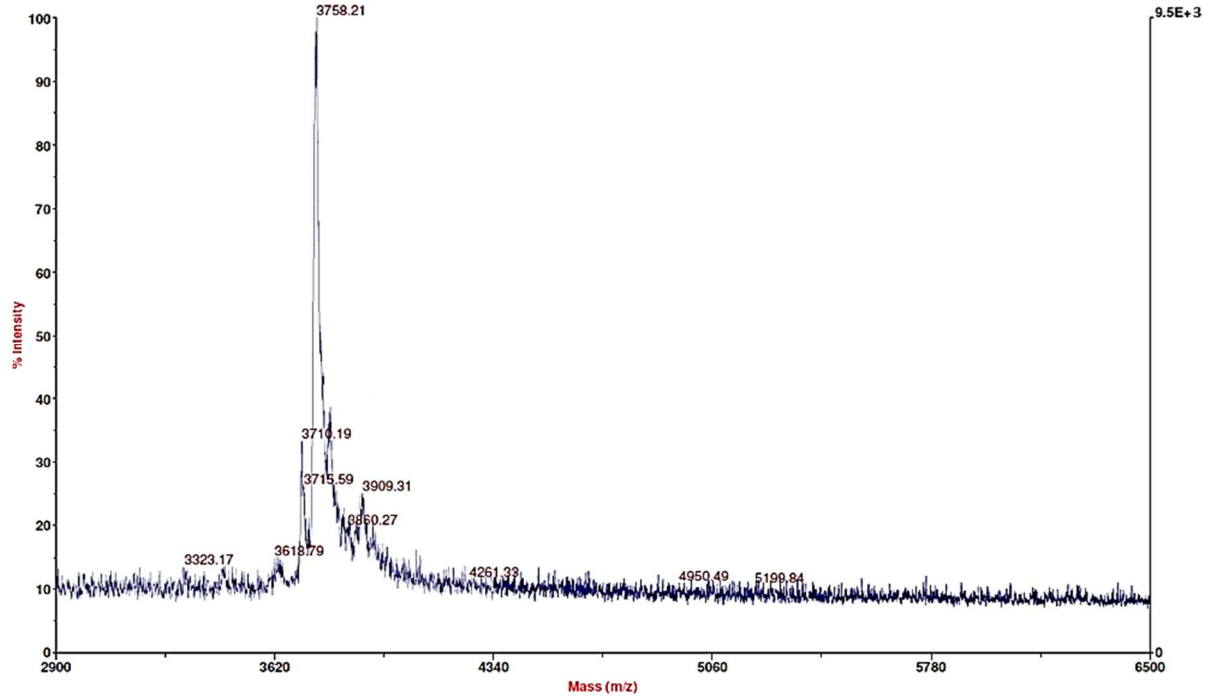

(b)

Figure 14: MALDI-TOF spectra of 12 bp ssDNA (a), the phosphoramidated conjugate on day 1 (b). The phosphoramidated conjugate after 7 days (c) and 14 days (d) upon storage at -20 °C (n=4).

Figure 14 continued

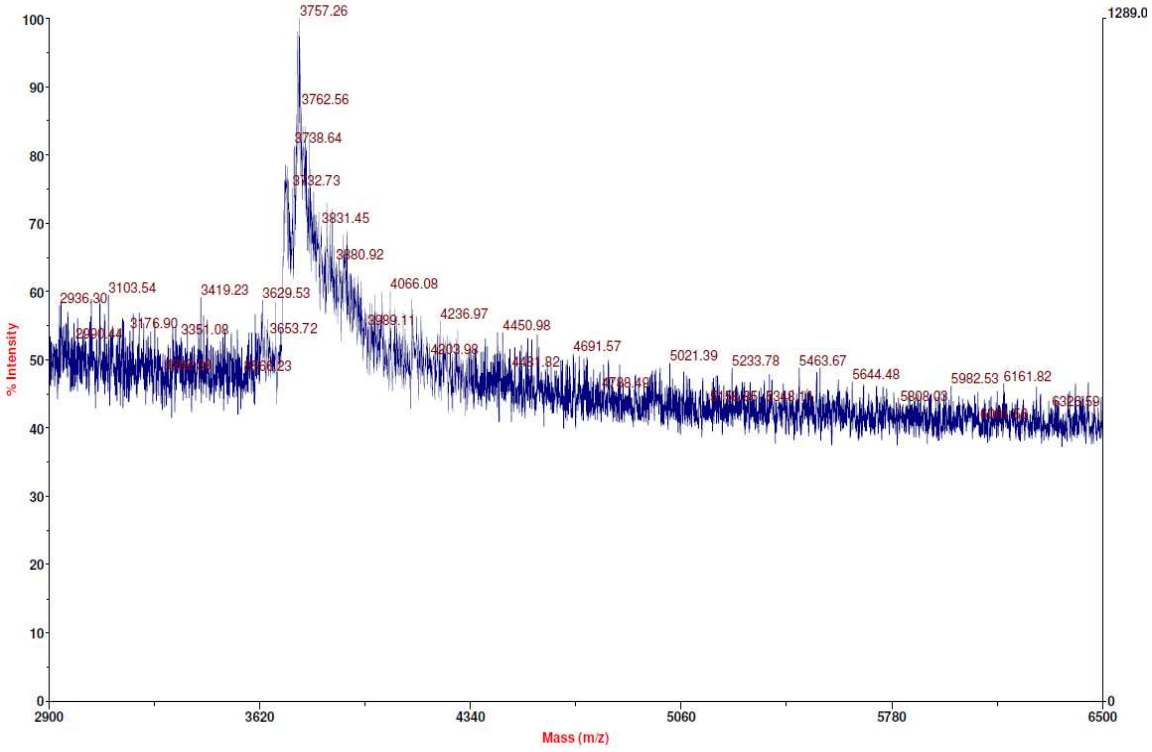

(c)

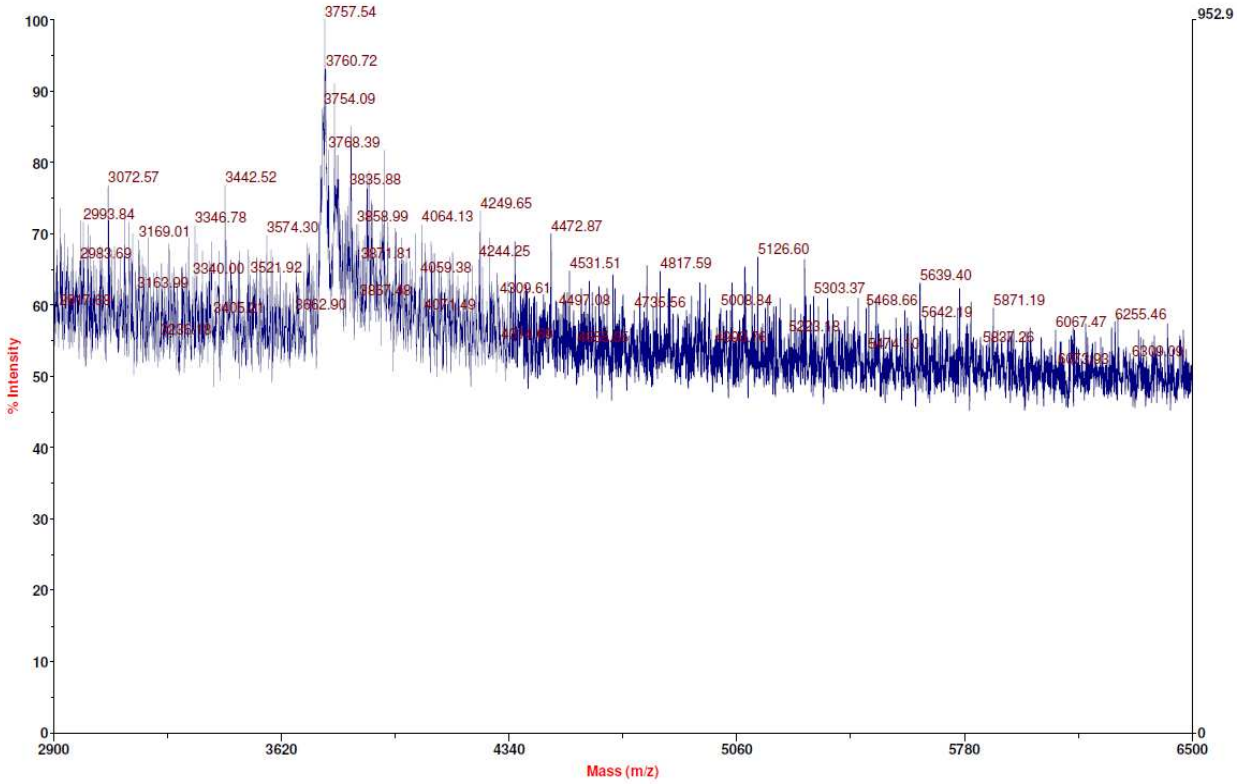

(d)

2.4.3 Phosphoramidation exclusively at 5'phosphate of ssDNA.

As suggested in previous literature, the ssDNA phosphate backbone can form adducts with EDC [77]. These adducts arise from non-covalent, electrostatic interactions between the phosphate groups and EDC. In order to investigate specific covalent bond formation at the open 5' phosphate of ssDNA, the EDC/Im reaction was conducted with nonphosphorylated ssDNA. As nonphosphorylated ssDNA lacks the open 5' phosphate group, there should not be any m/z signal owing to the expected phosphoramidated conjugate mass in MALDI results. As expected, no dominant, single peak was observed around 3758 m/z. Instead, multiple peaks were observed on MALDI, owing to adducts (Fig.15a). The spectra indicated mass additions to the starting reactant (5' phosphoryl ssDNA) ranging from 40 Da – 400 Da. This observation could be attributed to adduct formation via salt binding to the ssDNA phosphate backbone. It could also be due to temporary electrostatic interactions between the phosphate backbone of ssDNA and EDC and/or other small molecules. When MALDI runs were carried out with the same sample after 7 days of storage at -20 °C, the initially detected adduct peaks were not observed. Therefore, it was believed that none of the multiple peaks observed initially were due to stable, covalent bonds. It is validated by the observation that those signals no longer appeared on MALDI-TOF after 7 days, indicating dissociation caused by hydrolysis (Fig.15b). This indicates that the bonds formed initially were not covalent bonds. The masses greater than the starting material (<3641 Da) in here are expected to be gas phase dimerization results during MALDI-TOF analyses.

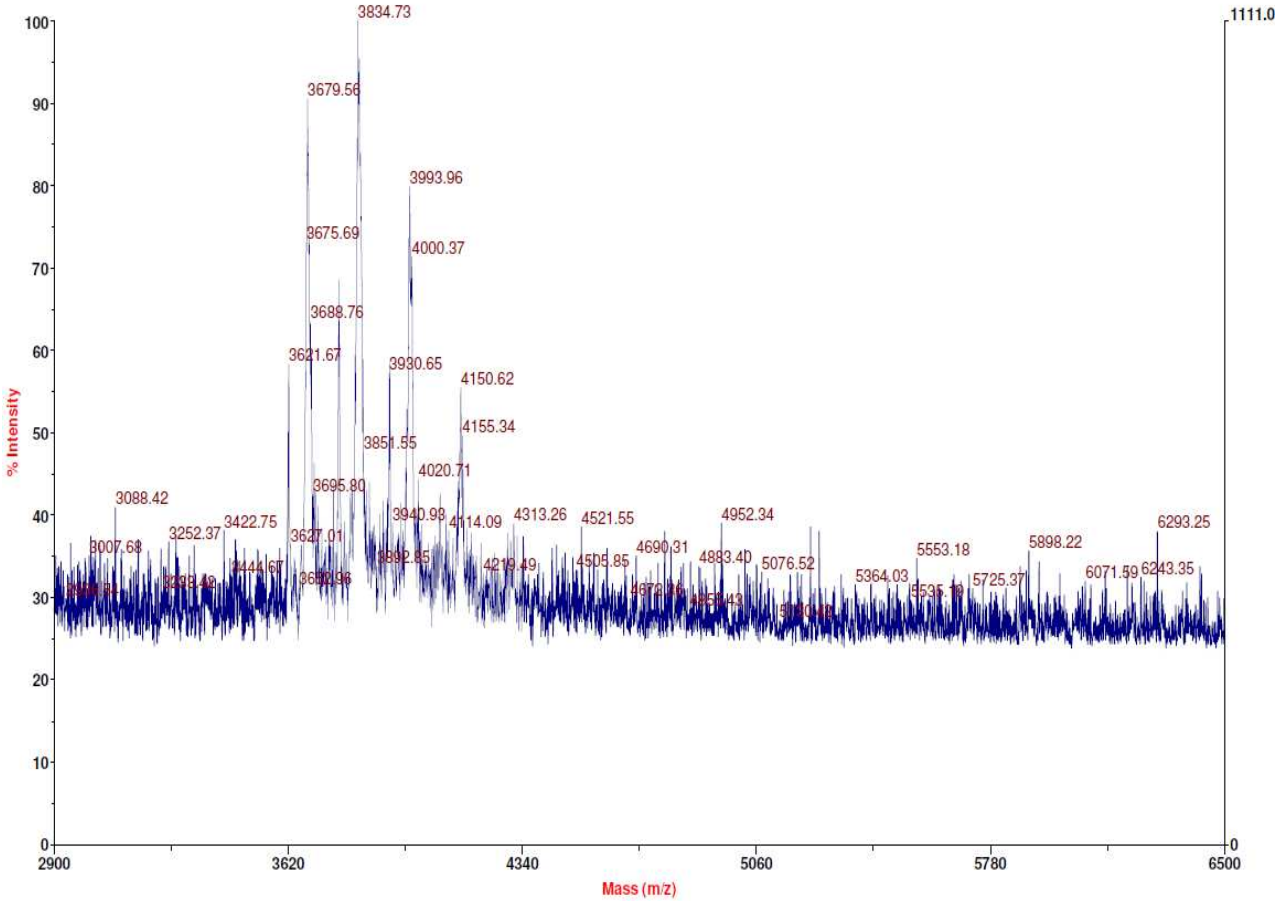

(a)

Figure 15: MALDI-TOF spectra indicating multiple peaks attributed to adduct formations (a). MALDI-TOF indicating deterioration of adducts after 7 days of storage at -20 °C (b).

Figure 15 continued

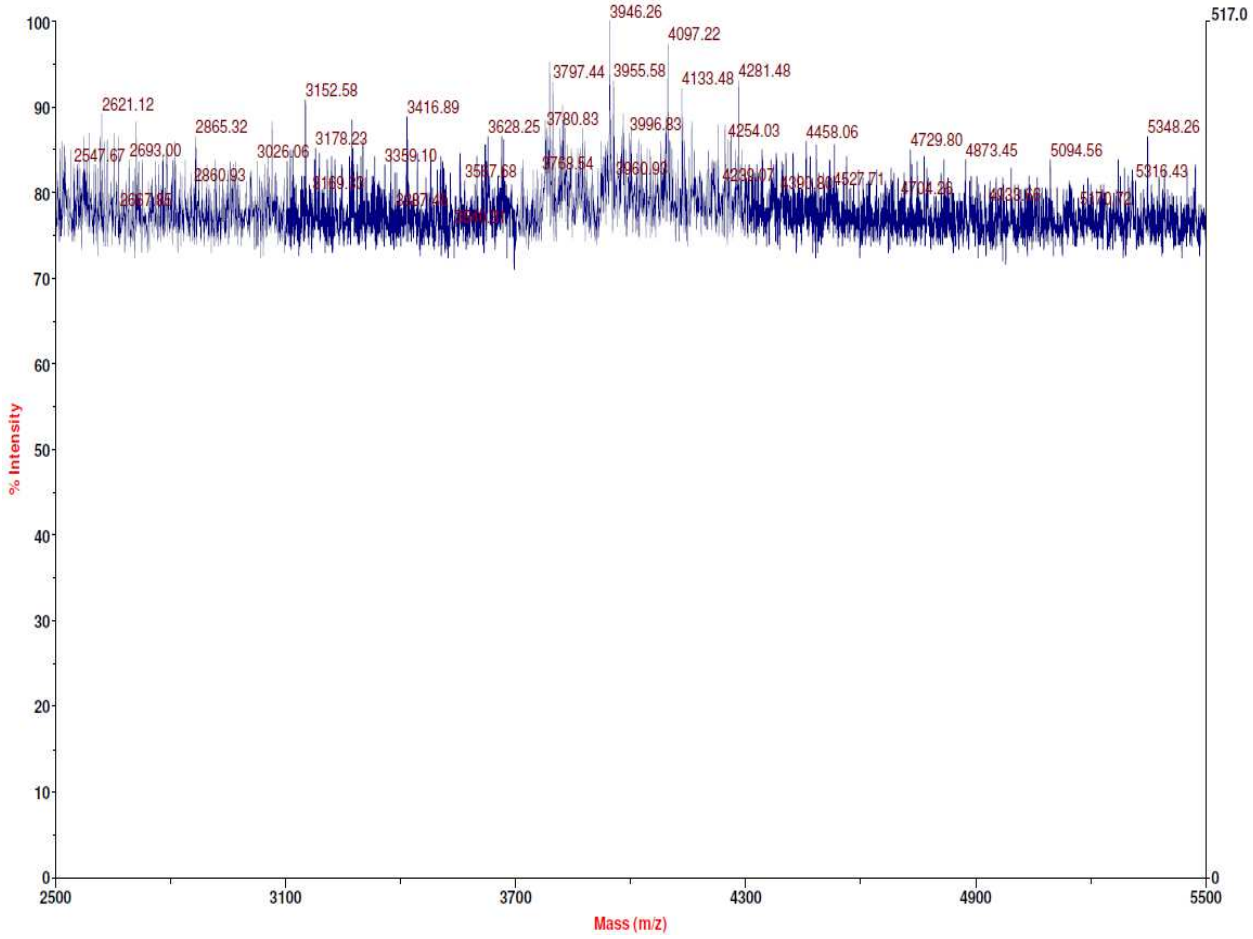

(b)

2.4.4 RP-HPLC: Method validation.

2.4.4.1 Linearity.

The calibration curve was constructed by linear regression using four 5' phosphoryl standards of known concentrations (Fig.16). The coefficient of determination (r^2) of the calibration curve was 0.9988. The linear regression equation was; y = 129,201·x + 1428205, where; y = area under the HPLC peak (µV·sec), and x = concentration of the analyte (µg/mL).

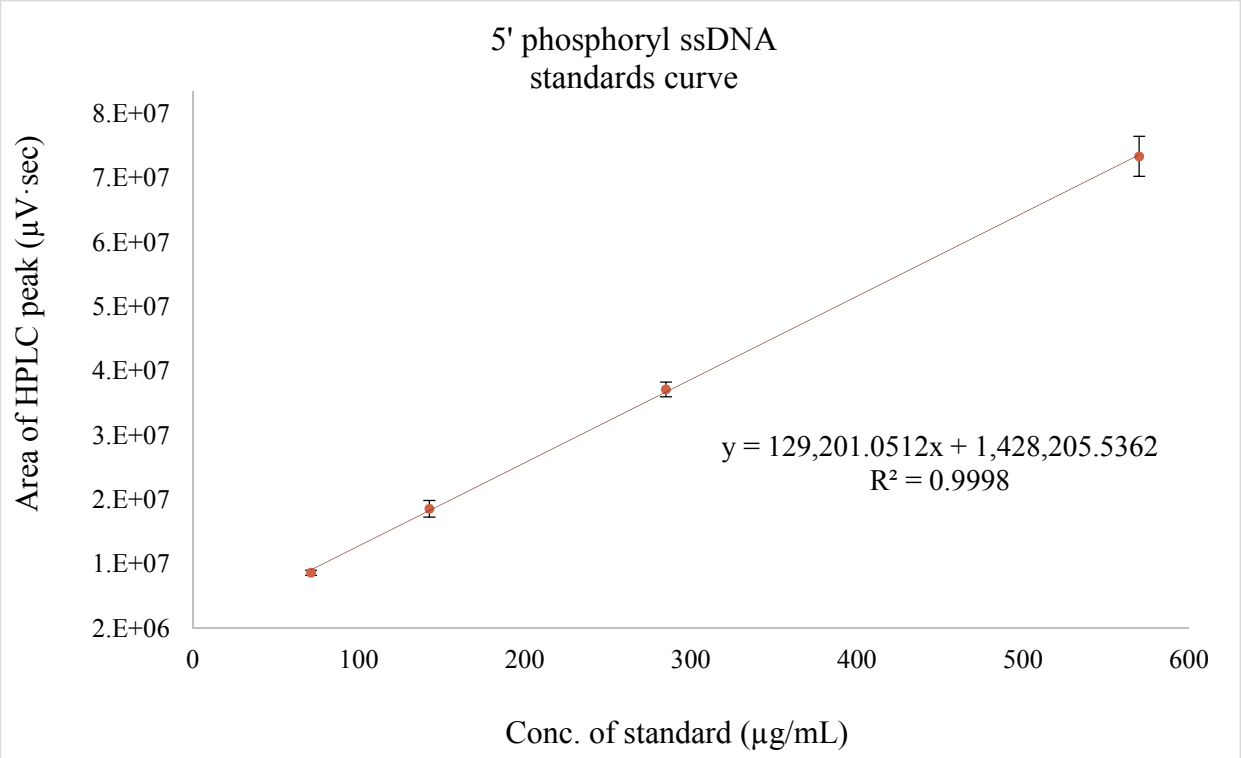

Figure 16: Standards calibration curve of 5' phosphoryl ssDNA.

Column dimensions: XTerra® MS C18 2.5 µm, 4.6 mm × 50 mm. Ion pairing reagent: 0.1 M TEAA, pH 9.70±0.05. Mobile phases: A; 5% acetonitrile in TEAA. B; 30% acetonitrile in TEAA. Gradient conditions: 90%A – 60%A in 16 min. 60% – 90% A in the next 14 min. Flowrate: 1.0 mL/min. Column and sample temperatures: 37°C, and 33°C. Injection volume: 100 µL. UV detector: 260 nm. Error bars represent ±SD of the peak areas from triplicate results.

2.4.4.2 Accuracy, precision, detection limit, and quantitation limit.

The accuracy and precision of the developed method are depicted from the %bias and the %CV respectively (Table 3). The %CV for all levels were well below 3%, and the %bias ranged from -5.1% – 1.2%. These are in agreement with a previously established acceptance criteria in a chromatographic study [80]. The detection limit (LOD) and quantitation limit (LOQ) determined as per the ICH Harmonized Tripartite Guidelines were 4.6 µg/mL and 13.9 µg/mL respectively. During product analysis later, all the detected concentrations of the phosphoramidated ssDNA conjugates were >278 µg/mL. They are well above the LOQ, and are well within the linear range of the analytical method.

Table 3: Recovery analysis and system suitability parameters – RP-HPLC.
(n=12 total determinations).

Nominal concentration (µg/mL)	Calculated concentration (µg/mL)	%Recovery	SD (±µg/mL)	%CV	%bias
570.0	568.3	99.7%	1.1	0.2%	-0.3%
285.0	288.3	100.0%	3.7	1.3%	1.2%
142.5	144.5	100.0%	3.3	2.3%	1.4%
71.3	67.6	94.9%	0.8	1.2%	-5.1%

2.4.5 RP-HPLC: Phosphoramidated ssDNA conjugate quantitation.

After assessing the developed IP-RP-HPLC method for suitability as reported above, the method was used to determine the phosphoramidated ssDNA conjugate yields obtained via the two reactions. The retention time (RT) of the reactant ssDNA was 7.5±0.2 min, while that of the ssDNA conjugate product was 6.1±0.4 min (Fig.17). The injection start point (time point zero) of both all the spectrographs illustrated here (Fig.17) were the same, as HPLC injections were performed automatically using Empower 2.0 software manager.

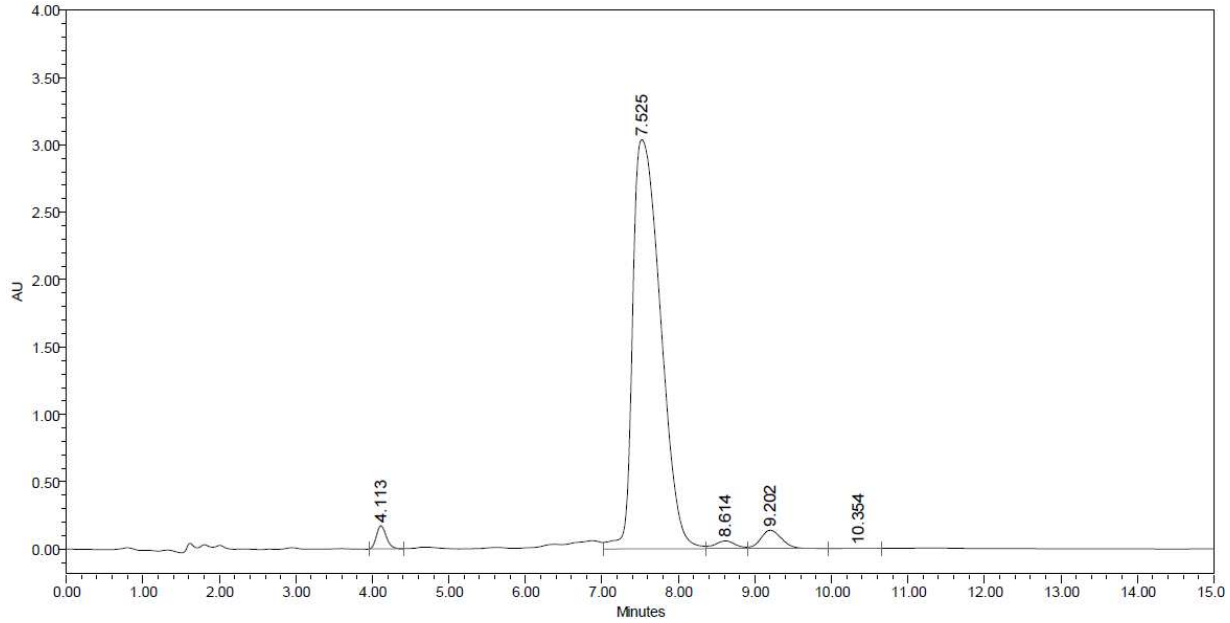

(a)

Figure 17: RP-HPLC chromatographic results of; The reactant phosphoryl ssDNA (a), the ssDNA bioconjugate product obtained via EDC/Im crosslinking method (b), the ssDNA bioconjugate obtained via EDC crosslinking method (c).

Column dimensions: XTerra® MS C18 2.5 µm, 4.6 mm × 50 mm. Ion pairing reagent: 0.1 M TEAA, pH 9.70±0.05. Mobile phases: A; 5% acetonitrile in TEAA. B; 30% acetonitrile in TEAA. Gradient conditions: 90%A – 60%A in 16 min. 60% – 90% A in the next 14 min. Flowrate: 1.0 mL/min. Column and sample temperatures: 37°C, and 33°C. Injection volume: 100 µL. UV detector: 260 nm. Error bars represent ±1 SD of the peak areas from triplicate results.

Figure 17 continued

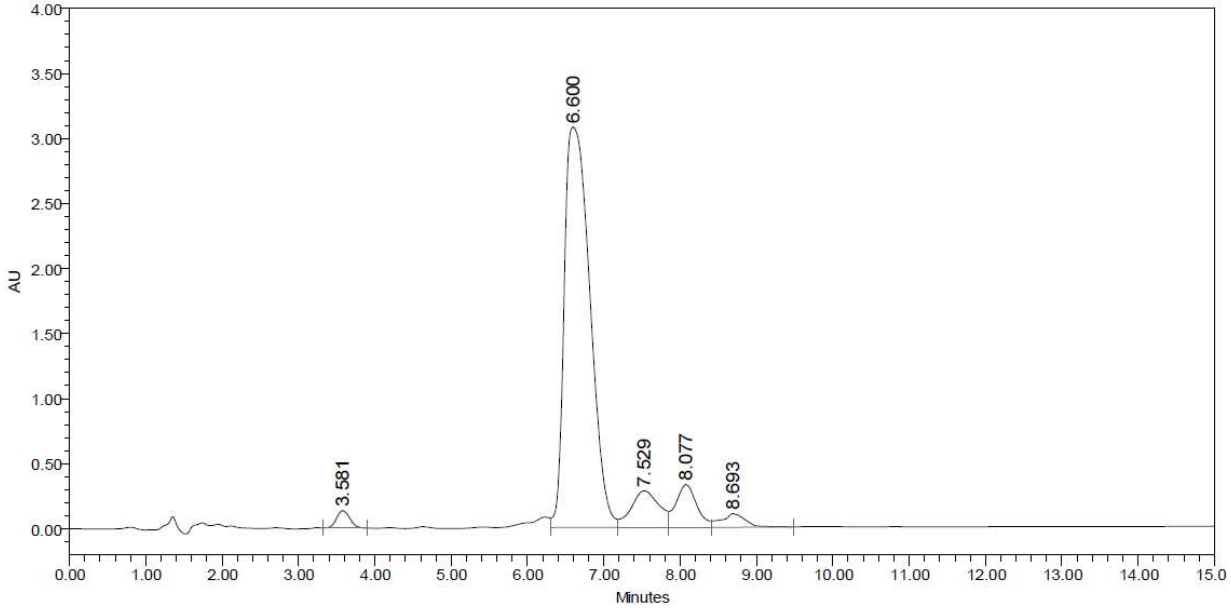

	Retention Time (min)	Area (uV*sec)	% Area	Height (uV)
1	3.581	1606739	1.8	132333
2	**6.6**	**71963620**	80.52	3077231
3	7.529	7142598	7.99	281191
4	8.077	6222254	6.96	328658
5	8.693	2298811	2.57	104925
6	9.832	137567	0.15	4774

(b)

Figure 17 continued.

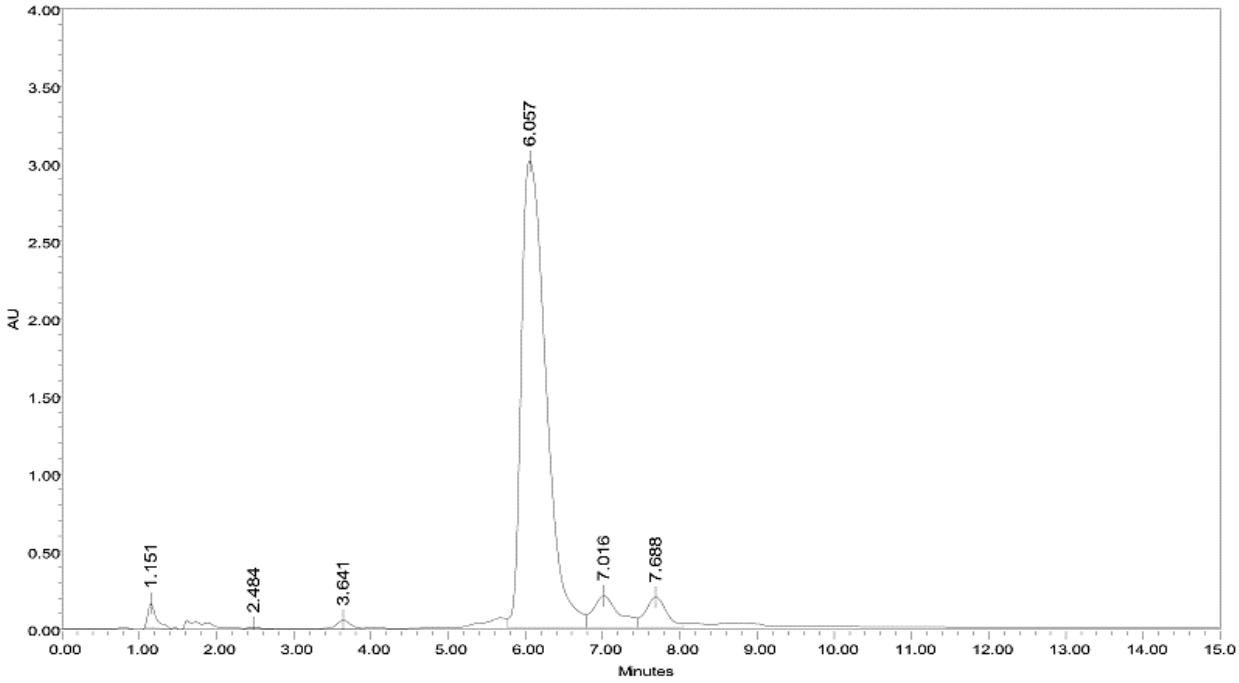

	Retention Time (min)	Area (uV*sec)	% Area	Height (uV)
1	1.151	1198776	1.55	157210
2	2.484	73618	0.1	7321
3	3.641	633906	0.82	53564
4	**6.057**	**66809570**	86.59	3015400
5	7.016	4766895	6.18	206117
6	7.688	3674803	4.76	196435

(c)

In order to calculate the amount of the bioconjugate product, the area underneath the major peak of the chromatograph was determined. Table 4 below illustrates raw HPLC peak area results obtained from bioconjugates formed via 12 independent crosslinking experiments.

Table 4: Compiled RP-HPLC results of the bioconjugate yields obtained via EDC/Im and EDC.

Replicate	Peak area (μV·sec)		Retention time. RT (min)	
	EDC/Im	EDC	EDC/Im	EDC
1	38886088	37441551	4.060	4.063
2	63556749	55672533	5.867	5.908
3	52793686	50537668	6.067	5.939
4	46294376	38590979	6.501	6.452
5	78428352	66809570	6.737	6.057
6	67143992	55344993	5.786	5.626

A Tukey's boxplot was used to determine the data outliers based on the peak area as well as the RT. The 25th percentile (Q1), and the 75th percentile (Q3), as well as the inter-quartile range (IQR) were determined. IQR is simply Q3 – Q1. Next, the lower bound was calculated using the equation; Q1– (1.5×IQR), and the upper bound was calculated using the equation; Q3+(1.5·IQR). Any data point beyond these two values were considered too far out, and hence were eliminated from the proceeding calculations. Like so, replicate 1 was eliminated from product yield calculations, as well as the Student's t-test.

Afterwards, using the area underneath the bioconjugate curve, and the standards calibration regression equation, the 'detected product concentration; was determined. Next, the injection volume, and the starting sample volume was used to calculate the 'detected amount (mg)' of the product. The division of the 'detected amount (mg)' and the 'reacted amount (mg)' yielded the conversion efficiency, i.e., product yield (Fig.18).

Standards Calibration Curve

slope =	129201.05
intercept =	1428205.54

$$x = \frac{y - intercept}{slope}$$

$$\text{concentration} = \frac{peak\ area - intercept}{slope}$$

Bioconjugate Product (i.e., Phosphoramidated ssDNA)

	Peak area (uV*sec)	Detected conc. (ug/mL)	Detected amount (mg)	*Conversion efficiency*
With Im	38886088	289.92	0.029	71.00%
	63556749	480.87	0.048	78.83%
	52793686	397.56	0.040	75.01%
	46294376	347.26	0.035	80.14%
	78428352	595.97	0.060	80.11%
	67143992	508.63	0.051	80.92%
			average =	**79.0%**
			SD =	**2.4%**
			%CV =	**3.0%**
W/O Im	37441551	278.74	0.028	68.26%
	55672533	419.84	0.042	68.83%
	50537668	380.10	0.038	71.72%
	38590979	287.64	0.029	66.38%
	66809570	506.04	0.051	68.03%
	55344993	417.31	0.042	66.39%
			average =	**68.3%**
			SD =	**2.2%**
			%CV =	**3.2%**

Figure 18: Calculations performed to determine the bioconjugate product yield.

Fig.19 illustrates the product yields obtained via the two separate reaction schemes investigated. Results showed that by following the EDC/Im reaction, the percent yield of the conjugate product increased by approx. 10%. The phosphoramidated ssDNA conjugate percent yield via the EDC/Im reaction method was 79.0±2.4% while that of the EDC reaction method alone was 68.3±2.2% (Fig.19).

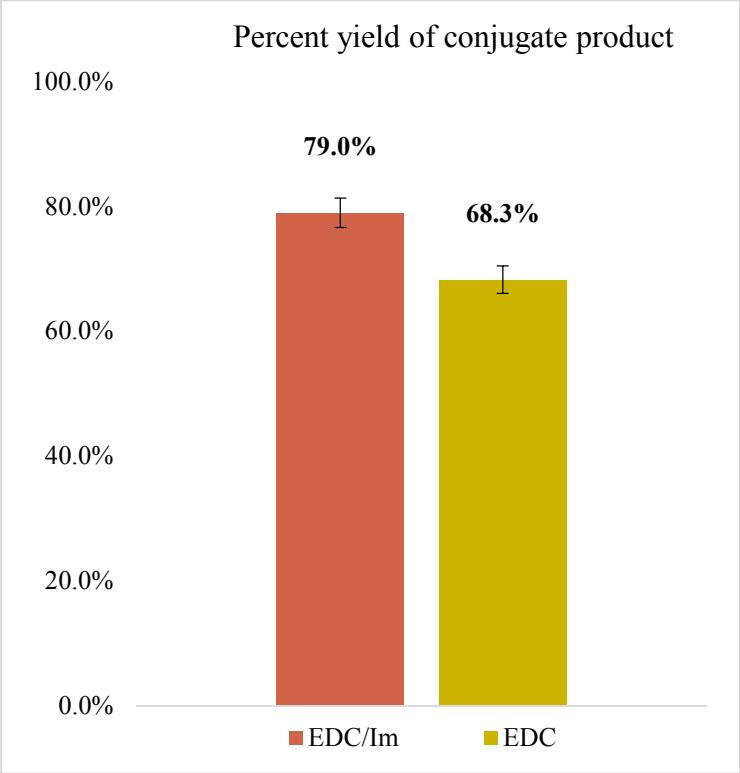

Figure 19: Percent yield of the phosphoramidated ssDNA conjugate obtained by following the conventional EDC scheme, and the modified EDC/Im strategy.

Error bars represent ±SD of the detected product concentrations from n=5 independent runs per reaction scheme.

An unpaired, two-tailed, Student's t-test indicated that there is a statistically significant difference between the product yields obtained via EDC/Im, and EDC reaction schemes (Fig.20).

t-Test: Two-Sample Assuming Equal Variances

	EDC/Im	*EDC*
Mean	**79.0%**	**68.3%**
Variance	0.0005537	0.0004842
Observations	5	5
Pooled Variance	0.000519	
Hypothesized Mean Difference	0	
df	8	
t Stat	7.4506641	
P(T<=t) one-tail	3.63E-05	
t Critical one-tail	1.859548	
P(T<=t) two-tail	**7.26E-05**	
t Critical two-tail	2.3060041	

Figure 20: Comparison of the product yield obtained via EDC vs. EDC/Im methods.

2.4.6 Molecular weight analysis of HPLC fractions.

In order to determine the molecular composition of the three dominant HPLC peaks, the corresponding HPLC fractions were collected as illustrated in Fig.21. Next, they were analyzed via MALDI-TOF. Results of the major peak (Fig.21, peak #1) indicated 3764.2±4.2 Da (Fig.22a). The fractions of one minor peak (Fig.21, peak #2) showed 3720.9±0.7 Da (Fig.22b), while the other minor peak (Fig.21, peak #3) resulted in 3874.6±1.8 Da (Fig.22c). Peak #1 is attributed to the product conjugate while peak #2 is attributed to unreacted starting material, 5'phosphoryl ssDNA, as the theoretical molecular weights agree with the observed molecular weights.

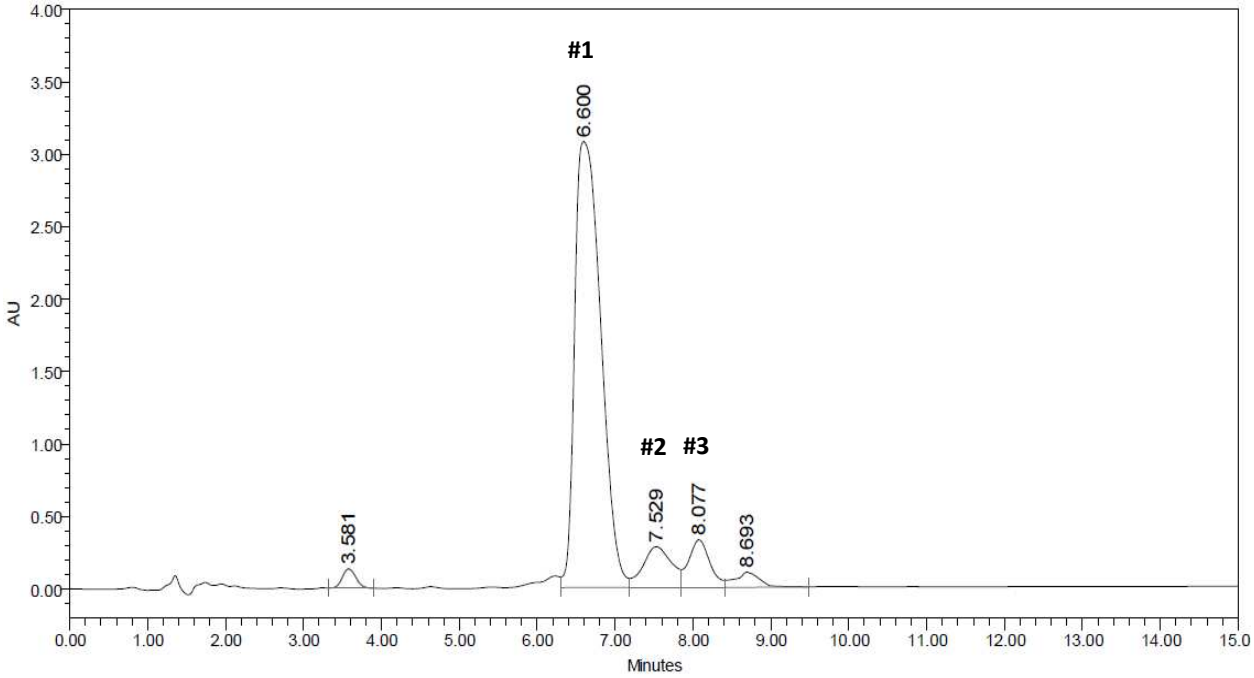

Figure 21: Chromatograph of the phosphoramidated ssDNA conjugate illustrating each peak collected for molecular weight analysis.

The fractions were collected for validation of the species in the major peak (#1) as well as the minor peaks (#2, #3).

Column dimensions: XTerra® MS C18 2.5 µm, 4.6 mm × 50 mm. Ion pairing reagent: 0.1 M TEAA, pH 9.70±0.05. Mobile phases: A; 5% acetonitrile in TEAA. B; 30% acetonitrile in TEAA. Gradient conditions: 90%A – 60%A in 16 min. 60% – 90% A in the next 14 min. Flowrate: 1.0 mL/min. Column and sample temperatures: 37°C, and 33°C. Injection volume: 100 µL. UV detector: 260 nm. Error bars represent ±1 SD of the peak areas from triplicate results.

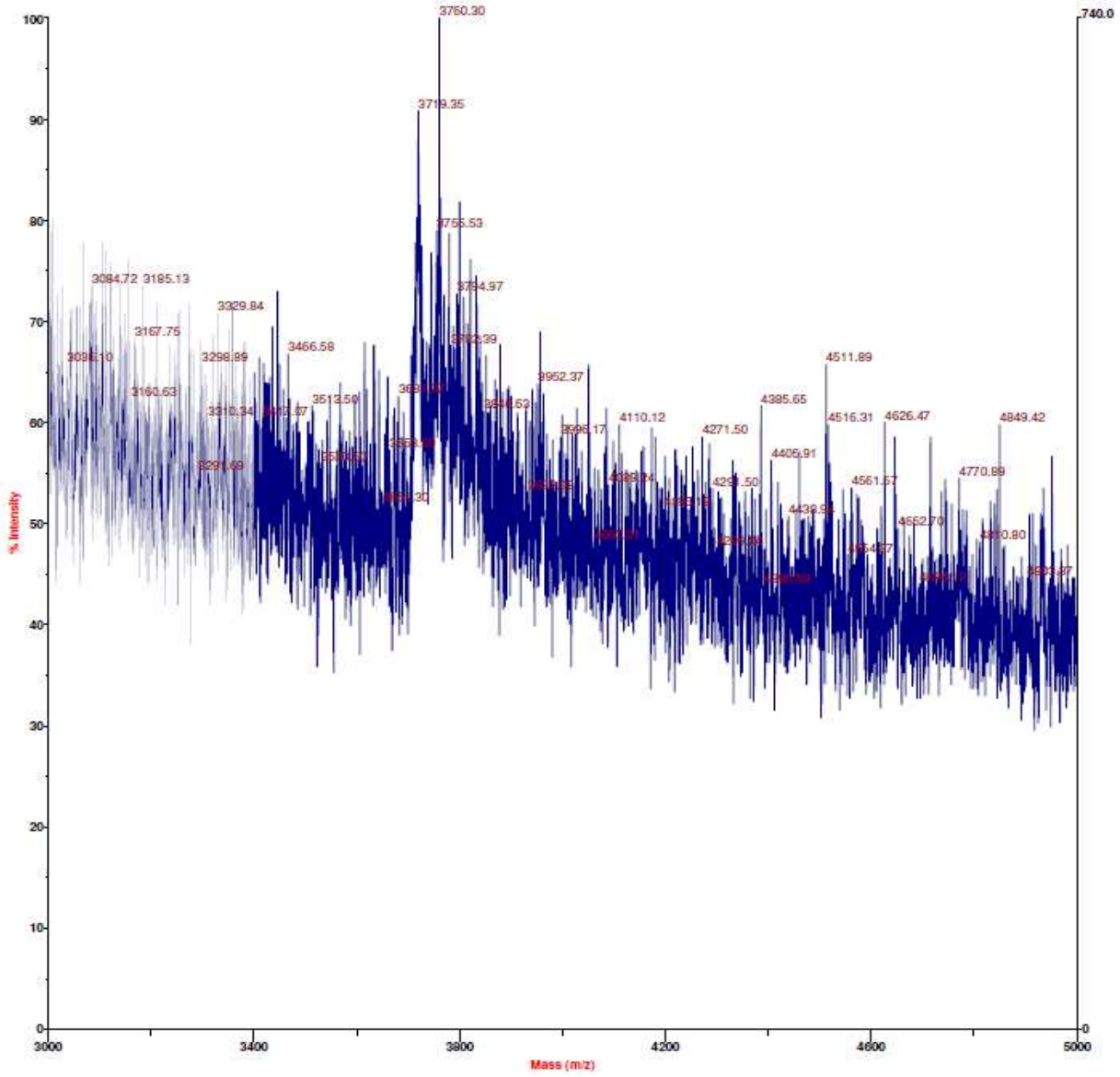

(a)

Figure 22: MALDI-TOF spectra illustrating the m/z values of the HPLC peaks (a) peak #1–phosphoramidated ssDNA. (b) peak #2–unreacted starting ssDNA. (c) peak #3–isourea intermediate derivative

(n=3).

Figure 22 continued

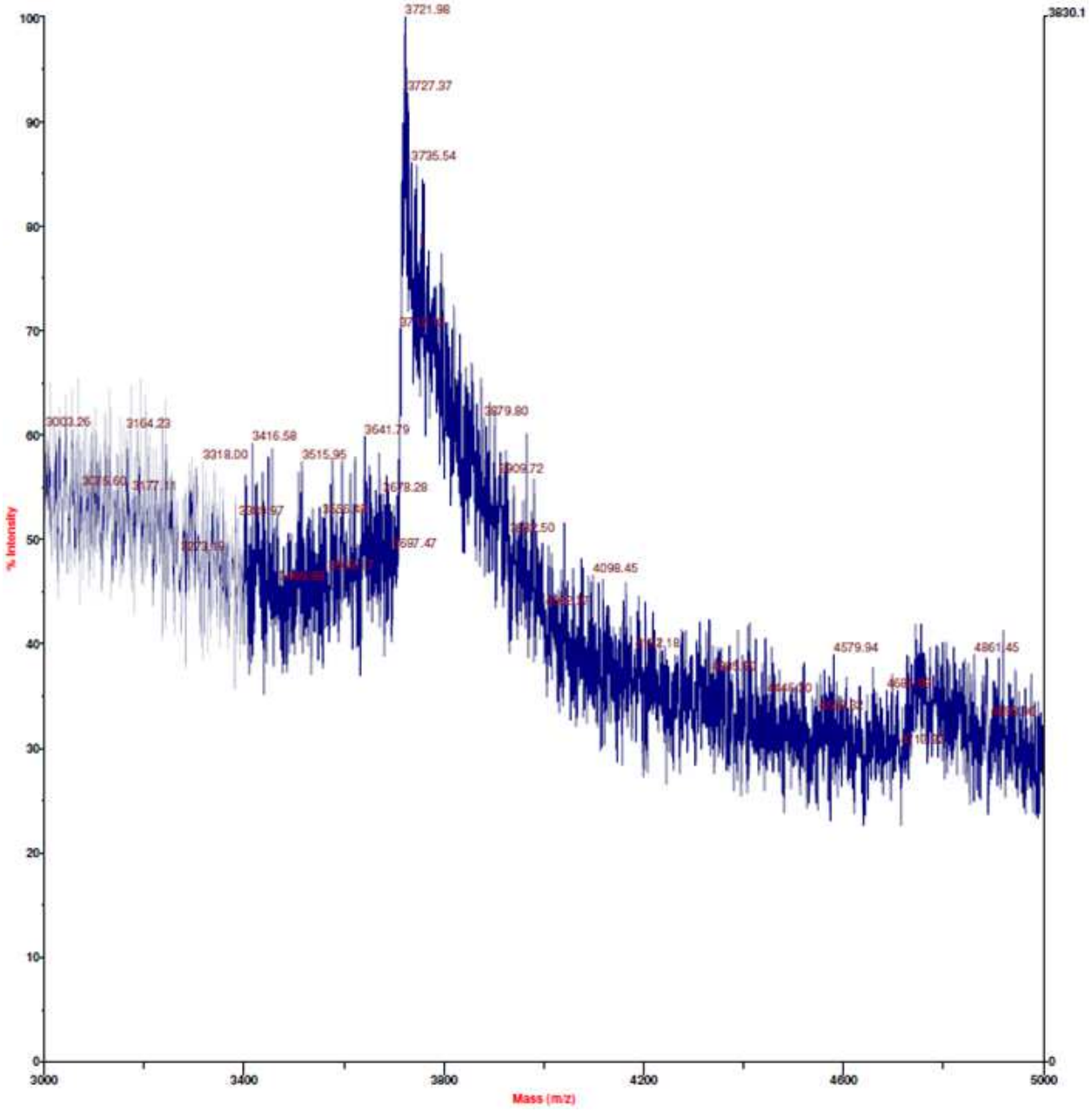

(b)

Figure 22 continued

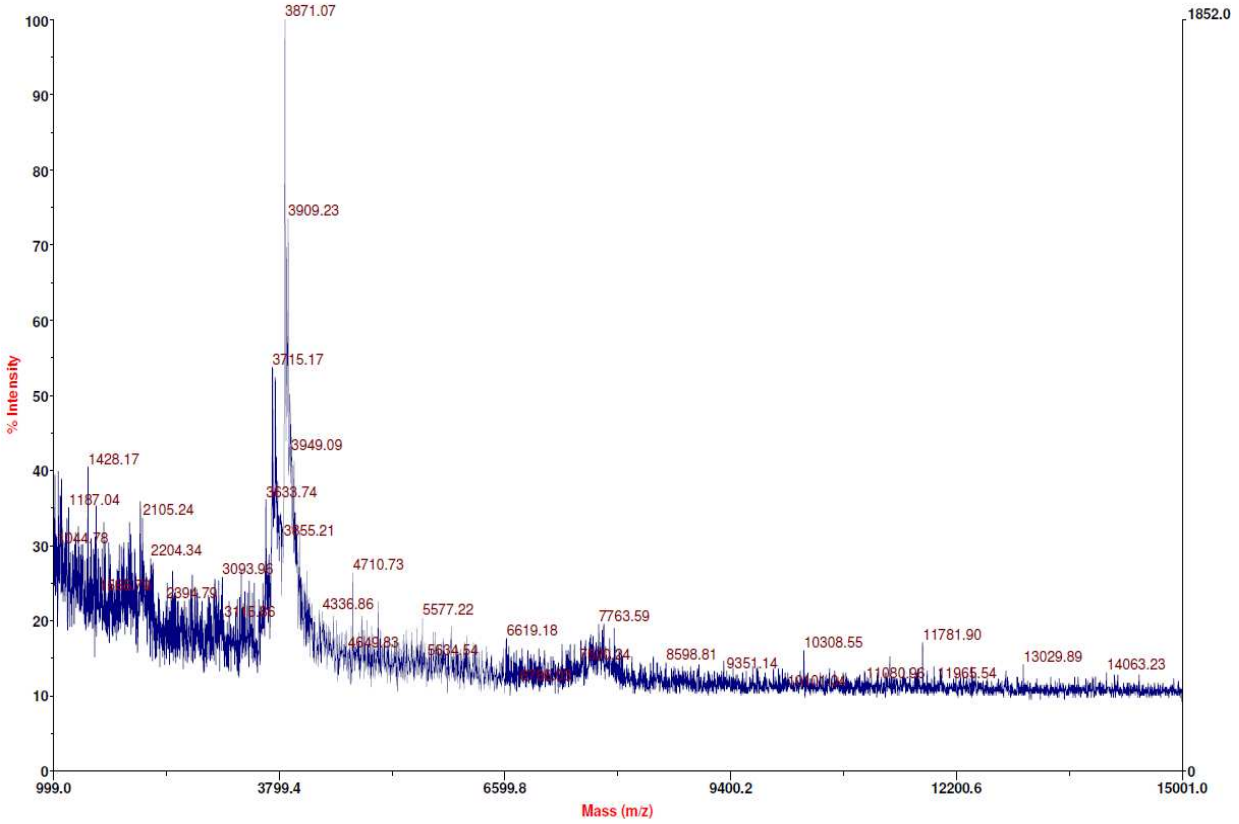

(c)

In order to determine possible molecular structures of the compound present in peak #3, (RT ~ 8.0 min), attention was directed to the byproducts possible from EDC side reactions. Previous researchers have speculated that, in the presence of excess EDC, O-acylisourea intermediate could react with the neighboring amine in EDC, forming N-acylisourea [2]. The theoretical molecular weight of both O-acyl isourea and N-acyl isourea derivatives are 3871 Da (Fig.23). MALDI-TOF experimental evidence suggests that molecular composition of the compounds in HPLC peak #3 could be an acylisourea derivative (Fig.22c).

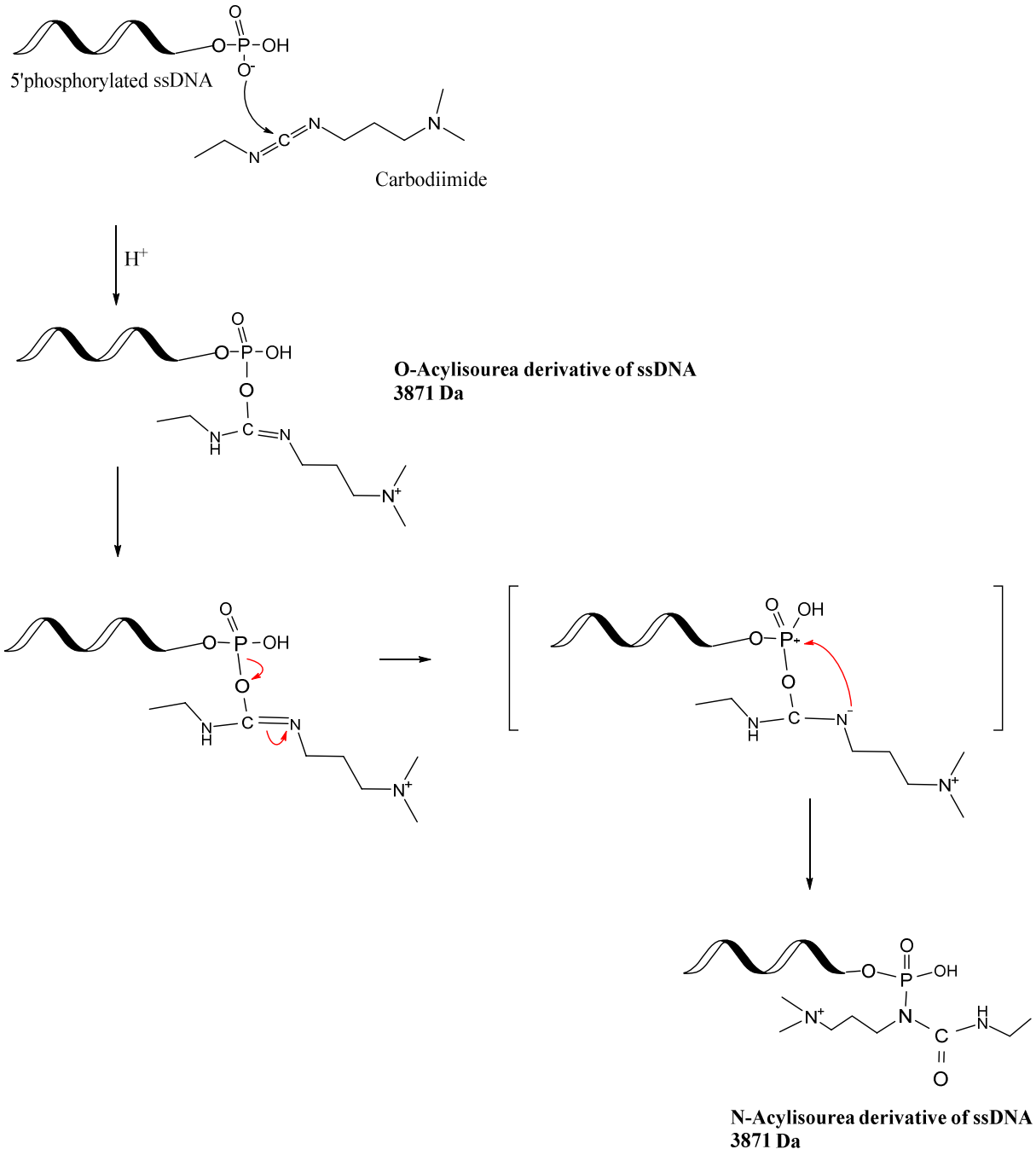

Figure 23: Reaction mechanism deduced for a possible EDC side reaction.
– modified from [1].

2.5 Conclusions

A novel phosphoramidated ssDNA was synthesized as a proof-of-concept modality to compare the conventional carbodiimide (EDC) reaction with an adapted strategy using EDC and

imidazole (EDC/Im). MALDI-TOF results indicated that a stable conjugate with the expected molecular weight is formed. The EDC/Im reaction method was compared to the conventional EDC reaction method in relation to reaction efficiencies. A RP-HPLC chromatographic analytical method was developed to determine the product yields. This method could also be used to purify other aminated and phosphorylated DNA compounds. The phosphoramidated ssDNA conjugate obtained from the EDC/Im method had a percentage yield of 79.0±2.4% while that of the conventional EDC method was 68.3%±2.2%. The improved EDC/Im method is applicable to synthesizing programmable DNA moieties, and constructing self-assembling macromolecules where there is a lack of experimental flexibility in adjusting reaction conditions.

CHAPTER 3. CONJUGATING SSDNA AND PEPTIDES VIA HOMOBIFUNCTIONAL AND HETEROBIFUNCTIONAL CROSSLINKERS

3.1 Abstract

This chapter discusses the preliminary results from the attempts to crosslink peptides to single stranded DNA (ssDNA). Results from experimentation with crosslinkers from the two major classes are reported herein. BS3 (bis(sulfosuccinimidyl) suberate) was the homobifunctional crosslinker utilized to crosslink amino ssDNA with peptides. Succinimidyl 4,4-azipentanoate (NHS-Diazirine) was the heterobifunctional crosslinker utilized to crosslink and amine modified ssDNA bioconjugate with peptides.

In the BS3 studies, we carried out experiments to determine the effect of reactant stoichiometry, reactant purity, buffer pH, sequence of reaction, the incubation temperature, and the peptide sequence. Matrix assisted laser desorption ionization time-of-flight (MALDI-TOF) was used to analyze the molecular weight of the bioconjugates formed. A reversed phase high performance liquid chromatography (RP-HPLC) method with detection at $\lambda_{260\,nm}$ was implemented to purify the starting amino ssDNA material. This method could be routinely used for both purifying and quantifying single stranded DNA, and their conjugates

The two-step reaction method with a 1:50:100 stoichiometry of amino ssDNA: BS3 crosslinker: peptide$_4$, at an incubation temperature of 4 °C yielded the desired amino ssDNA-BS3-peptide conjugate. However, all the subsequent MALDI-TOF results indicated conjugate molecular weights evidencing only partial bioconjugate formation (i.e., only one end of the crosslinker successfully reacting with one of the two biomolecules).

Although NHS-Diazirine crosslinking efforts with amino ssDNA bioconjugate and peptides did not indicate the expected final ssDNA–peptide bioconjugates, results showed that the crosslinker was successful in synthesizing a peptide$_4$–peptide$_4$ final bioconjugate.

At the conclusion of both BS3 and NHS-Diazirine crosslinking studies, we recognized that the key factor governing peptide conjugation is perhaps complete deprotonation of the peptide's

ammonium groups. Deprotonation is converting ammonium groups (NH_3^+) into amino groups (NH_2). If a peptide sequence with a high pI was chosen, complete deprotonation of the lysine groups would require a buffer media with very high pH values. This in return poses hydrolysis threats to the sulfo-NHS group in the BS3 crosslinker. Therefore, acidic peptide sequences such as $peptide_4$ used in this study would render more suitable for BS3 and NHS-Diazirine crosslinking. Due to lack of selectivity, SDA crosslinkers might be best suited for large scale studies as opposed to micro-scale bioconjugation studies.

3.2 Introduction

BS3 (bis(sulfosuccinimidyl) suberate)

BS3 is a selective, homobifunctional crosslinker with a 11Å length, 8-carbon spacer arm, with two negatively charged sulfo-NHS esters at both ends (Fig.24). DSS (disuccinimidyl suberate) which is the water immiscible analog of BS3 was not suitable for this study where the reactions are conducted in aqueous phase. Many non-sulfonated forms of NHS ester reagents are water insoluble, and must be used in organic solvents, such as DMSO and DMF. The solubility of NHS-ester reagents varies with buffer composition and the physical properties of the remainder of the molecular structure (e.g., spacer arm). The choice of buffer pH (ideal at ~7-9), and the type of conjugation buffer (amine free) will play a major role in preventing the NHS ester group's hydrolysis, and improve the selectivity of the coupling reaction. The sulfo-NHS groups are reactive towards primary amines and hence could be utilized to react naturally occurring peptides, enzymes and other biomolecules.

The sulfo-NHS functional group in the BS3 crosslinker is sensitive to the pH of the buffer and the type of buffer. It was important to carry out the reaction at a pH in the range of 7 – 9 in order to deprotonate the primary amine group. This facilitates the nucleophilic attack to the carbonyl carbon in the sulfo-NHS functional group. However, highly basic pH conditions could potentially hydrolyze the *N*-hydroxysulfosuccinimide (NHS) group. As extraneous amines present in the buffer could prevent conjugation, as opposed to Tris, glycine or imidazole buffers, we used a carbonate buffer at pH 8.5.

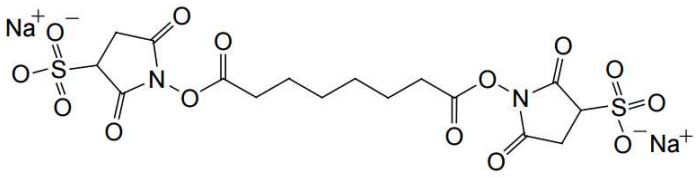

Figure 24: BS3 crosslinker depicting the two sulfo-NHS ester groups.

Although all previous reports used the BS3 crosslinker to link peptides and proteins, in this study, we utilized BS3 to react an amino ssDNA with a peptide (Fig.25).

While designing the ssDNA sequence for the study, we refrained from using too many Guanine (G) and Cytosine (C). Sequences rich in higher G and C contents are relatively inconvenient to synthesize. They also cause the T_m of the oligonucleotide sequence increase [81]. As we extended these crosslinking methods to ultimately crosslink enzymes with DNA, we maintained the melting temperature (T_m) of the DNA sequence as low as possible. The higher the T_m, the higher temperature we would need to provide in accomplishing DNA hybridization. Since, long oligonucleotide sequences can cause hindrances in the oligonucleotide synthesizing steps, and very small sizes could cause drawbacks in DNA hybridization (chapter 4), an average size was chosen after referring to several literature reports.

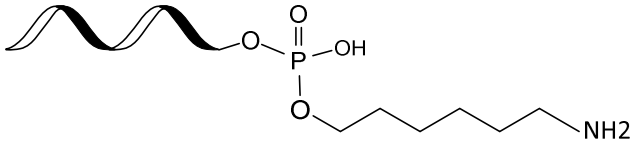

Figure 25: 5' amino-ssDNA obtained from IDT DNA®.

Succinimidyl 4,4-azipentanoate (SDA, NHS-Diazirine)

There are many crosslinkers in the heterobifunctional, Succinimidyl-diazirine (SDA) class, and only have begun to draw the attention of scientists very recently [75]. This class of crosslinkers have different spacer arm lengths, and are membrane permeable. The membrane permeability can prove very useful in post-purification steps such as dialysis. Succinimidyl 4,4-azipentanoate (SDA, NHS-Diazirine) is a member of the class heterobifunctional crosslinkers. In heterobifunctional crosslinkers, the two functional groups at the two ends of the spacer arm, are different. SDA has a

molecular weight of 225 Da, and has a 3.9 Å long spacer arm, with two different reactive groups at the end of it. At one end is a *N*-hydroxysuccinimide (NHS) ester which reacts with primary amine functional groups. On the other end is a diazirine ring in which, the nitrogen atoms very reactive (Fig.26a). The photoreactive groups available for crosslinking are diazirines, azides, and benzophenones [82]. The photoactivatable functional groups negate highly reactive free-radical intermediates upon photolysis. These intermediates exhibit almost no chemo-selectivity towards other functional groups. In SDA (succinimidyl 4,4-azipentanoate) class crosslinkers, the diazirine ring is photoactivatable, and readily undergoes reaction with any functional group. One major disadvantage of SDA class crosslinkers is the lack of specificity. Hence, this is more of a "shot gun" approach, and could lead to higher noise levels.

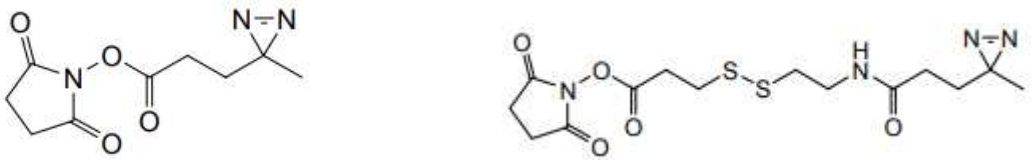

Figure 26: N-hydroxysuccinimide succinimidyl diazirine (NHS-Diarizine) (a) NHS-SS-Diazirine (SDAD) (b).

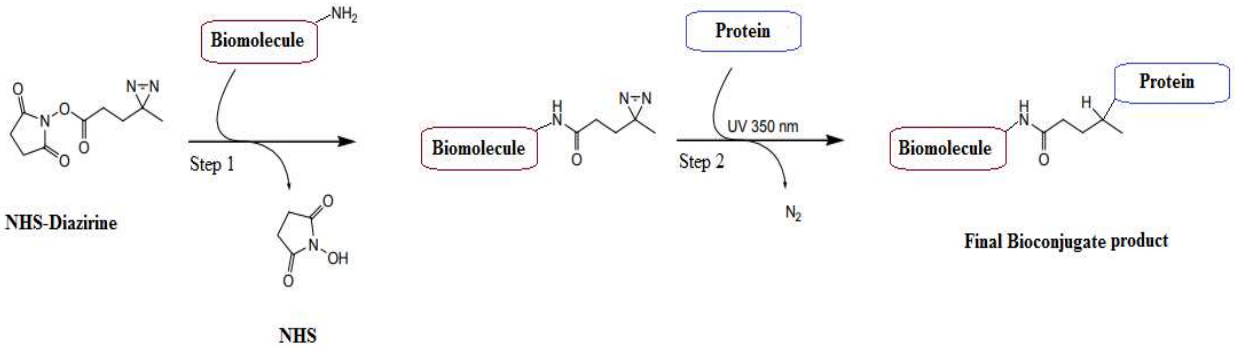

Figure 27: Schematic of the NHS-Diazirine (SDA) crosslinking reaction.
–modified from [83].

The reaction scheme of NHS-Diazirine is depicted in Fig.27. First, the NHS-ester is reacted with the primary amino groups in the first biomolecule. This reaction is most efficient in buffers with pH 7 – 9. After step one, the NHS acts as the leaving group while forming an amide bond between the crosslinker and the first biomolecule. In step 2, after introducing the protein into the sample, it is exposed to UV light (approx. 350 nm). The UV energy activates the diazirine ring (on the right side of the crosslinker), and creates a reactive carbine intermediate which is susceptible to react with any amino acid side group present on a protein. This reaction is a covalent bond formed in an 'addition' type reaction. The spacer arm of the crosslinker ultimately becomes a part of the final bioconjugate molecule. The molecular weight of the spacer arm is 83 Da. Therefore, the final molecular weight of any bioconjugate formed via this crosslinker is the summation of the crosslinker's spacer arm, and the molecular weights of the individual biomolecules (e.g. proteins, antibodies, peptide, DNA).

Albeit the non-selectivity of the diazirine ring, a variety of previous bioconjugate studies have been accomplished with diazirines. In one previous study, synthetic peptides, and myoglobin were used to demonstrate covalent bond formation by utilizing NHS-SS-Diazirine (SDAD) [83]. Their MALDI mass spectrometry results indicated high numbers of crosslinks [84]. Furthermore, the disulfide bond in the middle of SDAD crosslinkers could be particularly of interest in protein-protein interaction mapping. The chemical structure of SDAD is depicted in Fig.26b. Although SDAD and SDA are somewhat structurally different, the two functional groups of interest are the same.

In a different study, SDA was used to create photo-crosslinkable elastin-like proteins (ELP). These ELPs were next crosslinked to a common implant material Titanium, in a variety of geometries such as discs, screws, and rods [85]. They first reacted the crosslinker's NHS-ester with the amines present in ELPs. Next, these samples were spin coated onto the Titanium surfaces. Finally, diazirine ring was activated by exposing the spin-coated surface to 365 nm UV light, which facilitated the ELPs to functionalize on the Titanium surfaces.

NHS-Diazirine has also been used to synthesize photoactivatable crosslinking sugars to capture glycoprotein interactions [86]. In this study, monosaccharides were synthesized with

diazirine crosslinkers, and these sugars were incorporated onto cell surfaces, in order to study glycoprotein interactions.

Evidently, NHS-Diazirine has been used in previous academic applications to crosslink biomolecules and biomaterials. As the non-selectivity was viewed as an advantage, we attempted to use NHS-Diazirine in a controlled reaction. As any extraneous functional groups could bind to the activated diazirine ring, the salt concentrations in the buffer medium was heavily reduced in our experimentation.

Design of peptides

Some universal key design features were accounted for while designing the synthetic peptides for this study. Peptides are comprised of amino acids. Amino acids are also the building blocks of proteins in living organisms. There are over 500 amino acids found in nature. However, the human gene only directly encodes 20. Fig.28 illustrates the 20 essential amino acids and their characteristics. Among the considerations were water solubility, number of 1° amines, and the peptide purity. The solubility of a peptide is strongly influenced by the amino acid composition. Hence, amino acids with a high content of hydrophobic residues such as Leu, Val, Ile, Met, Phe and Trp should be avoided if the desired solvent system is polar. Peptides with hydrophobic amino acid contents higher than 50% could be partially or even completely insoluble in aqueous media. Additionally, in order to yield a peptide with very high solubility, it is best if at least 20% of the amino acids contain polar side groups. At pH values ~7 Asp, Glu, Lys, and Arg have charged side chains. From a synthesis perspective, peptides containing multiple Cys, Met, or Trp residues are cumbersome because these residues are prone to oxidation [87]. One other important structural concern is beta-sheet formation of peptides. Peptides tend to fold into secondary structures such as beta sheets or alpha helices in order to enhance its native stability.

But when beta sheets form, the peptide could undergo deletions and even truncations, resulting in a poor synthetic yield of the desired product. In order to avoid beta sheet formation, peptides with neighboring aromatic and hydrophobic residues such as Val, Ile, Tyr, Phe, Trp, Leu, Gln, and Thr are avoided [88,89].

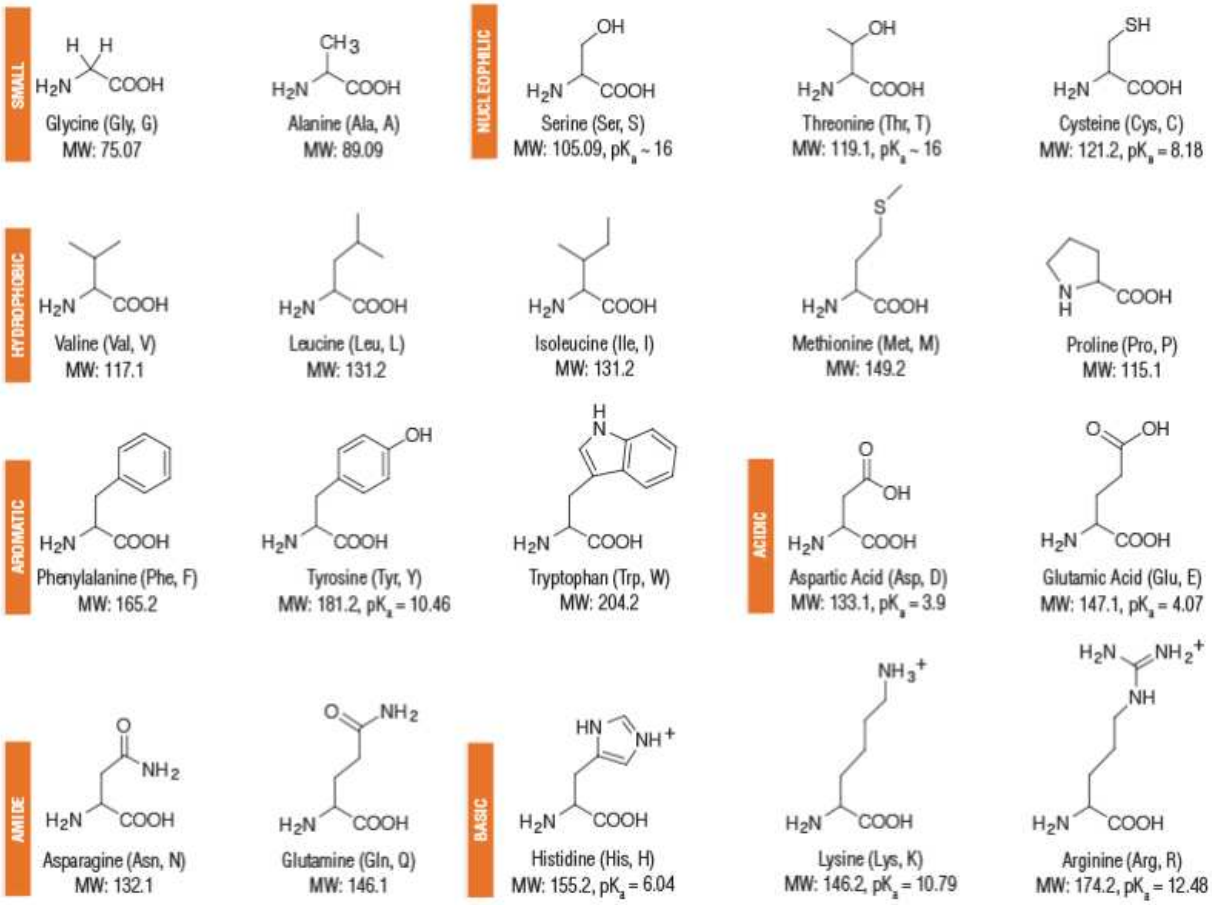

Figure 28: Properties and the chemical structures of the common amino acids [New England Biolabs].

The deduced electron pushing mechanism of this reaction is of S_N type (Fig.29, 30). The only functional groups involved in the reaction are esters and amines. The stoichiometry of amino ssDNA: BS3 crosslinker is important to ensure that amino ssDNA does not attach to both the sulfo-NHS ester moieties at the end. One end of the crosslinker should attach to the amino-ssDNA, while the other end attach to the amine in the peptide (Fig.30).

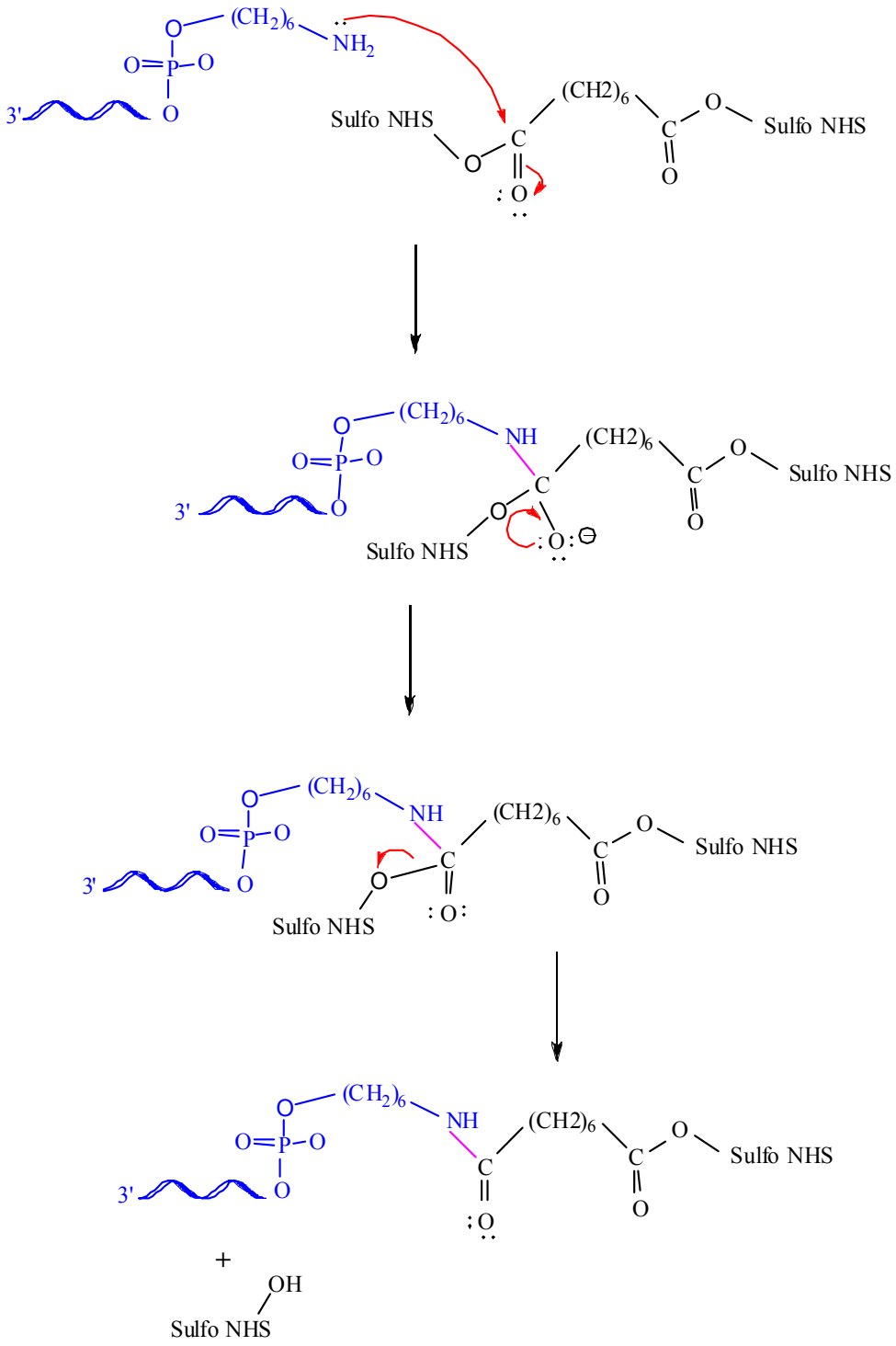

Figure 29: Electron pushing mechanism predicted for the S_N2 reaction between the 1° amine in amino ssDNA and one NHS-ester in BS3.

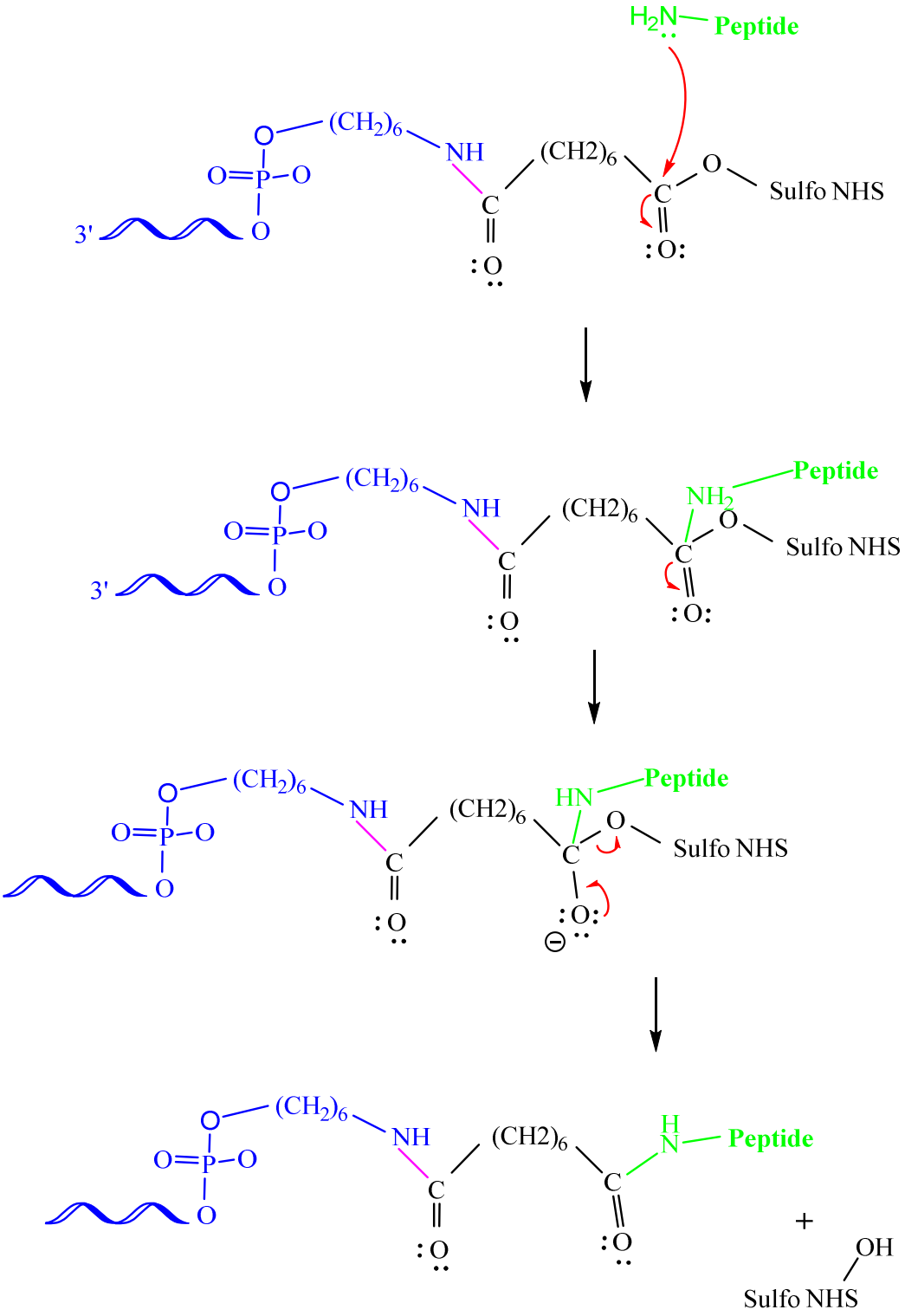

Figure 30: Electron pushing mechanism predicted for the S_N2 reaction between the 1° amine in a peptide and the other NHS-ester in BS3.

3.2 Materials and Methods

3.2.1 Materials – BS3 crosslinking.

3.2.1.1 Amino single stranded DNA (amino ssDNA).

The amino single stranded DNA (amino ssDNA); 5'amino/GTA GAT CAC TAT CAT 3', T_m 35.8 °C, molecular weights of 4730 Da was directly purchased from IDT® DNA.

3.2.1.2 Peptides.

The BS3 crosslinking was carried out using a small peptide and an amino ssDNA. In this study, we tested three different peptide sequences separately. The first and third were designed with several lysine groups in order to maximize the number of 1° amines available for amination with the crosslinker. The peptide properties calculated via the PepDraw 1.0 tool (Tulane University) are represented in table 5 below. Peptide sequence 2 and 4 were designed such that the pI of them was closer to, or less than physiological pH. Therefore, we expected their N-terminal ammoniums to be easily deprotonated at buffers near physiological pH, and react with the crosslinker. $Peptide_5$ was designed with several lysine groups in order to maximize the number of 1° amines available for amination with the crosslinker. Peptides 1 – 4 were directly purchased from NeoBioLab (Woburn, MA), while $Peptide_5$ was synthesized in-house.

Table 5: Properties of the synthetic peptides used in crosslinking studies.

Peptide #	Molecular weight (Da)	Sequence	Isoelectric point (pI)	Net charge
1	616.4	KRADK	10.6	2
2	457	GHTSG	7.91	0
3	643.4	KLKQK	10.86	3
4	576	DAEQD	2.71	-3
5	686	KRADGK	10.56	2

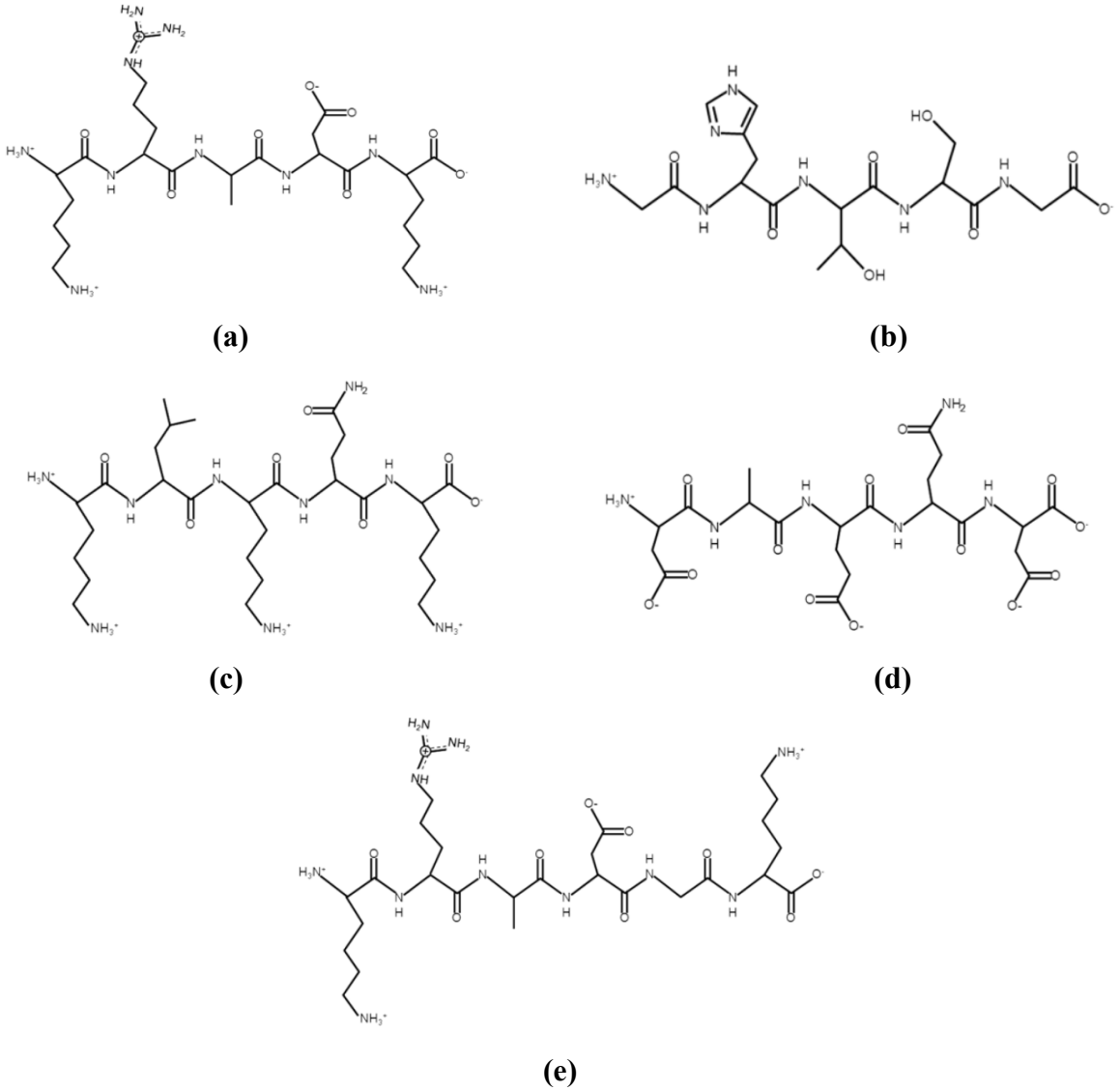

(a) **(b)** **(c)** **(d)** **(e)**

Figure 31: Molecular structures of Peptide; 1 (a), 2 (b), 3 (c), 4 (d), 5 (e).

3.2.2 Methods – BS3 crosslinking.

3.2.2.1.1 Crosslinking amino ssDNA with peptides.

Amino modified ssDNA; **5AmMC6/GTA GAT CAC TAT CAT** (Fig.25) were purchased from Integrated DNA Technologies (Coralville, IA). In a general crosslinking reaction the oligo samples were dialyzed using 2000 MWCO tubing prior to each experiment. First, amino ssDNA dissolved in 200 mM carbonate buffer was transferred to pre-weighed BS3. Unless specified otherwise, pH of the buffer was 8.5±0.2. Table 6 and the discussion below describes the

stoichiometry of reactants, incubation temperatures and various buffer pH values tested. In order to push the reaction towards amination, and reduce the effects of sulfo-NHS hydrolysis, a higher molar amount of peptides was used. Next, the mixture was incubated at the defined conditions (Table 6). After the incubation period, each sample was dialyzed against DI water at r.t. using 2000 MWCO tubes (ThermoFisher Scientific, IL) to remove any unreacted reactants and byproducts.

The preliminary reactions were conducted with $peptide_1$, as this peptide sequence contained a high no. of primary amines (a higher no. of lysine groups). We carried out sets of experiments to determine the effect of stoichiometry of reactants, purity of the reactants, peptide sequence, buffer pH, sequence of reaction and the incubation temperature (Table 6). In the initial experiments, we tried a one-pot reaction protocol. The peptide was added to the amino ssDNA, BS3 mixture within 5 s. By doing so, we allowed minimum time for the NHS to hydrolyze. The reactant stoichiometry in these experiments was maintained as indicated in *a, Table 6. They were incubated at room temperature (r.t.) and the incubation time period was 5 – 18 hrs.

Table 6: Illustration of the multiple alterations to the crosslinking protocols.

Designation	Step	Results Figure
Stoichiometry of amino ssDNA: BS3: $peptide_1$ = 1:50:50 One-pot reactions		
*a (n=3)	Amino ssDNA → BS3 → $peptide_1$	34
*b (n=2)	Reacting amino ssDNA with BS3, dialyzed the sample, then reacted with $peptide_1$.	34
*c (n=2)	Reacting $peptide_1$ with HPLC purified amino ssDNA.	39
Stoichiometry of amino ssDNA: BS3: peptide = 1:50:100		
*d (n=1)	Increased $peptide_1$ molar amount. Amino ssDNA: BS3: $peptide_1$ = 1:50:100	40

Table 6 continued

*e (n=3)	Increased buffer pH with $peptide_1$ (pH = 9.5).	41
*f (n=2,1,1)	Two-step reaction. Amino ssDNA reacted with BS3, incubated for 1 hr at the specified temp., then reacted with $peptide_2$. (a) ↓temperature (4 °C) (b) ↑temperature (40 °C) (c) conjugate from (b) acid washed using 6M HCl to remove adducts.	42 (a, b, c)
*g (n>5)	Replicates of *f(a)	43, 44
*h (n=3)	Replicated *f(a) with $peptide_3$.	45
*i (n=1)	Conjugating $peptide_4$ and $peptide_5$ in a one-pot BS3 crosslinking method.	47

In another experiment, the amino ssDNA was crosslinked with BS3, followed by dialysis. After incubating the amino ssDNA-BS3 at r.t. for about 1 hr, the product was purified using 2000 MWCO tubes. The recovered sample was then reacted with $peptide_1$ (*b, Table 6).

As impurities present in the starting material was suspected to be a plausible culprit for the lack of the desired bioconjugates, we developed a reversed phase HPLC procedure to remove truncated products from the starting material. The HPLC purified amino ssDNA was then crosslinked with $peptide_1$ utilizing BS3 (*c, Table 6). The procedure below discusses analytical chromatographic methods as well as preparative chromatographic methods.

3.2.2.2 Purifying amino ssDNA: Reversed phase high performance liquid chromatography (RP-HPLC)

If the truncated products in the starting amino ssDNA were reacting with BS3 crosslinker and $peptide_1$, the molecular formula of the final product would be unknown, and hence we would be unable to recognize it in our MALDI spectrographs. Therefore, we further purified the amino ssDNA ‘as received’ using RP-HPLC.

A C18 XTerra® (Waters, MA) 4.6 × 100 mm column with 3.5 µm particle diameter, and a guard column was used for reverse phase separation of the conjugates. High-performance liquid chromatography (HPLC) was performed on an Alliance 2695 separation module, using Empower version 2.0 software (Waters Corp., Milford, MA), equipped with a Waters 2496 UV/Vis detector (Waters Corp., Milford, MA). Detection was carried out at $\lambda_{260\ nm}$ as this is the wavelength that exhibits absorbance maxima of nucleotides. The two mobile phases were 0.1 M TEAA, pH 9.70±0.05 (triethylammonium acetate) buffer with 5% acetonitrile (ACN) and 30% ACN respectively. 0.1 M TEAA buffer was prepared by adding 5.6 mL of glacier acetic acid to 950 mL of deionized water. To this, 13.8 mL of TEA was added gradually, and the solution was stirred. Afterwards, the pH of the solution was adjusted to 7.3±0.05, and the final volume was brought to 1000 mL by adding water. Next, the mobile phases were prepared as follows; A: 5% acetonitrile in TEAA (v/v), B: 30% acetonitrile in TEAA (v/v). Finally, the solutions were filtered using qualitative-grade filter paper. The incorporated gradient is illustrated in Fig.32.

$$A := \begin{pmatrix} 92 \\ 77 \\ 60 \\ 60 \\ 100 \\ 100 \\ 92 \\ 68 \end{pmatrix} \qquad B := (100 - A) = \begin{pmatrix} 8 \\ 23 \\ 40 \\ 40 \\ 0 \\ 0 \\ 8 \\ 32 \end{pmatrix}$$

$$final := \left(\frac{5}{100} \cdot A\right) + \left(\frac{30}{100} \cdot B\right)$$

$$final = \begin{pmatrix} 7 \\ 10.75 \\ 15 \\ 15 \\ 5 \\ 5 \\ 7 \\ 13 \end{pmatrix} \quad \text{\% of organics in the final injection}$$

Figure 32: Calculations of the gradient incorporated into the Empower 2.0 software.

Analytical RP-HPLC methods.

Prior to conducting preparative RP-HPLC experimentation with the relatively expensive amino modified ssDNA, an analytical RP-HPLC procedure was conducted utilizing 15 bp ssDNA. These samples contained no modifications at the terminal ends, and had the same nucleotide sequence as those used in the amino ssDNA used for the crosslinking experiments. 15bp ssDNA 'as received' were resuspended in 0.1 M TEAA (pH 7.3) at a final oligo concentration of 2.4 mg/mL. It was then transferred to an HPLC vial, tightly secured with a septum, (Waters Corporation, MA) and placed in the auto sampler placeholder. A final gradient method with acetonitrile (ACN) percentage ranging from 7% – 13% was established (Fig.32). Suitability of the gradient was based on adequate baseline separation of the chromatograms.

Next, the same methods and column conditions were tested for the 5'amino 15 bp ssDNA 'as received' from the manufacturer. Initially, several injection volumes (10, 50, 100 µL) were used to test whether there would be an overloading limit in the C_{18} column. Upon confirming that there appear to be no such overload limit, 100 µL were used which enabled us to collect larger amounts of the desired fraction (described in "preparative methods").

Preparative HPLC methods.

Afterwards, 5' amino modified sample set 'as received' was resuspended in TEAA as previously described. Three runs were conducted, with an injection volume of 100 uL/run. With the aid of the real-time UV-detector screen, the fraction at RT= 16.9 min was collected from three injections. The total collected purified sample volume was approx. 12 mL. Next, the collection tube was left open in the fume hood overnight to evaporate acetonitrile in the sample. Afterwards, the sample was dialyzed using pre-washed 2000 MWCO dialysis tubes (ThermoFisher Scientific, IL). Each dialysis reservoir consisted of 1 L of DI water, and it was changed two times over the course of two days.

Next, the samples were recovered, and the volumes were further reduced by rotavapp'ing at 30 °C and -85 kPa for approximately 30 mins. The sample volume was reduced to 1 mL.

80 uL of the sample was predissolved in TEAA buffer, and re-run on the HPLC instrument using the same column, and methods. The purpose of the re-run was to confirm that we had removed all the truncated products observed in the amino ssDNA as received.

3.2.2.3 Crosslinking amino ssDNA with peptides contd.

The amino ssDNA samples collected from RP-HPLC were then crosslinked with increased $peptide_1$ molar amounts as indicated in *d, Table 6.

The pH of the reaction buffer was addressed next. As we deduced that deprotonation of the primary amines in the lysine groups was important, we pre-dissolved $peptide_1$ in carbonate buffers with pH 9±0.5. When the pH of the solution increases, the acidic and basic groups in a peptide or protein deprotonates. Furthermore in this case, the carboxylate anion converts from R-COOH to $R\text{-}COO^-$, and the ammonium cation converts from $R\text{-}NH_3^+$ to $R\text{-}NH_2$. The deprotonated amines are now more susceptible to undergo an S_N2 reaction with the sulfo-NHS group of the BS3 crosslinker (*e, Table 6). Since hydrolyzing peptide bonds at pH >10 was a risk, we did not attempt to reach to the pI 11 of the peptide (PepDraw 1.0, Tulane University).

Several variables were changed in the experimental procedure in *f. First, trials were conducted with $peptide_2$. Secondly, the one-pot reaction protocol used up until now was altered into a two-step reaction. Thirdly, the incubation temperatures were altered. In *f, *g, *h experimental procedures listed in Table 6. After reacting amino ssDNA with 50-fold molar excess, the sample mixture was incubated at 4 °C for one hour. Next, the sample was purified using 2000 MWCO dialysis tubes against DI water at room temperature (r.t.) for approx. 1hr. Next, the mixture was reacted with a 100-fold molar excess with respect to amino ssDNA. The final mixture was then incubated at 4 °C for approx. 5 hrs. Afterwards, the final sample mixture was dialyzed using 2000 MWCO dialysis tubes against DI water at r.t. overnight.

We altered the temperature conditions, as we questioned the stability of the crosslinker at r.t. In case the sulfo-NHS groups hydrolyze prior to undergoing amination, our MALDI-TOF observations (lack thereof) are quite explicable. Previous studies have indicated that the sulfo-NHS group is highly water labile, and that it has a half-life ranging from 10 min – 1 hr at r.t. [16,75] In order to prevent the hydrolysis of the sulfo-NHS group, we carried out experiments at 4 °C (*f(a), Table 6).

We also conducted the crosslinking reaction at 40 °C (n=1). This is slightly above the reported melting temperature (T_m) of the amino ssDNA. By doing so, we expected to loosen any

of the possible hairpin loop formations the amino ssDNA might have self-formed. We expected that increasing the temperature would relieve ssDNA from its secondary structures and increase the exposure of the terminal primary amine. This was expected to render the primary amine more accessible to react with the sulfo-NHS group (*f(b), Table 6).

As we consistently observed adduct formations, we also attempted to clear the result spectra by removing some of the adducts. In order to do this, we measured the pH of the final sample, and then neutralized it. The measured pH of the mixture was approx. 10, and this was brought down to a physiological pH of 7.4 by careful addition of 6M HCl.

Although results from *f(a) at 4 °C indicated successful conjugation, we were unable to replicate these results (*g, Table 6).

We conducted *f with $peptide_3$, to test whether the sequence plays a role in the success of bioconjugation (*h, Table 6). Lastly, we attempted crosslinking two different peptide molecules using BS3. In these attempts $peptide_1$ was reacted with $peptide_4$ in equimolar amounts, with incubation at 4 °C, followed by dialysis against DI water at r.t. (*i, Table 6).

Table 3 illustrates the molecular weights of the expected conjugates. The expected final conjugate molecular weight is calculated from summing the molecular weight of the amino ssDNA, the spacer arm of BS3, and the peptide. The ‘spacer arm’ of BS3 becomes a part of the final bioconjugate. The two sulfo-NHS groups at the two ends of BS3 are leaving groups.

Table 7: Molecular weights of the reactants and expected conjugates.

Reactant or conjugate	Molecular weight (Da)
Amino ssDNA (15 bp)	*4724*
BS3 crosslinker	572
Spacer arm of BS3	*140*
Sulfo-NHS group	200

Table 7 continued

Expected final bioconjugates	
amino ssDNA-BS3-peptide 1	**5480**
amino ssDNA-BS3-peptide 2	**5321**
amino ssDNA-BS3-peptide 3	**5507**

3.2.3 Materials – NHS Diazirine crosslinking.

10 mM sodium phosphate ($NaH_2PO_4 \cdot H2O$), 50 mM NaCl, buffer medium was pH adjusted to 7.2±0.2, and filtered. At the beginning of each experimentation, a 100 mM stock solution of NHS-Diazirine was freshly prepared in dimethyl sulfoxide (DMSO) immediately before use. NHS-Diazirine was purchased from ThermoFisher Scientific (Hanover Park, IL). All the crosslinking experimentation was conducted in a laboratory illuminated with very little light.

NHS-Diazirine crosslinking was carried out with a phosphoramidated single stranded DNA (phosphoramidated ssDNA) conjugate obtained from EDC crosslinking. $Peptide_4$ and $peptide_5$ were utilized for the NHS-Diazirine experiments (Table 5).

3.2.4 Methods – NHS Diazirine crosslinking.

3.2.4.1 Crosslinking two peptides with NHS-Diazirine.

The preliminary experimentation with NHS-Diazirine was conducted on two peptides. Prior to synthesizing ssDNA-peptide bioconjugates, it was important to discover whether the crosslinker could be used successfully to conjugate two different peptides together.

$Peptide_5$ was dissolved in 50 µL of PBS (pH 7.2±0.2). Into this, either a 50-fold, or 20-fold molar excess of NHS-Diazirine (with respect to peptides) was added from the 100 mM stock solution. The sample was incubated at room temperature (r.t.) for 30 min. Next, $peptide_5$ pre-dissolved in PBS was added in molar equivalence to $peptide_4$. The final molarity of the peptides was approx. 0.0012 M, while the final concentration of NHS-Diazirine in the reaction mixture was 0.003 M. Finally, the reaction mixture was gently vortexed, and exposed to 360 nm UV light using a 4 Watt, compact UV lamp (UVP, Upland, CA) for approx. 30 min. Afterwards, the sample was

incubated at r.t. for another 1 hr, and finally, the reaction was quenched by adding 50 mM Tris buffer to alter the pH of the reaction mixture. Next, the unreacted reactants and byproducts were removed by dialyzing the mixture against DI water, using 2000 MWCO dialysis filter tubes. The molecular weight of the constituents in the recovered reaction sample were analyzed on MALDI-TOF.

3.2.4.2 Crosslinking peptides and phosphoramidated ssDNA with NHS Diazirine.

Next, NHS-Diazirine was used to crosslink $peptide_5$ and $peptide_4$ separately with an in-house synthesized phosphoramidated ssDNA. In these experiments, the no. of mols of the phosphoramidated ssDNA was approx. 2×10^{-7} mols. A 20 – 50 molar excess of peptides was used in the crosslinking experiments. The procedure is the same described in the above section (3.2.4.1). The phosphoramidated ssDNA has a primary amino group available for amide bond formation with the NHS group in the NHS-Diazirine crosslinker. The method of synthesizing the phosphoramidated ssDNA bioconjugate is described in greater detail in chapter 2.

3.2.5 Bioconjugate analysis: (MALDI-TOF).

All the conjugates were analyzed using mass spectrometry to determine the conjugate molecular weights. MALDI-TOF results were obtained using an Applied Biosystems (Framingham, MA) Voyager DE PRO mass spectrometer. This instrument utilizes a nitrogen laser (337 nm UV laser) for ionization with a time-of-flight mass analyzer. Prior to MALDI-TOF, each sample was purified using a C_{18} – ZipTip column (Millipore Corporation, Billerica, MA). The ZipTip columns were conditioned using two 10 µL of acetonitrile followed by two 10 µL of 0.1% trifluroroacetic acid (TFA). As ssDNA contains functional groups which readily lose a proton, generally a negative linear mode was used (MH^-) to produce singly charged species.

3.3 Results and Discussion – BS3 crosslinker.

3.3.1 *Mass spectra of the reactants (peptides and ssDNA): MALDI-TOF*

The mass spectra of the starting material are illustrated in Fig.33.

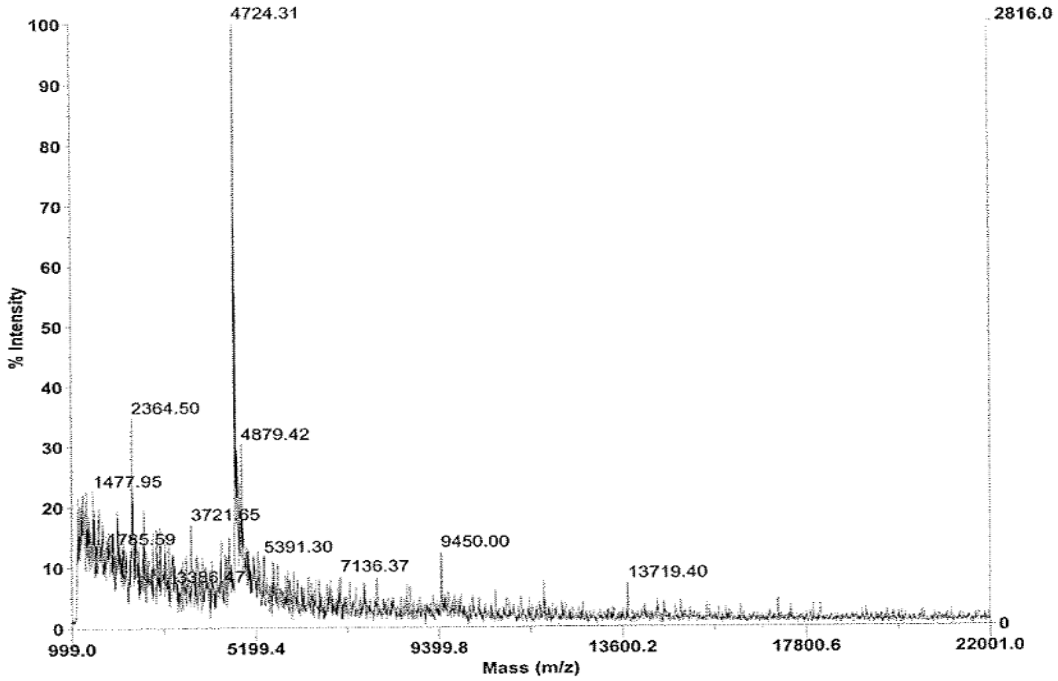

(a)

Figure 33: Mass spectrum of; amino ssDNA as received (a), $Peptide_1$ (b), $Peptide_2$ (c), $Peptide_3$ (d), $Peptide_4$ (e), $Peptide_5$ (f).

Figure 33 continued

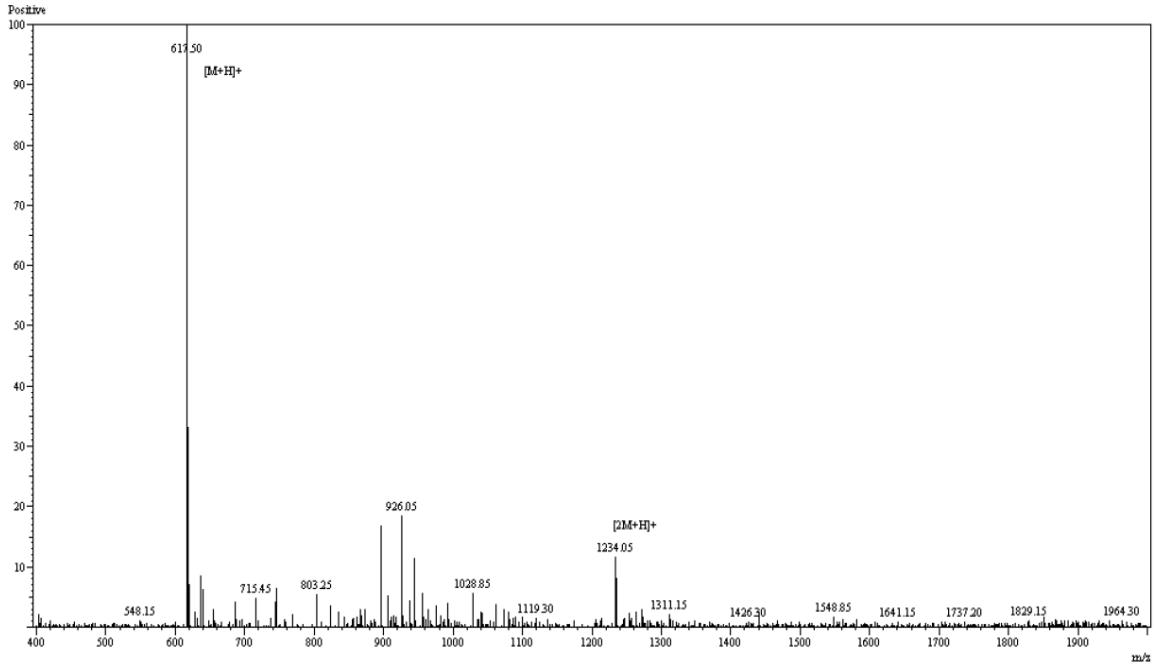

(b)

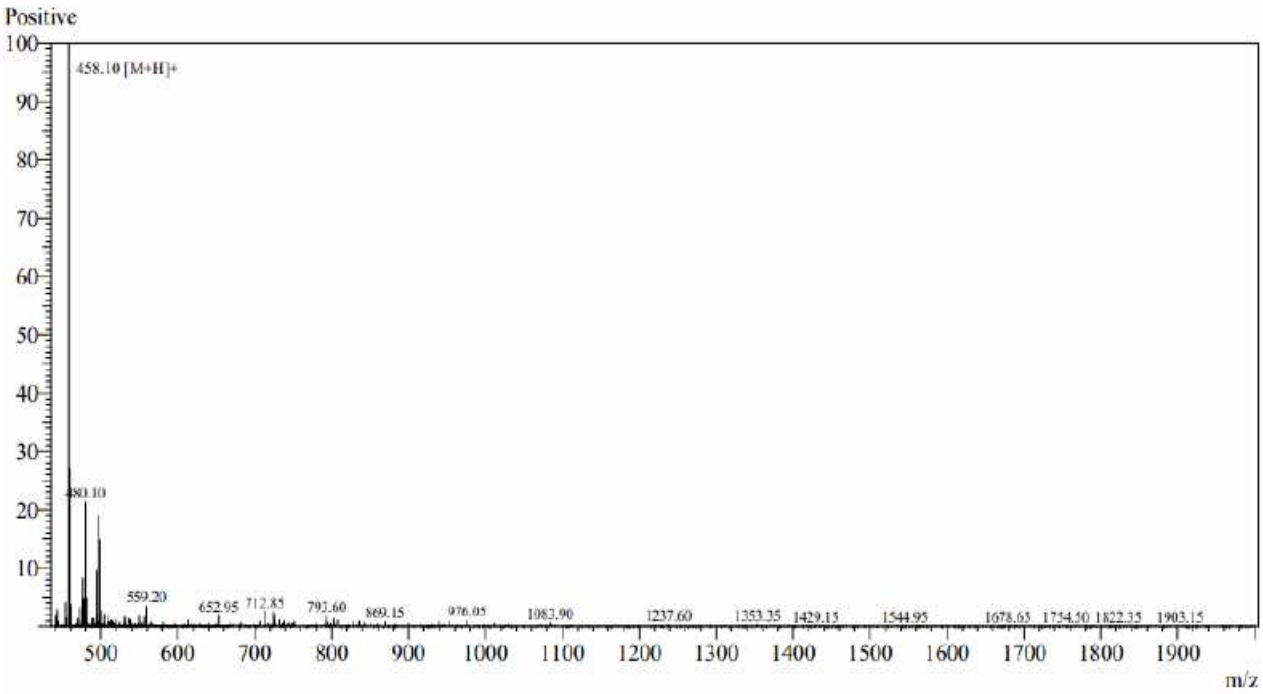

(c)

Figure 33 continued

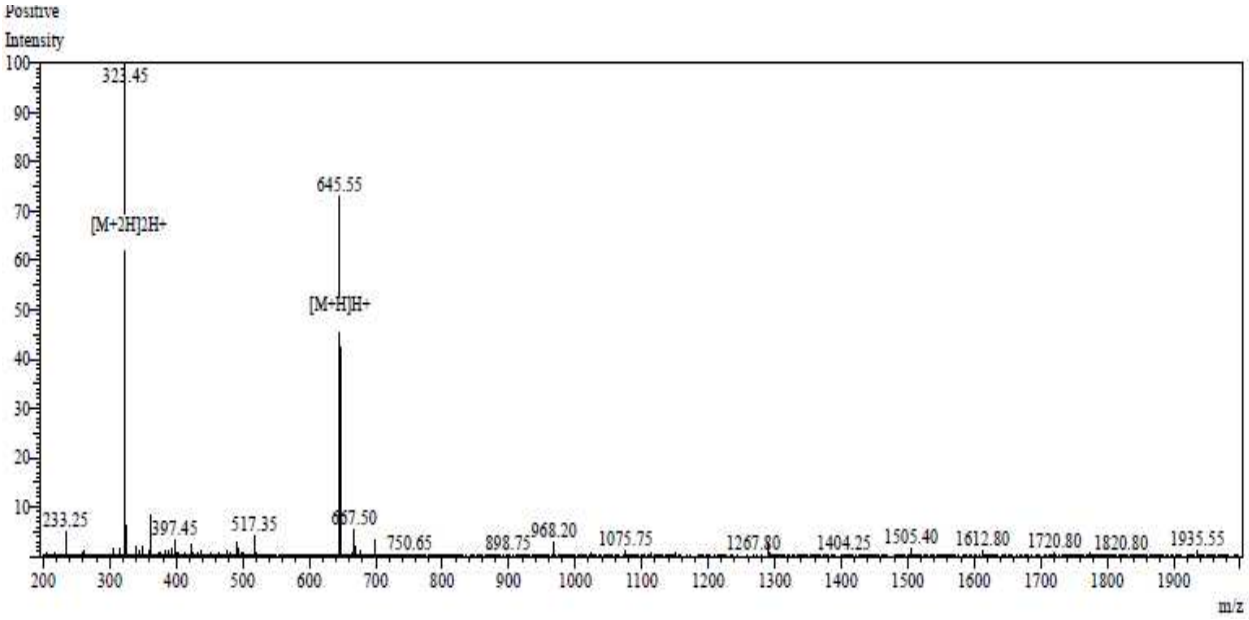

(d)

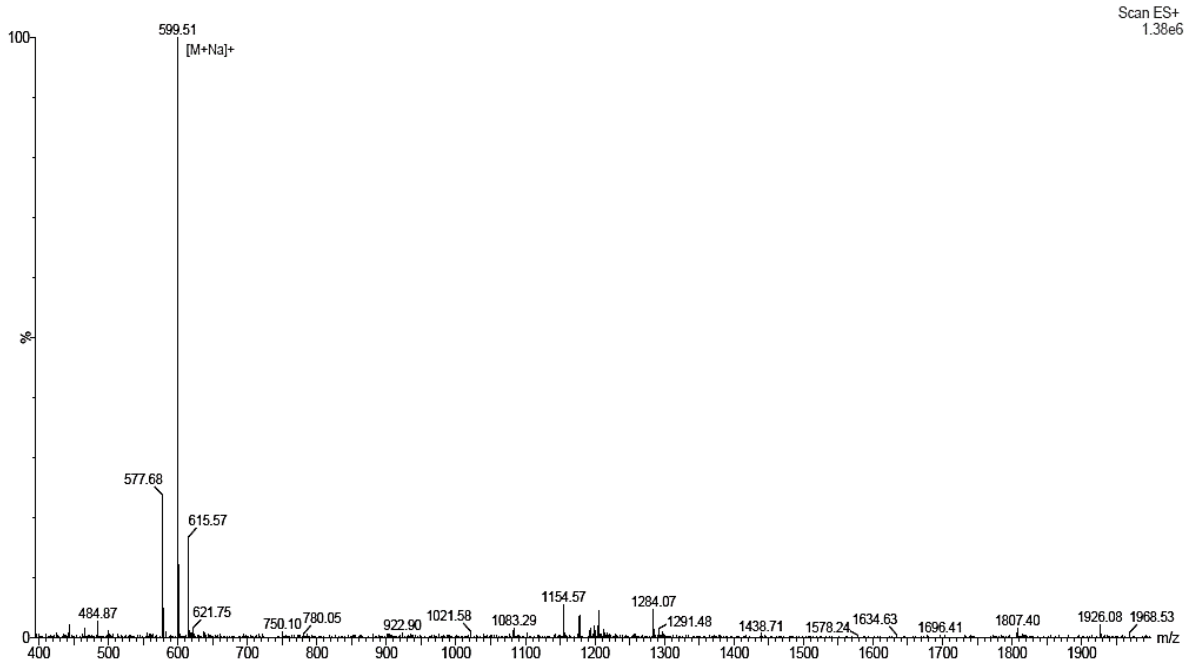

(e)

Figure 33 continued

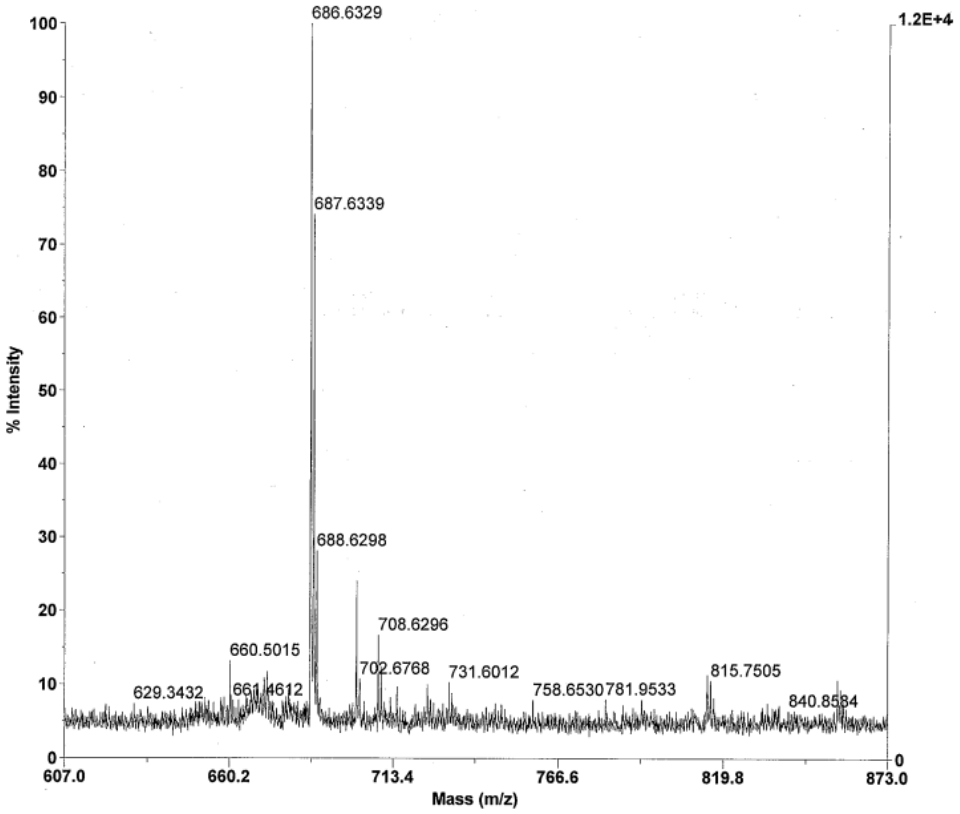

(f)

3.3.2 *Amino ssDNA-BS3-peptide conjugate analysis: MALDI-TOF*

MALDI-TOF results from the experimental procedure listed in *a , Table 6 indicated a major peak at 4731 m/z and a secondary peak at 4889 m/z (Fig.34). The peak at 4731 m/z corresponds to unreacted amino ssDNA. The secondary peak was attributed to the possible formation of a partial conjugate, and is discussed in greater detail later in Fig.46a. These mass spectrometry results indicated that the conjugation attempts with $peptide_1$ were not successful, as the expected amino ssDNA-BS3-$peptide_1$ conjugate signal at 5480 m/z was not observed.

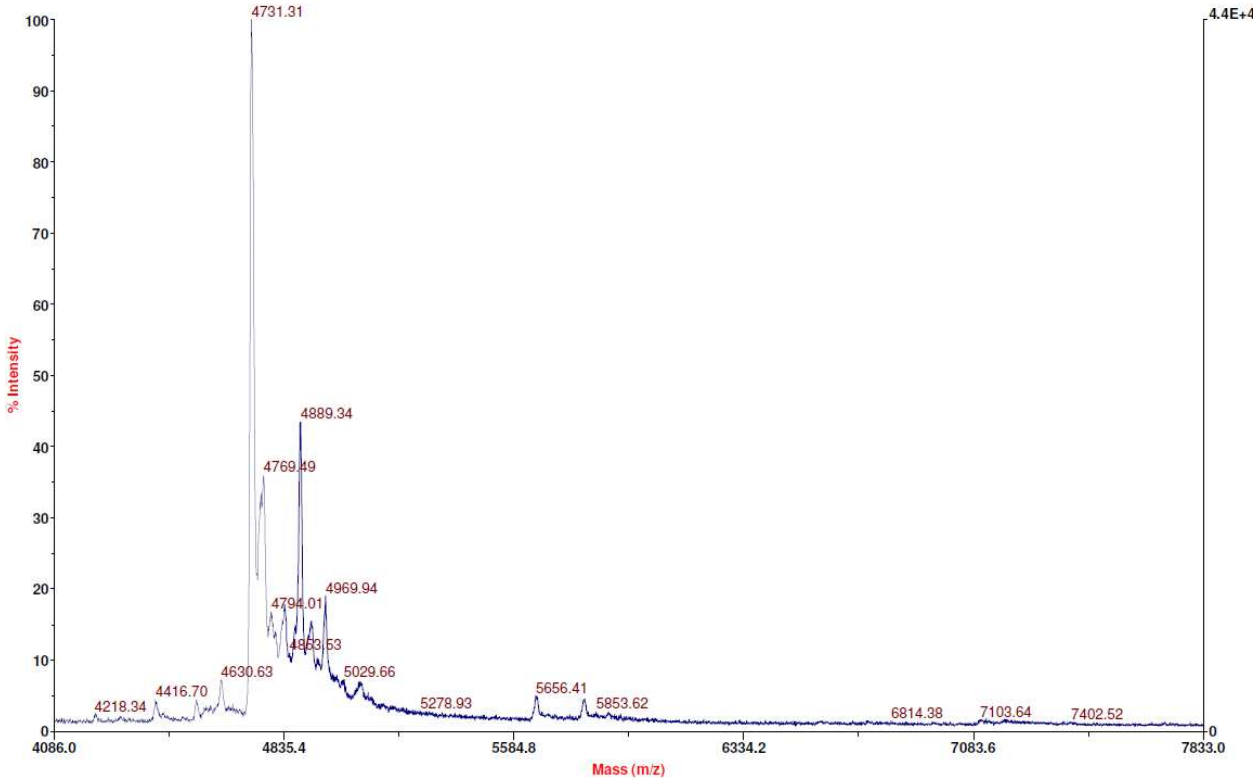

Figure 34: MALDI mass spectrum of conjugate obtained from experimental procedure, *a, Table 6.

Next, we purified the reaction sample using 2000 MWCO dialysis tubes after the first reaction (amino ssDNA with BS3). This was then reacted with 50-fold molar excess of peptide$_1$ (*b, Table 6). The MALDI spectrum of the resulting conjugate still indicated salt adducts at 4940 m/z, and partial conjugation structures at 4884 m/z, and 5078 m/z (Fig.35). The molecular structures of the possible partial conjugates are discussed in greater detail in Fig.46.

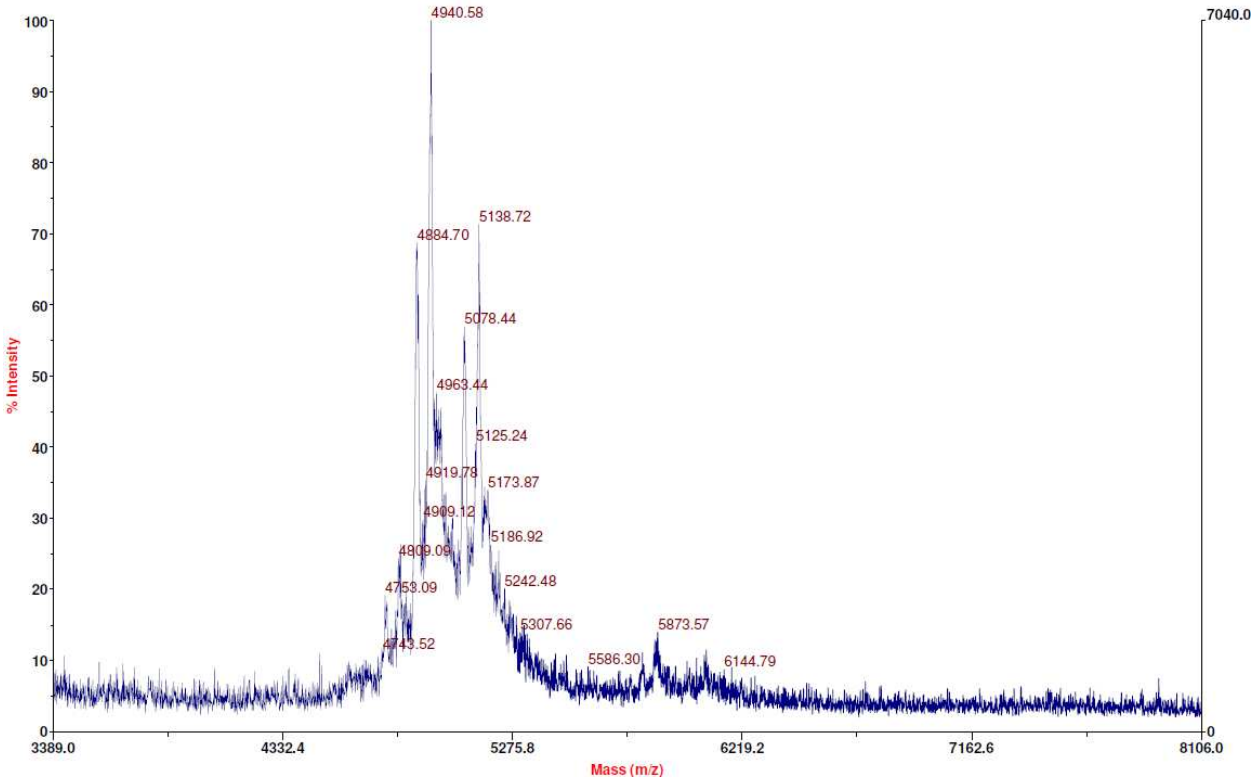

Figure 35: MALDI mass spectrum of conjugate obtained from experimental procedure, *b, Table 6 – with product purification in the intermediate step.

3.3.3 *Analytical RP-HPLC method.*

This sub-section discussed how RP-HPLC (reversed phase high performance liquid chromatoraphy) was used to purify the amino ssDNA as received. The RP-HPLC experiments with the standard 15 base pair ssDNA resulted in baseline resolved peaks, with one major component eluting at RT= 16.94 mins (Fig.36), and some significant, more hydrophilic impurities eluting initially. There was also some indication of additional truncated products eluting after the major component (Fig.36).

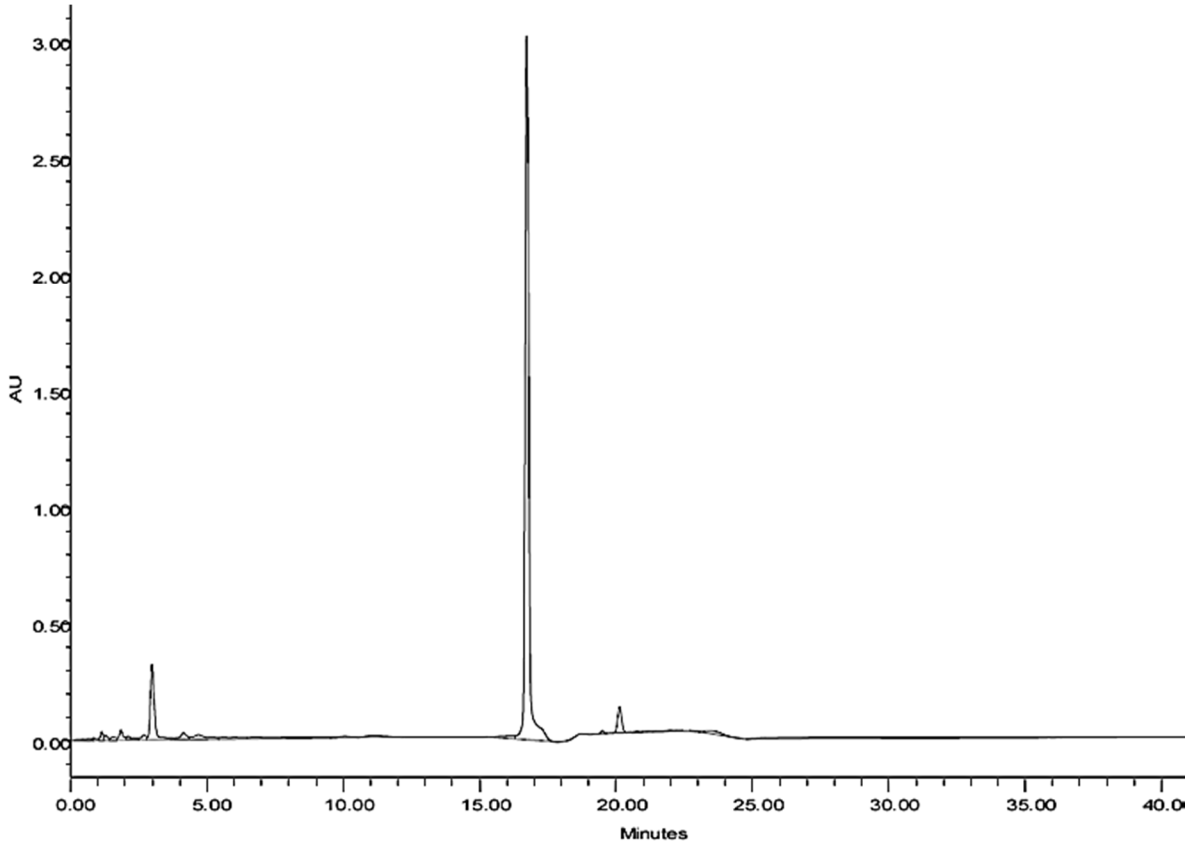

Figure 36: Standard 15 bp phosphoryl ssDNA chromatograph.

Column: XTerra® MS C_{18} 2.5 µm, 4.6 mm×50 mm. Mobile phases: A; 5% acetonitrile in 0.1 M TEAA (pH 7.01), B; 30% acetonitrile in 0.1M TEAA (pH 7.01). Flowrate: 1.0 mL/min. Gradient: 80% A to 20% A in 22 min. Column and sample temperatures: 33 °C and 35 °C. Injection volume: 100 µL. Detection: UV 260 nm.

The results of the isolated fractions indicate one highly resolved peak at a retention time (RT) of 16 min, as well as some indication of impurities much at retention times of 0.4 min, and 21 min. These could be due to residual material from the chromatographic column, the connection loops, or residual material from the dialysis tubes (glycerin). We ruled out all of these possibilities – (1) A "purge injector" and a column equilibration was performed in between each sample. (2) The MWCO tubes were always pre-washed using DI water for about 15 min. Therefore, the impurities attributed to any salts or truncated products in the material as received.

Afterwards, the developed RP-HPLC method was used to obtain chromatograms of the actual starting material; amino ssDNA. The results indicated truncated products in the amino

modifed ssDNA, just as it did on the 15 bp ssDNA (Fig.37). The largest peak corresponds to the desired material (60% peak area, RT=16.429 min).

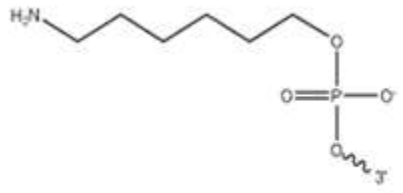

amino modified ssDNA

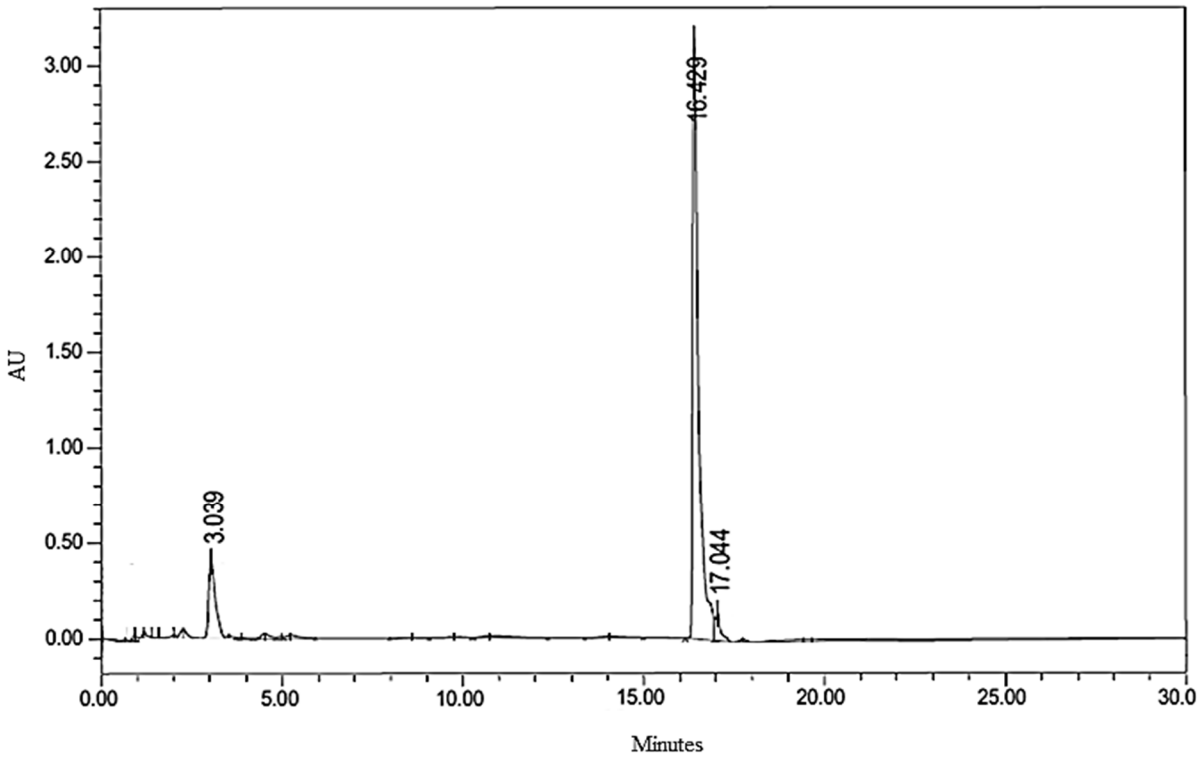

Figure 37: 15 bp amino ssDNA chromatograph.

Column: XTerra® MS C_{18} 2.5 µm, 4.6 mm × 50 mm column. Mobile phases: A: 5% acetonitrile in 0.1 M TEAA, pH 7.01, B: 30% acetonitrile in 0.1M TEAA, pH 7.01. Flowrate: 1.0 mL/min, Gradient: 80%A to 20%A in 22 min. Column temperature: 33°C, Injection volume: 100 µL. Detection: UV 260 nm.

3.3.4 *Preparative RP-HPLC results confirmation.*

A sample of the collected and purified fractions were further tested using the same analytical RP-HPLC method to determine whether we successfully removed all of the impurities

present in the original sample. Reults indicated that the method as well as the fraction collection steps were successful (Fig.38).

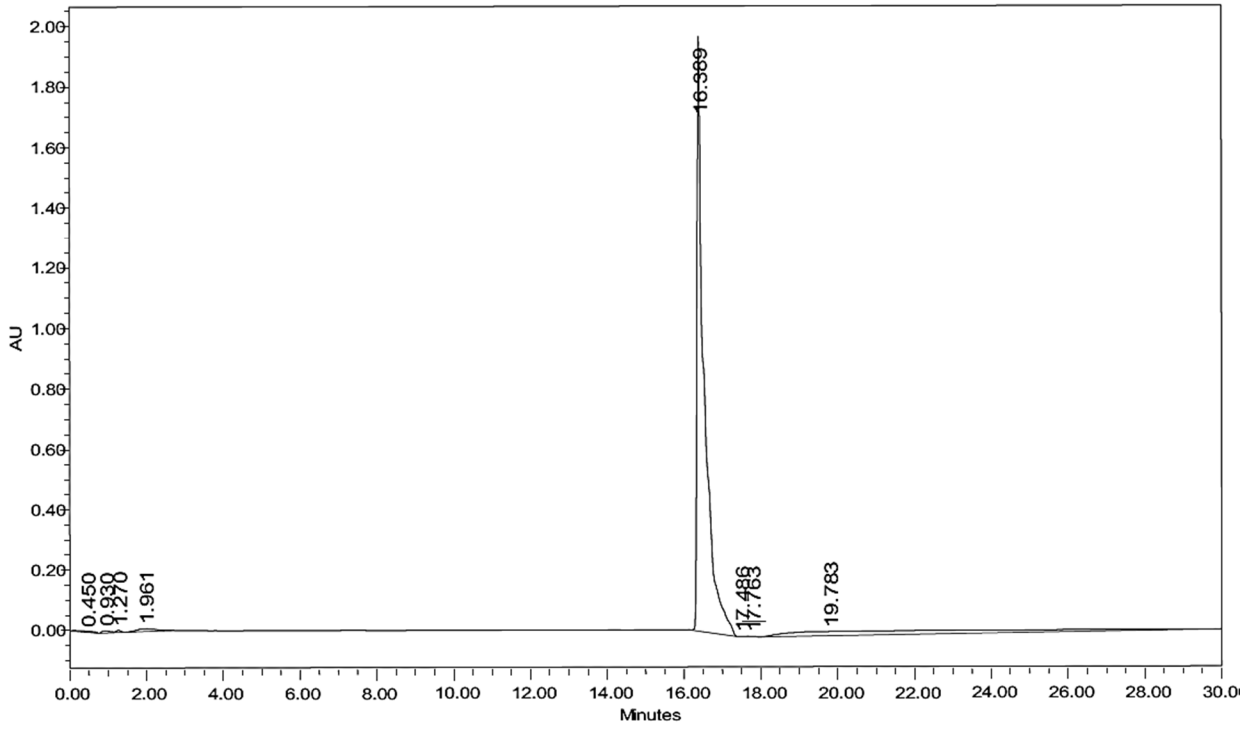

Figure 38: RP-HPLC purified 15 bp amino ssDNA.

Column: XTerra® MS C_{18} 2.5 µm, 4.6 mm × 50 mm column. Mobile phases: A: 5% acetonitrile in 0.1 M TEAA, pH 7.01, B: 30% acetonitrile in 0.1M TEAA, pH 7.01. Flowrate: 1.0 mL/min, Gradient: 80%A to 20%A in 22 min. Column temperature: 33°C, Injection volume: 100 µL. Detection: UV 260 nm.

3.3.5 *Amino ssDNA-BS3-peptide conjugate analysis contd.: MALDI-TOF*

Fig.39 illustrates the mass spectrum obtained from the crosslinked conjugate sample with the experimental conditions from *c, Table 6. These crosslinking experiments were conducted with the RP-HPLC purified starting material (i.e., carefully fraction collected, desalted and lyophilized 5'amino ssDNA). The largest peak appearing at 4935 m/z is attributed to a carbonate salt adduct of the the major product at a peak 4885 m/z. The amino ssDNA-BS3 conjugate is present at 5077 m/z. However, the desired amino ssDNA-BS3-peptide$_1$ peak at 5320 m/z is not observed (Fig.39).

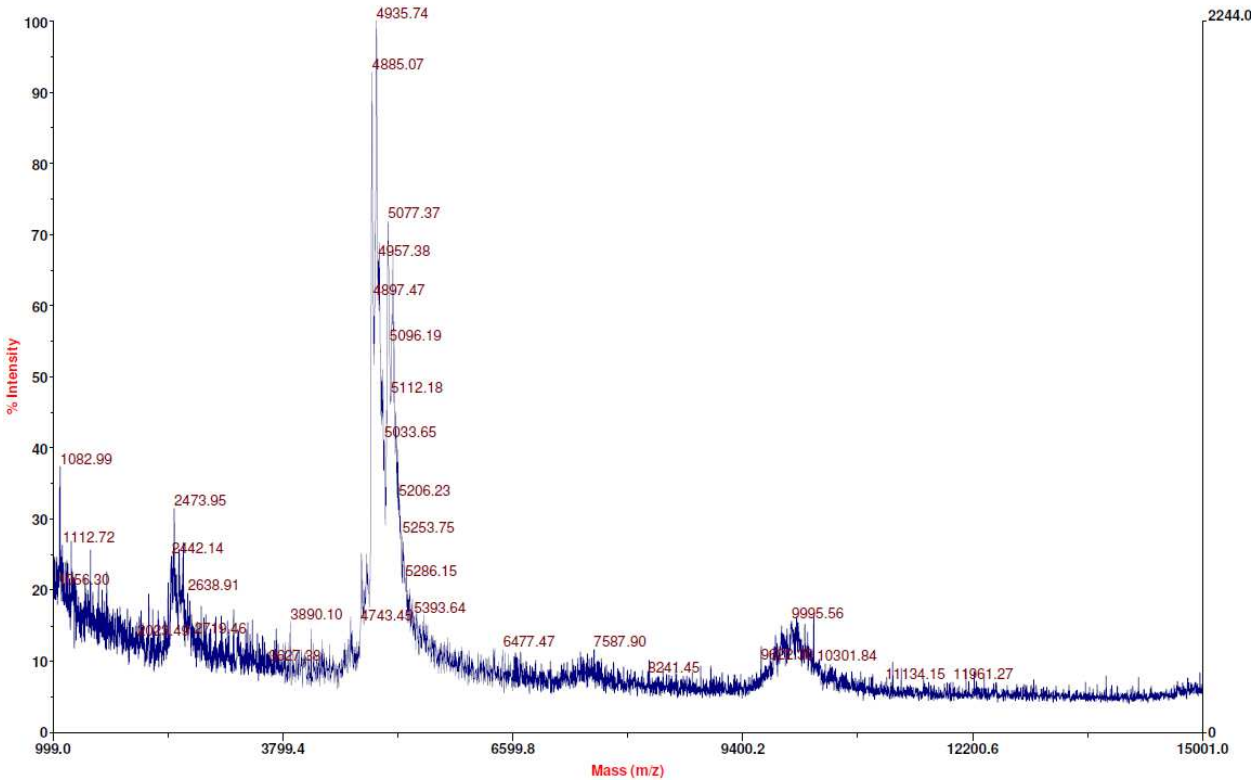

Figure 39: MALDI mass spectrum of conjugate obtained from experimental procedure, *c, Table 6 – RP-HPLC purified starting material (15 bp amino ssDNA).

The reaction carried out with an increased molar amount of peptide$_1$ (designation *d, Table 6) yielded a cluster of peaks (Fig.40). The peak at 4985 m/z is attributed to a salt adduct of the peak at 4884 m/z, which is the partial conjugate structure depicted in Fig.46b. The peak arising at 5082 m/z is attributed to the partial conjugate structure depicted and discussed in Fig. 46a. Results indicate that increasing the molar amount of peptide$_1$ does not have an impact on the extent of bioconjugation.

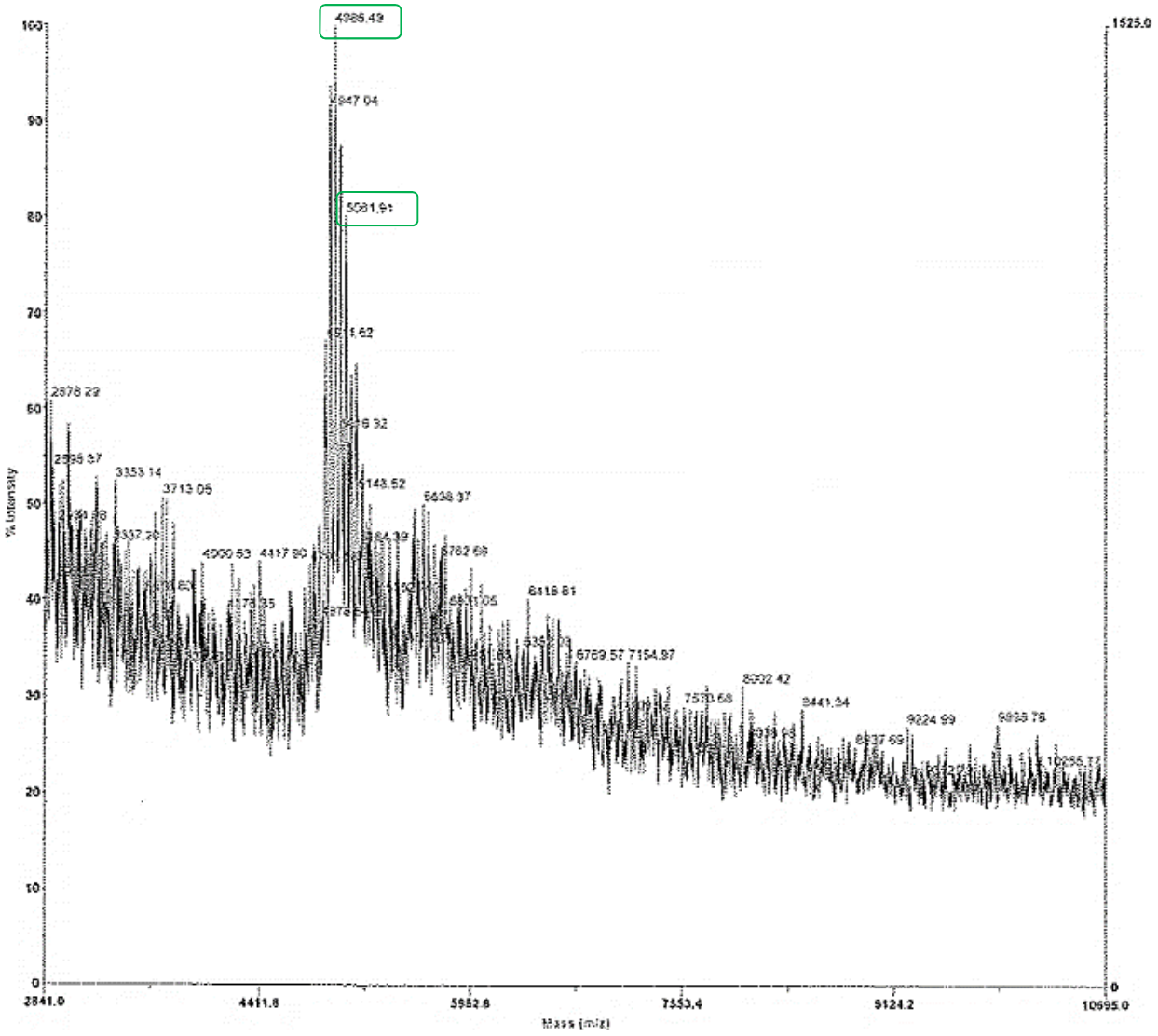

Figure 40: MALDI spectrum of conjugate obtained from experimental procedure, *d, Table 6 – Increased peptide$_1$ mols (1:50:100).

Our results with increased buffer pH did not indicate any bioconjugate products (Fig.41a). The major signals in Fig.41a correspond to the unreacted starting material amino ssDNA at 4730 m/z, and unreacted peptide$_1$ at 595 m/z. There is a peak arising at 981 m/z, which was attributed to a peptide$_3$-BS3 crosslinked. Another peak at 784 m/z could be due to the attachment of BS3 onto peptide$_3$ with one of the NHS groups hydrolyzing away. However, as these peaks are quite low in magnitude compared to the major two peaks, we conclude that increasing the pH of the reaction buffer does not result in the desired ssDNA-peptide conjugation.

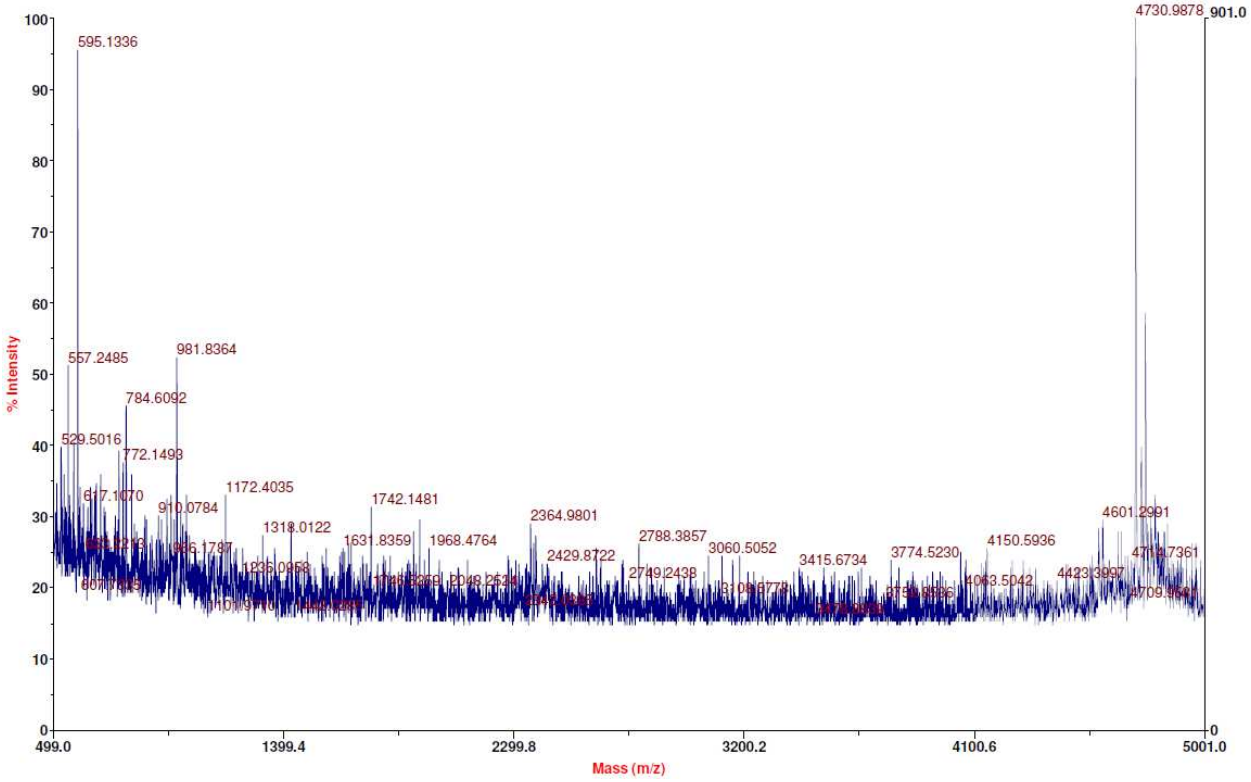

(a)

Figure 41: MALDI spectrum from *e, Table 6 – with peptide$_1$ at buffer pH near its pI

Our attempts with a 100-fold molar excess of peptide$_2$, followed by a two-step protocol yielded the desired amino ssDNA-BS3-peptide$_2$ conjugate (Fig.42a). In these experiments, the intermittent incubation was conducted at 4 °C (*f(a),Table 6). The peak arising at 5324 m/z corroborates with the theoretical molecular weight of the desired final bioconjugate where amino ssDNA is linked to the peptide$_2$ via BS3. Although we observed peaks corresponding to partial conjugation (at 4884 and 5081), we also observed complete bioconjugate formation (Fig.42a).

When the reaction was conducted at an increased temperature of 40 °C (*f(b), Table 6), we observed several peaks corresponding to salt adducts formed with the starting amino ssDNA molecules (Fig.42b). The major peaks were at 5104 and 4986 m/z, owing to salt adduct formations of a partial conjugate. The secondary peak was at 5061 m/z corresponding to a partial conjugate formation where the crosslinker is only attached to amino ssDNA (detailed discussion at Fig.46a).

The measured pH of the final reaction sample mixture was approx. 10. The pH was neutralized to 7.4 by careful addition of 6 M HCl (*f(c), Table 6). After neutralizing the sample, we expected to remove some of the salt adducts which appeared in the MALDI spectrum illustrated in Fig.42b. We observed that the peak at 5104 m/z had disappeared, but the adduct at 4907 m/z is still present (Fig.42c). Although the acid wash was able to yield more clarified peaks, we still observe the peak at 5062 m/z corresponding to the partial conjugate amino ssDNA-BS3, in these spectra as well (Fig.42c).

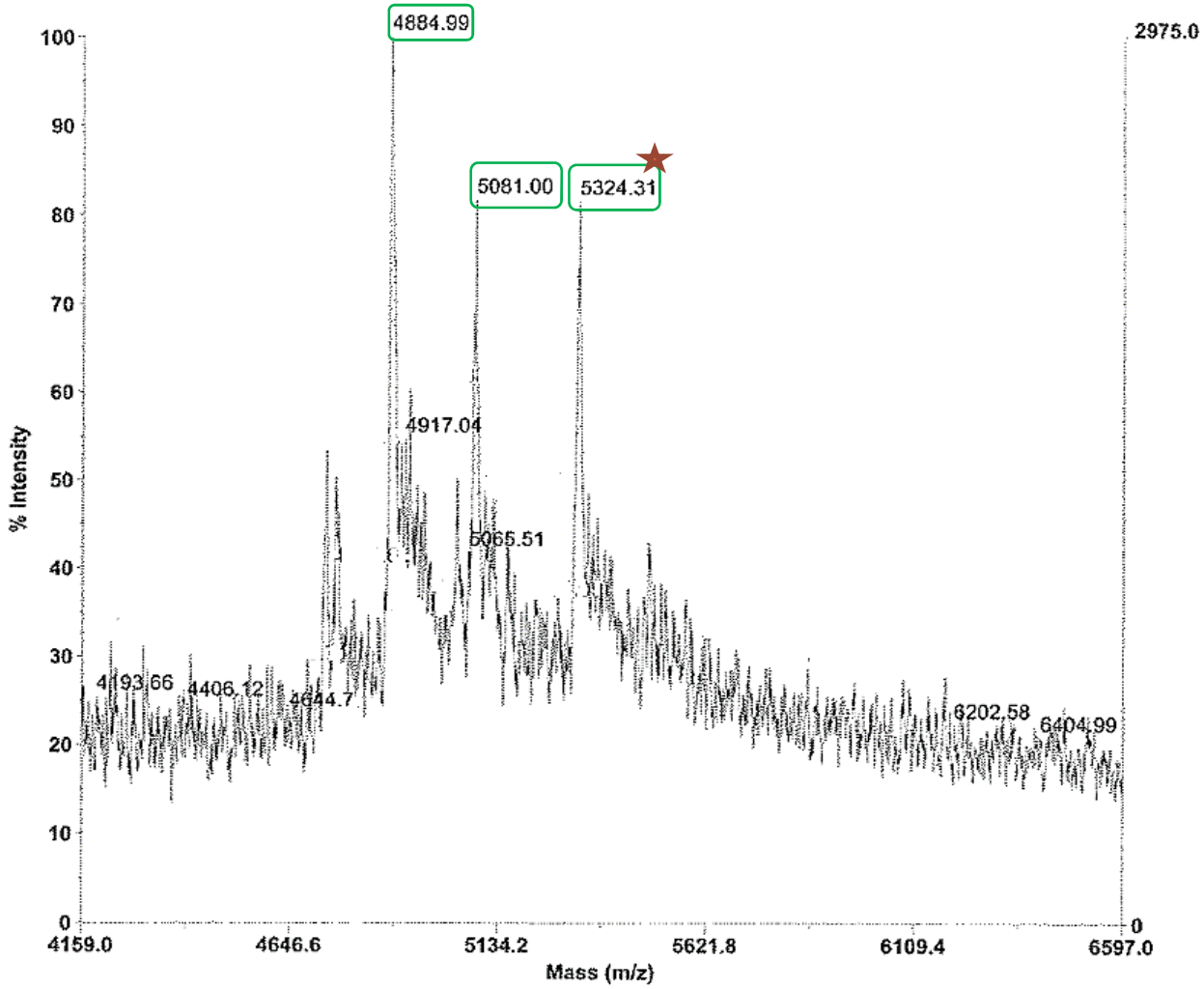

(a)

Figure 42: MALDI results indicating successful linkage of ssDNA to the peptide$_2$ (*fa, Table 6). (a). MALDI spectrum of the conjugate obtained from crosslinking at 40 °C (*fb, Table 6) (b). MALDI spectrum of the conjugate sample from after acid washing to remove adducts (c).

Figure 42 continued

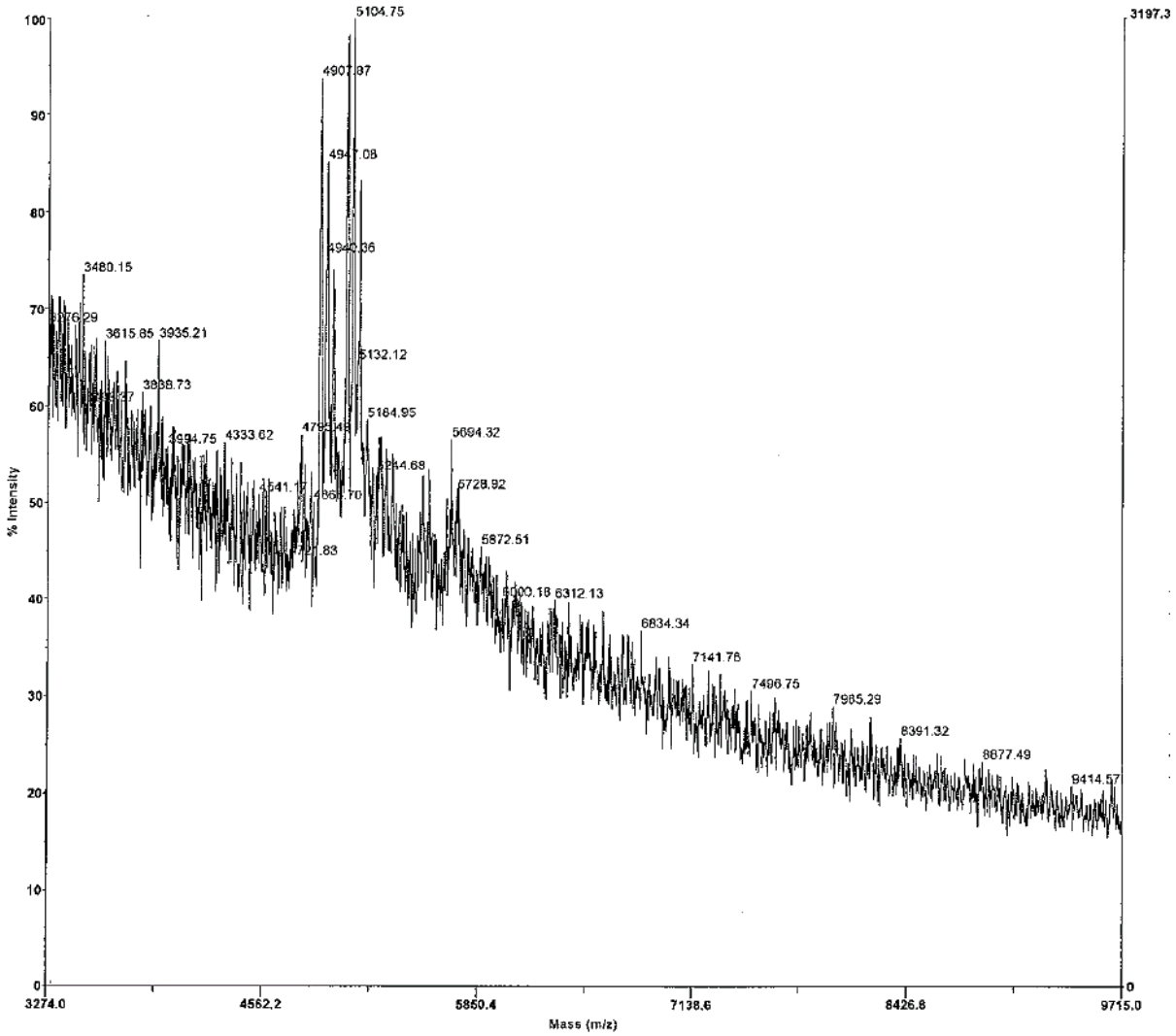

(b)

Figure 42 continued

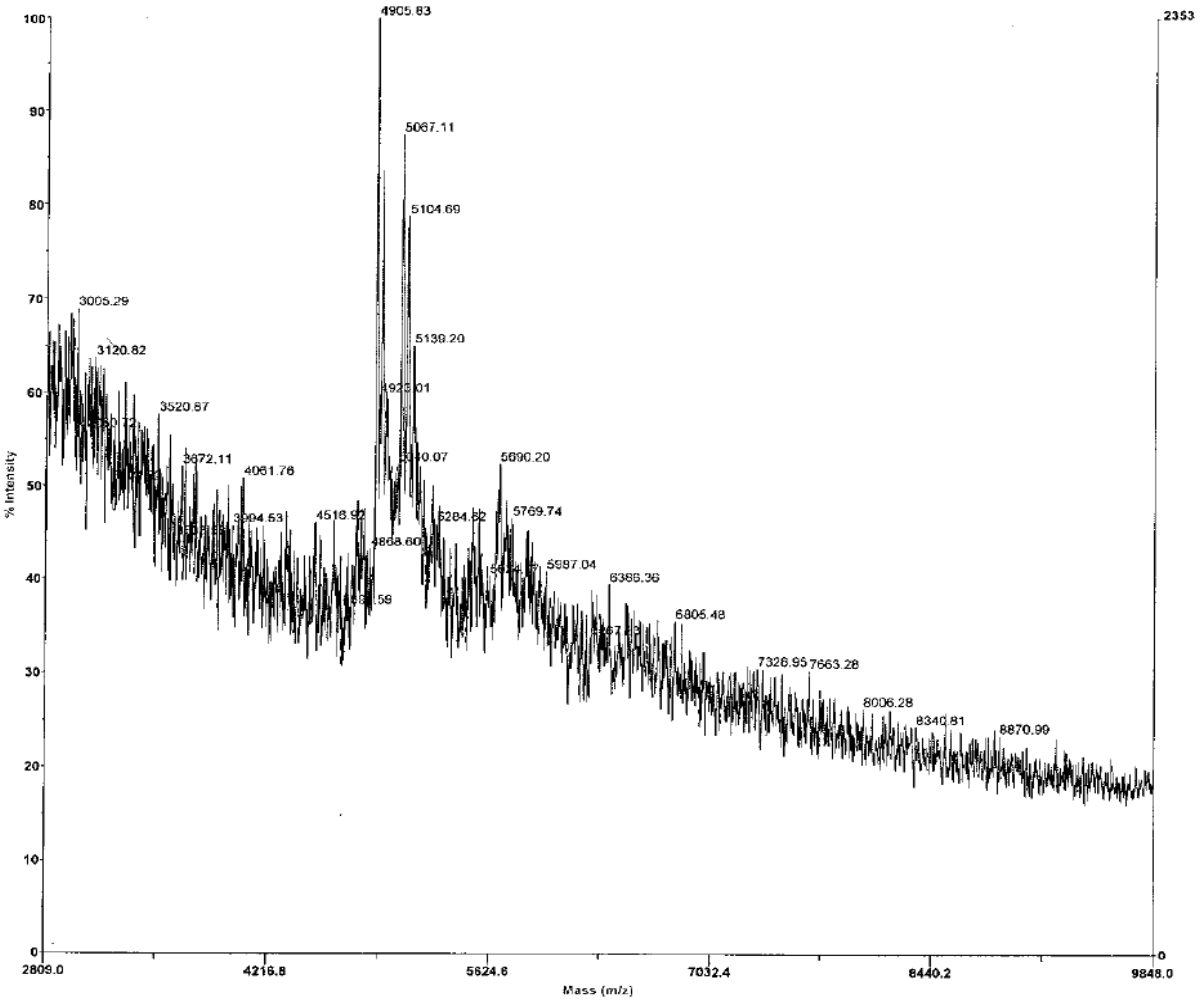

(c)

The successful two-step protocol with a 100-fold peptide molar excess, at 4 °C was repeated to confirm successful duplication abilities of the experiment (*g, Table 6). Although we observed a very weak peak around the expected m/z of 5082, the predominant peaks were still at 4728, and 4884 m/z (Fig.43a). Albeit adding a large molar excess of BS^3 crosslinker to the amino ssDNA, we noticed the possibility of unreacted amino ssDNA (4728 m/z). The peak at 4884 re-appeared in the replicate experiment as well (Fig.43a). The expected bioconjugate molecular weight was not observed in these MALDI results as well.

In Fig.20, the peaks arising at 2444, and 2544 Da are the doubly charged species of the major peaks at 4887 and 5082 m/z respectively. Doubly charged species arise when the molecules

in the analytical sample are ionized in the MALDI-TOF ionization chamber. If two electrons are knocked off from a single molecule in the ionization process, the charge on that molecule is now doubled, and hence the mass to charge ratio is 0.5. Hence, the doubly charged species of the same molecule will have an exact m/z signal at one half of the molecules molecular weight. For example, half of 4887 is 2444 Da.

There were no peaks at 4724 m/z. This observation could be attributed to two possibilities – Either there were no unreacted amino ssDNA, or, the unreacted amino ssDNA did not ionize in the MALDI-TOF laser ablation step. However, the strongest peak of the analytical sample occurs at 4887 Da. As one of the major peaks observed is at 5082 m/z, we concluded that the amino modified ssDNA was attached to one end of the BS3 crosslinkers (n>5) (Fig.43).

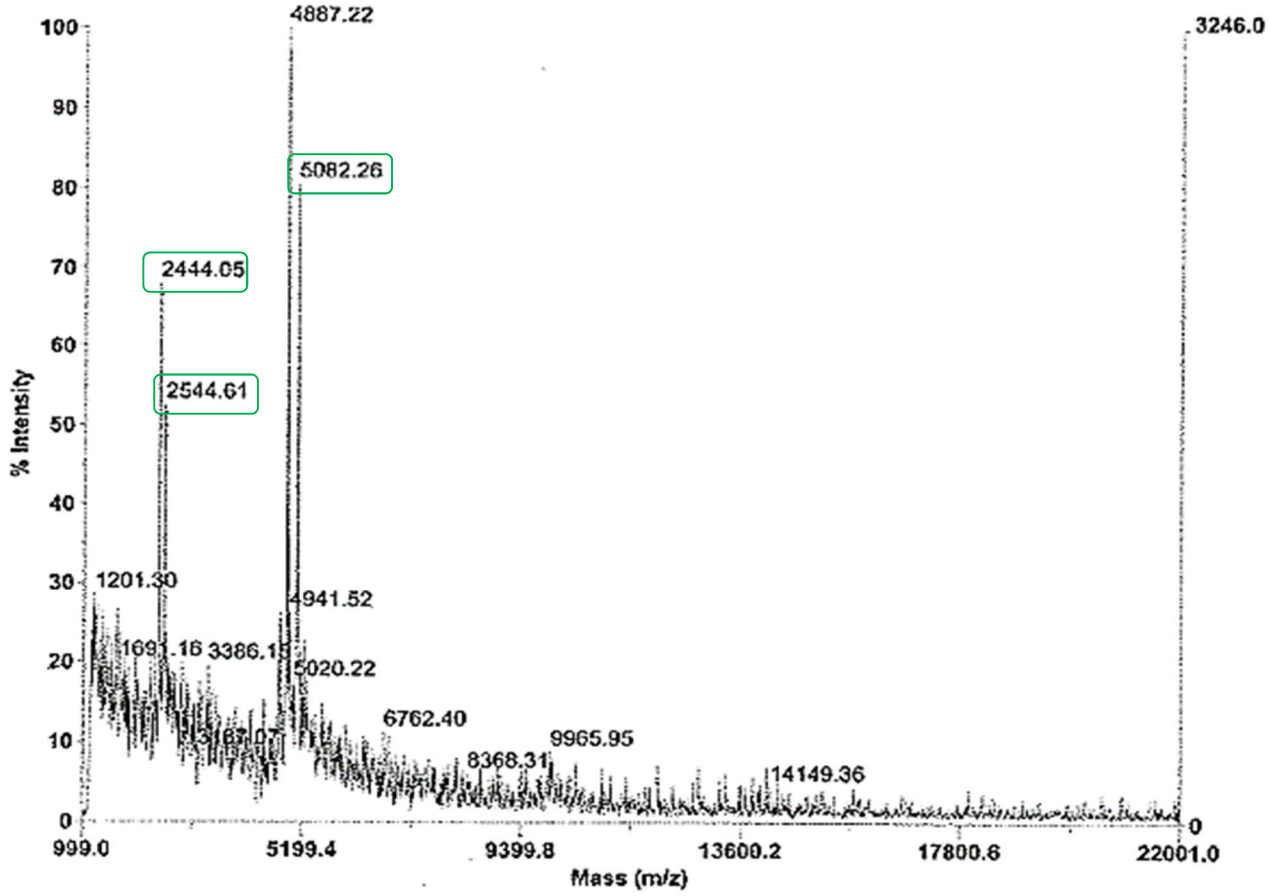

Figure 43: MALDI spectrum of *g, Table 6

When the same experiment was replicated, we obtained the same conjugate molecular weight at 4884 m/z (Fig.44). The peak arising at 4884 m/z was consistent in almost all of our mass spectrometry results.

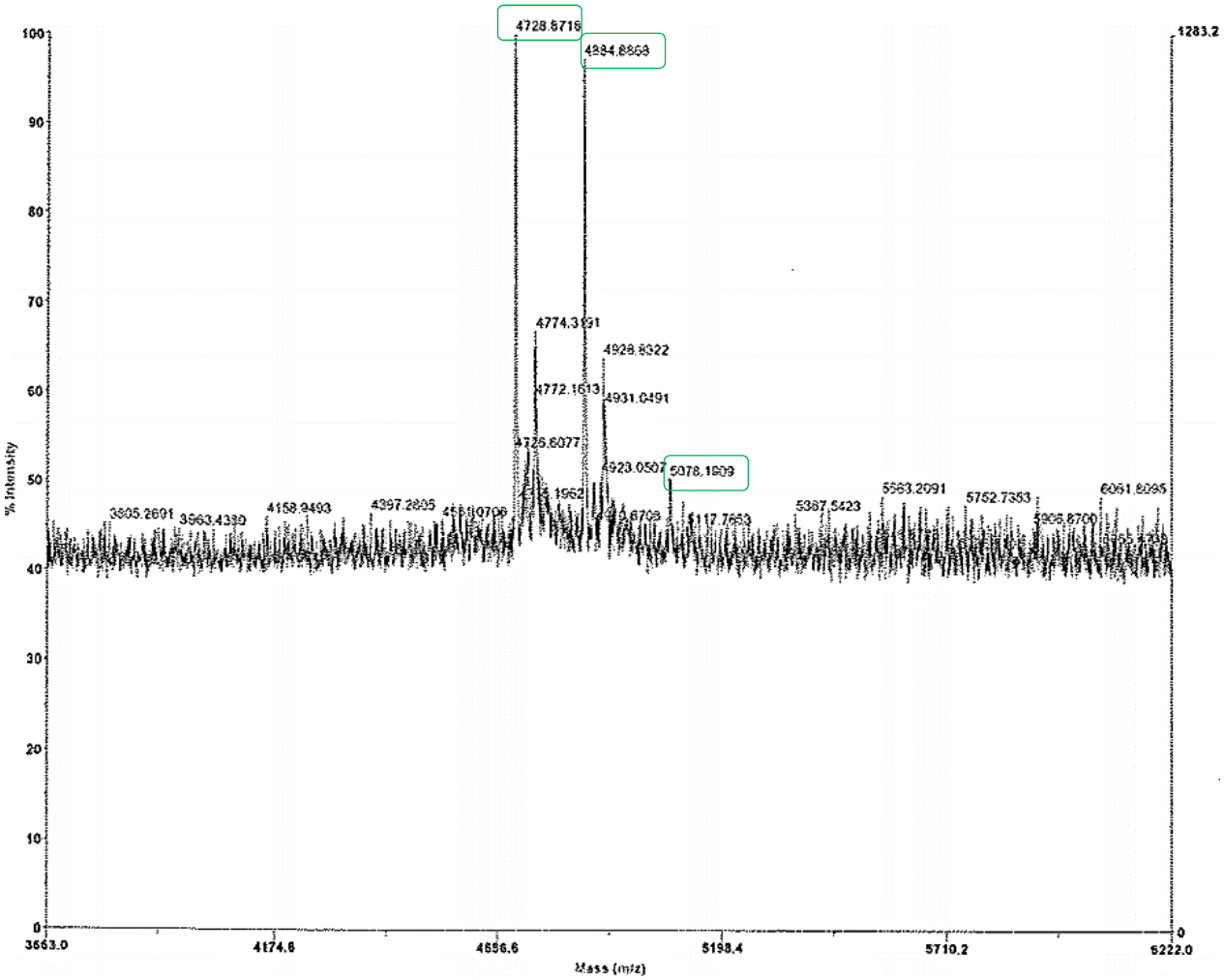

Figure 44: MALDI spectrum from replicates of *g, Table 6.

To discover a plausible attribute to the peak consistently arising at 4882 m/z, we performed mass calculations of the possible moieties. We deduced that this observation could be due to hydrolysis of one of the NHS groups in the BS3 crosslinker. If the amino ssDNA attached to one end of the BS3 crosslinker, while the other sulfo-NHS moiety was hydrolyzed, then the theoretical molecular weight of the resulting molecule is 4882 (Fig.46b). When one of the sulfo-NHS in the crosslinker does not undergo any reaction, it can hydrolyze, as these NHS groups have been recognized as water labile functional groups [16,75]. Therefore, the experimentally observed peak at

4884 Da could be explained by this phenomenon. Although NHS esters have good stability in aqueous conditions, it should be noted that amide bond formation and hydrolysis of the NHS ester both occur competitively. Which means that the susceptibility for hydrolysis is very high. There are several studies which have reported that both hydrolysis and amination increased with increasing the pH. An early study in 1972 reported that at a pH 8.6, and 4 °C the half-life of BS3 was only 10 mins [16]. Therefore, our observation could be attributed to this possibility. Another possibility is one end of the BS3 crosslinker successfully attaching to the amino group at the end of the amino ssDNA, while the other end remaining unreacted. In this case, the corresponding molecular weight of the partial conjugate structural molecular weight is 5079 Da (Fig.46a).

In order to determine whether another peptide sequence with high levels of lysine groups would deliver the expected bioconjugate, *f(a), Table 6 was conducted with peptide$_3$ (*h, Table 6). Results indicated peaks clustered around 5016 – 5762 m/z. These still indicate adducts and partial conjugation products (Fig.45).

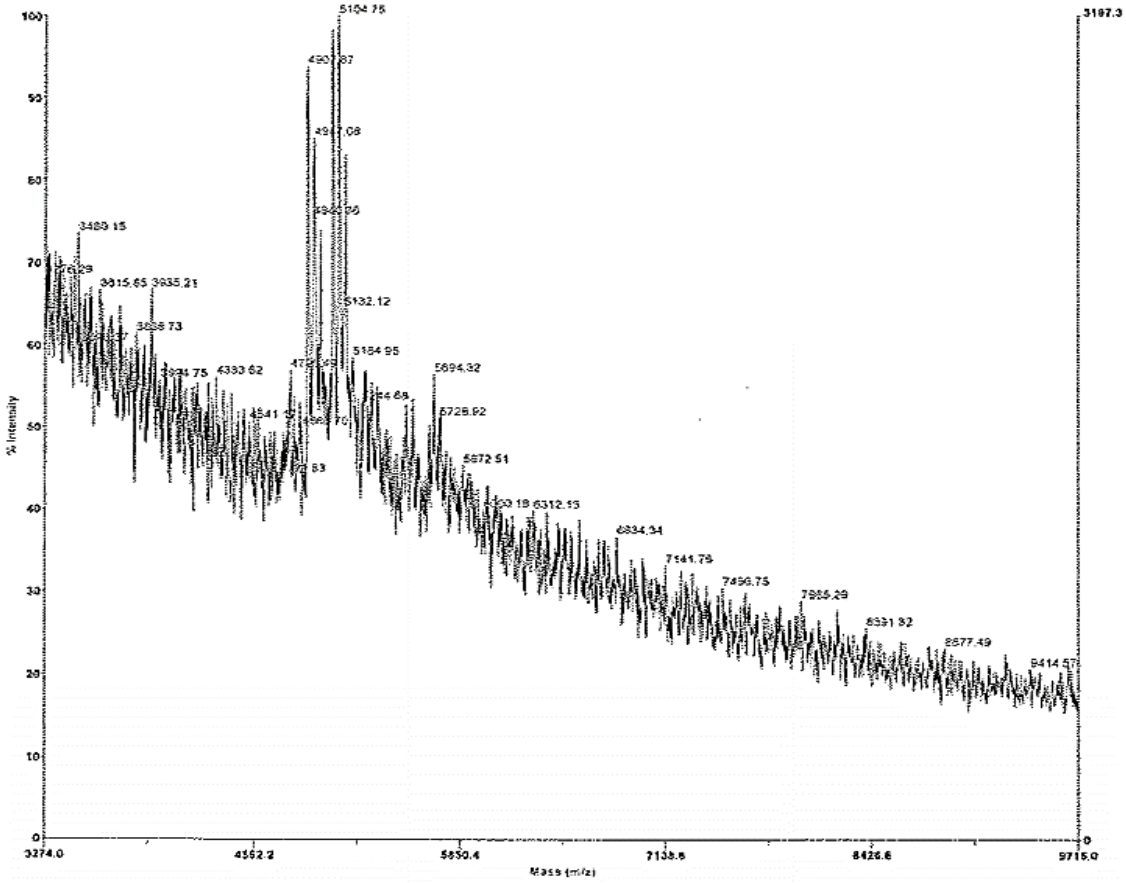

Figure 45: MALDI spectrum of *i, Table 6 – Peptide$_3$ crosslinked with amino ssDNA under *f(a) conditions.

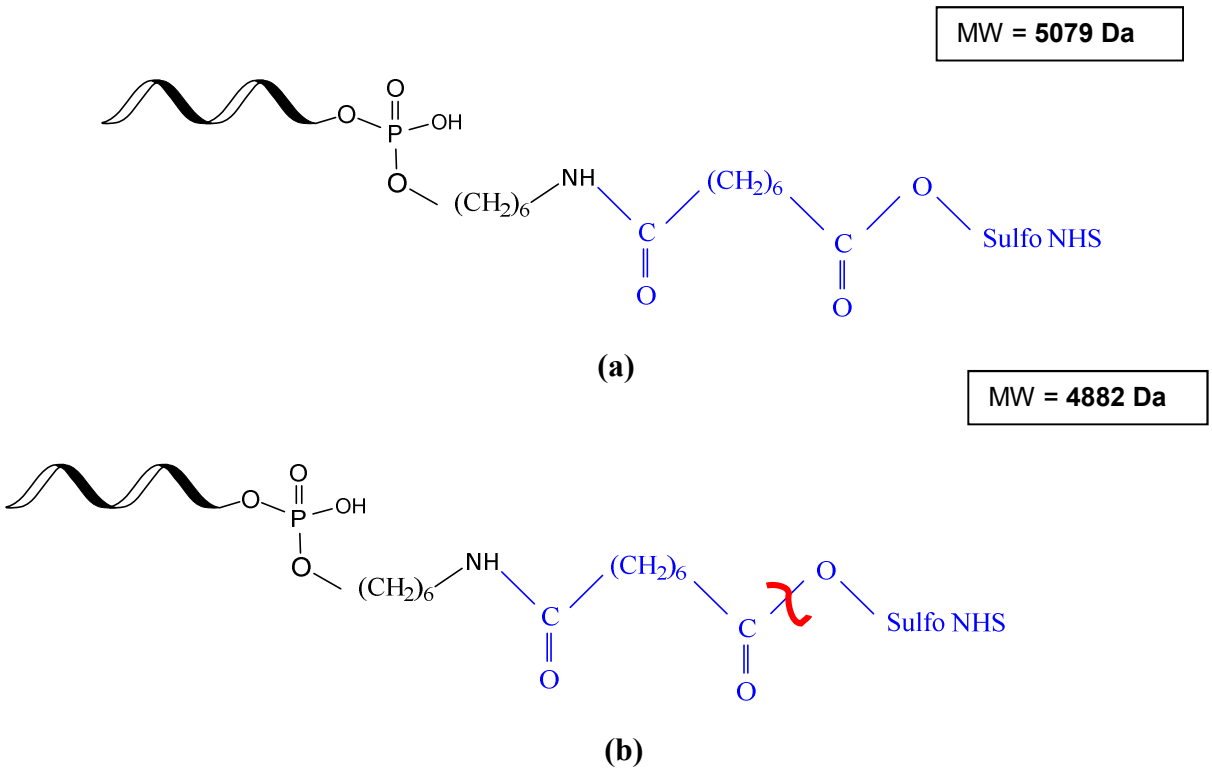

Figure 46: Molecular structures of partial conjugation; Amino ssDNA attached to one end of BS3 (a). Amino ssDNA attached to one end of BS3, while the other end hydrolyzes (b).

As a final attempt to demonstrate BS3 crosslinking, we tested whether the BS3 crosslinker would be successful in crosslinking two peptides. MALDI results does not indicate the expected peptide$_4$-BS3-peptide$_5$ bioconjugate (Fig.24). The molecular weight of the expected bioconjugate is 1402 Da, which was obtained by summing the molecular weights of peptide$_5$, BS3 spacer arm, and peptide$_4$.

However, two strong pieces of evidence suggest that we conjugated two molecules of peptide$_4$ together (Fig.24). First, the final bioconjugate molecular weight of peptide$_4$-BS3-peptide$_4$ is approx. 1250 Da. In our MALDI results, we observe an extremely minor peak in this region.

Furthermore, the major peak is at 686 m/z, which corresponds to unreacted peptide$_5$, hinting that peptide$_5$ did not participate in the reaction.

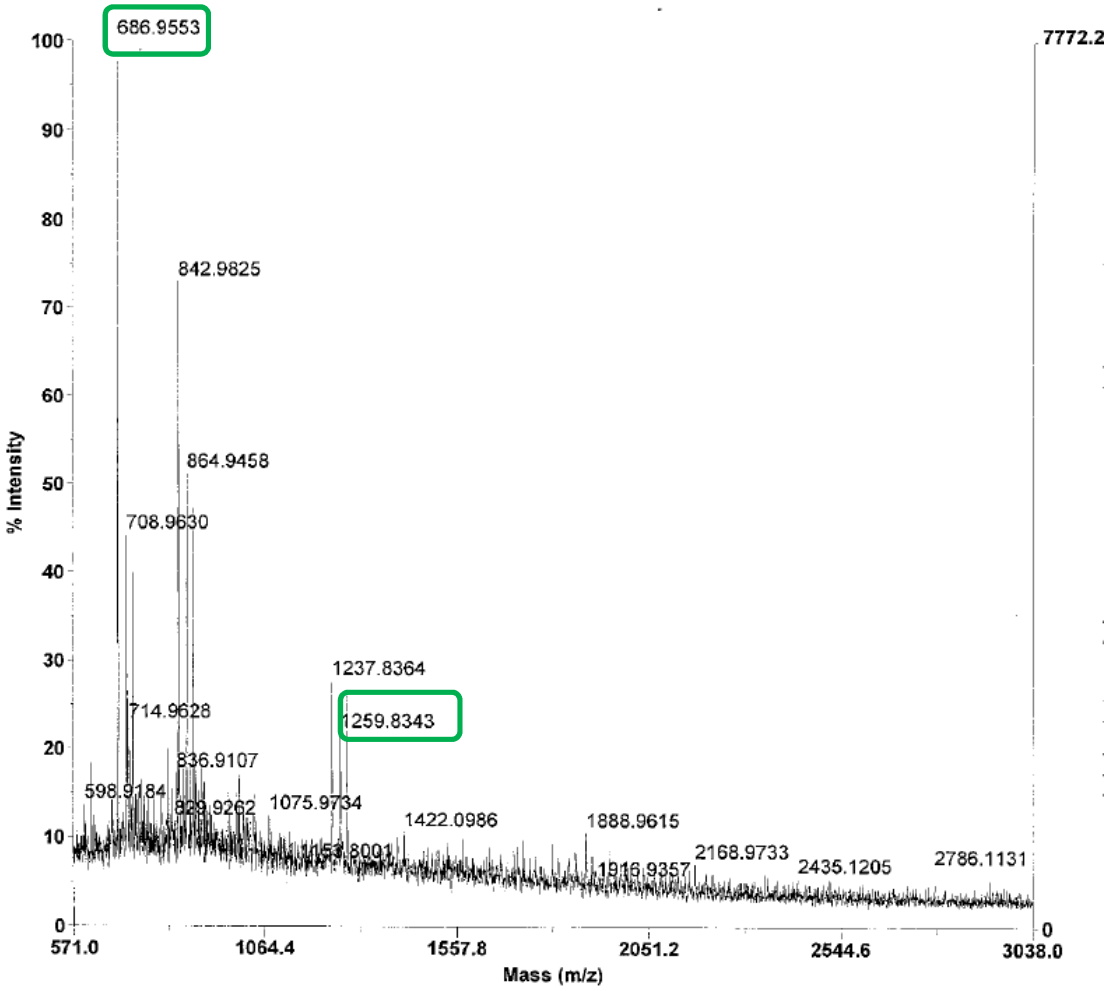

Figure 47: MALDI-TOF spectrum of *i, Table 6 – Peptide$_5$ crosslinked to Peptide$_4$ using BS3.

3.4 Results and Discussion – NHS Diazirine crosslinker.

3.4.1 Phosphoramidated ssDNA-peptide bioconjugate analysis: MALDI-TOF.

The conjugate product samples were characterized via MALDI-TOF. The mass spectra of the starting material phosphoramidated ssDNA is illustrated in Fig.48. The mass spectra of peptide$_4$ and peptide$_5$ are illustrated in Fig.31e and 31f.

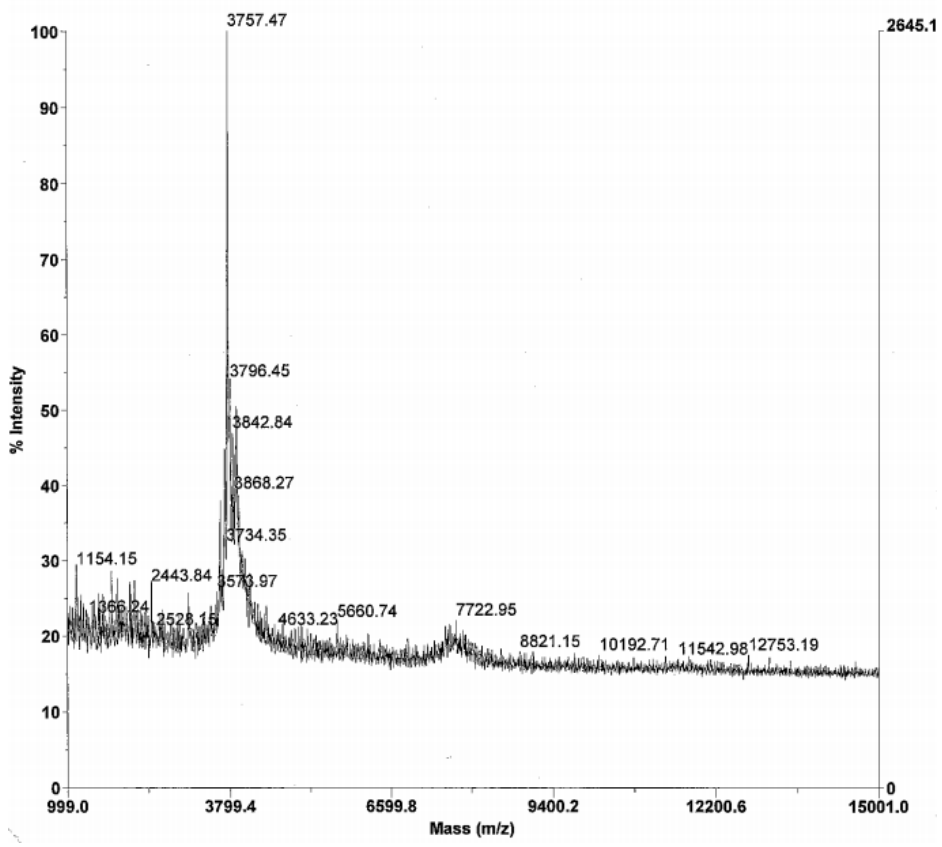

Figure 48: MALDI mass spectrograph of the phosphoramidated ssDNA.

MALDI results from the NHS-Diazirine crosslinking procedures did not indicate a peak at the theoretical molecular weight. The theoretical molecular weight is the summation of the molecular weights of phosphoramidated ssDNA, peptide, and the spacer arm of NHS-Diazirine. The expected MALDI peak of the conjugate was at a m/z of 4528 Da (Fig.49a). However, after the NHS-Diazirine crosslinking procedure was conducted, the resulting sample's MALDI-TOF scan did not indicate a peak at the expected molecular weight (Fig.49b). The peak at 3714 indicates unreacted ssDNA material (from the previous ssDNA crosslinking step), while the peak at 3760 m/z is indicative of the phosphoramidated ssDNA.

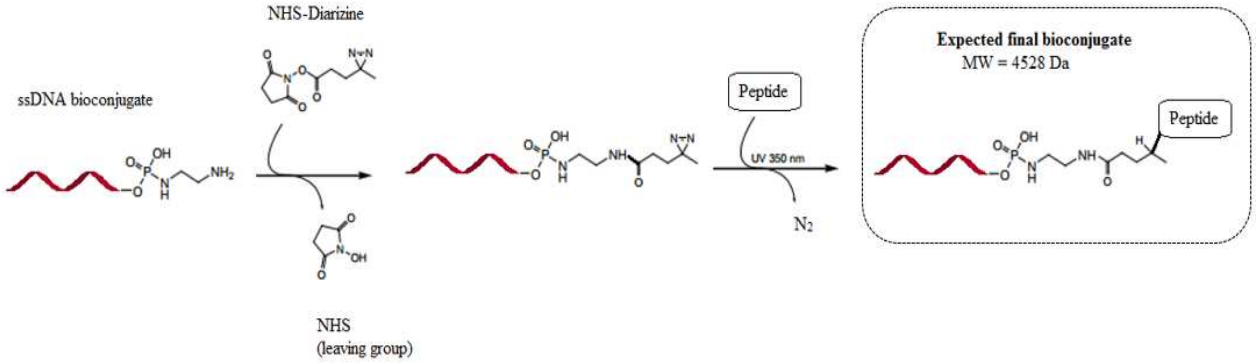

(a)

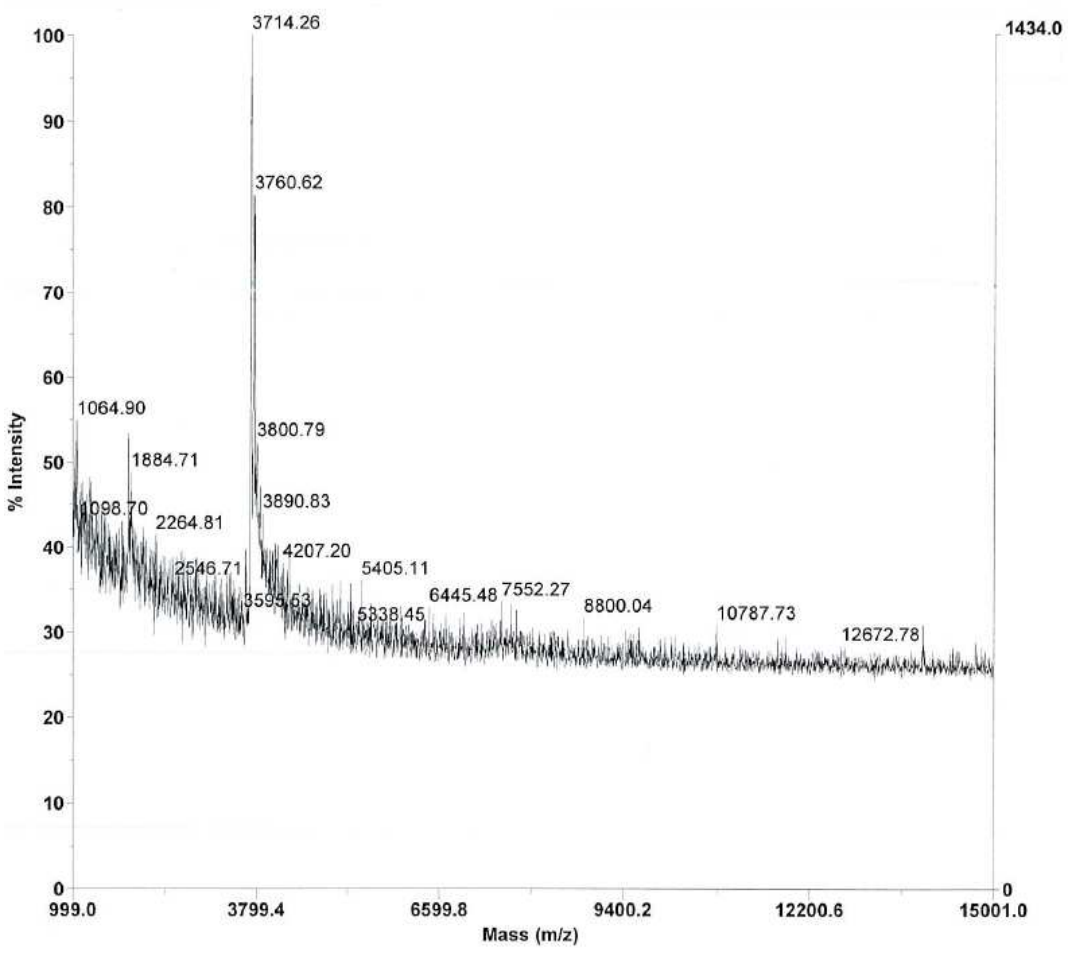

(b)

Figure 49: Schematic of the conducted crosslinking reaction, and the expected final bioconjugate (a). Observed MALDI-TOF results of the ssDNA bioconjugate (b).

3.4.2 Peptide-peptide bioconjugate analysis: MALDI-TOF.

As an attempt to understand whether the crosslinker could conjugate two separate peptides together, $peptide_4$ and $peptide_5$ were crosslinked using the same experimental procedure. The molecular weight of the expected $peptide_4$-diazirine-$peptide_5$ conjugate is 1347 Da, which was obtained by summing the molecular weights of the individual peptides and the NHS-Diazirine spacer arm. However, the observed results only indicate the unreacted $peptide_5$ (at 687 Da), salt adducts of $peptide_5$ (at 701 Da), and what we could speculate as a partial conjugate obtained by NHS-Diazirine crosslinking with one $peptide_5$ molecules (at 768 Da) (Fig.50a).

The NHS-Diazirine crosslinking experimentation conducted with phosphoramidated ssDNA, and $peptide_5$ did not indicate a peak at the expected bioconjugate molecular weight of 4526 Da (Fig.50b). The major peak at 3711, and 3754 indicates the unreacted phosphoryl ssDNA, and phosphoramidated ssDNA.

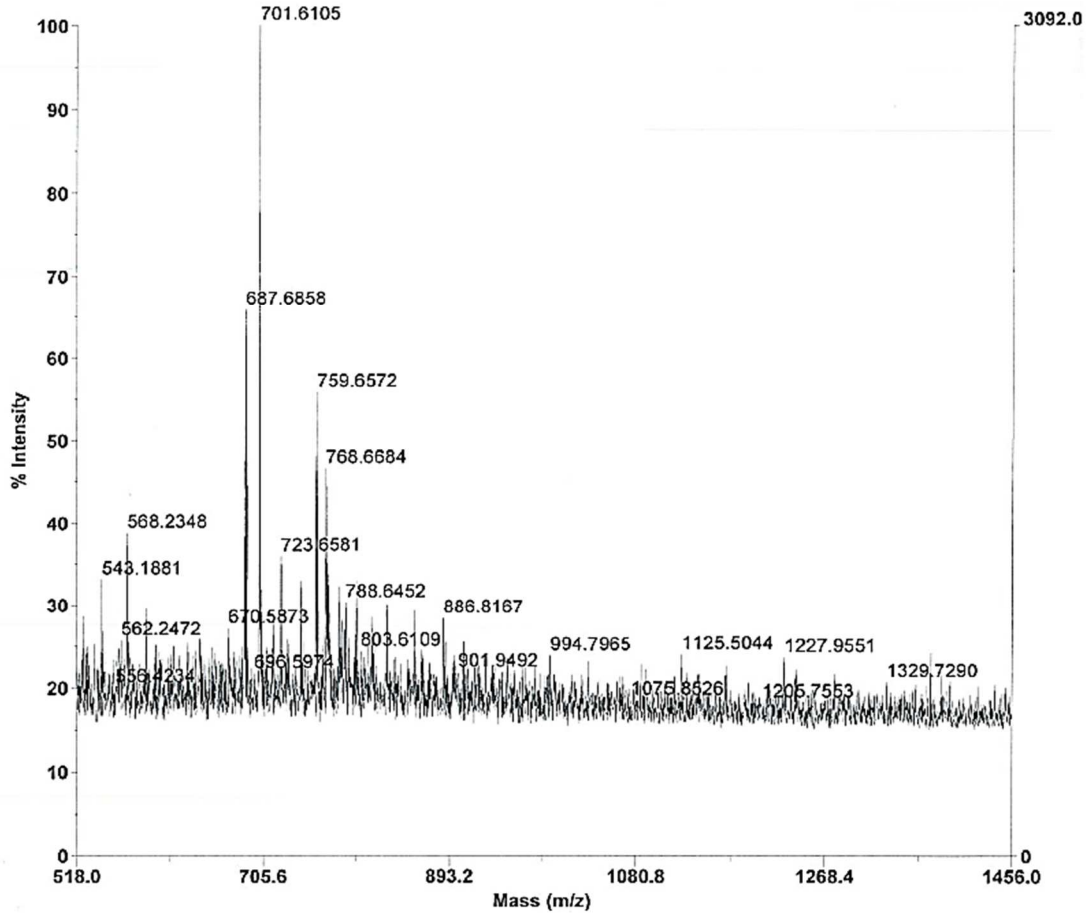

(a)

Figure 50: Observed MALDI-TOF results of; peptide$_4$-diazrine-peptide$_5$ (a). Phosphoramidated ssDNA-diazirine-peptide$_5$ (b).

Figure 50 continued

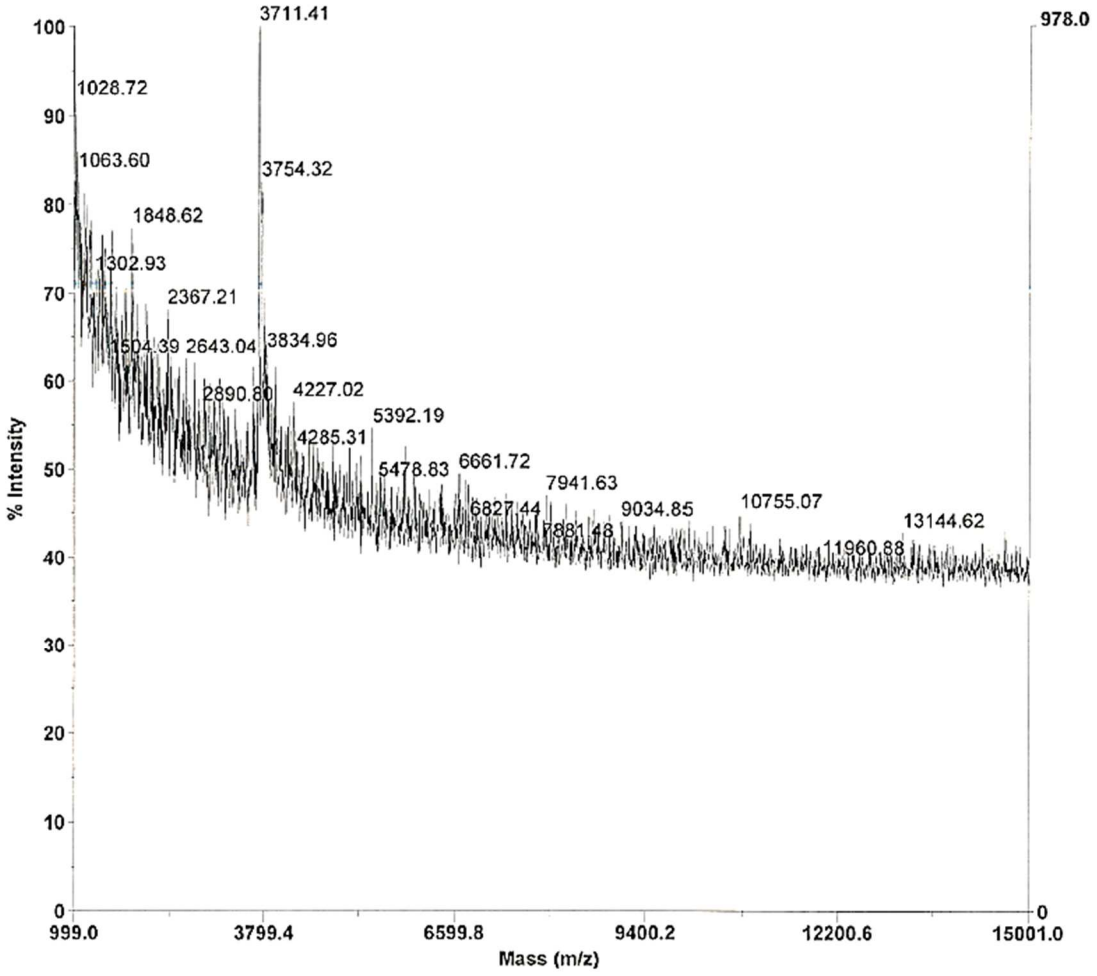

(b)

When peptide$_4$ and peptide$_5$ were reacted with only a 20-fold molar excess of NHS-Diazirine (as opposed to the previously used 50-fold molar excess w.r.t to the peptides) results indicated successful peptide$_4$-diazirine-peptide$_4$ conjugation. Although the desired peptide$_4$-diazirine-peptide$_5$ conjugate was not observed, interestingly, we observed two peptide$_4$ molecules conjugated together. The theoretical molecular weight of a peptide$_4$-diazirine-peptide$_4$ conjugate is 1235 Da. And the observed molecular weight from MALDI was 1228 Da (Fig.51).

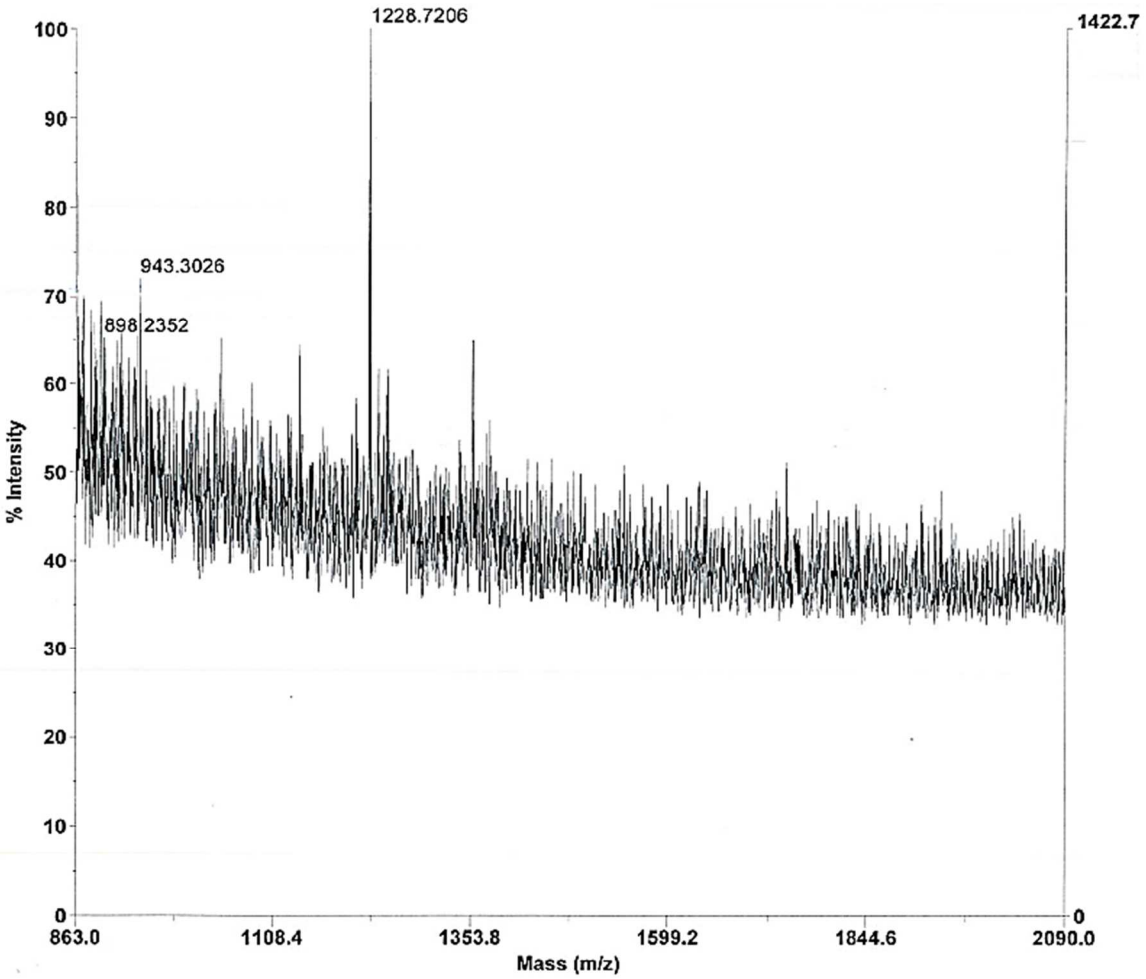

Figure 51: MALDI-TOF results indicating peptide$_4$-diazirine-peptide$_4$ conjugate formation.

3.5 Conclusions

In conclusion, we were able to crosslink BS3 to the amino terminal end of the 5'amino ssDNA. However, the primary amines in the peptides did not crosslink to the BS3 crosslinker. Results from Fig.24 (*i, Table 6), as well as Fig.19 (*fa, Table 6) both indicate that perhaps the most important factor to consider during peptide crosslinking is the pI of the peptide. Both of these figures illustrate that when peptide$_2$ and peptide$_4$ were used, the BS3 crosslinker was successful in crosslinking with them (albeit with low yields).

We report our results from Fig.19 and Fig.24 as the major evidence to state that the net charge of the peptide sequence should be seriously studied prior to conducting crosslinking with BS3. Although we chose three peptides (peptide$_1$, peptide$_3$, peptide$_5$) which has several amino

groups, and conducted experiments in pH 8 – 9.9 buffers, in order to deprotonate the ammonium groups we were unable to observe successful bioconjugate formation using the BS crosslinker. The purpose of increasing the buffer pH was to increase the nucleophilicity of the ammonium group in the lysine residues. The conjugate base of ammonium is always a stronger nucleophile, as nucleophilicity increases with increasing electron density on an atom. However, our experimental evidence suggest that unless the buffer solution pH does not exceed the pI of the peptide, the peptide is perhaps not fully deprotonated, and hence does not undergo any crosslinking. Therefore, if highly basic peptide sequences (pI >10) are used, we must use a solution which has a buffer pH >10 as well. Our results indicate that such high buffer systems do not yield any BS3 crosslinking. At such high pH values, the sulfo-NHS group in the BS3 crosslinker also faces high risks of hydrolyzing. When the sulfo-NHS group is hydrolyzed, the crosslinker no longer holds a reactive functional group to react with external primary amines.

The isoelectric point (pI) of a protein or peptide is defined as the pH at which the molecule contains no net charge. When the pH of the buffer used to dissolve the peptide is greater than the calculated pI of the peptide, the peptide will carry an overall negative charge, and vice versa (i.e., pH > pI, peptide has a negative charge). We obtained successful peptide conjugation results when we used peptides which contained a positive charge when dissolved in a buffer at pH 7.5 – 9.5. At a pH of 8.5, the acidic peptide sequence ($peptide_4$) is fully deprotonated at pH = 7.5. This may have caused complete deprotonation of the amino groups present in the lysine groups, resulting in a successful S_N reaction, leading to bioconjugation.

These results from the NHS-Diazirine experimentation also point in the direction of the major speculation derived from the BS3 experimentation results. Perhaps the pI of the peptide plays the biggest role in crosslinking with heterobifunctional crosslinkers as well. This is supported by the evidence we obtained from the crosslinking trials with $peptide_4$ and $peptide_5$. When equi-molar amounts of $peptide_4$ and $peptide_5$ were crosslinked with NHS-Diazirine, $peptide_5$ did not indicate any reaction at all. Instead, $peptide_4$, with the lowest pI value indicated successful bioconjugation with another $peptide_4$ molecule. This is perhaps due to the fact that when $peptide_4$ (having the lowest pI out of all the peptides used) was dissolved in the buffer system (PBS, pH 7.2±0.2), either the NH_2 in the Glutamine, or the N-terminus were fully deprotonated, allowing for a successful S_N2 type reaction with the NHS group of the NHS-Diazrine crosslinker.

In conclusion, if either BS3 or NHS-Diazirine crosslinkers were to be used in crosslinking trials, instead of choosing a peptide sequence which has a high pI (i.e. a basic sequence), a more acidic sequence should be chosen. This way, converting the ammonium groups (NH_3^+) to amino groups (NH_2) could be accomplished at pH values which does not hydrolyze the sulfo-NHS group in the BS3 crosslinker.

CHAPTER 4. DEMONSTRATING THERMALLY PROGRAMMABLE HYBRIDIZATION OF DNA

4.1 Abstract

This chapter discusses our studies related to determining the ability of single stranded DNA (ssDNA) to spontaneously hybridize with its complimentary sequence in an altered annealing protocol. In our altered protocol, the generally used hybridization temperature of 90 °C was reduced to 45 °C. In DNA hybridization protocols, the ssDNA mixture (i.e., equimolar amounts of ssDNA, and its complimentary ssDNA) is heated to very high temperatures in order to relieve the single strands from secondary structures such as hairpins. Secondary structures hinder proper DNA base pairing, leading to poor DNA hybridization. However, in thermal facilitation of glucose oxidase-ssDNA, and horseradish peroxidase-ssDNA conjugate assembly, utilizing such high annealing temperatures would degenerate the enzyme conjugates. Therefore, possibilities of accomplishing DNA hybridization at lowered annealing temperatures was investigated. The theory of hyperchromicity effect (UV absorption) was utilized to obtain qualitative data (n=6). UV study results indicate that even at a lowered annealing temperature of 45 °C, the expected hyperchromicity effect was observed. These results were also comparable to the annealing protocols conducted at the general temperature of 90 °C.

4.2 Introduction

4.2.1 Deoxyribonucleic acid (DNA)

A double stranded (i.e., double helical) DNA is comprised of two strands that run anti parallel to each other. The building blocks of the DNA structure are four nucleotide bases namely Adenine, Thymine, Cytosine, and Guanine (Fig.52a). Each base attaches to a sugar molecule, and a phosphate molecule. Altogether, the base, sugar, and the phosphate are referred to as a nucleotide. The phosphates form phosphodiesterase bonds to form a long oligonucleotide strand which is also referred to as single stranded DNA (ssDNA) (Fig.52a). The conjugated electrons in the ring structures of these nucleotide bases causes DNA to exhibit absorbance properties in the UV range. In UV-Vis spectrophotometric analyses, DNA has an absorbance maxima at 260 nm.

Each Guanine in one strand will form two H-bonds with a Cytosine in the opposite strand. Each Thymine in one strand will form three H-bonds with Adenine in the opposite strand (Fig.52b). This process alongside stacking interactions between nucleotides allows for DNA hybridization, and stabilizes the final double stranded DNA (dsDNA). In DNA complementarity (i.e., complimentary hybridization) when the nucleotides of one strand is aligned anti-parallel to the complimentary strand, they form very specific base pairs. This complementarity was first demonstrated by Watson and Crick. DNA denaturation, and/or DNA melting refers to the process of breaking the H-bonds between the base pairs, forming two single stranded DNA. For the purpose of all discussions in this thesis, DNA hybridization, annealing and DNA renaturation are used interchangeably.

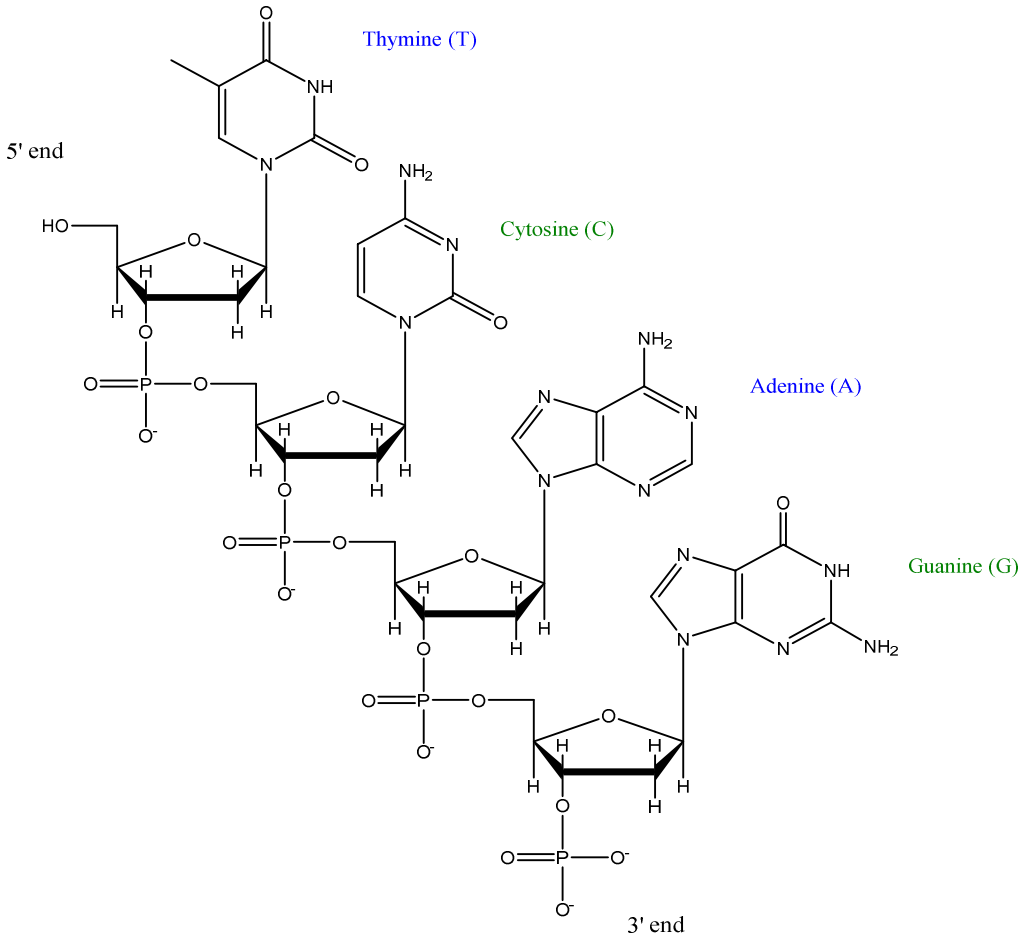

(a)

Figure 52: Illustration of the four building blocks (A, T, G, C nucleotides) of DNA, attached to a phosphate backbone (a). Deoxyribonucleoside base pairing facilitated by H-bonds (b).

Figure 52 continued

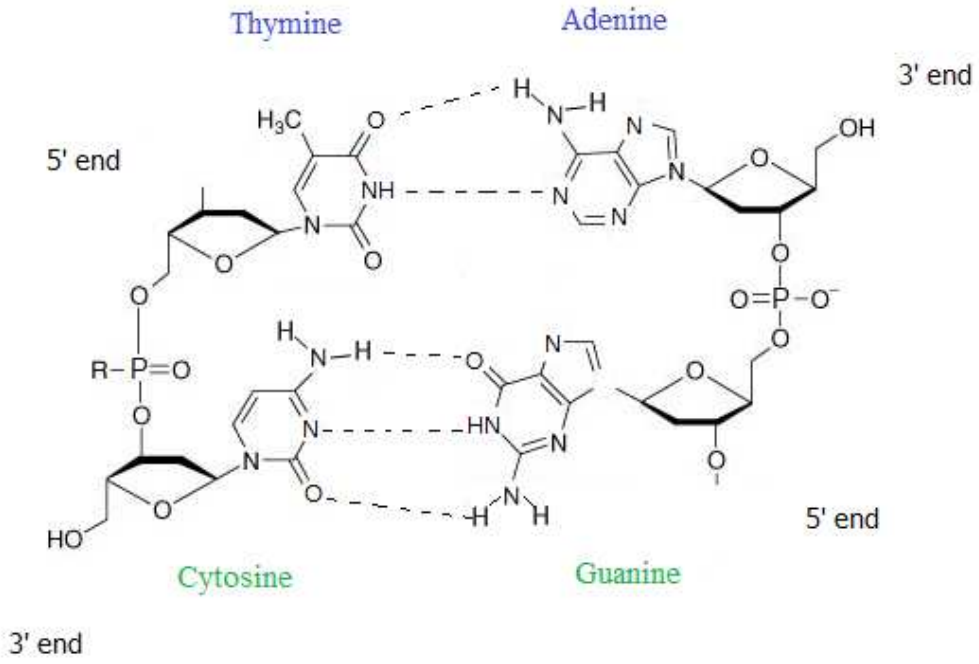

(b)

4.2.2 DNA profiling

DNA molecules are long strands found tightly wound in chromosomes which are contained in the nucleus of each human cell. Within each DNA strand are numbers of genes that determine the particular characteristics of an individual. DNA profiling which is also known as DNA fingerprinting, is the process of determining an individuals genetic makeup called a DNA profile. These DNA profiles differ in each individual. Therefore, it is a very common methodology used in forensic investigations, to identify individuals involved in a crime incident, by collecting biological samples (e.g. hair follicles, saliva, blood, skin) from the crime scene. It is also commonly used in paternity tests. Currently, there are three very common methods for DNA profiling.

The most common method is the famous polymerase chain reaction (PCR) technique. In this technique, extremely small amounts of DNA are collected from biological samples. Next millions of copies of it are made from it, using the PCR amplification steps. This creates enough DNA to allow scientists to generate the DNA profile of the individual. Another method called

restriction fragment length polymorphism (RFLP) analyzes the length of the strands of the DNA molecules with repeating base pair patterns. While about 5% of the gene compositions on DNA contain genetic information, the other 95% do not. These non-coding genes contain identifiable repetitive sequences of base pairs, which are called variable number tandem repeats (VNTR). In this technique, a Southern blot is performed and the DNA is analyzed via a radioactive probe. The restriction fragment length polymorphism analysis is used to detect the repeated sequences by determining a specific pattern to the VNTR, which becomes the individual's DNA fingerprint. The drawback with this system is that it requires a considerable amount of DNA in order to be used. Another method called short tandem repeat (STR) is a technique which is also based on features of PCR. It determines how many times the base pairs repeat themselves on a particular location on a strand of DNA [90].

4.2.3 Determining DNA characteristics

As opposed to DNA profiling, in many life science fields, scientists wish to reveal information about the DNA's identity, size and abundance. PCR techniques discussed above determines the DNA make up, but not physical characteristics of it. Southern Blotting is a famous technique used to separate DNA fragments from a sample, based on the fragments size. In this technique, DNA are first digested (i.e., not denatured, but cut into smaller pieces) using restriction enzymes. Next, they are separated according to the size of each fragment via non denaturing gel-electrophoresis. Afterwards, the DNA fragments are transferred to a nitrocellulose or nylon membrane support resulting in immobilization of the DNA. Due to this immobilization, the membrane carries a semi-permanent reproduction of the banding pattern of the gel. The immobilized DNA is covalently attached to the nylon membrane by briefly exposing the membrane (i.e., blot) to UV light. Transferring the DNA to the sturdy membrane is necessary because the fragile gel would fall apart during the next two steps in the process. Next, the membrane is bathed in a solution to denature (double stranded made single stranded) the attached DNA. Then a hybridization solution containing a small amount of single-stranded probe DNA that is complementary in sequence to a target molecule on the membrane. This probe DNA is labeled using fluorescent or radioactive molecules, and if the hybridization is performed properly, the probe DNA will form a stable duplex only with those DNA molecules on the membrane that are exactly complementary to it. Then, the non-hybridized probe is washed off and remaining

radioactive or fluorescent signal will appear in a distinct band when appropriately detected. Detection methods include autoradiography, Ethidium Bromide exposed to UV light, SYBR green fluorescent dye gel scanned with laser, and silver staining followed by photo development. The bands represents the presence of a particular DNA sequence within the mixture of DNA fragments [91]. The overall procedure of the Southern Blotting technique is illustrated in Fig.53.

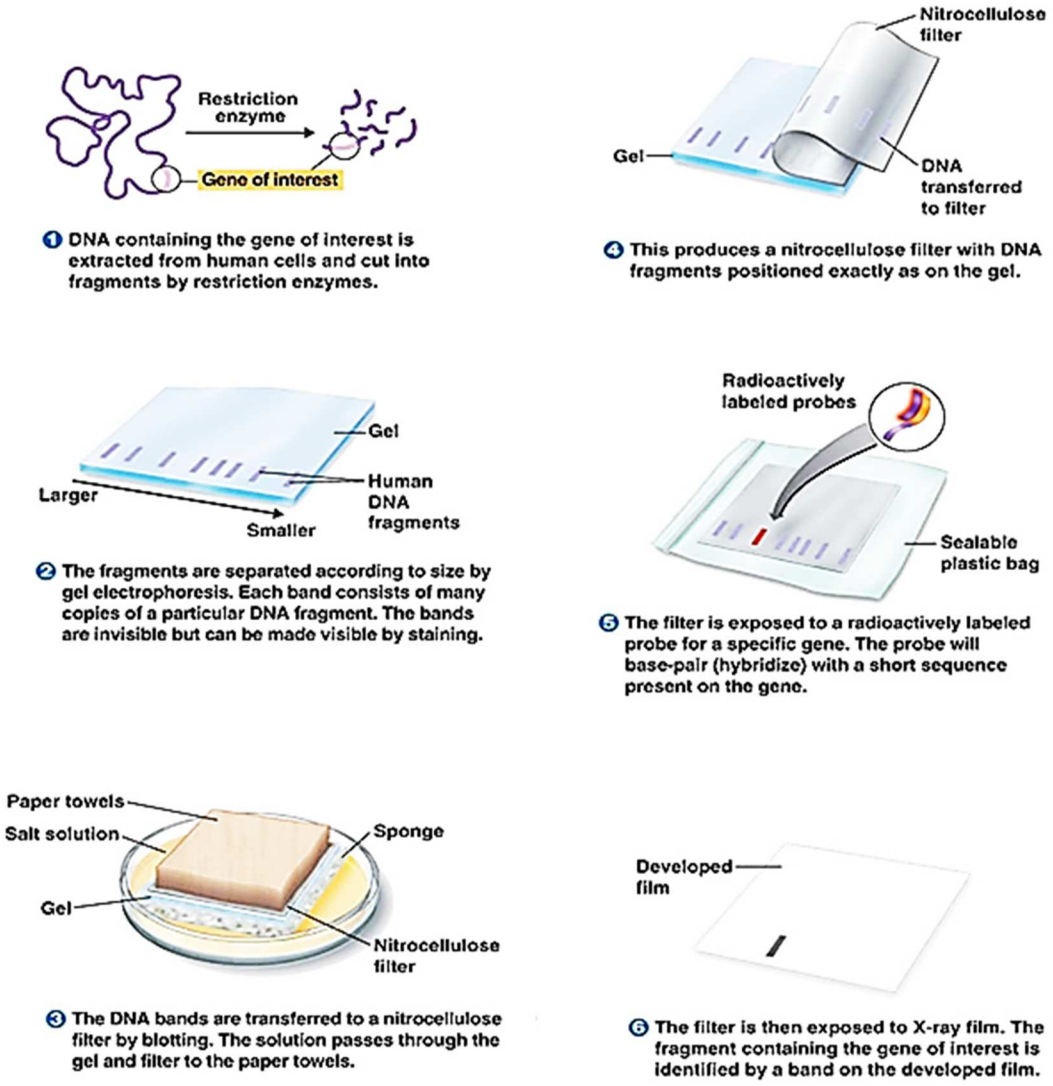

Figure 53: Schematic of the Southern Blotting procedure
[Copyright© Pearson Education, Inc.]

Native or non-denaturing gel electrophoresis is performed in the absence of sodium dodecyl sulfate. On the contrary, SDS-PAGE (sodium dodecyl sulfate polyacrylamide gel

electrophoresis) is a bioanalytical method where the proteins in a given sample are first denatured using the anionic surfactant SDS, and heating. This treatment forces unfolding of the preliminary tertiary structure of proteins. Next, these treated protein sample containing a mixture of fragments is introduced to the separation medium, which is the polyacrylamide gel. The electrophoretic mobility of protein fragments depend primarily on their molecular mass.

4.2.4 Optimizing DNA hybridization

As mentioned previously, DNA hybridization is the phenomenon of forming hydrogen bonds formed in between the A=T, and G≡C base pairs. To hybridize DNA in an aqueous system, optimizing and determining the synergistic effect of at least three main factors was important – *The melting temperature, salt concentration of the buffers, and the level of ssDNA self-dimerization.* In order to control the melting temperatures (T_m) of DNA, two key features could be controlled. The length of the ssDNA, and the nucleotide sequence. Shorter ssDNA fragments indicate high specificity during hybridization [81]. Longer ssDNA fragments result in higher T_m. However, the length of the sequence is not the only governing factor of T_m in an ssDNA. The amount of Guanine, and Cytosine present in the sequence largely contributes to the T_m as well. For our study, we require a balance in between these two features. If the T_m is too high, when we attempt to assemble different bioconjugates via DNA hybridization, the high temperatures applied to the bioconjugates could denature the enzymes. This dismantles the final anticipated macromolecular structure even before it is formed. If the T_m of the ssDNA is too low, it could result in poor molecule stability at room temperature. Therefore, the T_m of the single stranded DNA (ssDNA) used in this study was always approx. 32°C.

Melting temperature (T_m) – Since the two complimentary single stranded DNA will be obtained separately, it is important to calculate the correct effective melting temperature, in order to ensure hybridization. The DNA T_m is the temperature calculated at which, 50% of the ssDNA have recognized its exact complimentary sequence, i.e., the temperature at which, 50% of the mixture is in ssDNA form while, 50% is in the dsDNA form [81]. For ssDNA with lesser than 20 bps, an initial approximation for the melting temperature could be estimated by following a simple multiplication rule as such; $4\cdot(G+C) + 2\cdot(A+T)$. Generally, a 20 bps sequence with ~50% guanine and cytosine (G, C) content will have a T_m higher than 50 °C. Increasing the G, C content of an

ssDNA will further increase the melting temperature of the final sequence. This factor alongside with the difficulty of synthesis of high G, C content sequences owes to choosing a sequence containing a 33% G, C content. For more accurate T_m calculations for the final dsDNA duplex, the base stacking effects need to be considered as well. This "nearest neighbor effect (NN)" is mathematically solved using software tools, which uses experimentally determined thermodynamic parameters [81,92].

In order to predict the hybridization of DNA, it is important to study the kinetics and dynamics of the molecular binding. It is difficult to quantitatively characterize dsDNA hybridization or denaturation, because it is challenging to study hybridization or denaturation of specific base pairs individually. The level of complementary sequence annealing will be directly related to the temperature, at which each hybridization experiment is designed. In many PCR studies, the optimal hybridization temperature has been reported to be 2 – 5 °C below the calculated duplex T_m [93].

Buffer salt concentration – The desired hybridization should be mediated by using appropriate hybridization buffer such as SSC (saline sodium citrate) or a phosphate buffer at pH values of ~7.4. As the concentration of the salts (K^+, Na^+) in the solvent system increases, the T_m of the DNA duplex tends to be increased. High salt concentrations in the solvent refers to more cations floating in the system, which also means that these cations favor binding to the dsDNA, as opposed to their counterpart single strands. Therefore, with higher Na^+ concentrations, we could expect a better stabilized system of hybridized DNA [81,94].

Self dimerization – The OligoAnalyzer 3.1® tool allows us to determine and calculate the self-dimerization possibilities, and the possible hairpin structures of a given ssDNA sequence. Self-dimerization refers to two molecules in the sample interacting/binding with a complimentary nucleotide. In such a situation, the observed molecular weight the sample will be doubled. Hair-pin loop formation refers to the secondary structure formed when the same molecule bending and twisting in order to find a complimentary nucleotide within its own molecule. The molecular weight observed, remains the same. In our study, we minimize the probabilities of hairpin loop formation by carefully engineering the nucleotide sequence, and the length. In order to allow maximum hybridization probabilities with its complimentary strand, the T_m of the overall sequence

should be larger than any of the individual T_m numbers calculated for each hairpin structure. The dynamics of the hairpin folding are assumed to follow a *two-state model*, where the any ssDNA hairpin formation will alternate in between the folded loops and unfolded coils [95].

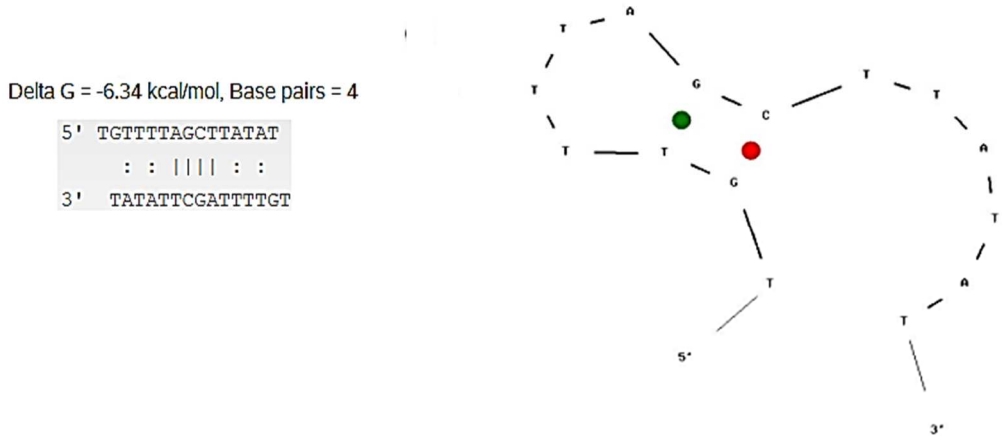

Figure 54: Illustration of possible hairpin loop formation of a single stranded DNA.

The contemporary method of synthetic oligonucleotide (i.e., ssDNA) synthesis is by sequential addition of one nucleotide at a time. Each reaction consists of five different steps – deprotection, coupling, capping, oxidation/stabilization and cleavage/detritylation/deblocking. After each nucleotide addition is accomplished via a cycle consisting each of these steps, they are desalted to remove any salts or contaminants. For ssDNA in nanomol amounts used in this study, further purification using HPLC or PAGE would result in significant product loss. Therefore, the ssDNA 'as received' were simply desalted prior to bioconjugation reactions.

4.2.5 Characterization techniques to analyze DNA hybridization

A recent study illustrated several physical and chemical DNA denaturation methods to study levels of DNA hybridization. DNA denaturation refers to the process of breaking the H-bonds between the base pairs, forming two single stranded DNA. They utilized physical methods such as heating, bead mills, and indirect & indirect sonication methods to first denature dsDNA. They also used chemical treatments such as sodium hydroxide (NaOH), and dimethyl sulfoxide (DMSO) to accomplish dsDNA denaturation. Next, they allowed the separated ssDNA strands to hybridize back into dsDNA, and studied the level of DNA hybridization accomplished after each denaturation method. After all of these treatments, the DNA denaturation and hybridization levels

were determined by means of hyperchromic effects. Fundamentals and methods related to hyperchromic studies are discussed further in section 5.4.1.

These dynamic physical denaturation techniques were not suitable for our studies because they are capable of disrupting the structural integrity of both enzymes and DNA in our final biomacromolecule. Since, the final biomacromolecule in our study consists of covalent linkages, using an extensive physical denaturation method could run the risk of bond cleavage. Moreover, using a chemical DNA denaturation technique such as alkaline (NaOH, formamide) could lead to undesired adducts with the nucleotides of ssDNA, i.e., sticky ends [96]. Therefore, we pursued thermal methods to accomplish DNA hybridization. In thermal denaturation and hybridization, a mixture of ssDNA and their complimentary ssDNA is heated to extremely high temperatures (generally, 90 °C). Afterwards, the mixture is slowly cooled down to room temperature (r.t.), which enables the strands to hybridize spontaneously, ultimately forming the double stranded, helical DNA structure.

Heating double stranded DNA (dsDNA) above their indicated melting temperature (T_m) disrupts the non-covalent H-bonds formed between the base pair nucleotides, which results in the two single stranded DNA strands to separate apart. This is referred to as denaturation, or melting of DNA. Fig.55 illustrates the how DNA hybridization is mediated thermally. Experimentally, DNA hybridization occurs when a mixture of ssDNA and its complimentary ssDNA strands are mixed together, heated, and cooled back down. Heating the mixture relieves secondary structures formed by single stranded DNA (ssDNA) self-folding on its self.

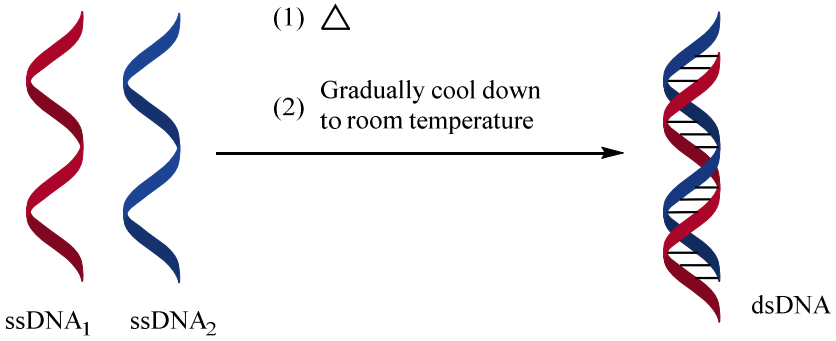

Figure 55: Principle of thermally induced DNA hybridization.

Many studies on bioconjugation have utilized Förster resonant energy transfer (FRET) techniques, autoradiography, and microscopy to study DNA hybridization (i.e., determining the proximity of molecules). FRET is a distance-dependent interaction between the electronic excited states of two dye molecules. The donor molecule in its electronically excited state transfers energy to an acceptor molecule *without emission of a photon.* The efficiency of FRET is dependent on the inverse sixth power of the intermolecular distance. Therefore, FRET is sensitive to very small changes in distances, making the technique highly useful in the dimensions of biological macromolecules. Although a highly successful technique, such fluorescent labelling was deemed unnecessarily complex in accomplishing our specific aim.

4.2.5.1 UV absorption hyperchromic effect

UV-Vis spectroscopy determines how well molecules absorb energy in the Ultraviolet-Visible region of the electromagnetic spectrum (200 – 700 nm).

$$absorbanc = \varepsilon \cdot b \cdot c$$

Where; ε= molar absorptivity, b= path length of cuvette, c= concentration of analyte.
The absorbance is in arbitrary units (au), and given the concentration of the analyte is in mol/L, and the pathlength is 1 cm, the molar absorptivity would be in $M^{(-1)}cm^{(-1)}$

DNA exhibits absorbance properties in the UV spectrum. Therefore, measuring the absorbance levels at 260 nm (Abs_{260}) could be used to determine the degree of regularity, i.e., degree of hybridization. Hyperchromicity studies is a label free detection method, and is unique compared to other methods of analyzing DNA hybridization.

With an increase in the polymer formation (DNA renaturation), the general observation is a decrease of the absorbance intensity (Fig.56). The separated two single stranded ssDNA, will have up to 40% higher absorbance, compared to that of its hybridized dsDNA structure [96]. As the ordered regions of stacked base pairs in the DNA duplex are disrupted, the UV absorbance increases. This difference in absorbance between the duplex and single strand states is due to an effect called hyperchromicity ("less color"), which is the result of NN (nearest neighbor) interactions of the base pairs. In the dsDNA state, interactions between base pairs causes the UV absorbance to decrease relative to that of single strands. When DNA is in the single strand state,

the interactions are much weaker due to the decreased proximity, and the UV absorbance is higher [97]. Upon denaturation (i.e., single strand state), the absorbance of the strands approaches that of the free bases [96,98]. In the hyperchromic method, it is assumed that DNA hybridization does not undergo intermediate states. This holds a valid assumption if we minimize the possibilities of hairpin formation of the ssDNA, and optimize the DNA hybridization conditions. Previous studies have successfully used hyperchromicity to measure DNA hybridization [96,98].

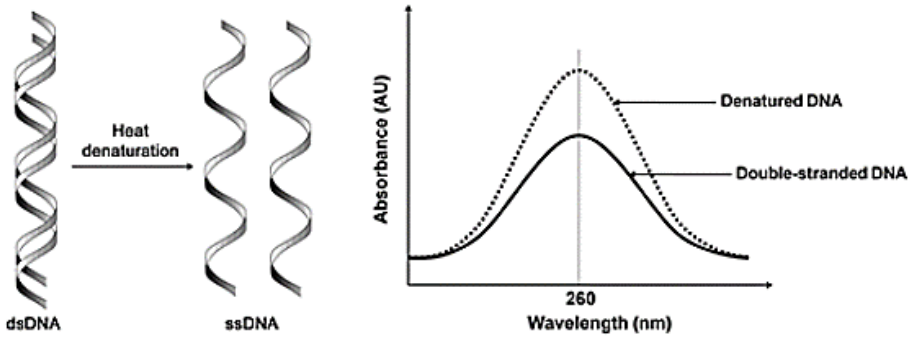

Figure 56: Illustration of the principle of hyperchromic effect observed in DNA hybridization.

4.2.5.2 Intercalating reagents and Fluorescence spectroscopy.

To characterize DNA hybridization, intercalating agents, and fluorescence spectroscopy were used. Intercalators are small dye molecules which insert themselves in the region where hydrogen bonding occurs between the specific DNA base pairs (Fig.57a). There are several types of intercalating agents which bind to different areas of a double stranded DNA (dsDNA); minor groove binders, major groove binders, external binders, and intercalators (Fig.57b). Since the DNA used in this study does not involve any nucleotide or DNA backbone modification, we had the major advantage of being able to use all three classes of the binder dyes. However, water solubility of the dye should be an important aspect to consider. Ethidium bromide (EtBr) was chosen given its high water solubility. Ethidium bromide (EtBr) binds with little or no sequence preference at a stoichiometry of one dye per 4–5 base pairs of dsDNA [99]. EtBr could be excited with wavelengths in the visible – near visible range. They are hence suitable for fluorescence microscopy, confocal laser-scanning microscopy, and fluorimetry. Once an intercalating agent such as ethidium bromide

(EtBr) are bound to nucleic acids, their fluorescence could be enhanced by approximately 10-fold (Fig.57c). And their excitation maxima are shifted ~30 – 40 nm to the red and their emission maxima are shifted ~15 nm to the blue [100].

Fluorescence spectroscopy is a technique which uses fluorescence emitted by molecules that absorb energy from electromagnetic radiation. At room temperature, most molecules reside in their "ground state" which is their lowest electronic vibrational state. When light energy (photons) is absorbed by these molecules, they are elevated to higher energy levels, which are called "excited states." However, they do not reside in such excited higher vibrational states because those states are unstable. These molecules soon drop down into their subsequent lower vibrational states, and eventually reach their ground state again. In the process of a molecule dropping to its ground state, it emits the initially absorbed energy, emitting photons. This process of re-emitting the absorbed photons is termed as fluorescence. Generally, the absorption spectrum resembles the emission spectrum. The difference between the absorption maxima and the emission maxima is termed as the Stokes shift [101].

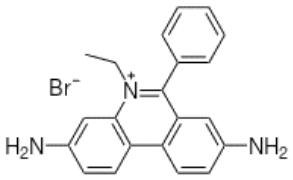

(a)

(b)

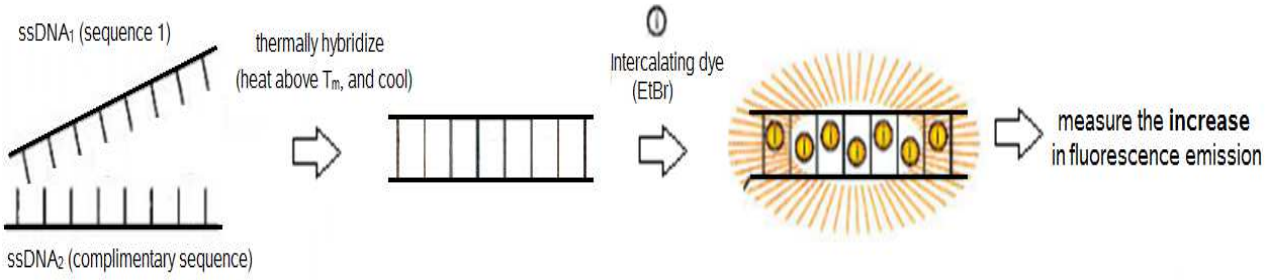

(c)

Figure 57: Ethidium bromide molecule (a). Depiction of where different types of intercalating agents bind to dsDNA (b). Schematic illustrating how EtBr increases its fluorescence after intercalating into dsDNA (c).

4.3 Materials and Methods

4.3.1 Materials

A 15 base pair ssDNA and their complimentary strands were purchased from IDT® DNA. The sequences were was designed with reduced G, C contents, and a medium length in order to avoid secondary structure formation. For the convenience of the reader, the sequences were termed as $ssDNA_1$, and $ssDNA_3$ while their complimentary strands were termed as $ssDNA_2$, and $ssDNA_4$ respectively (Table 8). It must be noted that the last two ($ssDNA_3$, and $ssDNA_4$) are the exact nucleotide sequences used in the DNA-Enzyme conjugation studies. In the conjugation study, 5' phosphorylated $ssDNA_3$ and Enzyme 1 were conjugated. Next, separately, Enzyme 2 and 3' phosphorylated $ssDNA_4$ were conjugated. Lastly, the final DNA-Enzyme macromolecule was assembled by thermally programmed DNA hybridization.

Table 8: Physical properties of ssDNA.
*Data obtained from OligoAnalyzer 3.1

Term	DNA Sequence	Molecular weight (Da)	*T_m (°C)	*Highest T_m (°C) of hairpin
$ssDNA_1$	5'-GTAGATCACTATCAT-3'	4551	35.8	32.1
$ssDNA_2$	5'-ATGATAGTGATCTAC-3'	4591	35.8	29.3
$ssDNA_3$	5'phosphoryl-TGTTTTAGCTTATAT-3'	4643	32.7	21.6
$ssDNA_4$	5'phosphoryl-ATATAAGCTAAAACA-3'	4657	32.7	N/A

4.3.2 Methods

4.3.2.1 Hyperchromicity effect.

The annealing PBS buffer (10 mM phosphate, 0.15 M NaCl) was freshly prepared, pH adjusted to 7.3±0.2, and filtered using laboratory grade filter papers.

In a general experimental procedure, the ssDNA sequence and its complimentary sequence were separately dissolved in PBS buffer in equi-molar amounts. It was imperative that both the

ssDNA samples were in equi-molar and equi-concentration, in order to prevent residual single-stranded ssDNA remaining after the annealing protocol has been conducted.

For the studies conducted with $ssDNA_1$ and $ssDNA_2$, a stock solution concentration of 100 μM was used. Serial dilution, was conducted to obtain four concentrations; 0.24, 0.12, 0.06, 0.03 mg/mL. Next, 1.75 μL aliquots were removed from each separate tube (i.e., total of eight tubes), and Abs_{260} data were gathered on a Thermo Scientific™ NanoDrop™ spectrophotometer (Wilmington, Delaware). These data were used to generate the ssDNA curve in the hyperchromicity graphs. For each sample, triplicate Abs_{260} measurements were obtained by multiple sampling of the same homogenous sample. Afterwards, the avg. of the data were obtained from both ssDNA strands (i.e., avg. of six data points) to generate the final ssDNA curve Fig. 10a.

Afterwards, the $ssDNA_1$ + $ssDNA_2$ mixture was used for the DNA hybridization protocol. The sample was first vortexed vigorously. Next, using a heat bath set to 45 °C, the sample mixture was heated for 3 – 5 min. Although the protocol published by the manufacturer specifies heating the ssDNA mixture up to 90 °C, lowered it to 45 °C in our modified protocol. The reason for using a temperature of 90 °C is to ensure that all the secondary structures present in the single stranded DNA are loosened. However, the sequence we chose in our ssDNA do not contain such significant secondary structures. That factor along with our inability to use temperatures higher than 50 °C in our final enzyme-DNA modality led us to test the ability of forming dsDNA at lowered heating temperatures. Next, the sample was removed from the heat and cooled down to room temperature gradually within 45 – 60 min. Next, 1.75 μL aliquots of this sample was used to obtain triplicate Abs_{260} data of the dsDNA using the NanoDrop™ spectrophotometer. These data were used to generate the final dsDNA curve in Fig.61a.

The same procedure was conducted at an annealing temperature of 90 °C instead of 45 °C, to compare the results qualitatively (Fig.61b).

We also conducted experiments with the actual DNA sequences used in the enzyme-ssDNA conjugate formations too (i.e., $ssDNA_4$ was used in glucose oxidase conjugates, while $ssDNA_3$ was used for horseradish peroxidase conjugates). The stock concentration of $ssDNA_3$ and $ssDNA_4$ were used the same as the final ssDNA concentrations enzyme-ssDNA conjugate reactions. Like so, for $ssDNA_3$ and $ssDNA_4$, the final concentration of the stock solution was 158

μM (0.74 mg/mL). Serial dilutions were conducted to obtain four concentration levels; 0.74, 0.37, 0.18, 0.09 mg/mL. The annealing protocol was the same as reported above.

The data reported Fig.61 were obtained from two independent replicates (two for 45 °C, and two for 90 °C). The data reported in Fig.58 were obtained from one annealing experiment (i.e., one for 45 °C, and one for 90 °C).

Data analyses was performed in the following manner. First, in the replicate 1, at a specific concentration (e.g. 0.74 mg/mL), the average of $ssDNA_3$ was obtained from triplicate Abs_{260} data. Next, the average of $ssDNA_4$ was obtained from the triplicate Abs_{260} data at the same concentration. Next, these two averages were averaged to obtain the final data point for that concentration value in one replicate. The procedure same procedure was conducted for all the four concentration values. Likewise, the same procedure was conducted on the replicate 2 data as well. The results illustrated are the average of the final average Abs_{260} values of the two replicates. So ultimately, one of the data points in the ssDNA curve illustrated in Fig.61, is the average of 8 determinations (i.e., avg. of 8 data points from two independent replicated experiments). The reported error bars in ssDNA curve are the standard deviations of the 8 independent data points generated at each concentration. The reported error bars in dsDNA curve are the standard deviations of 4 data points generated at each concentration.

4.3.2.2 EtBr and fluorescence spectroscopy.

4.3.2.2.1 Fluorescence spectrophotometer calibration.

At the beginning of each experimentation day, the fluorescence spectrophotometer was calibrated. First, the xenon lamp (i.e., excitation monochromator) was calibrated according to the Fluoromax-s v.2.0, 2001 operational manual. The excitation monochromator (xenon-lamp) spectrum generally exhibited a peak maxima of 0.11267 mV at 467 nm, as expected. The emission calibration check was performed to obtain a water Raman-emission spectrum at 397 nm. However, the exhibited peak maxima was generally at 394 nm. The water Raman scattering is due to the vibrations of the water molecule. This is a result of non-elastic scattering where the incident photon loses energy to the molecular vibrations, and then scatters at a higher wavelength. For a calibration excitation wavelength of 300 nm, Raman scattering should appear as a sharp emission peak at 397

nm [102]. Therefore, the water Raman-emission spectrum was always re-adjusted to the true and corrected wavelength, 397 nm.

4.3.2.2.2 Determination of EtBr excitation wavelength.

The manufacturer reported fluorescence excitation/emission wavelengths for nucleic acids suspended in different systems are as below.

Table 9: List of manufacturer reported excitation/emission wavelengths for EtBr [103].

Solvent system	Excitation wavelength (nm)	Emission wavelength (nm)
Aqueous	526	605
Phosphate buffered saline (PBS)	360	590
Tris buffer, pH 8.0	525	600

However, we found the optimal excitation wavelength by scanning the emission spectra in a very broad range of wavelength (320 nm – 900 nm). For scanning the emission spectrum, we chose an initial excitation wavelength of 300 nm. In order to pass the wavelength at which Rayleigh light scatter emission will occur, the acquiring start position in the emission spectrum was offset by 20 nm. Therefore, the starting wavelength for acquiring the emission spectrum was 320 nm. Pure water has two scattering peaks. The first one is Rayleigh scattering, which occurs when the photon absorbed and emitted, have the same energy level. Therefore, the peak corresponding to Rayleigh scattering of water will occur at the same wavelength as that of the excitation wavelength. It is to avoid this emission peak, we start acquiring the emission spectra at a lagged position from that of the excitation wavelength. The observed emission spectra exhibited a maxima at 600 nm (Fig.58).

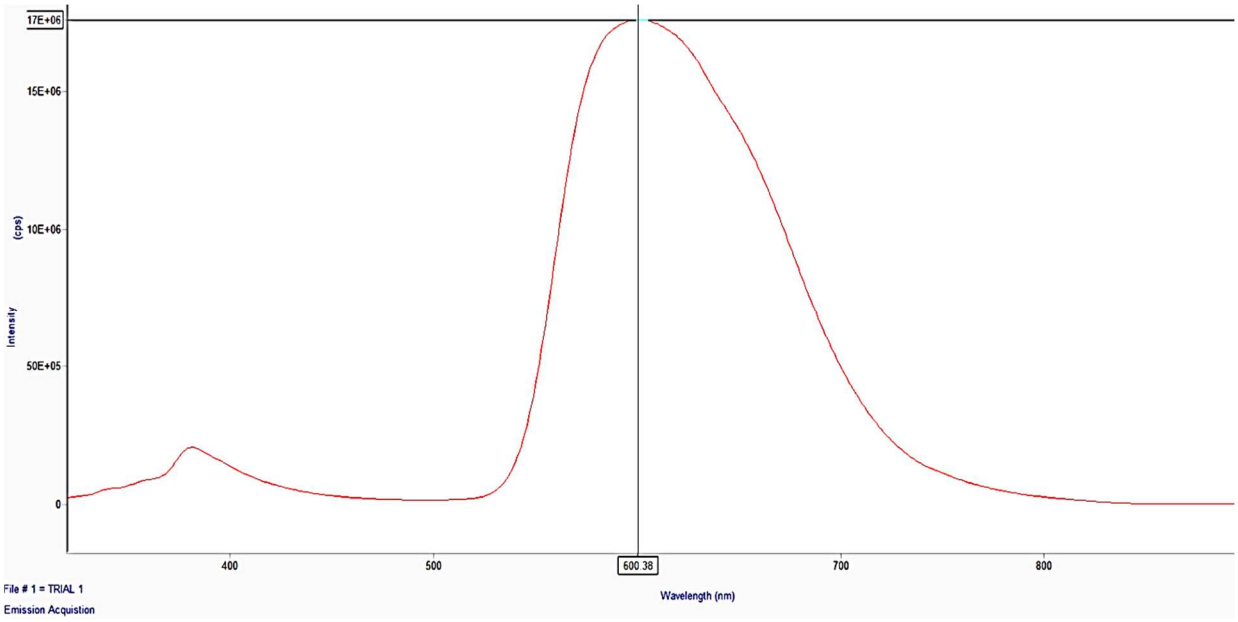

Figure 58: Emission spectrum exhibited by 5µg/mL of EtBr in 10 mM Tris buffer.

In the next step, the emission maxima was entered into the Fluoromax-3 instrument method, and scanning was conducted in "Excitation Acquisition" mode. In the excitation spectrum, two peaks occurred around 360 nm, and 512 nm. However, being the major peak out of the two, the maxima was determined as the peak appearing at 512 nm (Fig.59).

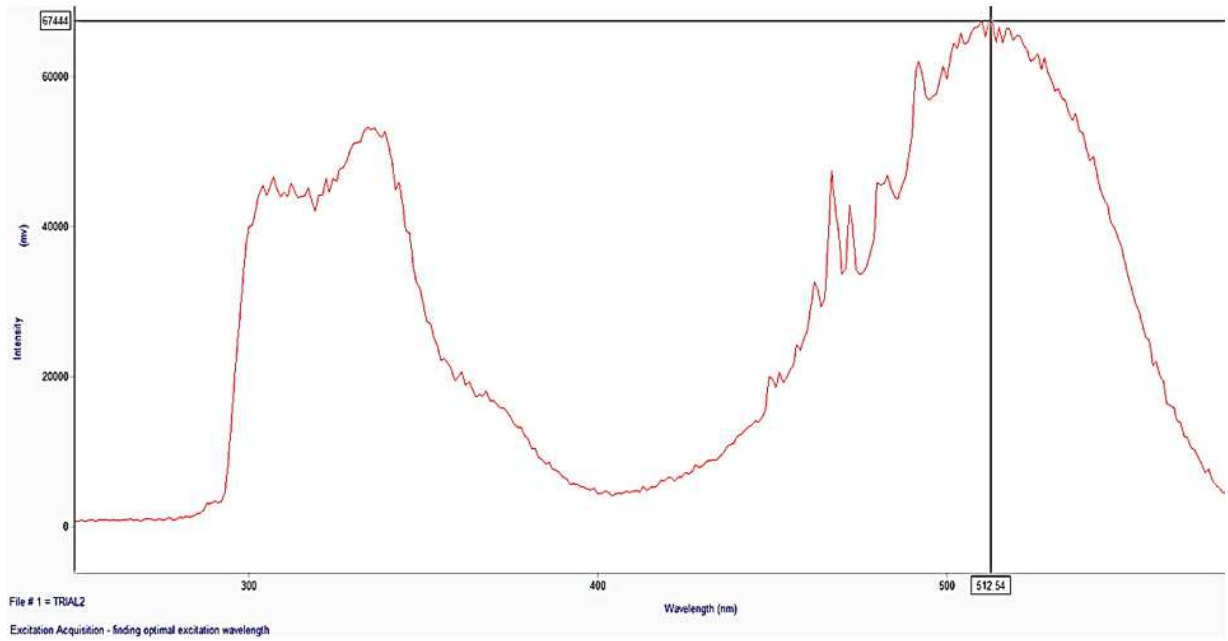

Figure 59: Excitation spectrum of by 5µg/mL of EtBr.

After determining the optimal excitation wavelength, the prepared ssDNA and dsDNA samples were analyzed on the same day, in order to minimize experimental variability. i.e. ssDNA spectra acquisition was conducted on the same day of dsDNA spectra acquisition. The results illustrated were obtained from $1.2 \cdot 10^{-7}$ mols, at a molarity of 100 mM.

4.3.2.2.3 DNA sample preparation for EtBr intercalation experimentations.

It is emphasized that all the EtBr protocols were carried out with person protective equipment (PPE) such as chemical resistant gloves (neoprene), N95 mask, goggles and lab coat. The annealing Tris buffer (10 mM Tris, 50 mM NaCl, 10 mM EDTA) was freshly prepared, pH adjusted to 7.4±0.2, and filtered using laboratory grade filter papers.

First, $ssDNA_1$ and $ssDNA_2$ were prepared in Tris buffer at equi-molar, equi-concentration. Another $ssDNA_1$ sample was also prepared at the equi-concentration, equi-molar to serve the purpose of the negative control (i.e., to obtain fluorescence intensity spectra of only single stranded DNA). The no. of mols of ssDNA in a typical experiment was approx. 1.5×10^{-7} mols, at a final concentration of 80 μM. Then, the two separate $ssDNA_1$ and $ssDNA_2$ samples were combined and vortexed vigorously. Next, the hybridization protocol was conducted by heating the $ssDNA_1$ and $ssDNA_2$ mixture up to 90 °C, and allowed to cool to r.t. gradually. The resulting sample is hybridized double stranded DNA (dsDNA).

Next, a 10 μg/mL EtBr stock solution was made using EtBr as received (ρ =10 mg/mL, Sigma Aldrich, St. Louis, MO). Aliquots from the stock solution were added to the $ssDNA_1$ and dsDNA samples so that the final EtBr concentration in each sample was 5 μg/mL. It is important to not use a very high final concentration of EtBr in the fluorescence spec analysis samples, due to possibilities of EtBr oversaturation. Previous studies have discussed that oversaturation would result in EtBr molecules aggregating, and ultimately resulting in largely erroneous overestimates of fluorescence intensities

Next, both the samples, ($ssDNA_1$ and dsDNA) were transferred to two separate quartz cuvette, and analyzed in a fluorescence spectrophotometer, FluoroMax-3 (Horiba Group). After several trials, the slit width was chosen as 2 nm. A spectrum acquisition increment of 2 nm, and

an integration time of 0.1 s was used. The excitation wavelength was set to 512 nm, while the emission wavelength was set to 600 nm.

4.4 Results

4.4.1 Hyperchromicity effect

4.4.1.1 ssDNA$_1$ and ssDNA$_2$

UV spectra (Abs$_{260}$ nm) of ssDNA$_1$ and ssDNA$_2$ are depicted in Fig.60a. The four separate curves in the descending order are of the four concentration levels at 0.24, 0.12, 0.06, and 0.03 mg/mL. As expected, with a decrease in the ssDNA concentration level, the Abs$_{260}$ nm decreases as well. Fig.60b illustrates the UV spectra of the dsDNA after ssDNA$_1$ and ssDNA$_2$ and were annealed after heating the ssDNA$_1$ and ssDNA$_2$ mixture up to 45 °C, followed by cooling. We observed a visual decrease in the Abs$_{260}$ levels after the annealing protocol had been completed.

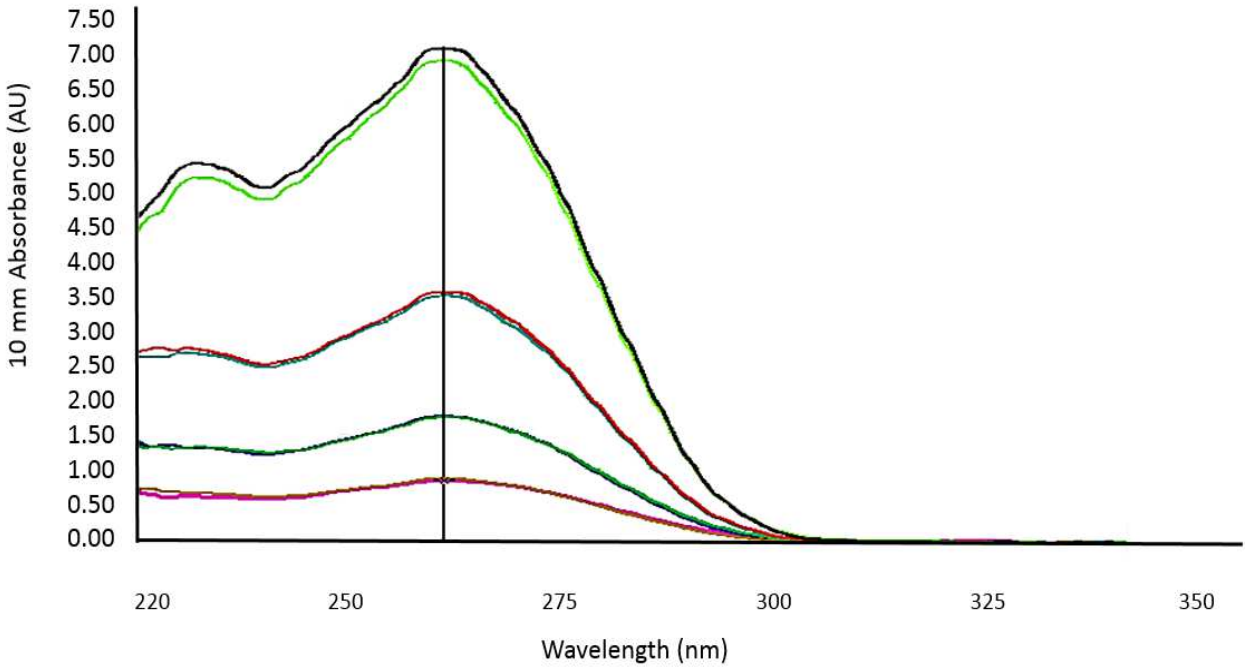

(a)

Figure 60: 260 nm absorbance data obtained at four different concentrations of DNA; Absorbance of ssDNA$_1$ and ssDNA$_2$ (a). Absorbance after ssDNA$_1$ and ssDNA$_2$ were hybridized after heating up to 45 °C and cooling (dsDNA) (b).

Figure 60 continued

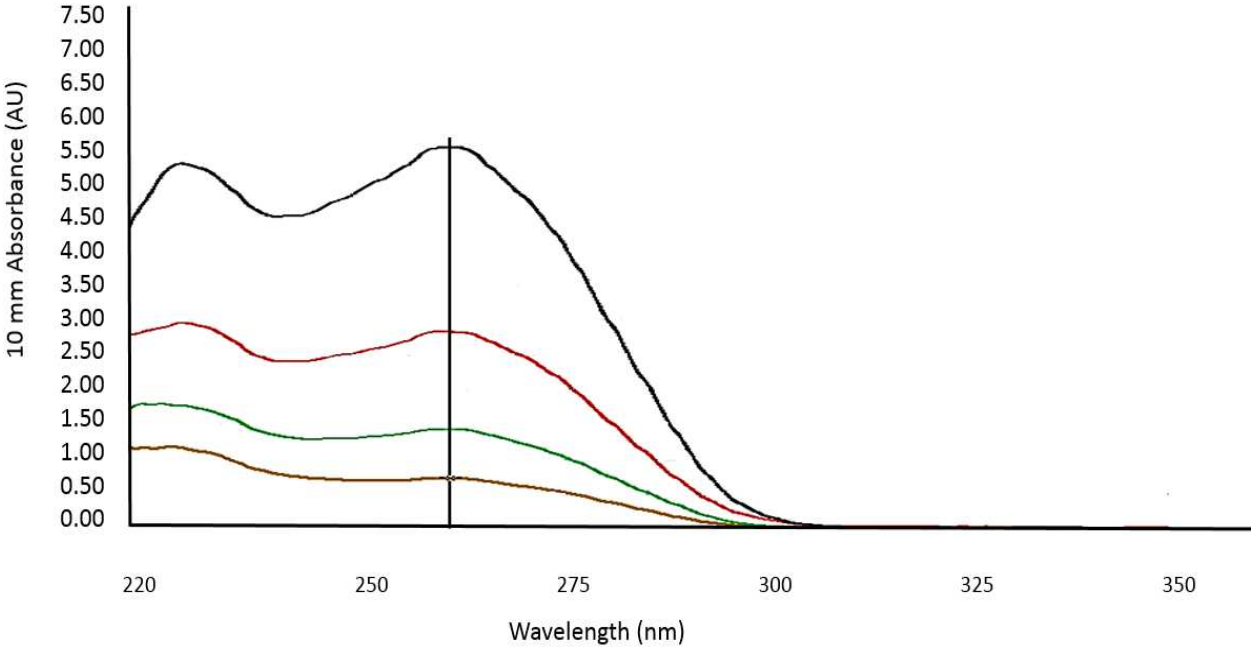

(b)

Fig.61 illustrates cumulative absorbance results obtained from a range of concentrations ssDNA, and dsDNA. Fig.61a depicts the Abs_{260} nm results from the annealing protocol conducted at 45 °C, while Fig. 61b is that of 90 °C. The coefficient of determination (r^2) of all four regression lines are greater than 0.999, indicating a high level of goodness of fit.

The regression lines of the dsDNA (yellow curves in Fig.61a and 61b), have similar linear regression equations. Although this is not quantitative evidence for a comparison between the two annealing methods (i.e., heated up to 45 °C, and 90 °C), it yields qualitative evidence to suggest that regardless the heating temperature, the phenomenon of $ssDNA_1 + ssDNA_2 \rightleftharpoons$ dsDNA could in fact be studied using the hyperchromicity principles.

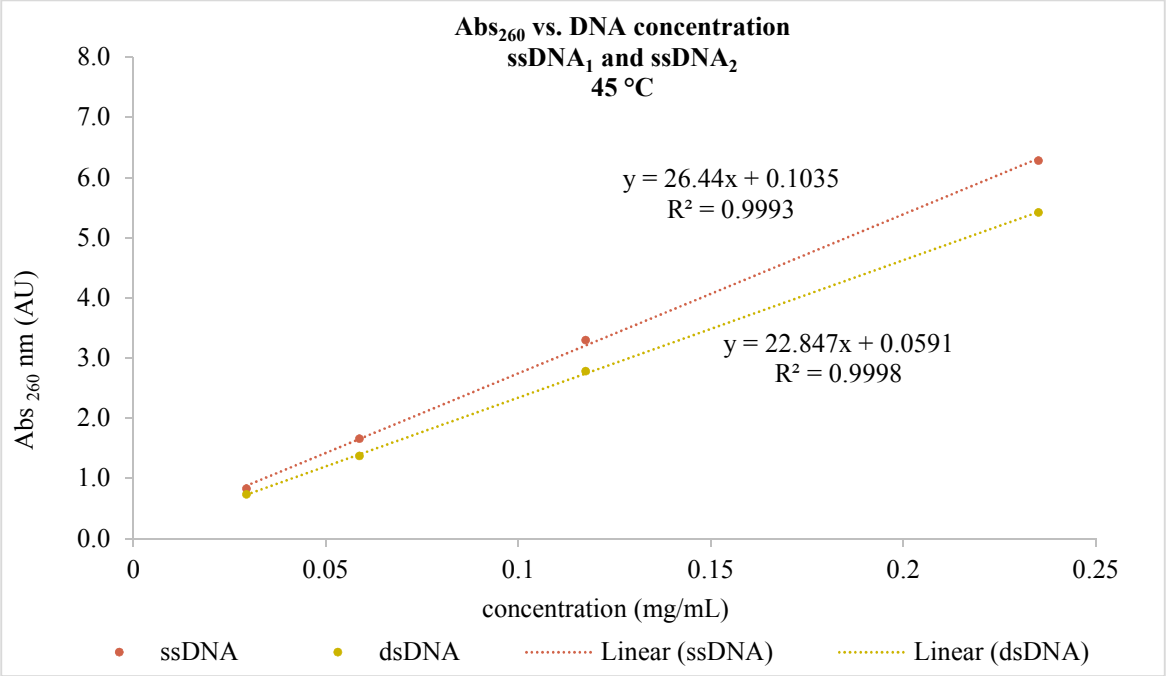

(a)

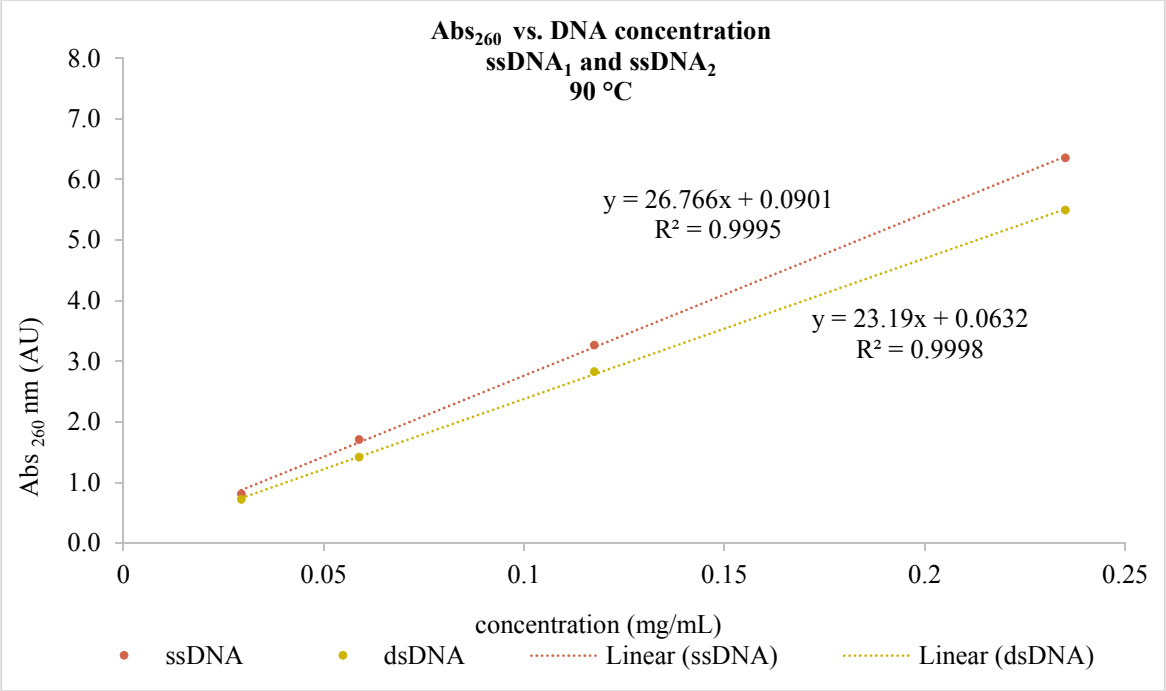

(b)

Figure 61: Hyperchromicity of $ssDNA_1$ and $ssDNA_2$ (before), and after annealing (dsDNA). Results of the annealing protocol conducted at the reduced temperature of 45 °C (a). Results of the annealing protocol conducted at the general temperature of 90 °C (n=1) (b).

4.4.1.2 ssDNA$_3$ and ssDNA$_4$

The two ssDNA sequences used for synthesizing the enzyme-ssDNA conjugates were also studied. Fig.62 illustrates that there is comparable differences in the Abs$_{260}$ measurements between ssDNA and dsDNA states. As the hyperchromicity phenomenon was experimentally observed in the nucleation process of ssDNA$_3$ + ssDNA$_4$ $\rightleftharpoons$ dsDNA, we could conclude that the heating method is an adequate approach to achieve DNA hybridization.

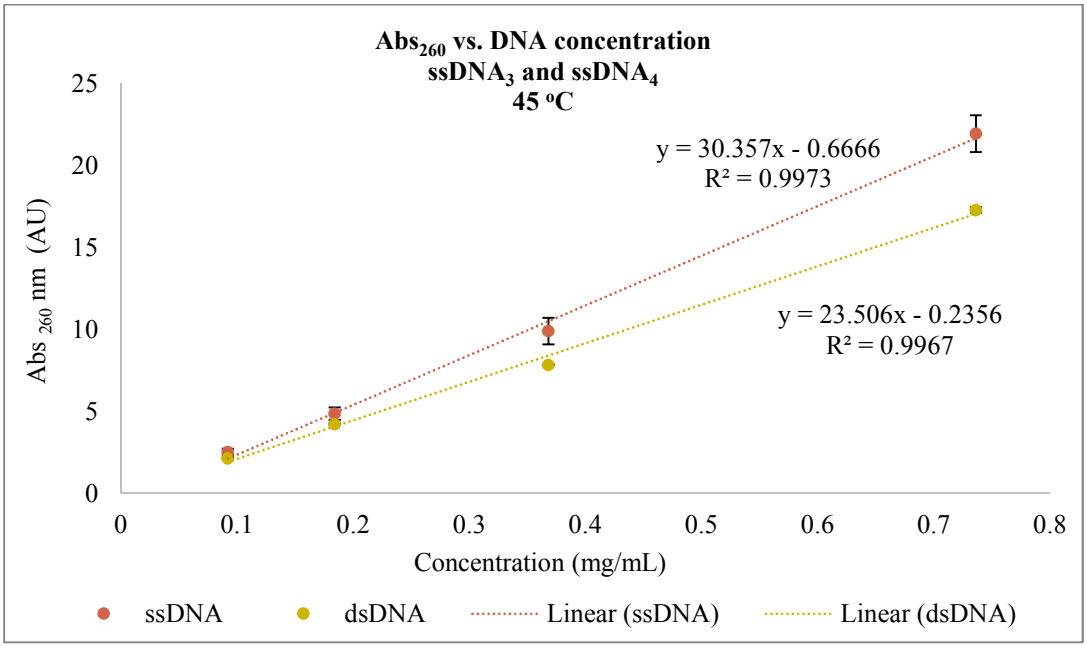

(a)

Figure 62: Hyperchromicity of ssDNA$_3$ and ssDNA$_4$ (before), and after annealing (dsDNA). Results of the annealing protocol conducted at the reduced temperature of 45 °C (n=2) (a). Results of the annealing protocol conducted at the general temperature of 90 °C (n=2) (b

Error bars represent ±SD of all the data points of the respective concentration level.

Figure 62 continued

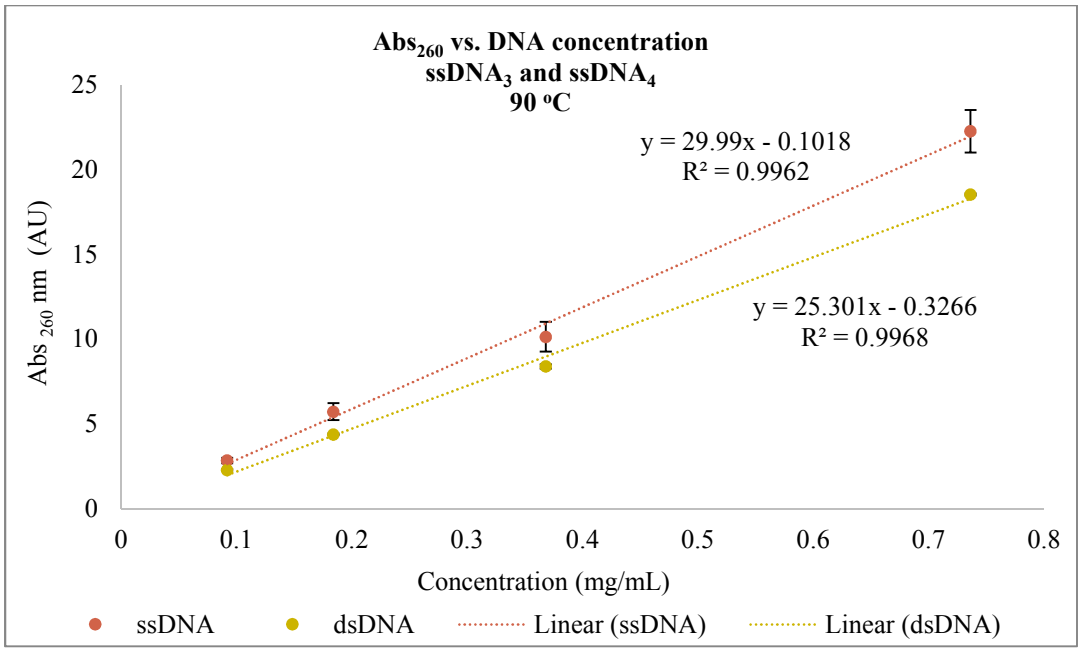

(b)

In a previous study, Wang and his team suggested that the best method for observing distinguishable differences between DNA denaturation (i.e., separation) and renaturation (i.e., hybridization) was via direct sonication [96]. Their characterization method was UV analysis at Abs_{260} nm. Their ultimate choice for DNA hybridization was based on their ability to quantitatively distinguish the Abs_{260} curve results before and after DNA hybridization. They concluded that they did not observe a high enough Abs_{260} difference between ssDNA, and dsDNA to validate the hyperchromicity effect experimentally. However, their observation could be explained as follows. Firstly, in their studies, they obtained DNA in dsDNA state. Their methodology was therefore in reversal to ours. The results they reported for the DNA in the ssDNA state were obtained immediately after denaturing (separation) the original dsDNA via heating at 95 °C. The lack of differences in the Abs_{260} could be explained by a technical limitation in their experimental method. Regardless how immediately they load their samples onto the NanoDrop stage, since the volume of the analytical sample is extremely small (2 µL), the sample contents perhaps undergo instantaneous cooling. Additionally, the heat loss facilitated by convection, as well as conduction (onto the sample loading stage) could highly likely result in hybridizing the separated ssDNA strands. In which case, the resulting absorbance measurements are essentially

from that of hybridized dsDNA. Therefore, when ssDNA, and dsDNA regression curves were compared, they might not have observed the expected differences in the absorbance levels. However, since in our study we have measured the absorbance measurements of physically separated two strands prior to carrying out the annealing protocol, we are able to compare the differences between the two states (ssDNA vs. dsDNA) successfully.

4.4.2 Fluorescence spectroscopy

In this set of experiments, we attempted to determine if the specific intercalation properties of EtBr would enable us to illustrate the DNA hybridization process qualitatively. At an excitation wavelength of 512 nm, and an emission wavelength of 600 nm, and a final EtBr concentration of 5 μg/mL, we noticed a comparable difference between the fluorescence intensities of starting single stranded DNA (ssDNA), and dsDNA after the annealing protocol was conducted (Fig.63). The final results show that there is an increase in the emitted wavelength intensities (counts) in the dsDNA in comparison to ssDNA. The difference was on average approximately 3×10^6 cps (n=4). This indicates that the way EtBr interacts with double stranded DNA results in enhancing the fluorescence emission levels. The theory of intercalation was observed in these experimental results, as the dsDNA fluorescence emission intensities always indicated higher values compared to those of the ssDNA.

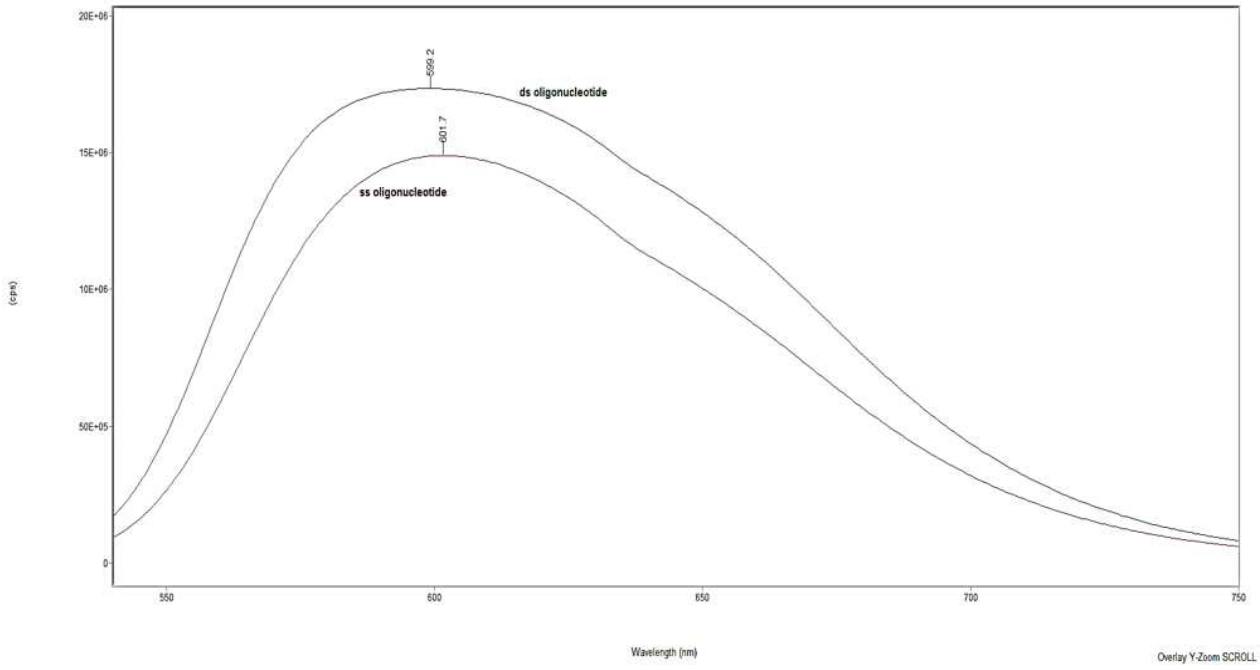

Figure 63: Fluorescence spectroscopy results of ssDNA vs. dsDNA at a final DNA concentration of 8.0×10^{-5} M, and a final EtBr concentration of 5 µg/mL.

4.5 Conclusions

DNA hybridization is a stochastic process where single strands form a duplex formation upon being introduced to their complimentary single strand. When the single strands of DNA has multiple secondary structure formation possibilities, the proceeding DNA hybridization process has to overcome an extra barrier. This is the enthalpy that needs to be provided to relieve such secondary structures. The single strands investigated in this study do not contain secondary structures (i.e., hair pin loops) which contains higher T_m values than the overall T_m of the strand. Therefore, the possible hairpin loops in these four strands investigated in this study were not presumed to interfere with DNA hybridization. Both EtBr intercalation studies, as well the UV hyperchromicity studies qualitatively suggest that DNA hybridization is achievable via simple heating methods. Accounting for all of the above as well as our experimental evidence, we conclude that DNA hybridization is a thermally programmable process. Hence, it is promising to utilize spontaneous DNA hybridization to form a final macromolecule of two separate enzyme-ssDNA complexes.

CHAPTER 5. SYNTHESIS AND ANALYSIS OF ENZYME-DNA MACROMOLECULES

5.1 Abstract

Synthesis and characterization of separate enzyme-single stranded DNA (enzyme-ssDNA) conjugates, and the final enzyme macromolecule ($enzyme_1$-dsDNA-$enzyme_2$), are discussed herein. EDC/Im crosslinking procedures were implemented to synthesize glucose oxidase-$ssDNA_4$ (GOD-$ssDNA_4$), and horseradish peroxidase-$ssDNA_3$ (HRP-$ssDNA_3$) conjugates separately. The absorbance maxima of glucose oxidase (GOD) was at 275 nm, while that of $ssDNA_4$ was at 260 nm. The Size exclusion chromatography (SEC) retention times of GOD and $ssDNA_4$ were at 58 min, and 73 min respectively. The GOD-$ssDNA_4$ conjugates produced from the EDC/Im crosslinking procedure were analyzed on SEC. The elution time of the GOD-$ssDNA_4$ conjugate was 55.9±0.2 min (n=3 determinations). The elution time of the control sample (an equi-molar mixture of GOD and $ssDNA_4$) was at 58 min. The elution time of the control sample resembles that of the GOD standard, while the GOD-$ssDNA_4$ conjugate results indicate a leftward skew (n=3). Separate fluorescence spectroscopy analyses were conducted with GOD enzyme (negative control), $ssDNA_4$ (positive control), SEC fractions of GOD-$ssDNA_4$ conjugate, and SEC fractions of the control experiment (equi-molar mixture of GOD and $ssDNA_4$). Fluorescence spectroscopy results indicated fluorescence intensity maximums at 21, 440, 150, and 94 AU for the GOD enzyme, $ssDNA_4$, GOD-$ssDNA_4$ conjugate, and the control experiment respectively.

The absorbance maxima of the horseradish peroxidase (HRP) enzyme and $ssDNA_3$ were at 415 nm, and 260 nm respectively. The size exclusion chromatography (SEC) retention times of HRP and $ssDNA_3$ were at 65 min, and 72 min respectively. The elution time of the GOD-$ssDNA_4$ conjugate was 65.45±0.58 min (n=6 determinations). Matrix assisted laser desorption ionization-time of flight (MALDI-TOF) of the HRP standard indicated m/z peak around 43,078 Da, while that of $ssDNA_3$ was 4643 Da. MALDI-TOF results of the purified HRP-$ssDNA_3$ fractions collected from the SEC experimentation yielded m/z peaks at 66,630 Da, and 71,110 Da. This is indicative of multiple mols of $ssDNA_3$ tethering onto one mol of HRP. These analytical results provide evidence to suggest that the EDC/Im crosslinking procedure has formed GOD-$ssDNA_4$,

and HRP-ssDNA$_3$ conjugates. Finally, SEC chromatographic results also indicate that the expected GOD-dsDNA-HRP macromolecule was synthesized via spontaneous DNA hybridization.

5.2 Introduction

5.2.1 Glucose oxidase (GOD)

Glucose oxidase is a flavoprotein with a molecular weight of ~160 kDa, and it belongs to the oxidoreductase, EC 1.1.3.4 category (Fig.64a). It catalyzes oxidation of β-D-glucose at its first hydroxyl group, utilizing O_2 as the external electron acceptor, to produce D-gluconic acid and hydrogen peroxide (H_2O_2). Glucose oxidase is a homodimeric enzyme, and has one iron atom, as well as one flavin adenine dinucleotide cofactor (FAD) molecule noncovalently bound at the active site of each 80 kDa subunit. Activators are not required for the catalytic activity of this enzyme. In the reduction half-step, D-glucose is enzymatically oxidized in to D-glucono-δ-lactone. This is then hydrolyzed into gluconic acid without enzymatic participation. Next, the Flavin adenine dinucleotide (FAD) of the glucose oxidase enzyme reduces to $FADH_2$. In the oxidation half-reaction, the reduced glucose oxidase is oxidized by the electron acceptor O_2, producing H_2O_2 [104].

Glucose oxidase was originally isolated and produced from the fungus *Aspergillus niger*, which remains the most common source of GOD production for glucose monitoring applications. Today, glucose oxidases are readily available commercially. The *A. niger* derived GOD has a pH optimum around 5.5, and has a very high substrate specificity for glucose [105]. Glucose oxidase is a very popular enzyme which has been historically used to detect glucose via spectrophotometric glucose assays, as well as fluorimetric assays [106]. Researchers have reported several analytical methods to determine the enzymatic activity of GOD (i.e., D-glucose oxidation rates) such as titrometric methods [107], Fourier transform infrared-FTIR methods [108], hydrophilic interaction chromatography-HILIC [109], and via spectrophotometric analysis from a coupled enzyme assay [110-112] The latter which is coupled enzyme assays is the most popular method to determine glucose oxidase activity. The technique is based on analyzing the amount of product formed in a the concomitant reaction (Fig.64b). As D-glucose is converted into D-glucono-δ-lactone, H_2O_2 is released too. Another enzyme which utilizes the H_2O_2 (horseradish peroxidase; HRP) is also added to the solution along with a chromogenic substrate (ABTS or o-dianisidine). Horseradish

peroxidase utilizes H_2O_2 as its substrate, and oxidizes the chromogenic substance producing a spectrophotometrically detectable signal at 420 – 475 nm (Fig.64b).

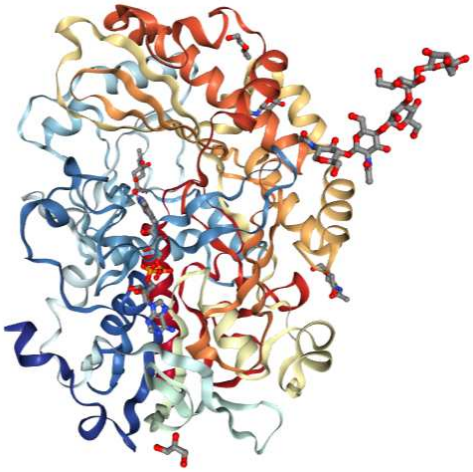

(a)

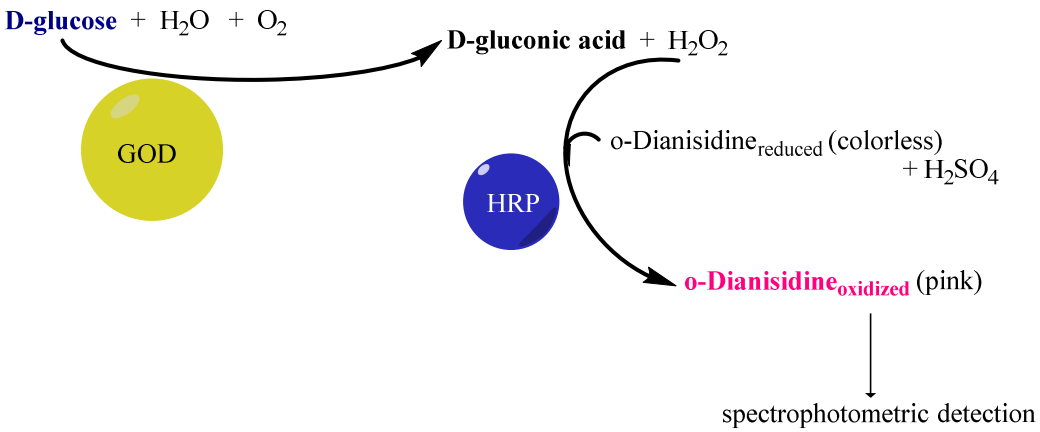

(b)

Figure 64: 3-D representation of GOD derived from *A. niger* (PDB) (a). Coupled enzyme assay to detect D-glucose conversion kinetics (b).

Most of the GOD surface immobilization research has been conducted to develop glucose detection sensors or probes. Some of such GOD functionalization have been accomplished on

noble metal nanoparticles [52], acrylic acid pre-treated polyaniline films [113], Whatman filter papers via EDC/NHS crosslinking [51], cellulose papers via TBHBA (2,4,6-tribromo-3-hydroxy benzoic acid) [114], and gelatin membranes [112]. Immobilization of oxioreductases have been shown to enhance the enzyme's heat stability, functional stability, pH tolerance, and to enhance the shelf life of the GOD detection probes [51,115].

As all the conjugation techniques utilized in this study are on aqueous solution phase systems, suitable analytical systems were researched. Like so, size exclusion chromatography, UV-Vis spectroscopy, and fluorescence spectroscopy were utilized to analyze the free enzymes, and the conjugated enzymes.

5.2.2 Horseradish peroxidase (HRP)

Horseradish peroxidase (HRP) is a commercially available, class III peroxidase, in the superfamily of plant peroxidases. This glycoprotein has two metal centers referred to as heme groups, and two calcium atoms. It has a globular structure, which mostly consists of α-helices, with a few β-sheets. There are two domains called distal and proximal, and the heme group (a.k.a. protoporphyrin IX cofactor) resides in between those. The heme group is typically linked to the HRP by a coordinate bond between the heme iron, and a conserved His170 residue. The N-terminal of HRP is blocked by pyroglutamate, however, there are several arginine residues on the enzyme surface which are susceptible for desired functionalization [116]. Furthermore, there are several surface lysine residues which could be directed towards enzyme immobilization via covalent linkages. On the surface of HRP C1A, three (Lys174, Lys232, Lys241) out of six lysine residues have been found accessible to chemical modifications [117].

HRP enzyme utilizes hydrogen peroxide (H_2O_2) to oxidize a variety of compounds. It not present in mammalian cells, and is obtained from the plant source, horseradish roots. However, recently, recombinant HRP has been expressed in eukaryotic systems (yeast) [118], as well as in prokaryotic systems (*E.coli*) [119]. Studies conducted on HRP dates to the nineteenth century. The first studies to report isolation, purification and characterization of the physical properties of seven distinct isoenzymes from HRP were in 1960s [120].

HRP activity can either be detected by the formation of a chromogenic or fluorogenic detector molecule product (e.g. ABTS, or o-dianisidine), or by an electrochemical signal due to the redox nature of HRP catalysis. The majority of studies on HRP in biosensor systems focuses on the detection of H_2O_2. Like so, it has been used extensively as a reporter enzyme in histochemical staining assays [121], biosensors [122], and medical diagnostics [123].

HRP used in bioremediation systems have shown that conjugating the enzyme with polysaccharides have improved the stability of the enzyme more than 6-fold, compared to the native HRP systems. The starch-conjugated HRP catalytic activity has been shown to be unaffected when attempted to decolorize synthetic dyes such as bromophenol blue [124]. Furthermore, in the last two decades, HRP enzyme has also been studied as a drug for cancer treatment. In a recent study, chitosan nanoparticles encapsulating HRP enzyme were demonstrated to induce cell death in human breast cancer cells. The encapsulation allowed for enhanced stability at 37 °C compared to the free HRP enzyme [125].

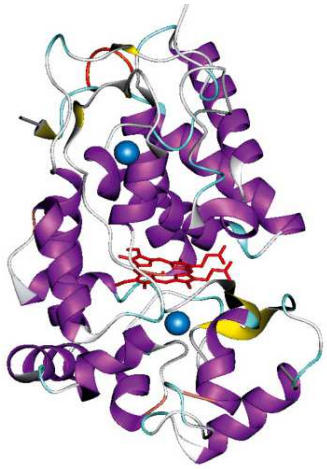

Figure 65: 3-D representation of HRP isoenzyme C [116].

5.2.3 Size Exclusion Chromatography

This is a separation technique in which the molecules in the analytical sample are separated based on their hydrodynamic radii, i.e., molecular size. In this type of chromatography, the stationary phase is composed of gel beads with pores. The mobile phase is the solvent. In size exclusion chromatography, the larger molecules elute faster because they spend less time getting trapped inside the gel beads. Smaller molecules have a higher residence time inside the column

because they enter the gel pores more frequently, and linger around, making their elution slower (Fig.66).

When size exclusion chromatography is used using organic solvents, the technique is referred to as Gel Permeation Chromatography (GPC). When size exclusion is performed with aqueous solvents, the technique is referred to as Gel Filtration.

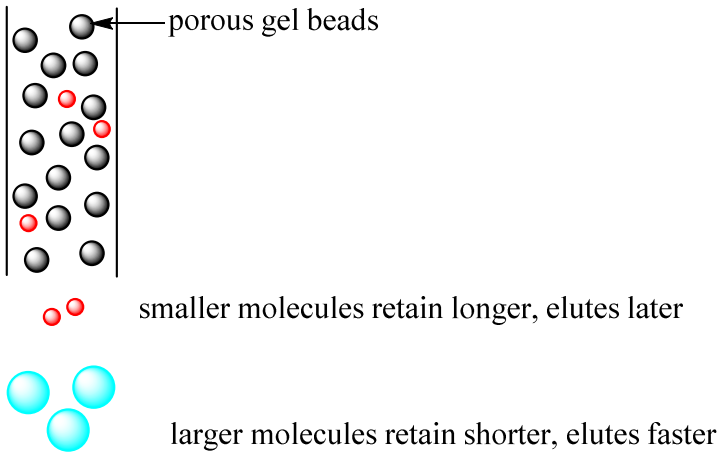

Figure 66: Illustration of the size exclusion chromatography principle.

Three types of polymers are mainly used in gel permeation beads – dextran, polyacrylamide, and agarose. The polysaccharide dextran is a composed of glucose monomers which are linked by α1-6 glycosidic bonds, and α1-3 branch linkages. In order to make gel bread with various pore sizes, these dextran molecules are crosslinked with epichlorohydrin to various extents. Such crosslinked dextran structures are called Sephadex. The higher the extent of crosslinking, the lesser the water retaining ability it has (e.g. Sephadex G-10). On the contrary, less crosslinked beads (e.g. Sephadex G-200), will swell more in the presence of water. Agarose, more commonly known as Sepharose, has pore sizes larger than those of crosslinked dextran. It is composed of D-galactopyranose monomers linked beta 1-4 to another alpha 1-3 linked 3,6-anhydro-L-galactopyranose. Whichever stationary phase gel is used, the basis of molecular separation in this technique is based on the size of the molecules.

The two enzymes reviewed above (GOD, and HRP) were utilized to synthesize separate enzyme-ssDNA conjugates. Next, using the complementarity of DNA, these two enzymes were co-localized to synthesize the final enzyme macromolecule. In the final biomacromolecule construct, the distance between the two enzymes was maximized. As DNA hybridization occurs from the 5'→3' direction, the reactive (via EDC/Im chemistry) phosphoryl groups were placed in the 5' terminal of both the ssDNA. The purpose of placing the enzymes as further as possible was to minimize steric hindrances possible due to the two large enzymes being on the same side.

$ssDNA_3$ was attached to horseradish peroxidase (HRP) while $ssDNA_4$ was attached to glucose oxidase (GOD). The purpose of heating the separated conjugates up to 45 °C was to relieve the $ssDNA_4$ and $ssDNA_3$ of their possible hair-pin loop formations. Fig.67 illustrates the architecture of the final biomacromolecule synthesized via spontaneous DNA hybridization.

This co-localized GOD-dsDNA-HRP macromolecule was separated based on size exclusion principles. There are several properties of biomolecules which could be exploited for identifying and separation, such as size, hydrophobicity, charge, ligand specificity and isoelectric point. Size exclusion chromatography (SEC) is an ideal candidate to separate molecules according to the size.

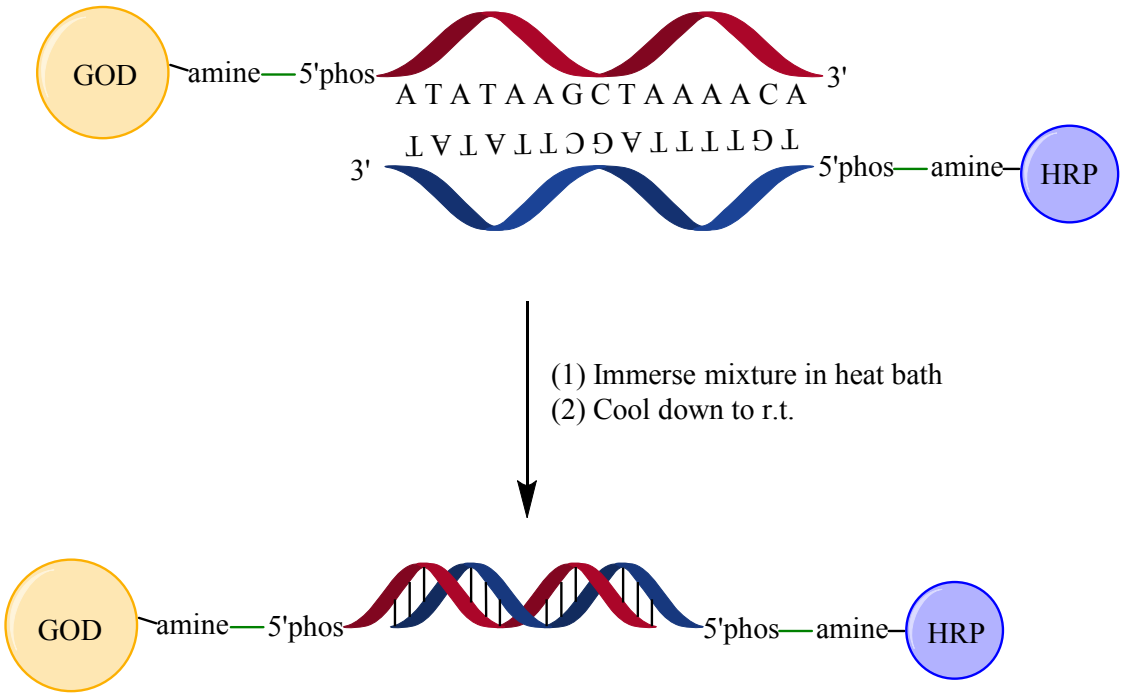

Figure 67: Illustration of the spontaneous assembly of the final biomacromolecule (GOD-dsDNA-HRP).
Bonds between amine and phosphoryl groups (in green) were formed via the established crosslinking technique (EDC/Im).

5.3 Materials and Methods

In order to synthesize the desired final enzyme macromolecule, enzyme-ssDNA conjugates were synthesized separately. Section 5.3.2.1 – 5.3.2.6 discusses the synthesis of separate enzyme-ssDNA crosslinking methods, and characterization techniques. Section 5.3.2.7 discusses the final enzyme macromolecule assembly via thermally facilitated DNA hybridization.

5.3.1 Materials

The ssDNA used for the glucose oxidase conjugation was, 5'phosphoryl-ATA TAA GCT AAA ACA-3'; T_m 32.7 °C; molecular weight 4657 Da. The chosen sequence for the ssDNA carried a T_m slightly above room temperature, but below the denaturation temperature of the two enzymes in the final macromolecule. The ssDNA used for the horseradish peroxidase was its complimentary sequence, 5'phosphoryl-TGT TTT AGC TTA TAT-3'; T_m 32.7 °C; molecular weight 4643 Da. These were purchased by IDT® DNA. For the convenience of addressing, the ssDNA used for glucose oxidase conjugation were termed $ssDNA_4$, while its complimentary sequence used in the horseradish peroxidase conjugation were termed $ssDNA_3$.

Imidazole (Im) and EDC were purchased from ThermoFisher Scientific. Glucose oxidase (GOD), and horseradish peroxidase (HRP) were purchased from Sigma Aldrich (St. Louis, MO). The 10 mM sodium phosphate ($NaH_2PO_4 \cdot H2O$), 0.15 M NaCl, buffer was prepared, pH adjusted to 6.2±0.2, and filtered. 0.1 M imidazole solutions were pH adjusted to 6.0±0.2, and filtered.

5.3.2 Methods

5.3.2.1 Crosslinking enzymes and ssDNA via EDC/Im crosslinking chemistry

Crosslinking GOD and $ssDNA_4$.

In order to manipulate the number of covalent bonds formed between the ssDNA 5'phosphoryl group and the primary amines in glucose oxidase (GOD), the molar ratio of $ssDNA_4$: GOD was maintained at 1:1. In an attempt to reduce non-specific EDC binding to the ssDNA phosphate backbone, the molar ratio of EDC: $ssDNA_4$ was reduced to a 150-fold excess, instead of the 430-fold molar excess suggested in literature [75].

First, $ssDNA_4$ (as received) was dissolved in PBS buffer, and transferred to EDC, followed by the addition of glucose oxidase pre-dissolved PBS buffer (pH 6). Finally, a molar equivalence (w.r.t to EDC) of 0.1 M Imidazole (Im) was added to the reaction mixture. EDC: Im molar ratio was maintained at 1:1 to avoid undesired byproduct formation. The reaction mixture was vortexed, and allowed to react at r.t. (room temperature) for >5 hrs. This adapted 1-ethyl-3-(3-dimethylaminopropyl) carbodiimide hydrochloride (EDC) crosslinking method is reported in chapter 2 in greater detail (Fig.68).

The GOD-$ssDNA_4$ product samples were subjected to exhaustive dialysis using 7000 MWCO dialysis tubes, to remove salts, unreacted ssDNA, EDC, and any other byproducts. The recovered sample was lyophilized and subjected to all further analytical methods (size exclusion chromatography, and fluorescence spectroscopy).

Crosslinking HRP and $ssDNA_3$.

First, $ssDNA_3$ (as received) was dissolved in PBS buffer, and was transferred to EDC, followed by the addition of enzymes pre-dissolved in PBS buffer (pH 6). A molar equivalence (w.r.t to EDC) of 0.1 M Im was added to the reaction mixture finally. The reaction mixture was vortexed, and allowed to react at r.t. (room temperature) for >5 hrs. The HRP-$ssDNA_3$ conjugate samples were subjected to exhaustive dialysis using 7000 MWCO dialysis tubes. The recovered sample was lyophilized and subjected to all further analytical, and characterization methods (size exclusion chromatography, and MALDI-TOF).

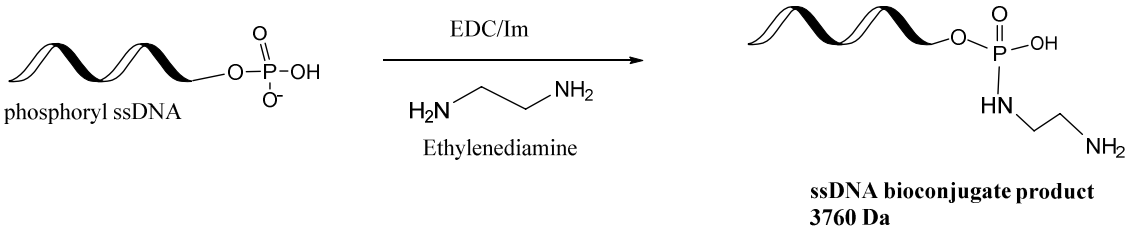

Figure 68: Schematic of the EDC/Im reaction scheme established in the current study.

5.3.2.2 UV-Vis spectroscopy

As the first step of enzyme-ssDNA studies, we conducted a broad UV-Vis wavelength scan of all the components involved in the bioconjugation study, i.e, glucose oxidase (GOD), horseradish peroxidase (HRP), and single stranded DNA ($ssDNA_4$, and $ssDNA_3$). The purpose was to determine the absorbance maxima of these compounds, in order to be utilized in the size exclusion studies. All UV-Vis studies were performed on a NanoDrop spectrophotometer (ThermoFisher Scientific, location). The samples were diluted in PBS buffer (pH 6.2±0.2), and 1.75 µL aliquots of them were analyzed on the NanoDrop machine, blanked against the same PBS buffer used in the crosslinking reactions.

5.3.2.3 GOD: Size exclusion chromatography

5.3.2.3.1 Analytical Chromatography

After determining the absorbance maxima of the compounds, those values were used in the size exclusion chromatography experiments to determine the suitability of the column. Size exclusion chromatography (SEC) was performed on a Superdex™ 200 10/30 GL capable of separating molecules in the range of 100,000 – 200,000 Da. SEC was utilized to separate unreacted GOD, and unreacted $ssDNA_4$ from the GOD-$ssDNA_4$ conjugates. Since the molecular weights of GOD and $ssDNA_4$ are 160 kDa and 4.6 kDa respectively, there is an adequate difference in the molecular weights to obtain adequate separation. However, we suspect that SEC would not remove any unreacted GOD enzyme from the GOD-$ssDNA_4$ conjugate samples due to the very small difference in the molecular weights between the free enzyme and the conjugates. This would be true unless there is a significant difference between the free enzyme and the conjugate due to several moles of $ssDNA_4$ (up to 30) conjugating with one mole of GOD.

The mobile phase used for separations was phosphate buffered saline (PBS). 10 mM sodium phosphate ($NaH_2PO_4 \cdot H2O$), 0.14 M NaCl, buffer medium was prepared with MilliQ water, pH adjusted to 7.20±0.15, and filtered using Whatman™ qualitative filter papers (Fisher Scientific). An isocratic method using a PBS buffer mobile phase (pH 7.20±0.15), was developed to separate and collect fractions of GOD-ssDNA$_4$ bioconjugates. High-performance liquid chromatography (HPLC) was performed on an Alliance 2695 separation module, using the Empower 2.0 software (Waters Corp., Milford, MA), equipped with a Waters 2496 UV detector (Waters Corp., Milford, MA). A flow rate of 0.35 mL/min, and a UV detection at 260 nm, and 275 nm were used to analyze the components in the reaction sample. Prior to conducting chromatography, each sample was filtered using 0.45 μm syringe filters to remove particulates.

Separate calibration curves were developed for GOD and ssDNA$_4$ standards at detection wavelengths of $\lambda_{275\ nm}$, and $\lambda_{260\ nm}$ respectively. For GOD calibration curve, three concentrations at 1.1, 0.55, and 0.275 mg/mL were tested. For ssDNA$_4$ six concentration levels at 0.81, 0.37, 0.405, 0.203, 0.101, and 0.051 mg/mL were analyzed to determine the methods linearity and range. Each calibration curve was developed using a minimum of 3 different concentrations in triplicates (i.e., at least 9 determinations).

5.3.2.3.2 Preparative chromatography on GOD-ssDNA$_4$ conjugates

For preparative chromatography, LC-10AT liquid chromatography system (Shimadzu, city, state), equipped with a Clarity light software was used to obtain chromatographic data. The instrument was equipped with two detection systems; a UV-Vis detector capable of analyzing 190 nm – 600 nm (Shimadzu Inc.) and a Varian Star 9040 RI detector. The flowrate of the mobile phase used in preparative chromatography was 0.3 mL/min.

As preparative chromatography was conducted on a different liquid chromatography instrument, standards runs were conducted again on the new separation module.

In order to subject GOD-ssDNA$_4$ conjugates for further analysis on fluorescence spectroscopy, corresponding conjugate fractions were collected. Fraction collection was performed manually from the tubes exiting the detector. Delay volume calculations were performed prior to fraction collections. Assuming the UV and RI detectors do not hold the

analytical sample for any duration, the tube length exiting from the detector is correlated to the travel time to the tube exit. The calculated delay volume is approx. 5 sec (Fig.69).

$ID_{tube} := 0.009in = 0.023 \cdot cm$ $\quad h := 76cm$ $\quad v_{rate} := 0.35 \frac{cm^3}{min}$

h = length of the tube exiting the detector (measured)
ID_{tube} = inner diameter of the collection tube (generic for LC instruments)
v_{rate} = volumetric flow rate in the method used.

$$t(v_{rate}, ID_{tube}) := \frac{\pi \cdot \left[\frac{(ID_{tube})}{2}\right]^2 \cdot h}{v_{rate}}$$

$t(v_{rate}, ID_{tube}) = 0.089 \cdot min$

$t(v_{rate}, ID_{tube}) = 5.347 s$

Figure 69: Calculations to compute the delay volume in SEC.

Therefore, during preparative chromatography, the real-time display on the detector monitor and the above calculated time were used to collect component fractions as accurately as possible. The detector screen was carefully monitored during the fraction collection process. As soon as the detector indicated an increase in the intensity (AU), approx. 5 sec were allowed to elapse prior to placing a collection tube at the end of the tube exiting the detector.

5.3.2.3.3 Control experiments on size-exclusion: mixture of GOD and ssDNA$_4$

It was important to validate that single stranded DNA (ssDNA$_4$) was in fact crosslinked to glucose oxidase (GOD). GOD is a positively charged enzyme, therefore, it can form electrostatic interactions with negatively charged anions, such as the oligonucleotides used in this study. Therefore, to test whether the single stranded DNA simply formed electrostatic interactions with GOD, or whether ssDNA$_4$ was in fact covalently attached to the enzyme, we also conducted a control experiment. In this control experiment, a sample mixture of GOD and ssDNA$_4$ was prepared. This control sample consisted each biomolecule at the same molar, and molarity as of that used in the crosslinking experiment. We did not conduct the carbodiimide/imidazole (EDC/Im) crosslinking procedure on this sample. Next, the sample was run on the same size exclusion

column (Superdex™ G-25, 10/30 GL). Fractions corresponding to the GOD enzyme were carefully collected. Generally, two fractions from two separate injections were collected (100 µL per injection). This was to ensure adequate sample weights to use in subsequent analytical characterization. The collected fractions were dialyzed for two days against DI, using 6–8k MWCO dialysis tubes, and finally lyophilized. The lyophilized samples were re-suspended in PBS (pH 6.2±0.15), and were subjected to fluorescence spectroscopy.

5.3.2.4 Fluorescence spectroscopy analysis of GOD-ssDNA$_4$ conjugates

The GOD-ssDNA$_4$ fractions collected and purified (exhaustive dialysis using 7000 MWCO tubes, against MilliQ water) from SEC were subjected to EtBr assisted fluorescence spectroscopy to determine the presence of single stranded DNA in the sample. Fraction collection was conducted manually from approx. 40^{th} – 60^{th} minute. This is discussed in greater details in section 5.4.3.

We initially attempted MALDI-TOF mass spectrometry to determine the molecular weight of GOD-ssDNA$_4$ conjugates, as MALDI-TOF is a high resolution method to obtain definitive answers regarding molecular weights of compounds. However, the resulting spectrographs did not indicate any peaks. We suspected this was due to the make-up of the enzyme. Although glucose oxidase (GOD) consists of ionizable amino side groups, the samples did not ionize in the mass spectrometry ionization chamber. Therefore, we resorted to an alternative analytical tool which yields qualitative results for the presence of DNA (i.e., fluorescence spectroscopy).

Fluorescence intensity data were obtained on a Cary Eclipse spectrophotometer (Varian, CA). The weighed GOD samples were first dissolved in PBS buffer (pH 6.2±0.2). Next, EtBr volumes from a 0.01 mg/mL stock solution was added to each GOD sample so that the final concentration of EtBr in the analytical sample was 6 µg/mL.

In order to determine whether GOD exhibits any EtBr intercalation, resulting in enhanced fluorescence emission, we also conducted calibration experiments using four different GOD concentrations. The fluorescence spectroscopy analytical concentration range captured the GOD concentration typically used in a crosslinking experiment. The final concentration of GOD were 0.5, 1.7, 3.8, and 7 mg/mL.

Fluorescence intensity data were analyzed in the following manner. First, triplicate fluorescence intensity data points were obtained by multiple sampling of the same homogenous sample. Next, the averaged result was subtracted from the results of a blank solution (i.e., same final concentration of EtBr dissolved in PBS buffer; pH 6.2±0.2) to obtain the results demonstrated in Fig.75 and 76.

5.3.2.5 HRP: Size exclusion chromatography

The sample preparations, analytical chromatography, and preparative chromatography techniques used to analyze and purify HRP-ssDNA$_3$ conjugates were the same as those described in GOD-ssDNA$_3$ methods.

Analytical chromatography was conducted on an Alliance 2695 separation module, using the Empower 2.0 software (Waters Corp., Milford, MA), equipped with a Waters 2496 UV detector (Waters Corp., Milford, MA). An isocratic flow rate of 0.35 mL/min was used. Both the column and sample temperature was 25 °C (at room temperature). Analytical chromatography was conducted to determine the suitability of the Superdex™ 200 10/30 GL column. For HRP, three concentration levels in triplicates each at 1.3, 0.65, and 0.33 mg/mL were tested to determine the methods linearity and range (i.e., at least 9 determinations). In the analytical procedure, the detection wavelength was 369 nm, as the UV detector was only capable of detecting wavelengths in the UV range. However, as the UV-Vis spectroscopy results from initial testing indicated that HRP exhibits absorbance at this wavelength, it was still deemed useful to use the 369 nm in the detection system.

Preparative chromatography was conducted on a LC-10AT liquid chromatography system (Shimadzu, Columbia, MD). The instrument was equipped with two detection systems; a UV-Vis detector capable of analyzing 190 nm – 600 nm (Shimadzu Inc.) and a Varian Star 9040 RI detector. The flowrate of the mobile phase used in preparative chromatography was 0.3 mL/min. As the separations module used for preparative size exclusion chromatography did not consist of an in-built mobile phase degasser unit, the mobile phase (PBS buffer; pH 7.4±0.15) were degassed via sonication. The purpose of sonication was to remove any air bubbles present in the mobile phase solution. When air bubbles trap inside the instrument system, the pressure build up poses high risks to the instrument and the column. For preparative chromatography of HRP, and ssDNA$_3$, UV

detection was conducted at 415 nm and 260 nm respectively. For the HRP-ssDNA$_3$ conjugates, UV detection was conducted at both 415 nm, and 260 nm .

5.3.2.6 Molecular weight analysis of the HRP-ssDNA$_3$ conjugates: MALDI-TOF

In order to determine whether EDC/Im crosslinking method was successful in synthesizing the desired HRP-ssDNA$_3$ conjugate, fractions collected from size exclusion chromatography were analyzed via MALDI-TOF mass spectrometry. Prior to analysis, each fraction was subjected to exhaustive dialysis on 7000 MWCO dialysis tubes. MALDI-TOF spectrometric results were obtained using an Applied Biosystems (Framingham, MA) Voyager DE PRO mass spectrometer, and Sinapinic acid as the matrix. Prior to MALDI-TOF, each sample was purified using a C_{18} – ZipTip column (Millipore Corporation, Billerica, MA). The ZipTip columns were conditioned using two 10 µL of acetonitrile followed by two 10 µL of 0.1% trifluroroacetic acid (TFA).

5.3.2.7 Assembly of the final enzyme macromolecule via DNA hybridiaztion

First, the GOD-ssDNA$_4$ conjugates (purified SEC fractions) were weighed and dissolved in 300 µL PBS buffer (pH 7.2) at a concentration of 35 mg/mL. Next, a HRP-ssDNA$_3$ conjugate (dialyzed SEC fractions) was weighed and dissolved in 300 µL PBS (pH 7.2) at a concentration of 40 mg/mL. Afterwards, the tubes containing the separate samples were heated to approx. 35 °C. The purpose of heating was to alleviate the single stranded DNA from any secondary structures it may have formed. Next, these samples were combined together, and the mixture was heated to 45 °C using a heat bath. The sample tube was immersed for 5 mins. Next, the tube was removed from heat, and was allowed to cool down to room temperature for 2 hours.

Afterwards, the final biomacromolecule sample was dialyzed using 10,000 MWCO dialysis tubes against MilliQ water for 2 hours. Finally, the recovered sample was analyzed on the Superdex 200™ 10/300 GL size exclusion column.

5.4 Results and Discussion

5.4.1 UV-Vis spectrophotometry.

As expected, for both sequences of single sranded DNA, the absorbance maxima was at 260 nm (Fig.70a,b). For glucose oxidase, absorbance maxima occurred at two wavelengths (Fig.70c). The maxima at 275 nm is general for proteins and enzymes, which is the result of the Tryptophan (Trp), tyrosine, (Tyr), and Phenylalanine (Phe) amino acid side groups. The peaks around 200 nm are caused by the peptide bonds present in the primary structures [51]. Our UV-Vis results corroborated well with previous spectroscopy results as well [111].

For horseradish peroxidase, maxima occurred at two peaks (Fig.70d). The peak at 275 nm is general for proteins and enzymes, which is the result of the Tryptophan (Trp), tyrosine, (Tyr), and Phenylalanine (Phe) amino acid side groups. Furthermore, disulfide bonds contribute minorly at 260 nm too [126]. The peaks around 200 nm are caused by the peptide bonds present in the primary structures [51]. The Abs maxima at 415 nm is due to the heme group present in HRP, which is also the reason for the brown color of the enzyme (Gong et al., 2016).

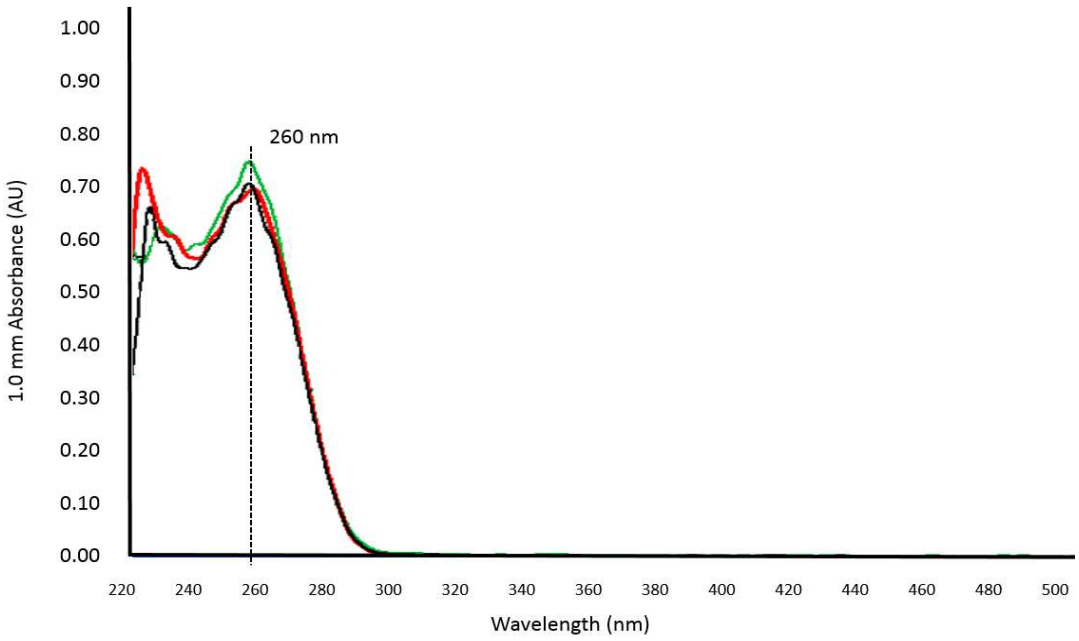

(a)

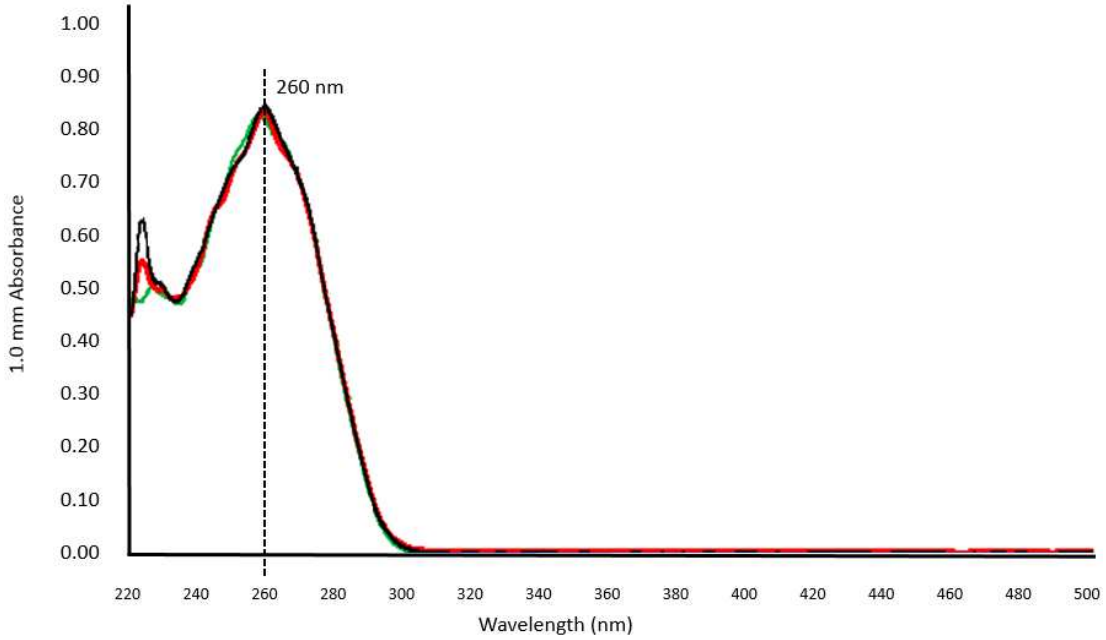

(b)

Figure 70: UV spectroscopy results of; $ssDNA_4$ at a concentration of 5×10^{-5} M (a), $ssDNA_3$ at 6×10^{-5} M (b), glucose oxidase enzyme (GOD) at a concentration of 8×10^{-5} M (c), horseradish peroxidase (HRP) standard at 3.28×10^{-5} M (d).

Figure 70 continued

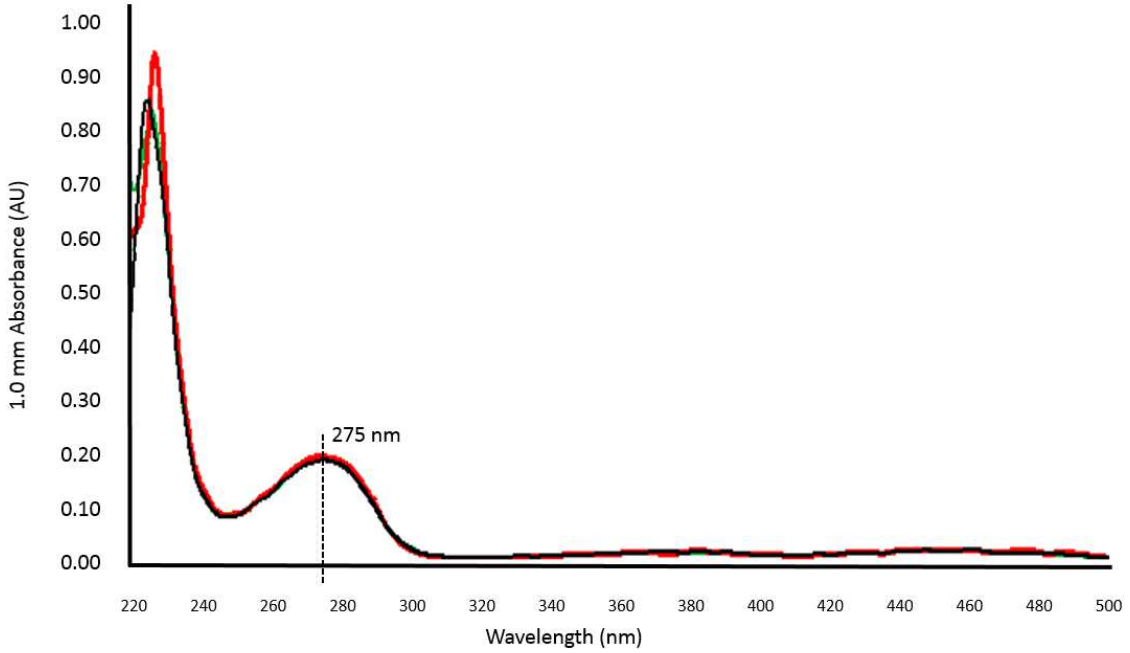

(c)

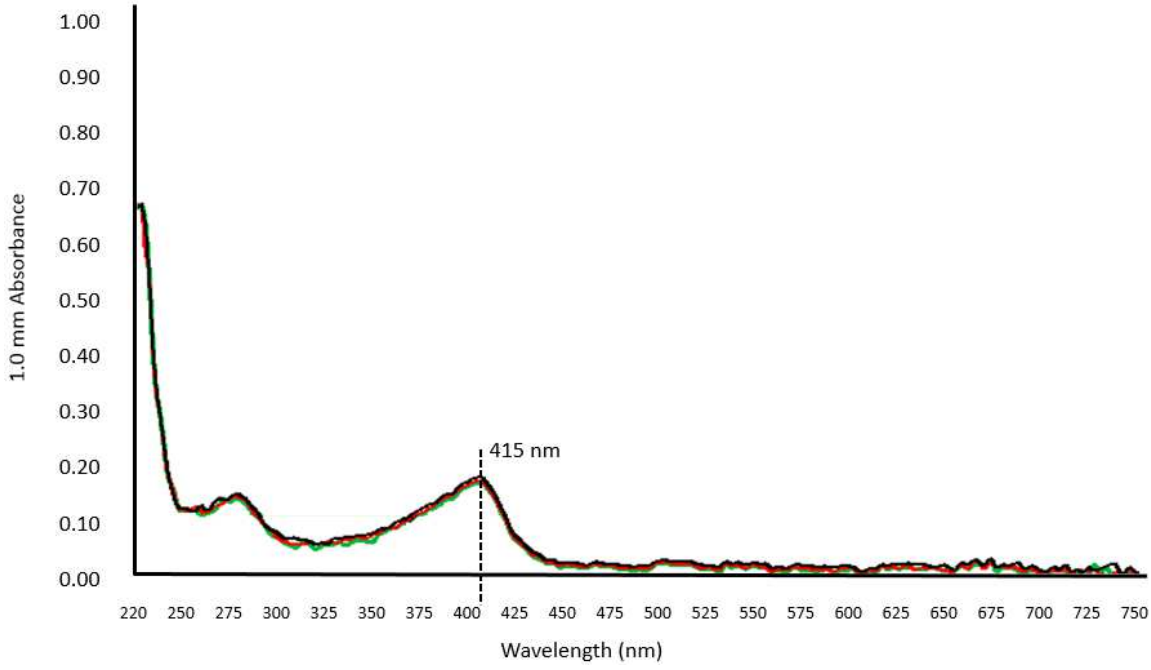

(d)

5.4.2 Size Exclusion Chromatography – GOD

5.4.2.1 Analytical size exclusion chromatography (GOD and ssDNA$_4$)

The calibration curves were constructed by linear regression using standards of known concentrations (Fig.71). The y-axis corresponds to the peak height, which is recorded in AU. The x-axis is the concentration of the analyte (mg/mL). The coefficients of variation (r^2) of both calibration curves are well above the acceptance criteria. The regression curves demonstrated linearity in the concentration range tested.

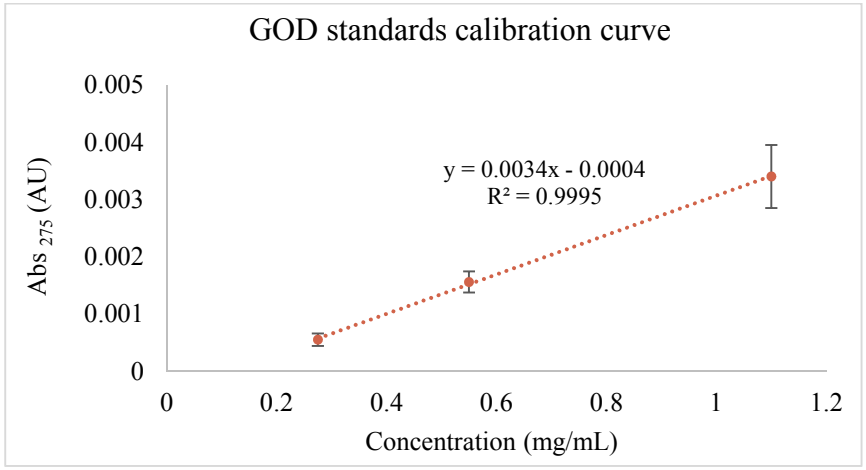

(a)

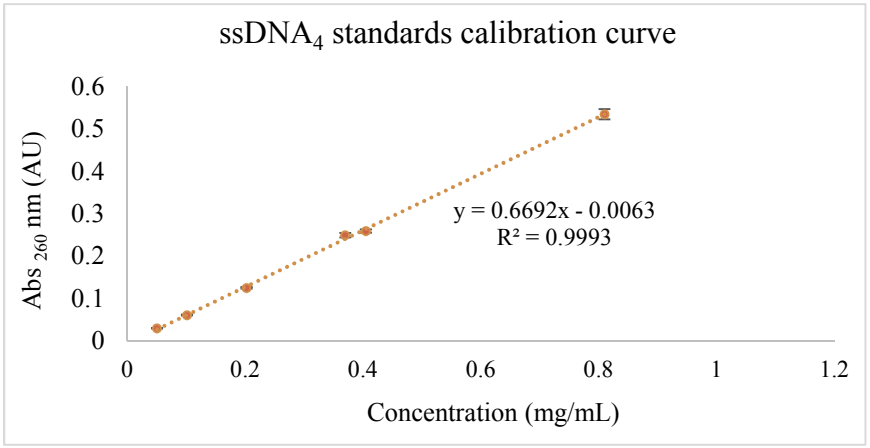

(b)

Figure 71: Standards calibration curves of; glucose oxidase enzyme (a), ssDNA$_4$ (b). Error bars represent ±SD of the peak areas from triplicate results.

Column: Superdex 200™ 10/300 GL. Mobile phase: 10mM sodium phosphate, 0.14 M NaCl, (pH 7.2±0.15). Flowrate: Isocratic, 0.35 mL/min. Column and sample temperature: 25 °C.

Injection volume: 100 µL. UV detection: 275 nm, and 260 nm for GOD and ssDNA$_4$ respectively.

5.4.2.2 Preparative size exclusion chromatography: GOD-ssDNA$_4$ conjugates.

Size exclusion results from the glucose oxidase (GOD) standard, and ssDNA$_4$ indicate that GOD eluted from the size exclusion column at a retention time of 58.4 min, while the ssDNA$_4$ elutes at a retention time of 72.7 min (Fig.72). This corroborates well with size exclusion principles, as the smaller molecular weight biomolecule (i.e., single stranded DNA) elutes later.

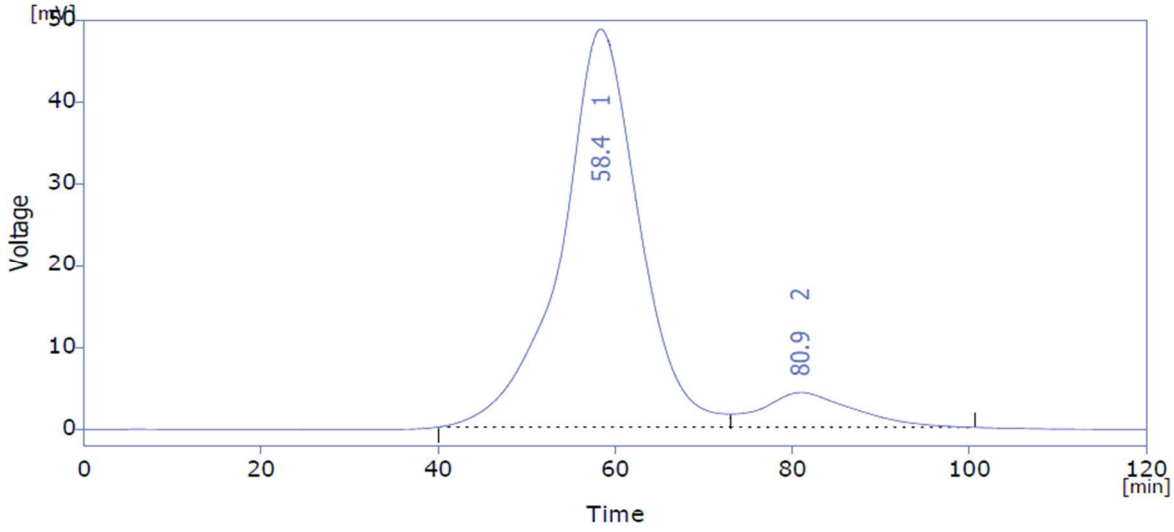

	Reten. Time [min]	Area [mV.s]	Height [mV]	Area [%]	Height [%]
1	58.358	29669.709	48.648	90.6	92.0
2	80.882	3084.444	4.251	9.4	8.0
	Total	32754.153	52.899	100.0	100.0

(a)

Figure 72: Size exclusion chromatographic results of; glucose oxidase (GOD) standard, at 3.4×10^{-6} M (a). ssDNA$_4$ standard at 4.4×10^{-6} M (b).

Column: Superdex 200™ 10/300 GL. Mobile phase: 10mM sodium phosphate, 0.14 M NaCl, (pH 7.2±0.15). Flowrate: Isocratic, 0.3 mL/min. Column and sample temperature: 25 °C. Injection volume: 100 µL. UV detection: 275 nm.

Figure 72 continued

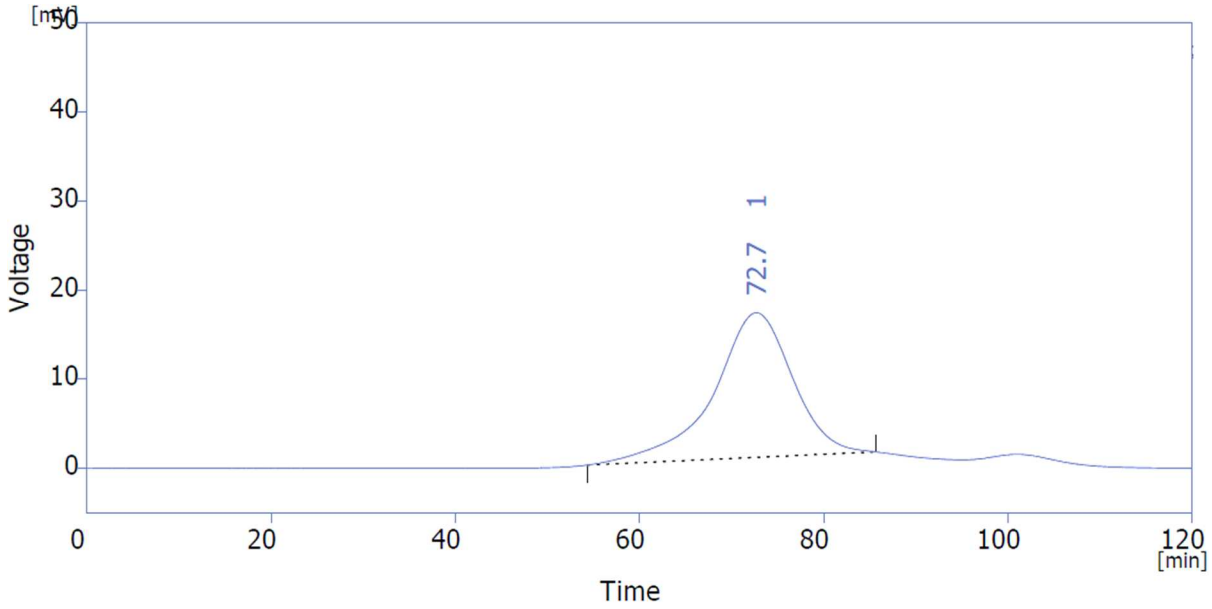

	Reten. Time [min]	Area [mV.s]	Height [mV]	Area [%]	Height [%]
1	72.736	9613.011	16.146	100.0	100.0
	Total	9613.011	16.146	100.0	100.0

(b)

After the EDC/Im crosslinking procedure, the GOD-ssDNA$_4$ conjugates were analyzed on size exclusion chromatography. Fig.73 illustrates the chromatogram profile of the GOD-ssDNA$_4$ conjugate. The elution profile is bimodal. The first peak elutes at 55.9±0.2 min, while the second major peak elutes at 70.1±0.2 min (n=3). The first peak closely resembles that of free GOD enzyme, while the second peak closely resembles that of free ssDNA$_4$. However, the major observation is the leftward shift of both peak and 2. Compared to the GOD and ssDNA$_4$ standards, the elution of both peak 1 and 2 have shifted to the left. While the GOD standard elutes at approx. 58 min, the peak 1 in the GOD-ssDNA conjugate sample elutes earlier, at 55 min. This is preliminary evidence supporting that the expected GOD-ssDNA$_4$ conjugate was formed. Conjugating a molecule with a 4600 Da size to a 160,000 Da sized enzyme would yield a small difference in molecular weights. However, the GOD enzyme has 30 primary amines available for conjugation, while each ssDNA$_4$ molecule has 1 phosphoryl group available for conjugation. As the ssDNA$_4$ and GOD were reacted at a molar equivalence, not a molar equivalence of the functional groups, there is a high probability that several ssDNA$_4$ molecules conjugated with one GOD molecule. The functional group molar

ratio is described as amine: phosphoryl, while the molar ratio is described as GOD: ssDNA$_4$. The used GOD: ssDNA$_4$ molar ratio was 1:1. However, the used amine: phosphoryl molar ratio was 30:1. Even if functional group molar equivalences were used, controlled bioconjugation is nearly impossible to obtain when there are multiple reactive sites present in a biomolecules. i.e., if there are 5 GOD molecules (each with 30 primary amines), it is nearly impossible to distribute an equal ratio of the amine-phosphoryl reactions among all 5 GOD molecules.

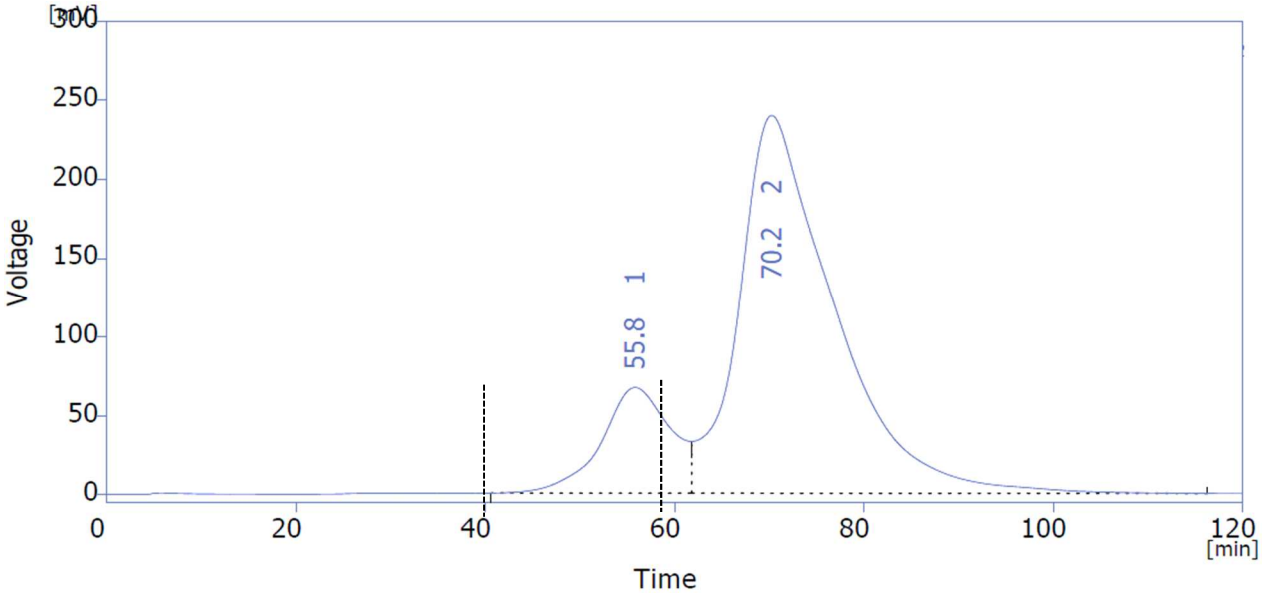

	Reten. Time [min]	Area [mV.s]	Height [mV]	Area [%]	Height [%]
1	55.787	34058.549	66.924	16.9	21.8
2	70.240	168007.951	239.467	83.1	78.2
	Total	202066.500	306.390	100.0	100.0

Figure 73: Size exclusion chromatographic results of the GOD-ssDNA$_4$ conjugate.

Column: Superdex 200™ 10/300 GL. Mobile phase: 10mM sodium phosphate, 0.14 M NaCl, (pH 7.2±0.15). Flowrate: Isocratic, 0.3 mL/min. Column and sample temperature: 25 °C. Injection volume: 100 µL. UV detection: 275 nm.

In order to investigate how a mixture of GOD and ssDNA$_4$ behaves during size exclusion chromatography, a control experiment was conducted. Results indicate a similar elution profile compared to that of the GOD-ssDNA$_4$ conjugates (Fig.74). However, the elution times of peak 1, and peak 2 very closely resemble the retentions times GOD, and ssDNA$_4$ standards (Fig.72).

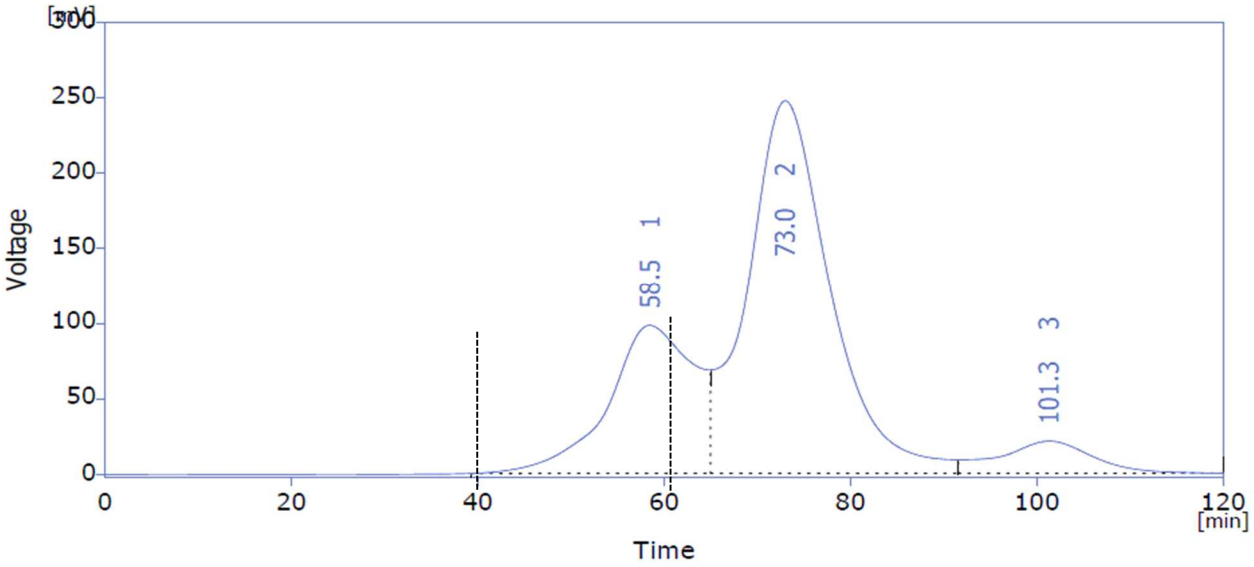

	Reten. Time [min]	Area [mV.s]	Height [mV]	Area [%]	Height [%]
1	58.482	62731.075	97.995	27.2	26.7
2	72.993	153031.881	247.362	66.4	67.5
3	101.320	14851.932	21.267	6.4	5.8
	Total	230614.888	366.624	100.0	100.0

Figure 74: Size exclusion chromatographic results of the control experiment: An equi-molar (1.68×10^{-7} mols) mixture of GOD enzyme and $ssDNA_4$ (not crosslinked).

Column: Superdex 200™ 10/300 GL. Mobile phase: 10mM sodium phosphate, 0.14 M NaCl, (pH 7.2±0.15). Flowrate: Isocratic, 0.3 mL/min. Column and sample temperature: 25 °C. Injection volume: 100 µL. UV detection: 275 nm.

In conclusion, the SEC experimental evidence depicted in Fig.74 suggests that the two biomolecules in the control experiment resemble those of the native GOD, and $ssDNA_4$. However, the leftward shift in the chromatogram profiles provides preliminary evidence to state that the EDC/Im crosslinking method had altered the surface of the GOD enzyme (i.e., synthesized a GOD-$ssDNA_4$ conjugate) (Fig.73).

5.4.3 Fluorescence spectroscopy

MALDI-TOF analyses conducted on glucose oxidase standards did not yield any peaks in the spectrographs. We suspected this was due to the structure of the enzyme. Although glucose oxidase has several ionizable amino acid side groups, our MALDI attempts were not able to ionize the glucose oxidase molecules. Therefore, we resorted to an alternative, indirect approach to detect the presence of single stranded DNA in the GOD-$ssDNA_4$ conjugates. The fluorescence

spectroscopy results obtained from separate crosslinking reactions are depicted in Fig.75. All the curves were generated after subtracting the fluorescence emission intensity values of a blank solution. The blank was made by dissolving EtBr at a final concentration of 6 μg/mL, in PBS; pH 6.2±0.2. This was the same final concentration of EtBr in all analytical samples. GOD-ssDNA$_4$ conjugate fluorescence study replicates were obtained from two SEC fractions collected from two separate crosslinking experiments. The fraction collection occurred from 40 min – 60 min (Fig.73). The concentrations of the GOD-ssDNA$_4$ fractions used in replicates 1 and 2 were 1.3 mg/mL, and 1.5 mg/mL respectively, while that of the GOD control was 1.7 mg/mL (1.06×10^{-5} M). There are clear indications of an increase in fluorescence emissions between the two curves (Fig.75).

We also observe a notable red shift in the emission spectra among ssDNA$_4$ (positive control), GOD-ssDNA$_4$, and GOD enzyme (negative control) (Fig.75). The emission maxima of ssDNA$_4$ occurs at 597 nm, while that of the GOD-ssDNA conjugates occur at an average of 605 nm. The emission maxima of the GOD enzyme occurs at 617 nm. The fluorescence emission wavelength experimentally observed in our ssDNA samples correlates with the previously reported maxima wavelength for ssDNA in PBS buffer medium as well [103]. Note that the fluorescence emission results from the positive control (ssDNA$_4$) at the equi-molar amount to that of the negative control (GOD only) yielded fluorescence intensity results outside the instrument's range (max=1000 a.u). Therefore, the ssDNA$_4$ results shown here are from a half-fold molarity. However, the most important curves (GOD control and GOD-ssDNA$_4$ conjugates) for comparison are at the same final concentration. Results indicate that there is a notable difference in the fluorescence intensities as well as the wavelength where the emission maxima occurs (Fig.75).

The control experiments were conducted with size exclusion fractions collected from an equi-molar mixture of GOD and ssDNA sample. In Fig.75, these controls are labeled as 'mock' experiments. The EDC/Im crosslinking chemistry was not conducted on these control samples. The fractions used in the 'mock' experiments were collected during SEC from 40 min – 62 min (Fig.74). The fluorescence emission intensities of the control experiments indicated higher intensities when compared to that of only the GOD enzyme (negative control). The increase in the fluorescence could be attributed to the presence of ssDNA on the control experiment sample as well. However, this could be due to two reasons. First, although fraction collection was stopped at minute 62, there may have been coelution of compounds from the neighboring peak. As peak no.2

is attributed to $ssDNA_4$ (Fig. 74), the increase in the fluorescence spec results could have been due to such coelution. However, as the fractions collected from SEC were further purified using 7000 MWCO tubes, prior to fluorescence spectroscopy, this is an unlikely scenario. The second possibility is electrostatic interactions. As GOD enzyme are positively charged molecules, the highly negatively charged ssDNA could have resulted in forming electrostatic interactions with the GOD enzyme. Regardless, the fluorescence emission of GOD-$ssDNA_4$ fractions are still approx. 56 a.u. higher than the control experiment fractions (Fig.75).

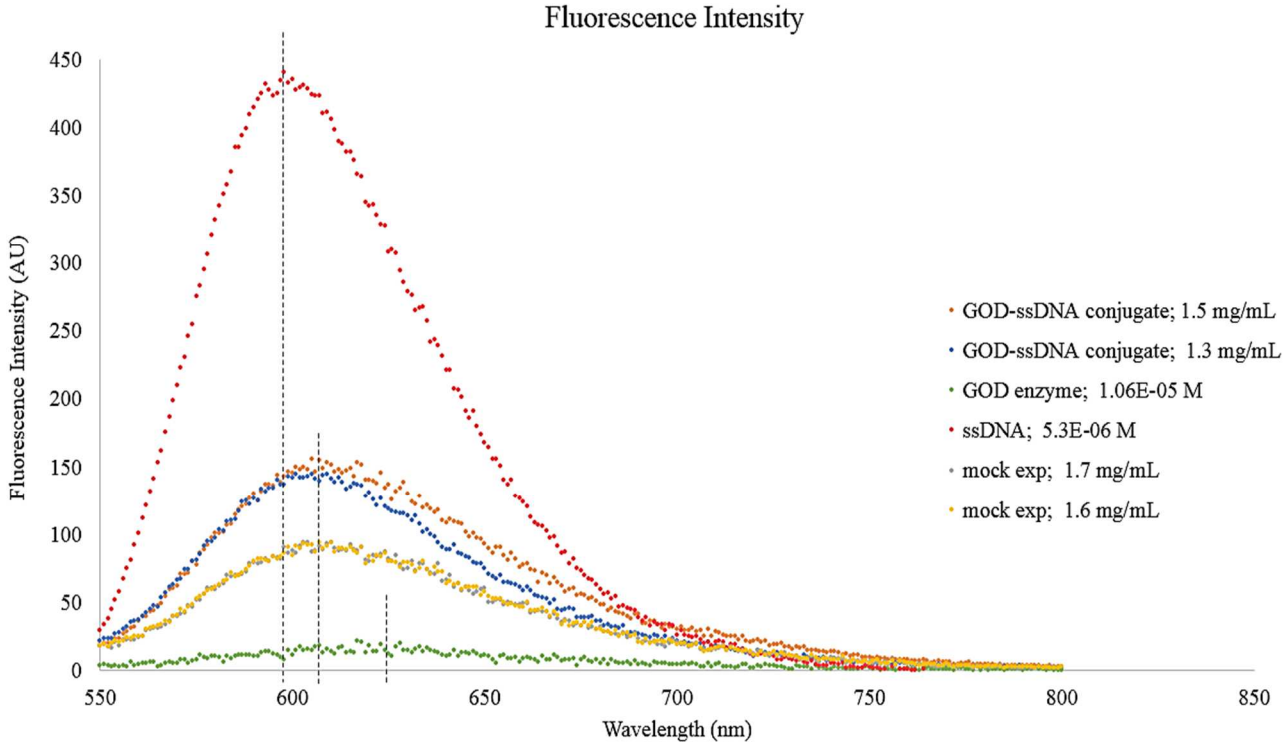

Figure 75: Fluorescence spectroscopy results of the conjugates and controls.

The results of the GOD calibration standards are depicted in Fig.76. As the concentration of GOD was increased, the intensity of the solution color increased proportionally too (Fig.76a). The fluorescence emission maxima exhibited by GOD was 622.2±7.1 nm (Fig.76). It appears that there is dismal fluorescence exhibited by GOD. However, we do observe a direct proportionality in the fluorescence emission intensity vs. the GOD concentration.

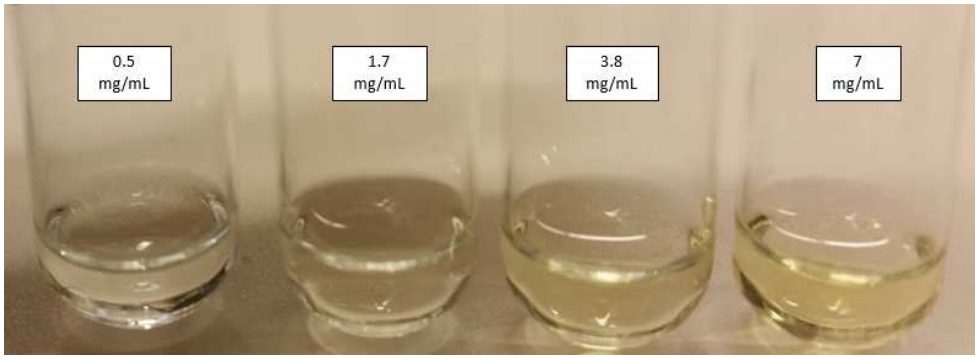

(a)

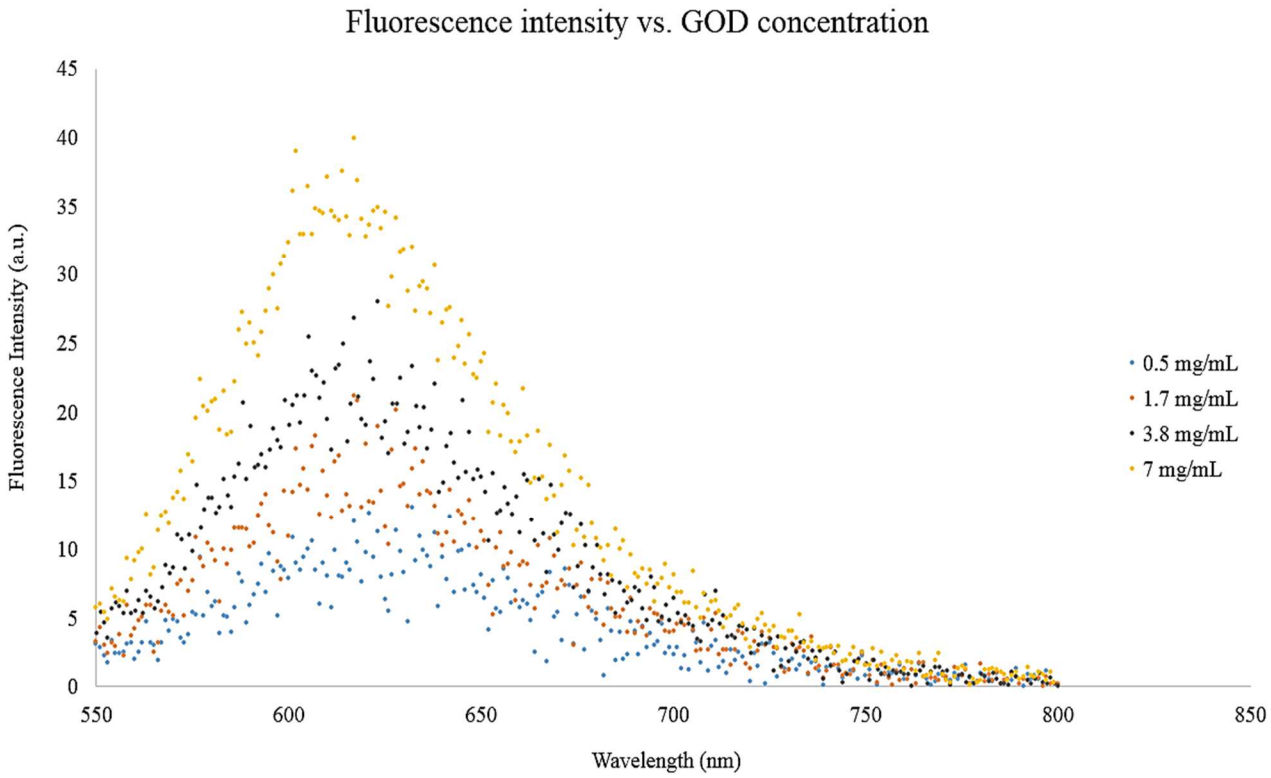

(b)

Figure 76: Digital images of GOD in PBS (a). Fluorescence spectroscopy results of the GOD calibration standards (b).

This increasing trend is unlikely to be caused by EtBr intercalation with the GOD enzymes. However, the observation of intensity increase could be attributed to differences in proton transfer due to the increase in GOD enzyme concentrations. A previous study conducted on the solvent effects explained fluorescence quenching of EtBr by proton transfer to the solvent[127]. Olmsted and Kearns developed a mechanism using protonated EtBr in ground state (EH^+), excited state

protonated EtBr (EH^{+*}), excited state deprotonated EtBr (E^{*}), and solvent (S) to explain their speculation. They suggested that EtBr molecules in their excited state (after absorbing the excitation energy supplied to it) could be quenched by proton transferring into the solvent. They attributed the increase in fluorescence intensity to reduction in the proton transfer rate. Perhaps the increase in fluorescence intensity we observe is due to an increase in the localized protons available in the GOD samples. When the localized protons in a GOD sample increases, the EH^{+*}might be present predominantly. If the increasing GOD concentrations increases the available protons, thereby decreasing proton transfer rate from EH^{+*} molecules to the buffer solvent, our observation could be explained well by the above theory.

5.4.4 Size exclusion chromatography – HRP.

5.4.4.1 Analytical size exclusion chromatography (HRP and ssDNA$_3$)

The HRP enzyme calibration curve was constructed by linear regression using standards of three known concentrations (Fig.77). The coefficients of variation (r^2) of the calibration curve was well above the general acceptance criteria. The regression curve demonstrated linearity in the concentration range tested. The y-axis corresponds to the peak height, which is recorded in AU. The x-axis is the concentration of the analyte (mg/mL).

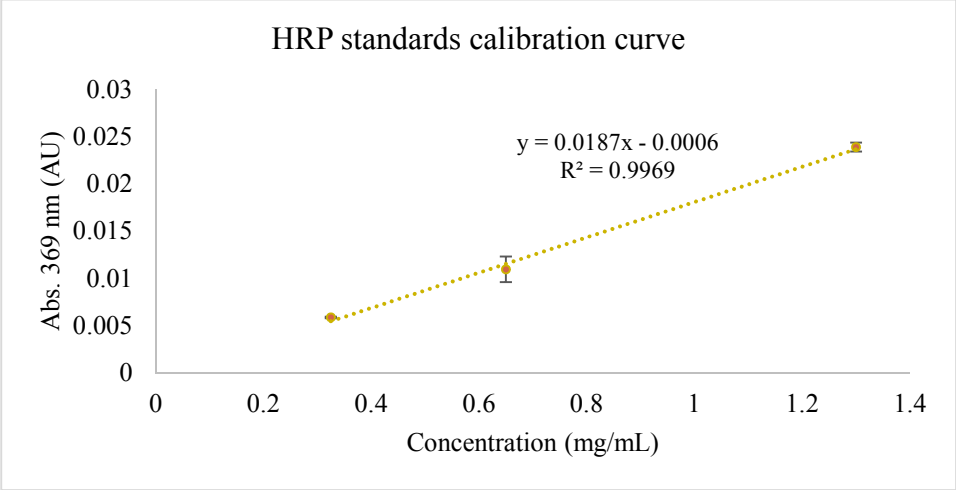

Figure 77: Standards calibration curve of horseradish peroxidase (HRP). Error bars represent ±1 SD of the peak areas from triplicate results.

Column: Superdex 200™ 10/300 GL. Mobile phase: 10mM sodium phosphate, 0.14 M NaCl, (pH 7.2±0.15). Flowrate: 0.35 mL/min. Injection volume: 100 µL. UV detection: 369 nm.

5.4.4.2 Preparative size exclusion chromatography: HRP-ssDNA$_3$ conjugates

Size exclusion results from the horseradish peroxidase (HRP) standard, and ssDNA$_3$ indicate that HRP elutes at a retention time of 65.4 min, while the ssDNA$_3$ elutes at a retention time of 72.4 min (Fig.78).

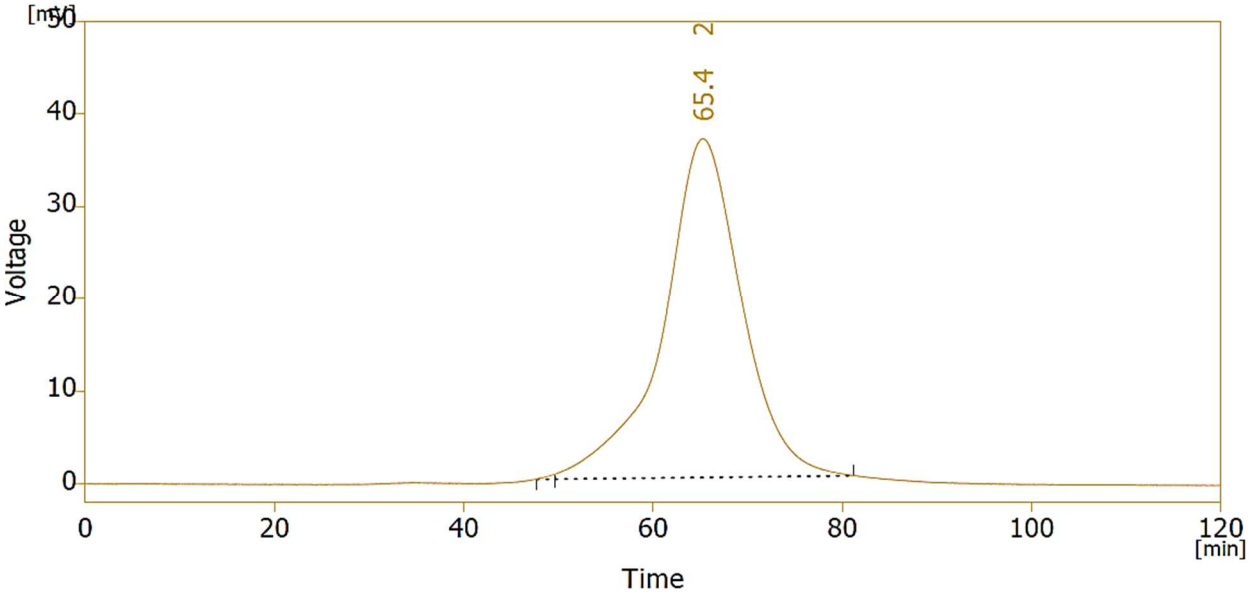

	Reten. Time [min]	Area [mV.s]	Height [mV]	Area [%]	Height [%]
1	49.604	30.596	0.537	0.1	1.4
2	65.384	21130.629	36.627	99.9	98.6
	Total	21161.225	37.164	100.0	100.0

(a)

Figure 78: Size exclusion chromatographic results of; horseradish peroxidase (HRP) standard, at a final concentration of 1.2×10^{-4} M, detection at 415 nm (a) ssDNA$_3$ standard at a final concentration of 1.2×10^{-4} M, detection at 260 nm (b).

Column: Superdex 200™ 10/300 GL. Mobile phase: 10mM sodium phosphate, 0.14 M NaCl, (pH 7.2±0.15). Flowrate: 0.3 mL/min. Injection volume: 100 µL. *Note: The y-axis scales of the two chromatograms are different.

Figure 78 continued

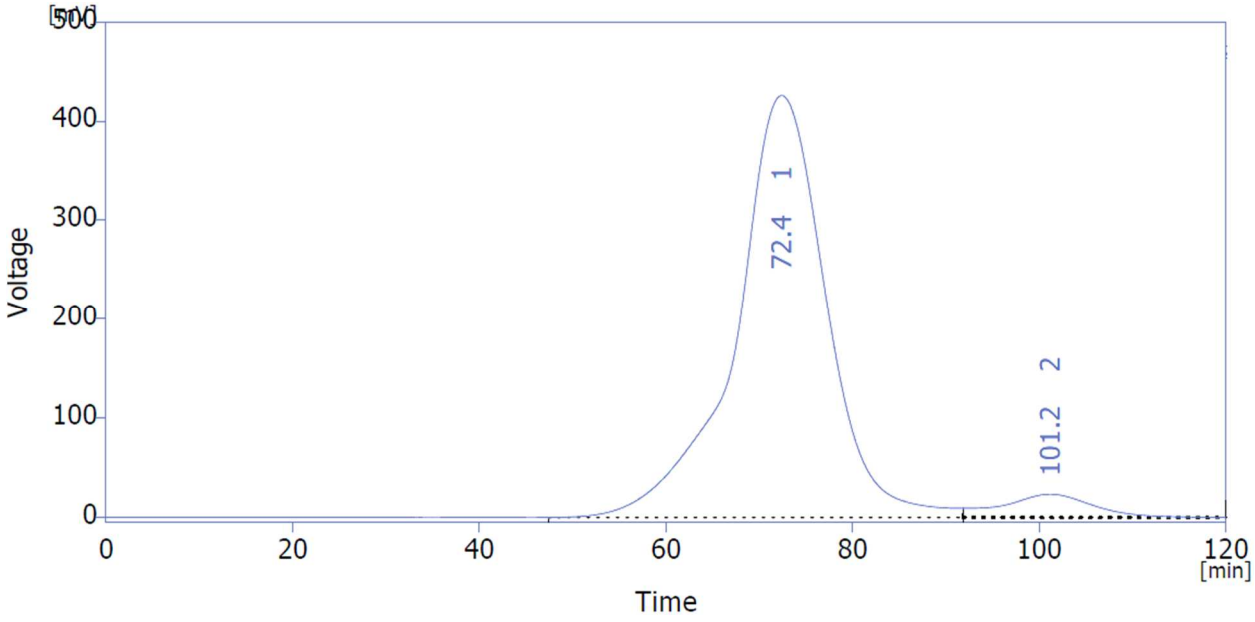

	Reten. Time [min]	Area [mV.s]	Height [mV]	Area [%]	Height [%]
1	72.422	287275.363	425.980	94.8	94.8
2	101.182	15784.118	23.406	5.2	5.2
	Total	303059.481	449.386	100.0	100.0

(b)

SEC was utilized to collect fractions of the HRP-ssDNA$_3$ conjugates from the 45th min – 70th min. Results indicated that the retention time of the conjugate is 65.45±0.58 min (n=6 determinations). Two separate conjugate reactions were conducted, and each conjugate sample was analyzed on SEC in triplicates. Fig.79 illustrates the resulting chromatographs of the HRP-ssDNA conjugates.

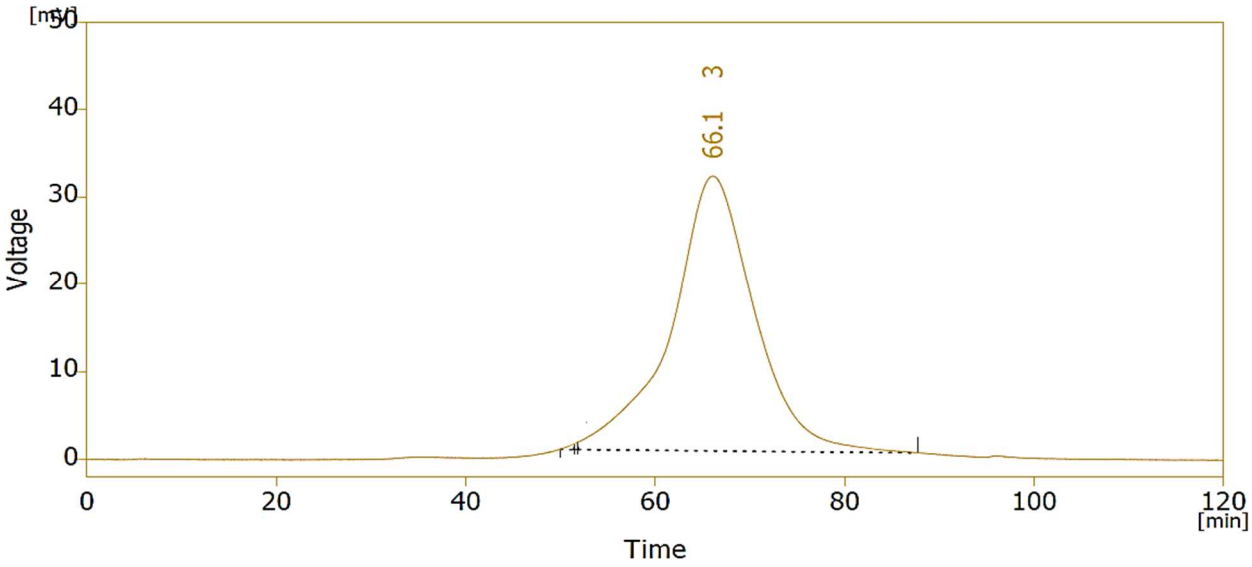

	Reten. Time [min]	Area [mV.s]	Height [mV]	Area [%]	Height [%]
1	51.404	27.873	0.644	0.1	2.0
2	51.822	19.730	0.842	0.1	2.6
3	66.116	19135.752	31.434	99.8	95.5
	Total	19183.355	32.920	100.0	100.0

Figure 79: Size exclusion chromatographic results of the HRP-ssDNA$_3$ conjugate. Column: Superdex 200™ 10/300 GL. Mobile phase: 10mM sodium phosphate, 0.14 M NaCl, (pH 7.2±0.15). Flowrate: 0.3 mL/min. Injection volume: 100 µL. UV detection: 415 nm.

It was important to determine the profile of a mock-experiment. SEC experiments were conducted with an equi-molar mixture of HRP and ssDNA$_3$ without carrying out the EDC/Im crosslinking protocol. Fig.80(a) and 80(b) indicate the size exclusion chromatograms obtained under UV-Vis detection at 260 nm, and at 415 nm respectively. The retention time of major peak of the HRP, ssDNA$_3$ mixture detected at 260 nm resembles the chromatograph obtained for the ssDNA$_3$ standard (Fig.80a). The retention time of the major peak of the HRP, ssDNA$_3$ mixture detected at 415 nm resembles the chromatograph obtained for the HRP standard (Fig.80b).

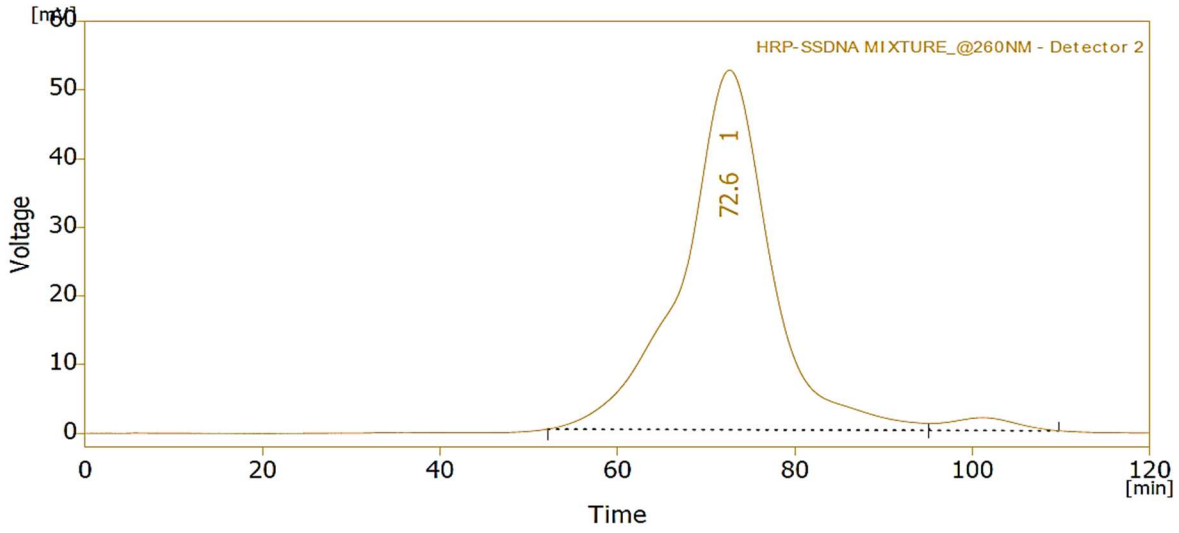

	Reten. Time [min]	Area [mV.s]	Height [mV]	Area [%]	Height [%]
1	72.633	35945.639	52.370	97.3	96.6
2	101.269	985.839	1.862	2.7	3.4
	Total	36931.478	54.232	100.0	100.0

(a)

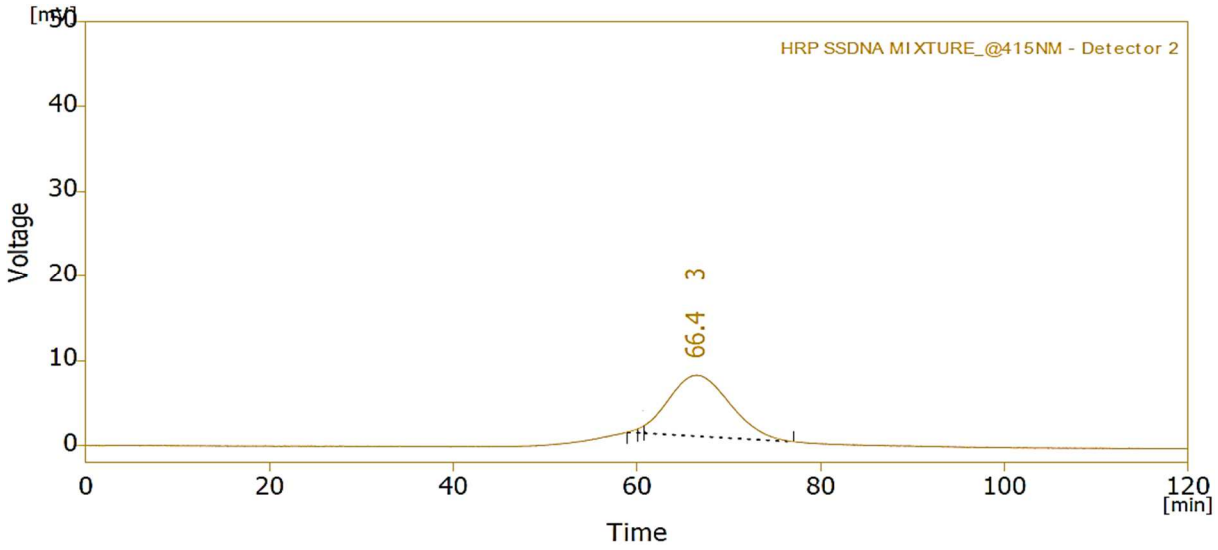

	Reten. Time [min]	Area [mV.s]	Height [mV]	Area [%]	Height [%]
1	60.071	15.713	0.473	0.5	5.5
2	60.800	29.010	0.923	0.9	10.8
3	66.382	3311.972	7.173	98.7	83.7
	Total	3356.695	8.570	100.0	100.0

(b)

Figure 80: Size exclusion chromatographic results of an equi-molar (3.86×10^{-8} mols) mixture of HRP enzyme and $ssDNA_3$; at 260 nm detection (a), at 415 nm detection (b).

Column: Superdex 200™ 10/300 GL. Mobile phase: 10mM sodium phosphate, 0.14 M NaCl, (pH 7.2±0.15). Flowrate: Isocratic, 0.3 mL/min. Injection volume: 100 µL.

5.4.5 Molecular weight analysis of HRP-ssDNA$_3$ conjugates: MALDI-TOF

MALDI-TOF results from the horseradish peroxidase samples indicated a major peak at 43,078 Da (Fig.81a), corroborating well with the manufacturer reported avg. molecular weight (44,000 Da). The molecular weight of the ssDNA$_3$ is at 4643 Da (Fig.81b).

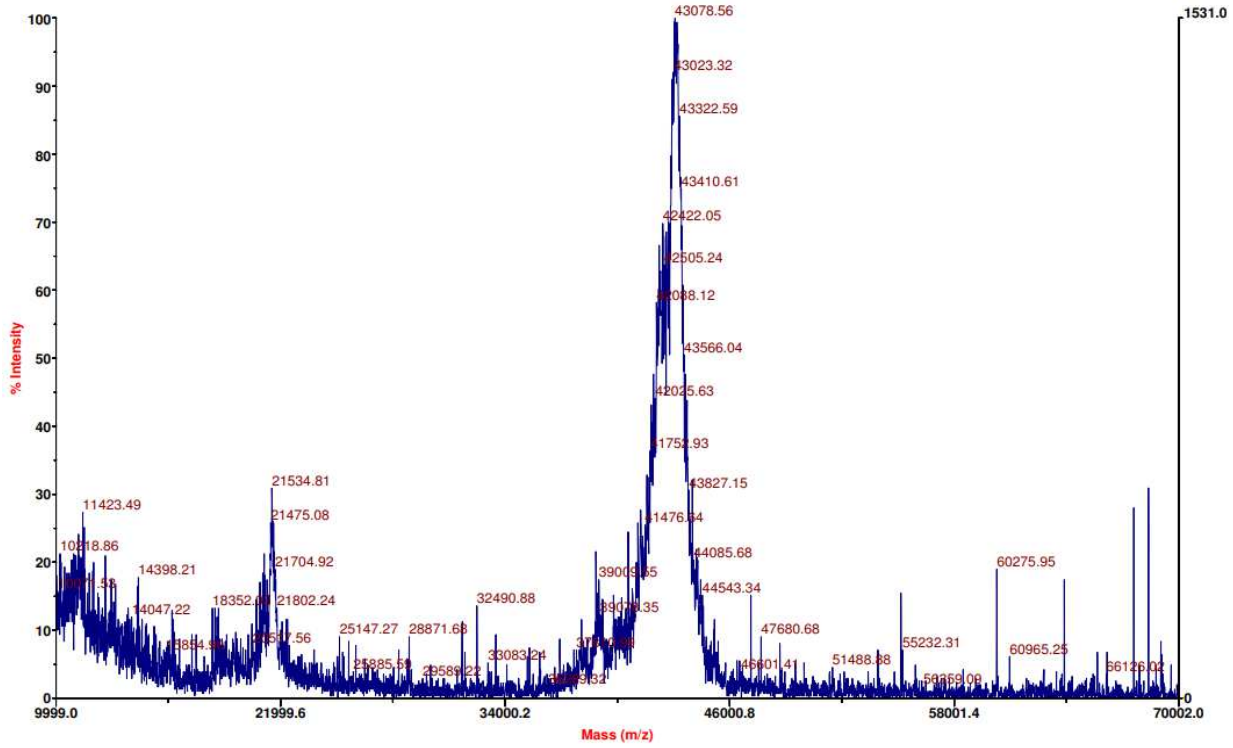

(a)

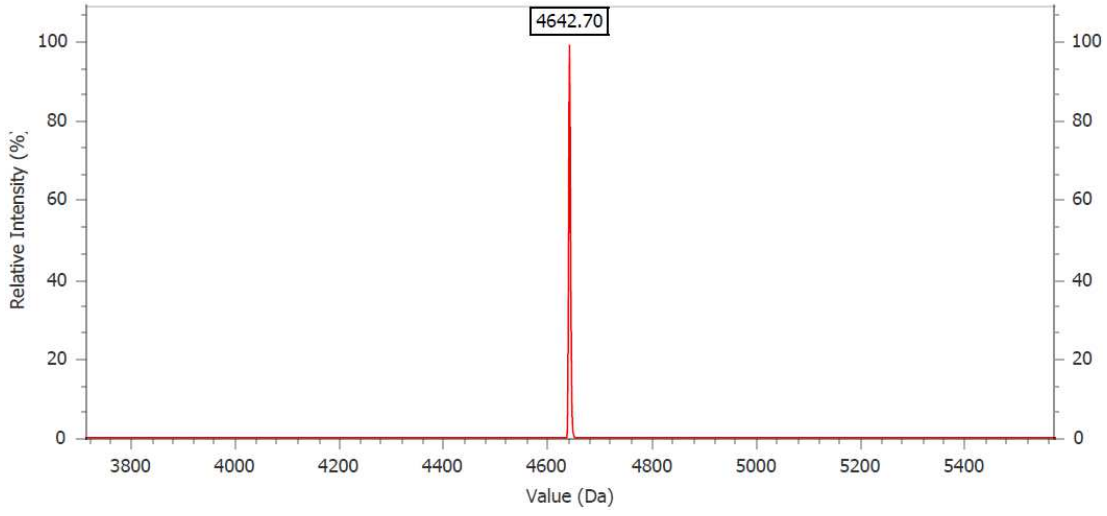

(b)

Figure 81: MALDI-TOF mass spectrum of HRP (a), ESI mass spectrum of $ssDNA_3$ (b).

In order to determine whether the expected HRP-$ssDNA_3$ conjugates were formed, MALDI-TOF analyses were conducted. Two major peaks (no.1 and 2, Fig.82) were observed at approx. 66,360 Da, and 71,100 Da. When each of these two molecular weights are subtracted from that of the HRP standard's molecular weight, the resulting values are 23,286 Da, and 28,039 Da. These resulting values indicate how much mass was added to the original HRP enzyme. When each are divided by the molecular weight of the starting material $ssDNA_3$ (4643 Da), we obtain the number of $ssDNA_3$ attached to the HRP enzyme. Like so, peak 1 and 2 are the resulting conjugates from attaching 5 mols of $ssDNA_3$, and 6 mols of $ssDNA_3$ onto one mole of HRP enzyme (Fig.82).

HRP has six available amino groups on the surface of the HRP enzyme [59]. The experimental procedure was conducted with 1:1 molar ratio of HRP: $ssDNA_3$. Therefore, there is a probability of more than one $ssDNA_3$ molecules functionalizing onto one molecule of HRP. Like so, up to six phosphoramidate bonds could be formed in one HRP molecule.

The process of bioconjugation, under the most controlled and optimal conditions, can result in a number of different structural species making up the final composition. When two components are reacted together and at least one of them has multiple sites for covalent attachment. Therefore, with HRP containing multiple amines, the resultant bioconjugate could likely have a distribution of molecular weights around an average mass. This is the explicable reason for the multiple ssDNA additions onto one HRP molecule.

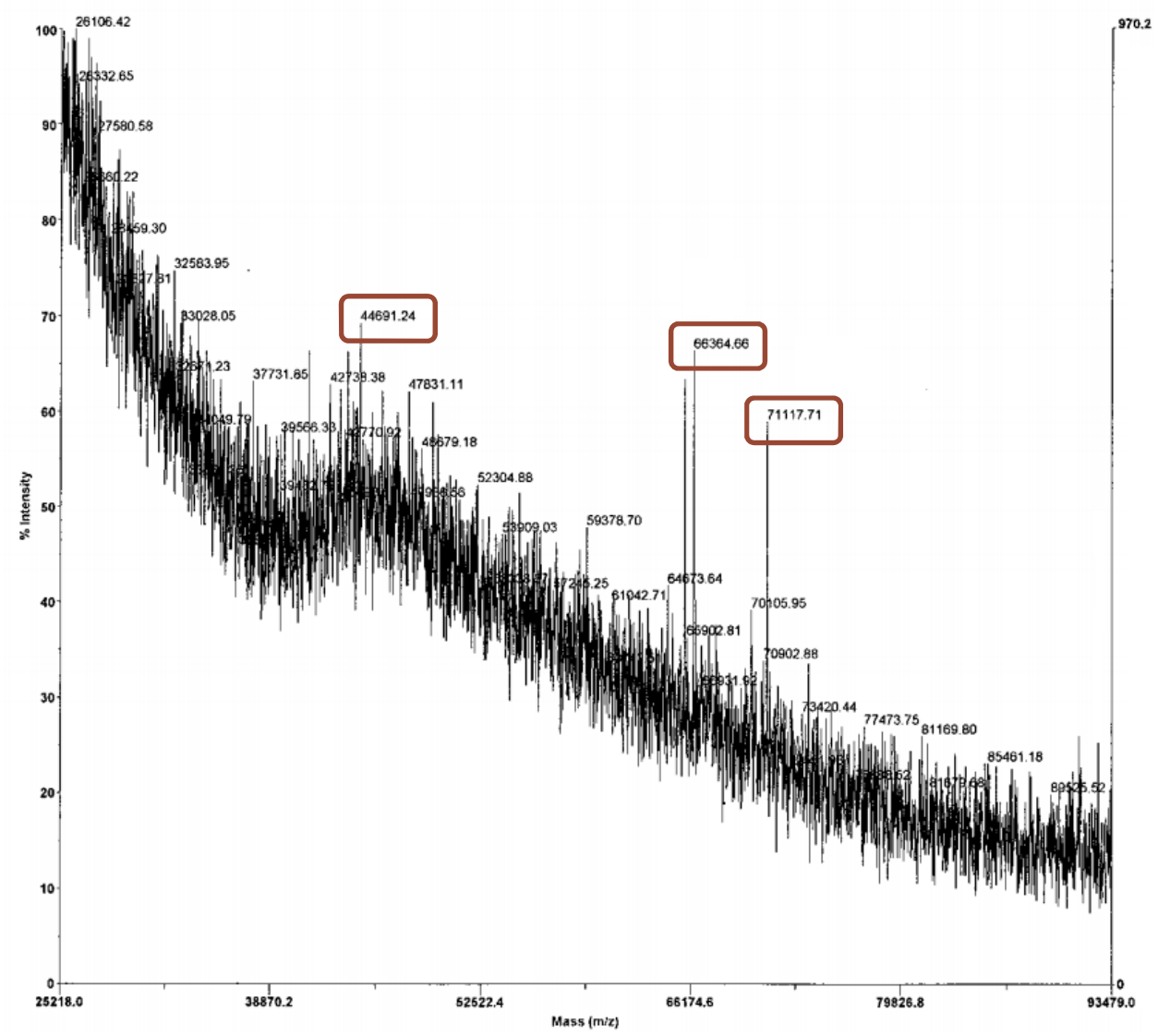

Figure 82: MALDI-TOF mass spectrum of the purified HRP-ssDNA$_3$ conjugate.

In order to determine whether the SEC fractions collected from the HRP-ssDNA$_3$ conjugates contained any unreacted ssDNA$_3$, we conducted MALDI-TOF analyses on the recovered samples after exhaustive dialysis on 7000 MWCO tubes. The scans obtained from the purified HRP-ssDNA$_3$ conjugate fractions indicate no signs of unreacted ssDNA$_3$ (Fig.83). If there was any unreacted ssDNA$_3$, we would expect to observe a signal around 4657 Da, which is the molecular weight of ssDNA$_3$. Fig.83 below illustrates that there is no m/z peak in that range, indicating that our purification steps have successfully removed any unreacted ssDNA$_3$. This is

important because any residual ssDNA lingering from either enzyme-ssDNA conjugates could lead to undesired products during the final macromolecule assembly, i.e., residual $ssDNA_3$ and $ssDNA_4$ remaining in the final samples will lead to dsDNA formations during the DNA hybridization at final aim in our study. If so, the separate dsDNA material eluting peaks could confound with the major peak of the GOD-dsDNA-HRP macromolecule.

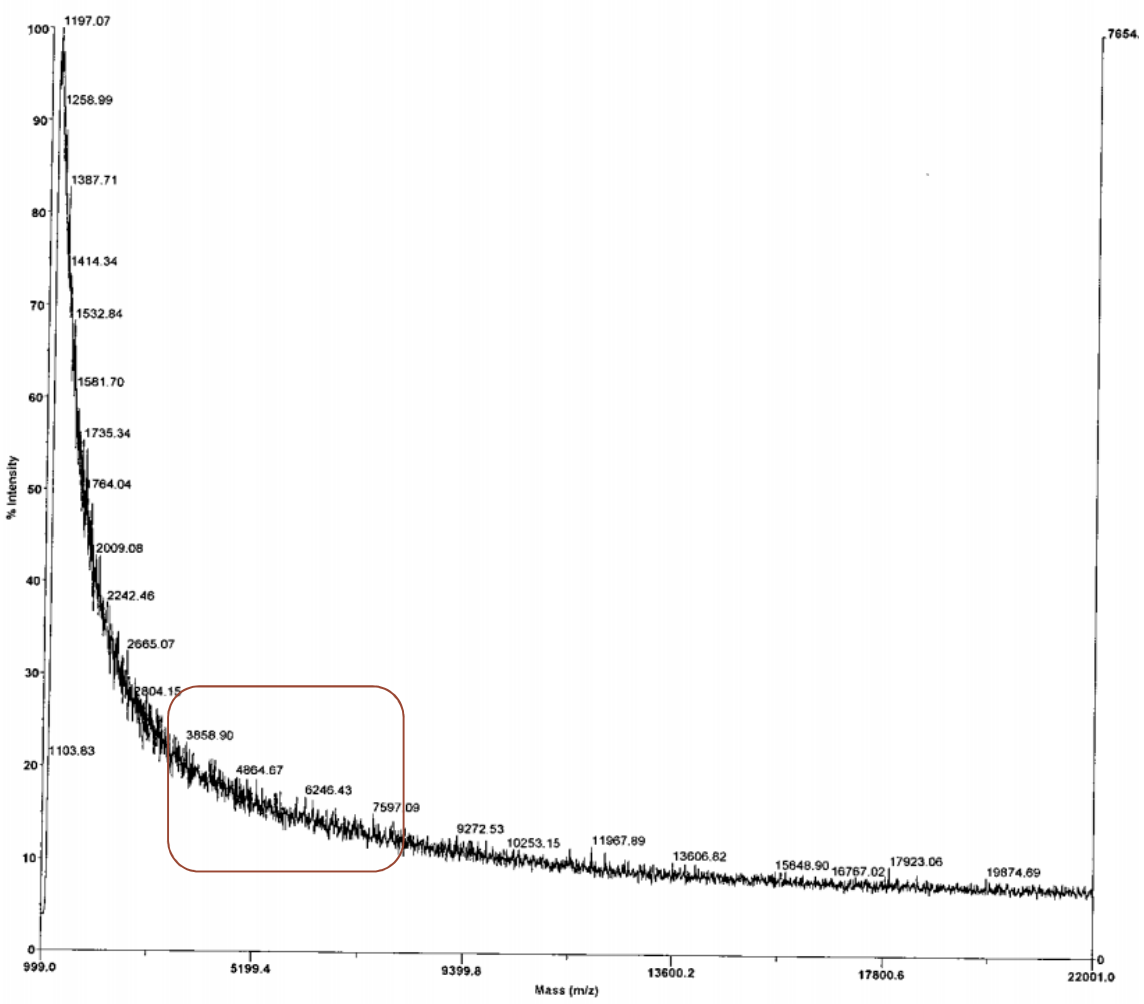

Figure 83: MALDI-TOF results of the purified HRP-$ssDNA_3$ conjugates, contd.

In a typical enzyme-ssDNA bioconjugate purification procedure via size exclusion chromatography, approx. 0.0008 g of enzyme-ssDNA bioconjugate was recovered from one SEC injection (injection volume = 100 µL). Therefore, when scaled-up to the original volume in the

bioconjugate product sample, the total recovered product was determined to be approx. 0.008 g. This corresponds to an approximation of 53% enzyme-ssDNA bioconjugate product yield.

5.4.6 Final GOD-dsDNA-HRP macromolecule: Size exclusion chromatography

Size exclusion results of the final biomacromolecules obtained from two independent reaction samples are indicated in Fig.84. The results showed a single, broad peak spanning from 45^{th} min – 95^{th} min (Fig.84). These chromatographs provide preliminary evidence directing in two possibilities; (1) DNA hybridization has enabled the formation of the GOD-dsDNA-HRP final macromolecule. (2) The GOD-ssDNA$_4$ and HRP-ssDNA$_3$ conjugates are all simply co-existing in the final sample, and are co-eluting.

Firstly, it is important to note that GOD-ssDNA$_4$ and HRP-ssDNA$_3$ fractions were collected separately. The fraction of the GOD-ssDNA$_4$ collection spanned from 40^{th} min – 58^{th} min (Fig.73). The fraction of the HRP-ssDNA$_3$ collection spanned from the 45^{th} min – 70^{th} min (Fig.79). Both the fractions collected from SEC were further purified using 7000 MWCO dialysis tubes.

Secondly, our MALDI-TOF results of the HRP-ssDNA$_3$ did not indicate any unreacted ssDNA$_3$ in the spectrographs. Lastly, the final reaction sample (i.e., after GOD-ssDNA$_4$ and HRP-ssDNA$_3$ were annealed via hybridization) was also purified using 7000 MWCO dialysis tubes. Considering all of the above factors, we can state that the purified enzyme-ssDNA fractions did not contain any residual ssDNA. Therefore, the singular peak we observe in the final GOD-dsDNA-HRP macromolecule can not be due to residual single stranded DNA.

The elution time of the final enzyme macromolecule is later than expected. However, it is important to remember that in size exclusion, it is the Stokes radius of the molecules which determine their elution from the size exclusion column matrix. Perhaps the shape of the final GOD-dsDNA-HRP macromolecule was the reason for the inexplicable its elution from the size exclusion column. When macromolecules vary in shape such as globular, or rigid rod-like shapes, the Stokes radius does not correlate with the molecular weight. Therefore, based on the final shape, and orientation of our enzyme-DNA macromolecule, perhaps the Stokes radius contributed largely to the elution of our final macromolecule at a later time. Therefore, the uniform singular peak illustrated in Fig.84 was attributed to GOD-dsDNA-HRP macromolecule.

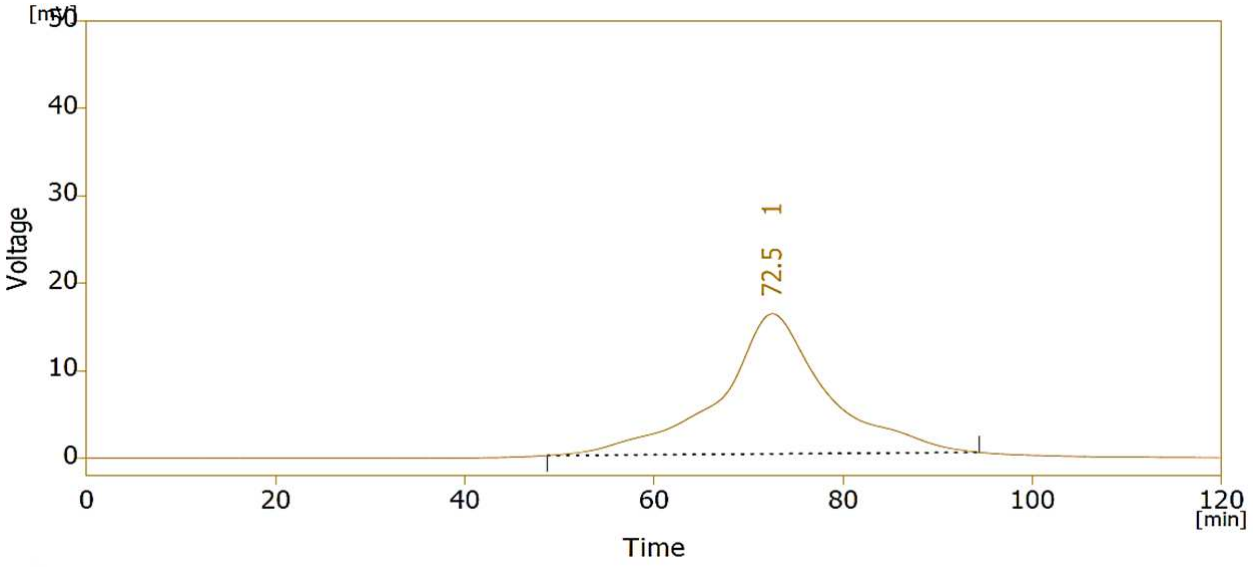

	Reten. Time [min]	Area [mV.s]	Height [mV]	Area [%]	Height [%]
1	72.502	12543.469	16.021	100.0	100.0
	Total	12543.469	16.021	100.0	100.0

(a)

Figure 84: Size exclusion chromatographic results of the final biomacromolecule, GOD-dsDNA-HRP; detected at 275 nm (a), at 260 nm (b), at 415 nm (c).

Column: Superdex 200™ 10/300 GL. Mobile phase: 10mM sodium phosphate, 0.14 M NaCl, (pH 7.2±0.15). Flowrate: Isocratic, 0.3 mL/min. Column and sample temperature: 25 °C. Injection volume: 100 µL.

Figure 84 continued

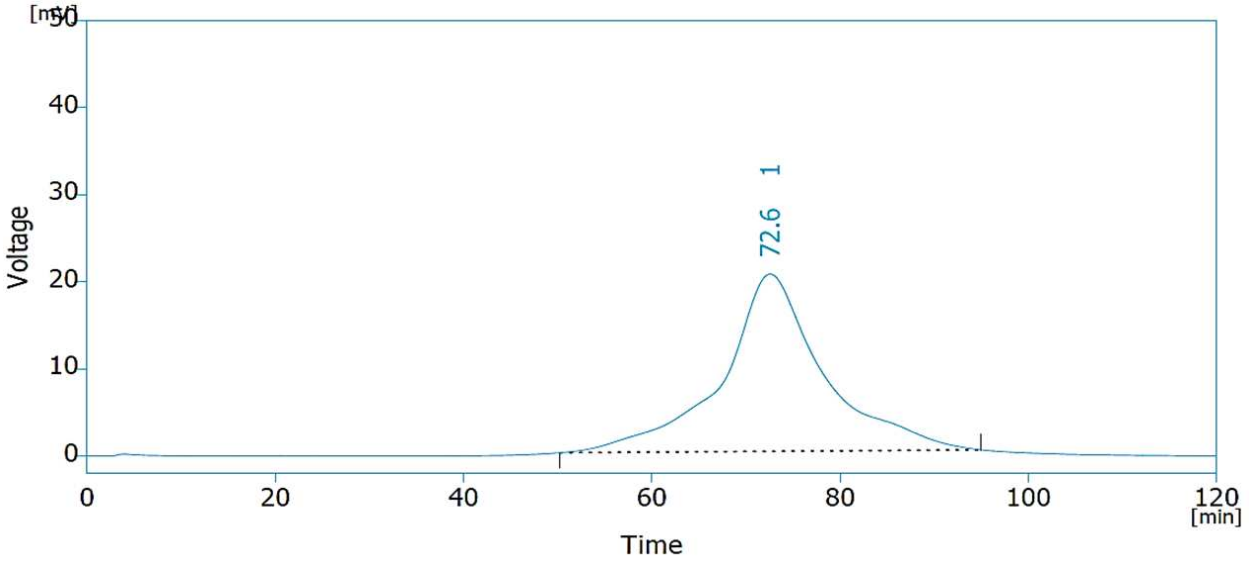

	Reten. Time [min]	Area [mV.s]	Height [mV]	Area [%]	Height [%]
1	72.600	15201.450	20.351	100.0	100.0
	Total	15201.450	20.351	100.0	100.0

(b)

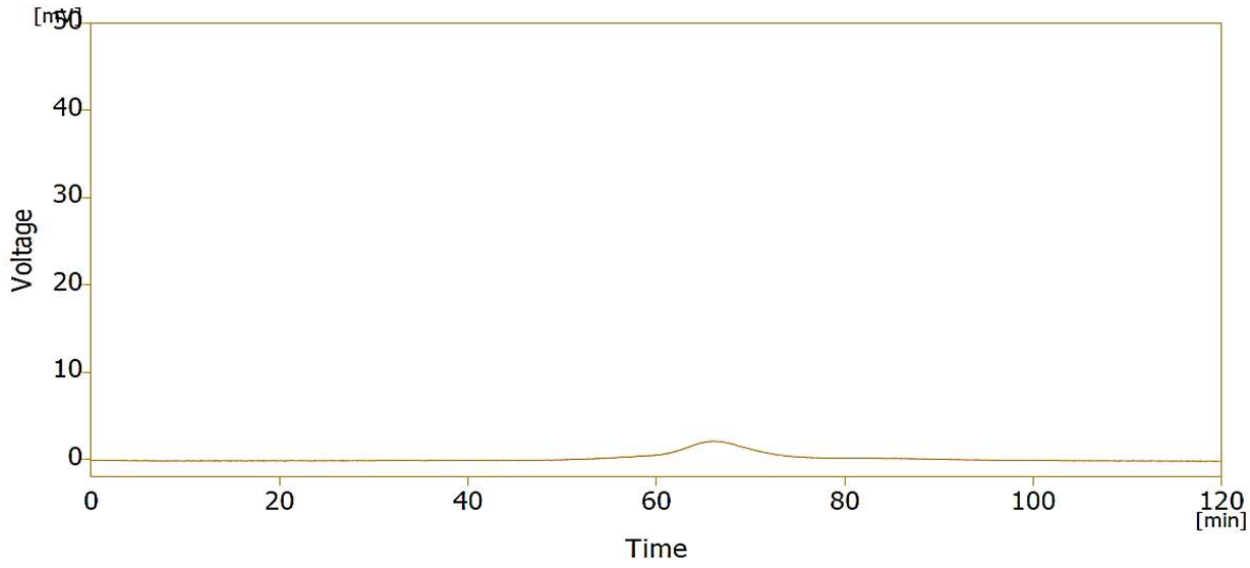

(c)

5.5 Conclusions

Glucose oxidase is an enzyme which contains up to 30 lysine residues on the wild-type enzyme's surface. The amino functional groups of these lysine residues, and the terminal phosphoryl group of a single stranded DNA ($ssDNA_4$) was crosslinked using a previously demonstrated carbodiimide/imidazole (EDC/Im) crosslinking method. The resulting GOD-$ssDNA_4$ conjugates were analyzed using size exclusion chromatographic (SEC) methods and fluorescence spectroscopy. The observed differences in the SEC elution times of the GOD-$ssDNA_4$ conjugates compared to those of the GOD and ssDNA control experiments provided evidence to suggest successful crosslinking. Further analyses on fluorescence spectroscopy conducted from purified GOD-$ssDNA_4$ conjugates showed that the GOD-$ssDNA_4$ conjugates exhibit enhanced fluorescence intensities compared to those of the controls. Altogether, these results suggest that the EDC/Im crosslinking method was successful in producing the expected GOD-$ssDNA_4$ conjugates.

Horseradish peroxidase is an enzyme which contains up to 6 lysine groups on the enzyme's surface. The amino functional groups of these, and the terminal phosphoryl group of a single stranded DNA ($ssDNA_3$) were crosslinked using the same EDC/Im crosslinking technique. The resulting HRP-$ssDNA_3$ conjugates were analyzed on SEC, and MALDI-TOF. As the elution times of the HRP standard and the HRP-$ssDNA_3$ conjugates were very close, SEC results alone were not able to determine successful HRP-$ssDNA_3$ conjugation. Therefore, HRP-$ssDNA_3$ molecular weight analyses was conducted using MALDI-TOF. These results showed that the crosslinking procedure has successfully attached several mols of $ssDNA_3$ onto one mol of HRP enzyme.

The two separate enzyme-ssDNA conjugates formed herein were utilized in a final enzyme macromolecule construction, facilitated by DNA hybridization. The resulting GOD-dsDNA-HRP macromolecule was re-analyzed on size exclusion chromatography. A singular peak was observed spanning from 45 – 95 min, which was attributed to the expected hybrid enzyme macromolecule. The elution time of the final enzyme macromolecule is later than expected. However, it is important to remember that in size exclusion, it is the Stokes radius of the molecules which determine their elution from the size exclusion column matrix. When macromolecules vary in shape, e.g., globular, or rigid rod-like shapes, the Stokes radius does not correlate with the

molecular weight. Therefore, based on the final shape, and orientation of our enzyme-DNA macromolecule, perhaps the Stokes radius contributed largely to the elution of our final macromolecule at a retention time later than expected.

CHAPTER 6. CONCLUSIONS AND FUTURE WORK

6.1 Conclusions

Bioconjugation techniques is a fast growing area of research. These powerful methods enable researchers to manipulate diverse biological molecules in order to synthesize multi-functional molecules. Multifunctional molecules obtained via bioconjugation techniques are frequently used in constructing biomaterials, biosensors, bioassays, and next-generation vaccines. Therefore, there is a need to study and optimize bioconjugation techniques because these powerful techniques hold the foundation to molecular nanotechnology.

Bioconjugation is generally accomplished via bottom-up syntheses, where small components of the final macromolecule are assembled sequentially. Bioconjugation techniques could be divided into two major categories called site-specific techniques, and random techniques. Site-specific methods such as “click” reactions enable researchers to control the final bioconjugate product yields. However, one of the biggest drawbacks in site-specific bioconjugation techniques is the necessity for derivatizing each biomolecule with the necessary functional groups required for the bioconjugation reaction to take place. Such prior derivatization is time consuming, and are not universally extensible to wild-type peptides, proteins, enzymes, and antibodies. Furthermore, if an enzyme’s active site is perturbed during a derivatization step, it could result in loss of enzyme functionality. On the contrary, random bioconjugation techniques such as crosslinking do not require prior derivatization of naturally occurring biomolecules. The trade-off in crosslinking is poor bioconjugate product yields due to possible side-reactions.

Direct crosslinking of enzymes limits the ability to control the distance between enzymes. The maximum spacer arm length of crosslinkers available up-to-date is approx. 15 Å. Depending on the enzymes used in a bioconjugation study, the lack of ability to control the distance, could bring the enzymes too close together. This could lead to steric clashes of the two enzymes, as well

as potential product inhibition due the proximity of enzymes in the micro-environment. As this was recognized as a drawback, giving rise to kinetic limitations of an enzymatic system, we investigated the ability to attach single stranded DNA to enzymes, to synthesize enzymatic cascades with the flexibility to control the distance between enzymes.

Accounting for all of the above factors, the major focus of this investigation was to determine relatively inexpensive, less complex, and universal bioconjugation techniques with the flexibility to control the distance between wild-type enzymes or proteins.

In the first aim of the study, an adapted strategy from the conventional 1-ethyl-3-(3-dimethylaminopropyl) carbodiimide hydrochloride (EDC) was developed to form a novel phosphoramidated single stranded DNA (ssDNA) bioconjugate. A phosphoramidate bond was formed between a 5' terminal phosphoryl group in ssDNA, and a primary amine group in ethylenediamine. Previously EDC has been used to crosslink carboxyl groups with amine groups. However, the current study demonstrates that phosphoryl functional groups could be used instead of carboxyl groups to carry out EDC crosslinking. The phosphoramidation reaction between a phosphoryl and a primary amine was mediated by the crosslinker, EDC. The adapted method (EDC/Im) was tested where imidazole (Im) was used during the EDC reaction scheme. The EDC/Im reaction method was compared to the conventional EDC reaction method in relation to reaction efficiencies. An RP-HPLC chromatographic analytical method was developed to determine the product yields. The analytical procedure's accuracy, precision, linearity, limit of detection (LOD), and limit of quantitation (LOQ) were determined. Afterwards, the yield of the phosphoramidated ssDNA bioconjugate was determined using the developed analytical procedure. The bioconjugate yield obtained from the EDC/Im method had a percentage yield of 79.0±2.4% while that of the conventional EDC method was 68.3%±2.2%. The approx 10% increase in the yield percentage obtained from the EDC/Im method was statistically significant. MALDI-TOF results of the ssDNA bioconjugate indicates that the phosphoramidate bond is stable up to 14 days. If this ssDNA bioconjugate were to be utilized in future studies, it is recommended that the dialyzed bioconjugate sample is lyophilized and stored at -20 °C. In our attempts to determine suitable crosslinkers, another crosslinker (BS3) was also investigated to accomplish bioconjugation between ssDNA, and a small peptide. However, MALDI-TOF results indicated conjugate molecular weights evidencing only partial bioconjugate formation (i.e., only one end of

the crosslinker successfully reacting with one of the two biomolecules). At the conclusion of the BS3 crosslinking studies, we speculated that the key factor governing successful amide bond formation between the NHS-ester in the crosslinker owes to complete deprotonation of the primary amine containing biomolecule.

In the next aim, the successful EDC/Im crosslinking technique was implemented to synthesize glucose oxidase-ssDNA$_4$ (GOD-ssDNA$_4$), and horseradish peroxidase-ssDNA$_3$ (HRP-ssDNA$_3$) conjugates separately. These enzyme-ssDNA conjugates were analyzed, and purified using size exclusion chromatography (SEC). Fluorescence spectroscopy was used to determine the presence of ssDNA in the GOD-ssDNA$_4$ bioconjugates, while MALDI-TOF spectrometry was used to determine the molecular weights of the HRP-ssDNA$_3$ bioconjugates. Analyses on fluorescence spectroscopy conducted from carefully purified GOD-ssDNA$_4$ conjugates showed that the GOD-ssDNA$_4$ conjugates exhibit enhanced fluorescence intensities compared to those of the controls. MALDI-TOF analyses on HRP-ssDNA$_3$ conjugates showed that the EDC/Im crosslinking procedure has successfully attached several mols of ssDNA$_3$ onto one mol of HRP enzyme. Altogether, size exclusion chromatography, fluorescence spectroscopy, and MALDI-TOF results suggest that the EDC/Im crosslinking method was successful in producing the expected enzyme-ssDNA conjugates.

In order to spontaneously assemble the GOD-ssDNA$_4$, and HRP-ssDNA$_3$ bioconjugates, DNA hybridization was utilized. However, high annealing temperatures used in the general heating-cooling protocols has the potential to degenerate these enzyme conjugates. Therefore, possibilities of accomplishing DNA hybridization at lowered annealing temperatures was investigated as well. UV and fluorescence spectroscopy results illustrated that spontaneous DNA hybridization is achievable via a simple heating-cooling process, at a temperature slightly above the T_m of the DNA (at 45 °C).

After facilitating DNA hybridization between GOD-ssDNA$_4$ and HRP-ssDNA$_3$, the final enzymatic macromolecule was analyzed on size exclusion chromatography. Results indicated a single peak which was attributed to the final expected GOD-dsDNA-HRP macromolecule. However, albeit consisting of a much larger molecular weight, the macromolecule indicated an elution at approx. 73 min. We speculate that the unexpected retention time of the final enzymatic

macromolecule could be due to its final structure or shape. As the macromolecule consisted of two enzymes with largely disparate molecular weights, the final shape of the macromolecule was perhaps no longer globular. This difference in shape could have resulted in a Stokes radius which governed the macromolecule's elution from the size exclusion column. Future work encompassing further confirmation of this plausibility are discussed in the next section.

6.2 Future work

The random bioconjugation techniques, reaction optimization, and bioconjugate characterization discussed in the preceding chapters holds some areas of possible expansion via future studies. First, further optimization could be implemented on the EDC/Im crosslinking reaction. As illustrated and discussed in Chapter 2 (Fig.11), the amination reaction is favored under basic conditions. Therefore, a future design of experiments should encompass increasing the pH of the solution containing imidazole (Im), and the amine containing biomolecule. Furthermore, bond characterization techniques such as Fourier transform infrared spectroscopy (FTIR) could be utilized to confirm formation of a phosphoramidate bond between the phosphoryl group in ssDNA and the primary amine in ethylenediamine.

Using size exclusion chromatography to purify ssDNA material prior to usage is also a fascinating approach. As truncated impurities present in starting ssDNA material will consist of much lesser molecular weights, perhaps size exclusion chromatography (SEC) could be utilized to further purify the reactant ssDNA. Furthermore, future work should also test the correlation of Stokes radius to the retention time, by utilizing a variety of biomolecules containing different molecular weights and shapes.

In order to confirm that DNA hybridization facilitated spontaneous assembly of the final enzymatic macromolecule, two methodologies could be followed. First, chemical dsDNA denaturation (i.e., separation of dsDNA into two ssDNA strands) methods such as increasing the buffer alkalinity could be explored. Superdex™ size exclusion columns generally contain a pH stability range of 3 – 12. Therefore, if the recovered final product is re-suspended in a more basic buffer (c.a. PBS; pH 9), and analyzed on SEC, the dsDNA structure could be denatured into their corresponding ssDNA structure. This essentially means that the final enzymatic assembly is now

separated into the two separate enzyme-ssDNA bioconjugates. Secondly, enzyme-ssDNA bioconjugation experiments could be conducted with non-complimentary DNA sequence. Then, after combining the two separate bioconjugates, we would not expect DNA hybridization to take place. This would then fail to form the expected GOD-dsDNA-HRP macromolecule.

In both of these approaches, during the SEC analytical procedure, the expected elution profile would correspond to the respective GOD-ssDNA, and HRP-ssDNA bioconjugate elution profiles, as opposed to the singular peak owing to the final enzymatic macromolecule.

Lastly, future investigations for this study could be aligned in determining enzyme kinetics of the co-localized enzymatic model (i.e., GOD-dsDNA-HRP macromolecule), and comparing them to those of a non co-localized GOD and HRP enzymatic system (i.e., free-floating). A Michaelis-Menten (M-M) modeling should be performed to compare the differences of kinetic parameters (V_{max}, K_m) of the two disparate systems. In such a kinetic study, the experimental outputs are the time elapsed (min), and the intensity of the spectrophotometric detection signal (Abs_{540} nm) (Fig.86b).

The future design of experiments (DOE) of a glucose oxidase-horseradish peroxidase (GOD-HRP) enzyme assay should include several controls. For example, experimentation for the M-M parameterization assay should be performed with; (1) free GOD, (2) free HRP, (3) GOD-HRP free floating, (4) GOD-dsDNA-HRP enzymatic macromolecule. Furthermore, a number of variables such as the assay temperature, final concentration of enzymes/conjugates, and the buffer medium pH should also be tested.

Both GOD and HRP enzymes are Michaelis-Menten enzymes, and does not follow competitive inhibition, noncompetitive inhibition, or allosteric enzyme kinetics. The future work could be governed by the following two major hypotheses:

H1: Since $product_1$ formed by the first enzyme (GOD) is the substrate of the second enzyme (HRP), $product_1$ will be continuously removed by the second enzyme, in the final reaction (i.e., no product inhibition) (Fig.86a). This is because the product of the first enzyme, is the substrate of the second enzyme.

H2: Due to minimization of product$_1$ diffusion limitations, and creating a high local concentration of product$_1$, the co-localized enzymatic modality (Fig.86b) will result in enhanced reaction kinetics compared to the corresponding free-floating system.

The characteristic kinetic profile of the systems are expected to be a hyperbola, with two asymptotic parameters; V_{max}, and K_m. In order to validate the parameters obtained by fitting experimental velocity data into the M-M mathematical model, a range of substrate (D-glucose) concentrations should be used to obtain the product formation rates.

The o-dianisidine (probe) used for determining the rate of substrate conversion (kinetics) has an Abs_{max} at 504 nm. Abs_{max} of DNA, GOD, and HRP are at 260 nm, 275 nm, and 415 nm respectively. Therefore, in an enzyme assay of the co-localized model, absorbance readings will not be interfered with those of any components of the GOD-dsDNA-HRP macromolecules. Like so, interference will not be a concern when analyzing the enzyme kinetics of the GOD-DNA-HRP macromolecule.

However, o-dianisidine produces an intense pink color at Abs_{540} only when it reacts with sulfuric acid. If the addition of the sulfuric acid is foreseen as a contributing factor which would dissociate the GOD-dsDNA-HRP macromolecules, a different reducing agent (the colorimetric reagent in the assay) such as 2,2'-azino-bis(3-ethylbenzthiazoline-6-sulfonic acid (ABTS) could be easily utilized. The ABTS protocol follows the same procedure, without the addition of sulfuric acid. The oxidized $ABTS^{2+}$ exhibits absorbance at 725 nm. The important factor to note is the stoichiometry of D-glucose to ABTS. As opposed to o-dianisidine, $ABTS_{reduced}$ utilizes two mols of H_2O_2 to form $ABTS_{oxidized}$.

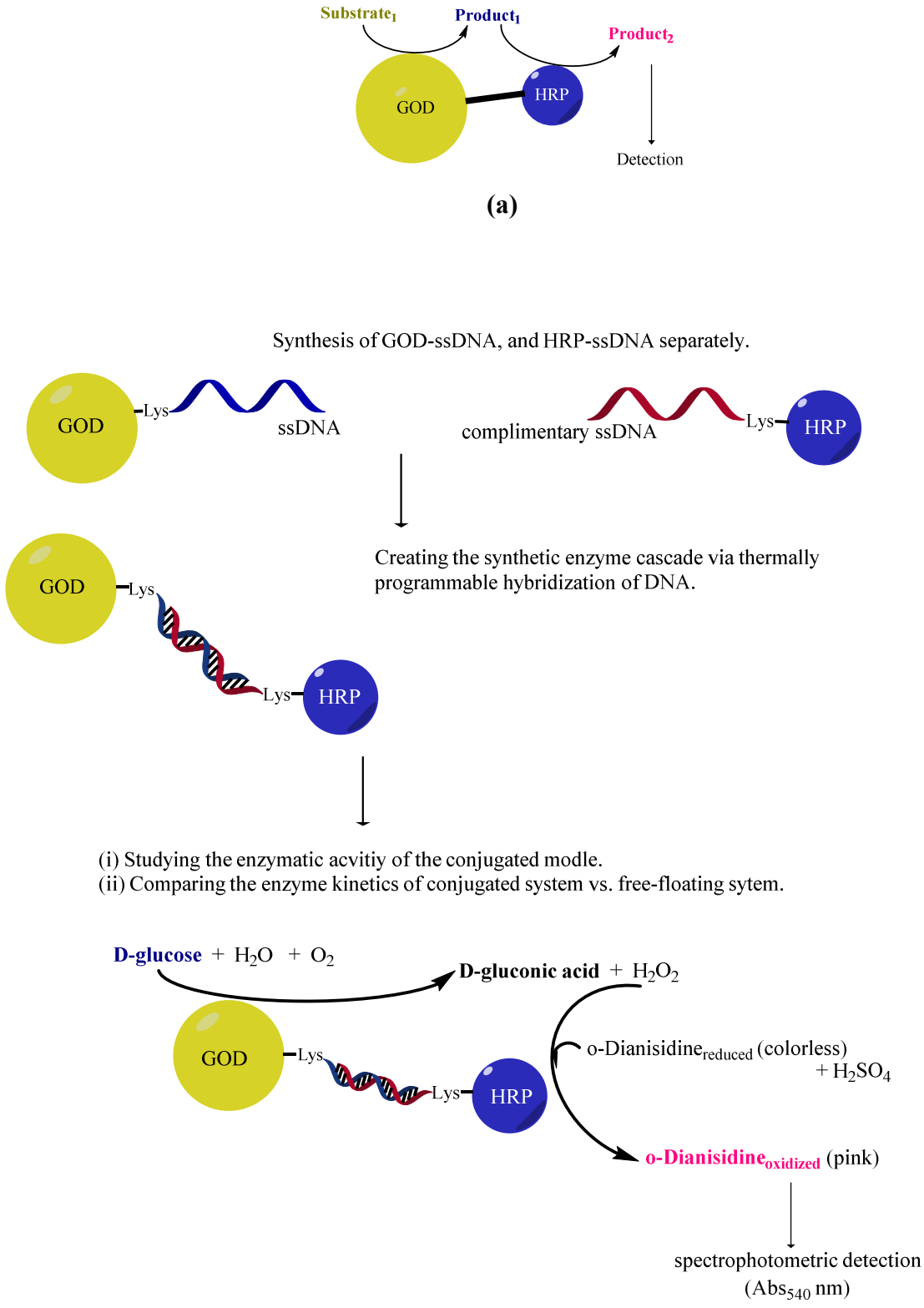

Figure 85: Theory of a continuous assay (a). Detailed schematic of the enzyme cascade reaction, and detection (b).

When synthesizing GOD-dsDNA-HRP macromolecules for future M-M kinetic comparison studies, attention should be directed to the T_m of the DNA. The manufacturer's protocol (Sigma Aldrich, St. Louis, MO) reports that the optimal temperature of the GOD-HRP continuous assay is at 37 °C. However, if the system temperature of the GOD-dsDNA-HRP macromolecules is increased up to 37 °C, the annealed dsDNA will be denatured (i.e., separated into two ssDNA strands). This is because the T_m of DNA used in the current GOD-dsDNA-HRP macromolecule is 32 °C. Therefore, heating the system up to 37 °C could ultimately cause the co-localized GOD and HRP to separate. Therefore, in future experimentation, the kinetics of both systems (co-localized enzymatic macromolecule vs. free-floating enzymatic system) should be conducted at a temperature below the T_m of the ssDNA. If not, synthesis of the GOD-dsDNA-HRP macromolecule should be conducted with ssDNA strands with a slightly higher T_m. In order to accomplish a higher T_m, either a new sequence, and/or a longer ssDNA could be designed. However, the T_m of the ssDNA should be maintained below 45 °C in order to not affect the enzyme functionalities. The optimal temperature range for GOD is 40 – 60 °C [104], while for HRP it is 45 – 50 °C [128].

Furthermore, future work should also encompass determining the optimal distance between GOD, and HRP in the final GOD-dsDNA-HRP macromolecule. This could be attained by synthesizing GOD-dsDNA-HRP macromolecules with ssDNA strands consisting of varied lengths, such as, low, medium, and high (e.g., 10, 20, 40 base pairs).

During the enzymatic reaction, two possible scenarios could occur in the co-localized GOD-dsDNA-HRP system. (1) Since the HRP enzyme could constantly remove (i.e., utilize) H_2O_2 from the microenvironment, the rate of o-dianisidine oxidation should increase ideally. This in return, would indicate enhanced enzyme kinetics. (2) Due to the concentric nature of the system, the accumulation of D-gluconic acid in the system could act as a weak competitive inhibitor. Although this inhibition is not well documented, there are some reports indicating the possibility of D-gluconic acid to act competitively with the substrate, D-glucose [127,128]. The outcomes of an experimental design constructed with the all the above considerations would be able to address whether a spatially concerted (i.e., co-localized) enzymatic model could get rid of substrate diffusion limitations, or whether it would inflict product inhibition.

REFERENCES

1 Sanchez, F. & Sobolev, K. Nanotechnology in concrete – A review. *Construction and Building Materials* **24**, 2060-2071, doi:https://doi.org/10.1016/j.conbuildmat.2010.03.014 (2010).

2 Hermanson, G. T. *Bioconjugate techniques*. (Academic press, 2013).

3 Schaeffer, P. M. & Dixon, N. E. Synthesis and applications of covalent protein-DNA conjugates. *Australian Journal of Chemistry* **62**, 1328-1332 (2009).

4 Rostovtsev, V. V., Green, L. G., Fokin, V. V. & Sharpless, K. B. A Stepwise Huisgen Cycloaddition Process: Copper(I)□Catalyzed Regioselective "Ligation" of Azides and Terminal Alkynes. *Angewandte Chemie* **114**, 2708-2711, doi:doi:10.1002/1521-3757(20020715)114:14<2708::AID-ANGE2708>3.0.CO;2-0 (2002).

5 El-Sagheer, A. H. & Brown, T. Click chemistry with DNA. *Chemical Society Reviews* **39**, 1388-1405, doi:10.1039/B901971P (2010).

6 Wang, X., Huang, B., Liu, X. & Zhan, P. Discovery of bioactive molecules from CuAAC click-chemistry-based combinatorial libraries. *Drug Discovery Today* **21**, 118-132, doi:https://doi.org/10.1016/j.drudis.2015.08.004 (2016).

7 Agard, N. J., Prescher, J. A. & Bertozzi, C. R. A strain-promoted [3+ 2] azide− alkyne cycloaddition for covalent modification of biomolecules in living systems. *Journal of the American Chemical Society* **126**, 15046-15047 (2004).

8 Khatwani, S. L. *et al.* Covalent protein-oligonucleotide conjugates by copper-free click reaction. *Bioorganic & medicinal chemistry* **20**, 4532-4539, doi:10.1016/j.bmc.2012.05.017 (2012).

9 Prescher, J. A. & Bertozzi, C. R. Chemistry in living systems. *Nature Chemical Biology* **1**, 13, doi:10.1038/nchembio0605-13 (2005).

10 Görmer, K., Waldmann, H. & Brunsveld, L. in *Comprehensive Natural Products II* 531-585 (Elsevier, 2010).

11 ThermoFisher. (ed ThermoFisher Scientific) (U.S, 2009).

12 Sleiman, H. (ed Hanadi Sleiman).

13 Franken, K. L. M. C. *et al.* Purification of His-Tagged Proteins by Immobilized Chelate Affinity Chromatography: The Benefits from the Use of Organic Solvent. *Protein Expression and Purification* **18**, 95-99, doi:https://doi.org/10.1006/prep.1999.1162 (2000).

14 Creighton, J. A., Blatchford, C. G. & Albrecht, M. G. Plasma resonance enhancement of Raman scattering by pyridine adsorbed on silver or gold sol particles of size comparable to the excitation wavelength. *J. Chem. Soc., Faraday Trans. 2* **75**, 790-798 (1979).

15 Hayat, M. A. (ed M.A. Hayat) (Cambridge University Press, Cambridge University Press, Cambridge, United Kingdom, 2000).

16 Cuatrecasas, P. & Parikh, I. Adsorbents for affinity chromatography. Use of N-hydroxysuccinimide esters of agarose. *Biochemistry* **11**, 2291-2299, doi:10.1021/bi00762a013 (1972).

17 Erben, C. M., Goodman, R. P. & Turberfield, A. J. Single□molecule protein encapsulation in a rigid DNA cage. *Angewandte Chemie* **118**, 7574-7577 (2006).

18 Płoskoń, E. *et al.* Controlled Assembly of Artificial Protein–Protein Complexes via DNA Duplex Formation. *Bioconjugate chemistry* **26**, 427-434 (2015).

19 Goodman, R. P. *et al.* Rapid chiral assembly of rigid DNA building blocks for molecular nanofabrication. *Science* **310**, 1661-1665 (2005).
20 Yan, H., Park, S. H., Finkelstein, G., Reif, J. H. & LaBean, T. H. DNA-templated self-assembly of protein arrays and highly conductive nanowires. *Science* **301**, 1882-1884 (2003).
21 Rothemund, P. W. Folding DNA to create nanoscale shapes and patterns. *Nature* **440**, 297-302 (2006).
22 Hendrickson, E. R., Truby, T. M. H., Joerger, R. D., Majarian, W. R. & Ebersole, R. C. High sensitivity multianalyte immunoassay using covalent DNA-labeled antibodies and polymerase chain reaction. *Nucleic acids research* **23**, 522-529 (1995).
23 Lovrinovic, M. *et al.* Synthesis of protein–nucleic acid conjugates by expressed protein ligation. *Chemical Communications*, 822-823 (2003).
24 Niemeyer, C. M. The developments of semisynthetic DNA–protein conjugates. *Trends in biotechnology* **20**, 395-401 (2002).
25 Ghosh, S. S., Kao, P. M., McCue, A. W. & Chappelle, H. L. Use of maleimide-thiol coupling chemistry for efficient syntheses of oligonucleotide-enzyme conjugate hybridization probes. *Bioconjugate chemistry* **1**, 71-76 (1990).
26 Nykypanchuk, D., Maye, M. M., van der Lelie, D. & Gang, O. DNA-guided crystallization of colloidal nanoparticles. *Nature* **451**, 549-552 (2008).
27 Alivisatos, A. P. *et al.* Organization of'nanocrystal molecules' using DNA. (1996).
28 Mirkin, C. A., Letsinger, R. L., Mucic, R. C. & Storhoff, J. J. A DNA-based method for rationally assembling nanoparticles into macroscopic materials. (1996).
29 Zhang, Y., Lu, F., Yager, K. G., van der Lelie, D. & Gang, O. A general strategy for the DNA-mediated self-assembly of functional nanoparticles into heterogeneous systems. *Nature nanotechnology* (2013).
30 Jawalekar, A. M. *et al.* Conjugation of nucleosides and oligonucleotides by [3+ 2] cycloaddition. *The Journal of organic chemistry* **73**, 287-290 (2008).
31 Burbulis, I., Yamaguchi, K., Gordon, A., Carlson, R. & Brent, R. Using protein-DNA chimeras to detect and count small numbers of molecules. *Nat Meth* **2**, 31-37 (2005).
32 Corey, D. & Schultz, P. Generation of a hybrid sequence-specific single-stranded deoxyribonuclease. *Science* **238**, 1401-1403 (1987).
33 Duckworth, B. P. *et al.* A universal method for the preparation of covalent protein–DNA conjugates for use in creating protein nanostructures. *Angewandte Chemie* **119**, 8975-8978 (2007).
34 Bock, C. *et al.* Photoaptamer arrays applied to multiplexed proteomic analysis. *Proteomics* **4**, 609-618 (2004).
35 Curiel, D. T. *et al.* High-efficiency gene transfer mediated by adenovirus coupled to DNA-polylysine complexes. *Human gene therapy* **3**, 147-154 (1992).
36 Yamaguchi, S., Chen, Y., Nakajima, S., Furuta, T. & Nagamune, T. Light-activated gene expression from site-specific caged DNA with a biotinylated photolabile protection group. *Chemical Communications* **46**, 2244-2246 (2010).
37 Bochet, C. G. Photolabile protecting groups and linkers. *Journal of the Chemical Society, Perkin Transactions 1*, 125-142 (2002).
38 Gianneschi, N. C. & Ghadiri, M. R. Design of Molecular Logic Devices Based on a Programmable DNA□Regulated Semisynthetic Enzyme. *Angewandte Chemie* **119**, 4029-4032 (2007).

39 Seo, T. S., Li, Z., Ruparel, H. & Ju, J. Click Chemistry to Construct Fluorescent Oligonucleotides for DNA Sequencing. *The Journal of Organic Chemistry* **68**, 609-612, doi:10.1021/jo026615r (2003).

40 Staudinger, H. & Meyer, J. Über neue organische phosphorverbindungen III. Phosphinmethylenderivate und phosphinimine. *Helvetica Chimica Acta* **2**, 635-646 (1919).

41 Kretschy, N., Sack, M. & Somoza, M. M. Sequence-Dependent Fluorescence of Cy3- and Cy5-Labeled Double-Stranded DNA. *Bioconjugate Chemistry* **27**, 840-848, doi:10.1021/acs.bioconjchem.6b00053 (2016).

42 Kernohan, K. D. & Bérubé, N. G. Three dimensional dual labelled DNA fluorescent in situ hybridization analysis in fixed tissue sections. *MethodsX* **1**, 30-35, doi:10.1016/j.mex.2014.04.001 (2014).

43 Ishizuka, T., Liu, H. S., Ito, K. & Xu, Y. Fluorescence imaging of chromosomal DNA using click chemistry. *Scientific Reports* **6**, 33217, doi:10.1038/srep33217 (2016).

44 Wu, S. M. *et al.* Quantum□Dot□Labeled DNA Probes for Fluorescence In Situ Hybridization (FISH) in the Microorganism Escherichia coli. *ChemPhysChem* **7**, 1062-1067, doi:doi:10.1002/cphc.200500608 (2006).

45 Brodin, J. D., Auyeung, E. & Mirkin, C. A. DNA-mediated engineering of multicomponent enzyme crystals. *Proceedings of the National Academy of Sciences* **112**, 4564-4569 (2015).

46 De Filette, M. *et al.* An influenza A vaccine based on tetrameric ectodomain of matrix protein 2. *Journal of Biological Chemistry* **283**, 11382-11387 (2008).

47 Teal, A. R. W. P. E. O. B. S. B. A. t. S. C. G. *Enzymes and their role in biotechnology*. (Biochemical Society, 1993).

48 Anbu, P., Gopinath, S. C. B., Cihan, A. C. & Chaulagain, B. P. Microbial Enzymes and Their Applications in Industries and Medicine. *BioMed Research International* **2013**, 2, doi:10.1155/2013/204014 (2013).

49 Shuler, M. L., Kargi, F. & DeLisa, M. *Bioprocess engineering: basic concepts*. Vol. 576 (Prentice Hall Englewood Cliffs, NJ, 2017).

50 Brady, D. & Jordaan, J. Advances in enzyme immobilisation. *Biotechnology Letters* **31**, 1639, doi:10.1007/s10529-009-0076-4 (2009).

51 Nery, E. W. & Kubota, L. T. Evaluation of enzyme immobilization methods for paper-based devices—A glucose oxidase study. *Journal of Pharmaceutical and Biomedical Analysis* **117**, 551-559, doi:https://doi.org/10.1016/j.jpba.2015.08.041 (2016).

52 Xia, X., Long, Y. & Wang, J. Glucose oxidase-functionalized fluorescent gold nanoclusters as probes for glucose. *Analytica Chimica Acta* **772**, 81-86, doi:https://doi.org/10.1016/j.aca.2013.02.025 (2013).

53 Pierre, A. C. The sol-gel encapsulation of enzymes. *Biocatalysis and Biotransformation* **22**, 145-170, doi:10.1080/10242420412331283314 (2004).

54 Onaizi, S. A. & Leong, S. S. J. Tethering antimicrobial peptides: Current status and potential challenges. *Biotechnology Advances* **29**, 67-74, doi:http://dx.doi.org/10.1016/j.biotechadv.2010.08.012 (2011).

55 Tran, C. T., Nosworthy, N. J., Kondyurin, A., McKenzie, D. R. & Bilek, M. M. CelB and β-glucosidase immobilization for carboxymethyl cellulose hydrolysis. *RSC Advances* **3**, 23604-23611 (2013).

56 Sheldon, R. A. Enzyme Immobilization: The Quest for Optimum Performance. *Advanced Synthesis & Catalysis* **349**, 1289-1307, doi:10.1002/adsc.200700082 (2007).

57 Seyhan Tükel, S. & Alagöz, D. Catalytic efficiency of immobilized glucose isomerase in isomerization of glucose to fructose. *Food Chemistry* **111**, 658-662, doi:http://dx.doi.org/10.1016/j.foodchem.2008.04.035 (2008).

58 Zhang, Y., Tsitkov, S. & Hess, H. Proximity does not contribute to activity enhancement in the glucose oxidase–horseradish peroxidase cascade. *Nature Communications* **7**, 13982, doi:10.1038/ncomms13982 (2016).

59 Wilner, O. I. *et al.* Enzyme cascades activated on topologically programmed DNA scaffolds. *Nature Nanotechnology* **4**, 249, doi:10.1038/nnano.2009.50 https://www.nature.com/articles/nnano.2009.50#supplementary-information (2009).

60 Saxena, U. & Goswami, P. Silk Mat as Bio-matrix for the Immobilization of Cholesterol Oxidase. *Applied Biochemistry and Biotechnology* **162**, 1122-1131, doi:10.1007/s12010-010-8923-2 (2010).

61 Pollard, T. D., Earnshaw, W. C., Lippincott-Schwartz, J. & Johnson, G. *Cell Biology E-Book*. (Elsevier Health Sciences, 2016).

62 Carter, J. D. & LaBean, T. H. Coupling strategies for the synthesis of peptide-oligonucleotide conjugates for patterned synthetic biomineralization. *Journal of nucleic acids* **2011** (2011).

63 Grabarek, Z. & Gergely, J. Zero-length crosslinking procedure with the use of active esters. *Analytical Biochemistry* **185**, 131-135, doi:http://dx.doi.org/10.1016/0003-2697(90)90267-D (1990).

64 Staros, J. V., Wright, R. W. & Swingle, D. M. Enhancement by N-hydroxysulfosuccinimide of water-soluble carbodiimide-mediated coupling reactions. *Analytical Biochemistry* **156**, 220-222, doi:http://dx.doi.org/10.1016/0003-2697(86)90176-4 (1986).

65 Liberelle, B. *et al.* Impact of Epidermal Growth Factor Tethering Strategy on Cellular Response. *Bioconjugate Chemistry* **21**, 2257-2266, doi:10.1021/bc1002604 (2010).

66 Keefe, A. J., Brault, N. D. & Jiang, S. Suppressing Surface Reconstruction of Superhydrophobic PDMS using a Superhydrophilic Zwitterionic Polymer. *Biomacromolecules* **13**, 1683-1687, doi:10.1021/bm300399s (2012).

67 Zhang, Z., Chen, S. & Jiang, S. Dual-Functional Biomimetic Materials: Nonfouling Poly(carboxybetaine) with Active Functional Groups for Protein Immobilization. *Biomacromolecules* **7**, 3311-3315, doi:10.1021/bm060750m (2006).

68 Vashist, S. K. Comparison of 1-Ethyl-3-(3-Dimethylaminopropyl) Carbodiimide Based Strategies to Crosslink Antibodies on Amine-Functionalized Platforms for Immunodiagnostic Applications. *Diagnostics* **2**, 23 (2012).

69 Bartczak, D. & Kanaras, A. G. Preparation of Peptide-Functionalized Gold Nanoparticles Using One Pot EDC/Sulfo-NHS Coupling. *Langmuir* **27**, 10119-10123, doi:10.1021/la2022177 (2011).

70 Xu, C., Wang, B. & Sun, S. Dumbbell-like Au−Fe3O4 Nanoparticles for Target-Specific Platin Delivery. *Journal of the American Chemical Society* **131**, 4216-4217, doi:10.1021/ja900790v (2009).

71 Wang, C., Yan, Q., Liu, H.-B., Zhou, X.-H. & Xiao, S.-J. Different EDC/NHS activation mechanisms between PAA and PMAA brushes and the following amidation reactions. *Langmuir* **27**, 12058-12068 (2011).

72 Mangalam, A. P., Simonsen, J. & Benight, A. S. Cellulose/DNA Hybrid Nanomaterials. *Biomacromolecules* **10**, 497-504, doi:10.1021/bm800925x (2009).

73 Nguyen, C. V. *et al.* Preparation of nucleic acid functionalized carbon nanotube arrays. *Nano letters* **2**, 1079-1081 (2002).

74 Sam, S. *et al.* Semiquantitative Study of the EDC/NHS Activation of Acid Terminal Groups at Modified Porous Silicon Surfaces. *Langmuir* **26**, 809-814, doi:10.1021/la902220a (2010).

75 ThermoFisher. in *Crosslinking Technical Handbook* (2009).

76 Chu, B. C., Wahl, G. M. & Orgel, L. E. Derivatization of unprotected polynucleotides. *Nucleic acids research* **11**, 6513-6529 (1983).

77 Rasmussen, S. R., Larsen, M. R. & Rasmussen, S. E. Covalent immobilization of DNA onto polystyrene microwells: the molecules are only bound at the 5′ end. *Analytical biochemistry* **198**, 138-142 (1991).

78 Gu, L.-s. *et al.* Immobilization of a phosphonated analog of matrix phosphoproteins within cross-linked collagen as a templating mechanism for biomimetic mineralization. *Acta Biomaterialia* **7**, 268-277, doi:http://doi.org/10.1016/j.actbio.2010.07.036 (2011).

79 Biotechnology, N. C. f. (National Center for Biotechnology Information, PubChem compound Database, 2017).

80 Uney, K., Altan, F. & Elmas, M. Development and validation of a high-performance liquid chromatography method for determination of cefquinome concentrations in sheep plasma and its application to pharmacokinetic studies. *Antimicrobial agents and chemotherapy* **55**, 854-859 (2011).

81 IDT. (Integrated DNA Technologies, 2011).

82 Zybailov, B. L., Glazko, G. V., Jaiswal, M. & Raney, K. D. Large Scale Chemical Cross-linking Mass Spectrometry Perspectives. *Journal of proteomics & bioinformatics* **6**, 001, doi:10.4172/jpb.S2-001 (2013).

83 FisherScientific. Amine reactive Diazirines. (2017). <https://www.thermofisher.com/order/catalog/product/26167>.

84 Gomes, A. F. & Gozzo, F. C. Chemical cross-linking with a diazirine photoactivatable cross-linker investigated by MALDI- and ESI-MS/MS. *Journal of Mass Spectrometry* **45**, 892-899, doi:10.1002/jms.1776 (2010).

85 Raphel, J. *et al.* Engineered protein coatings to improve the osseointegration of dental and orthopaedic implants. *Biomaterials* **83**, 269-282, doi:https://doi.org/10.1016/j.biomaterials.2015.12.030 (2016).

86 Tanaka, Y. & Kohler, J. J. Photoactivatable Crosslinking Sugars for Capturing Glycoprotein Interactions. *Journal of the American Chemical Society* **130**, 3278-3279, doi:10.1021/ja7109772 (2008).

87 Bodanszky, M. *Peptide chemistry*. (Springer, 1988).

88 Milton, R. C. d. L., Milton, S. C. F. & Adams, P. A. Prediction of difficult sequences in solid-phase peptide synthesis. *Journal of the American Chemical Society* **112**, 6039-6046, doi:10.1021/ja00172a020 (1990).

89 Fauchere, J. & Pliska, V. Hydrophobic parameters-pi of amino-acid side-chains from the partitioning of n-acetyl-amino-acid amides. *European Journal of Medicinal Chemistry* **18**, 369-375 (1983).

90 Carey, G. in *The New Genetic Technologies* (Sage Publications, 2001).

91 Dalgleish, R. in *Encyclopedia of Immunology (Second Edition)* 2194-2198 (Elsevier, 1998).

92 Xia, T. *et al.* Thermodynamic parameters for an expanded nearest-neighbor model for formation of RNA duplexes with Watson-Crick base pairs. *Biochemistry* **37**, 14719-14735 (1998).
93 Dieffenbach, C., Lowe, T. & Dveksler, G. General concepts for PCR primer design. *PCR Methods Appl* **3**, S30-S37 (1993).
94 Owczarzy, R., Moreira, B. G., You, Y., Behlke, M. A. & Walder, J. A. Predicting stability of DNA duplexes in solutions containing magnesium and monovalent cations. *Biochemistry* **47**, 5336-5353 (2008).
95 Yin, Y. & Zhao, X. S. Kinetics and Dynamics of DNA Hybridization. *Accounts of Chemical Research* **44**, 1172-1181, doi:10.1021/ar200068j (2011).
96 Wang, X., Lim, H. J. & Son, A. Characterization of denaturation and renaturation of DNA for DNA hybridization. *Environmental Health and Toxicology* **29**, e2014007, doi:10.5620/eht.2014.29.e2014007 (2014).
97 Volkov, S. Some aspects of the DNA hypochromic effect theory. *International Journal of Quantum Chemistry* **16**, 119-132 (1979).
98 Wang, X. & Son, A. Effects of pretreatment on the denaturation and fragmentation of genomic DNA for DNA hybridization. *Environmental Science: Processes & Impacts* **15**, 2204-2212 (2013).
99 Glazer, A. N., Peck, K. & Mathies, R. A. A stable double-stranded DNA-ethidium homodimer complex: application to picogram fluorescence detection of DNA in agarose gels. *Proceedings of the National Academy of Sciences* **87**, 3851-3855, doi:10.1073/pnas.87.10.3851 (1990).
100 Sun, J.-S. *et al.* Sequence-specific intercalating agents: intercalation at specific sequences on duplex DNA via major groove recognition by oligonucleotide-intercalator conjugates. *Proceedings of the National Academy of Sciences* **86**, 9198-9202 (1989).
101 Valeur, B. (Wiley-VCH, 2001).
102 Lawaetz, A. J. & Stedmon, C. A. Fluorescence Intensity Calibration Using the Raman Scatter Peak of Water. *Applied Spectroscopy* **63**, 936-940, doi:10.1366/000370209788964548 (2009).
103 Sigma-Aldrich. *Ethidium Bromide*, <https://www.sigmaaldrich.com/technical-documents/articles/biology/ethidium-bromide.html> (2018).
104 Witt, S., Wohlfahrt, G., Schomburg, D., Hecht, H. J. & Kalisz, H. M. Conserved arginine-516 of Penicillium amagasakiense glucose oxidase is essential for the efficient binding of beta-D-glucose. *Biochemical Journal* **347**, 553-559 (2000).
105 Bankar, S. B., Bule, M. V., Singhal, R. S. & Ananthanarayan, L. Glucose oxidase — An overview. *Biotechnology Advances* **27**, 489-501, doi:https://doi.org/10.1016/j.biotechadv.2009.04.003 (2009).
106 Galant, A. L., Kaufman, R. C. & Wilson, J. D. Glucose: Detection and analysis. *Food Chemistry* **188**, 149-160, doi:https://doi.org/10.1016/j.foodchem.2015.04.071 (2015).
107 Tongbu, L., Xinyu, P., Huiying, Y. & Liangnian, J. The production of glucose oxidase using the waste myceliums of Aspergillus niger and the effects of metal ions on the activity of glucose oxidase. *Enzyme and Microbial Technology* **19**, 339-342, doi:https://doi.org/10.1016/S0141-0229(96)00004-X (1996).
108 Karmali, K., Karmali, A., Teixeira, A. & Curto, M. J. M. Assay for glucose oxidase from Aspergillus niger and Penicillium amagasakiense by Fourier transform infrared

spectroscopy. *Analytical Biochemistry* **333**, 320-327, doi:https://doi.org/10.1016/j.ab.2004.06.025 (2004).

109 Jandera, P. Stationary and mobile phases in hydrophilic interaction chromatography: a review. *Analytica Chimica Acta* **692**, 1-25, doi:https://doi.org/10.1016/j.aca.2011.02.047 (2011).

110 Witt, S., Singh, M. & Kalisz, H. M. Structural and kinetic properties of nonglycosylated recombinant Penicillium amagasakiense glucose oxidase expressed in Escherichia coli. *Appl Environ Microbiol* **64**, 1405-1411 (1998).

111 Gong, C. *et al.* A glucose biosensor based on the polymerization of aniline induced by a bio-interphase of glucose oxidase and horseradish peroxidase. *Analytical Methods* **8**, 1513-1519, doi:10.1039/C5AY02762D (2016).

112 De Luca, P. *et al.* Glucose Determination by Means of Steady-state and Time-course UV Fluorescence in Free or Immobilized Glucose Oxidase. *Sensors* **7**, doi:10.3390/s7112612 (2007).

113 Li, Z. F., Kang, E. T., Neoh, K. G. & Tan, K. L. Covalent immobilization of glucose oxidase on the surface of polyaniline films graft copolymerized with acrylic acid. *Biomaterials* **19**, 45-53, doi:https://doi.org/10.1016/S0142-9612(97)00154-3 (1998).

114 Cha, R., Wang, D., He, Z. & Ni, Y. Development of cellulose paper testing strips for quick measurement of glucose using chromogen agent. *Carbohydrate Polymers* **88**, 1414-1419, doi:https://doi.org/10.1016/j.carbpol.2012.02.028 (2012).

115 Guzik, U., Hupert-Kocurek, K. & Wojcieszynska, D. Immobilization as a strategy for improving enzyme properties-application to oxidoreductases. *Molecules (Basel, Switzerland)* **19**, 8995-9018, doi:10.3390/molecules19078995 (2014).

116 Veitch, N. C. Horseradish peroxidase: a modern view of a classic enzyme. *Phytochemistry* **65**, 249-259, doi:https://doi.org/10.1016/j.phytochem.2003.10.022 (2004).

117 O'Brien, A. M., Ó'Fágáin, C., Nielsen, P. F. & Welinder, K. G. Location of crosslinks in chemically stabilized horseradish peroxidase: Implications for design of crosslinks. *Biotechnology and Bioengineering* **76**, 277-284, doi:doi:10.1002/bit.1194 (2001).

118 VLAMIS-GARDIKAS, A., SMITH, A. T., CLEMENTS, J. M. & BURKE, J. F. Expression of Active Horseradish Peroxidase in Saccharomyces cerevisiae. *Biochemical Society Transactions* **20**, 111S-111S, doi:10.1042/bst020111s (1992).

119 BURKE, J. F. *et al.* (Portland Press Limited, 1989).

120 Shannon, L. M., Kay, E. & Lew, J. Y. Peroxidase isozymes from horseradish roots I. Isolation and physical properties. *Journal of Biological Chemistry* **241**, 2166-2172 (1966).

121 Veillette, M. *et al.* Conformational Evaluation of HIV-1 Trimeric Envelope Glycoproteins Using a Cell-based ELISA Assay. *Journal of Visualized Experiments : JoVE*, 51995, doi:10.3791/51995 (2014).

122 Kafi, A. K. M., Wu, G. & Chen, A. A novel hydrogen peroxide biosensor based on the immobilization of horseradish peroxidase onto Au-modified titanium dioxide nanotube arrays. *Biosensors and Bioelectronics* **24**, 566-571, doi:https://doi.org/10.1016/j.bios.2008.06.004 (2008).

123 Alonso Lomillo, M. A., Ruiz, J. G. & Pascual, F. J. M. Biosensor based on platinum chips for glucose determination. *Analytica Chimica Acta* **547**, 209-214, doi:https://doi.org/10.1016/j.aca.2005.05.037 (2005).

124 Krainer, F. W. & Glieder, A. An updated view on horseradish peroxidases: recombinant production and biotechnological applications. *Applied Microbiology and Biotechnology* **99**, 1611-1625, doi:10.1007/s00253-014-6346-7 (2015).
125 Cao, X., Chen, C., Yu, H. & Wang, P. Horseradish peroxidase-encapsulated chitosan nanoparticles for enzyme-prodrug cancer therapy. *Biotechnology Letters* **37**, 81-88, doi:10.1007/s10529-014-1664-5 (2015).
126 Antosiewicz, J. M. & Shugar, D. UV–Vis spectroscopy of tyrosine side-groups in studies of protein structure. Part 2: selected applications. *Biophysical Reviews* **8**, 163-177, doi:10.1007/s12551-016-0197-7 (2016).
127 Olmsted, J. & Kearns, D. R. Mechanism of ethidium bromide fluorescence enhancement on binding to nucleic acids. *Biochemistry* **16**, 3647-3654, doi:10.1021/bi00635a022 (1977).
128 Chattopadhyay, K. & Mazumdar, S. Structural and Conformational Stability of Horseradish Peroxidase: Effect of Temperature and pH. *Biochemistry* **39**, 263-270, doi:10.1021/bi990729o (2000).

VITA

MALITHI WICKRAMATHILAKA

EDUCATION

Ph.D. Candidate, Agricultural & Biological Engineering, Purdue University, IN. May, 2018
M.S. Biological Engineering, University of Missouri, MO. May, 2013
B.S. Chemical Engineering, University of Wyoming, WY. July, 2011

RESEARCH INTERESTS

- Synthesis of self-assembling and functional macromolecules/bioconjugates.
- Polymeric implantable devices, drug elution studies, and physicochemical characterization.
- Chromatographic assay development and method validation.
- Reaction kinetics, numerical modeling, process (unit operations) simulations.

RESEARCH EXPERIENCE

Research Assistant, Purdue University, Dept. of Agricultural & Biological Engineering
August 2013 – May 2018

Ph.D. Dissertation. Investigating cost-effective crosslinking strategies to synthesize protein-DNA conjugates with minimum surface modifications, to generate a spontaneously assembling multifunctional enzyme cascade with enhanced enzymatic activities.

August 2014 – May 2016

Characterization and Evaluation of Zero-Length Covalent Crosslinking Strategies for DNA Based Applications. A comparison of the extent of product formation via a conventional coupling chemistry, and an adapted version, and a comprehensive method validation as per ICH guidelines was conducted for product quantitation.

February 2017 – June 2017

Changes on antioxidant activity of microwave-treated protein hydrolysates after simulated gastrointestinal digestion. Developed and conducted Size Exclusion Chromatography (SEC) and RP-HPLC methods to purify microwave-treated fish protein hydrolysates based on peptides' size and hydrophobicity, and determined their antioxidant properties.

April 2017 – December 2017

Modeling thermal and non-thermal methods for Food Processing. Developing RP-HPLC methods, troubleshooting, and developing preliminary method validation by constructing standards calibration curves to determine the vitamin C content in heat-treated orange juice.

Research Assistant, University of Missouri, Dept. of Biological Engineering
August 2011 – May 2013

Supercritical water gasification of waste residues – Parameterization of rate law. Investigated supercritical water gasification (SCWG) of used motor oil in a batch reactor, and studied the effects of amounts, residence time, temperature and emulsification, on the gasification efficiencies, and biofuel product composition.

Rate determination of supercritical water gasification of primary sewage sludge as a replacement for anaerobic digestion. Initiated literature review and sample collection, developed a safe operational protocol for in-house reactors, and performed preliminary experiments to yield gasification rates/efficiencies. Assisted with data analysis.

Exploration of High Pressure Separations of Supercritical Nitrogen and Carbon Dioxide. Collected biofuel samples from the in-house gas separation columns, and assisted with GC analysis of the biofuel.

PROFESSIONAL EXPERIENCE

Development Engineering Intern, COOK Biotech Inc., West Lafayette, IN
May 2017 – August 2017

Developed an automated, novel process to manufacture a polymeric bioabsorbable fiber, and investigated the effect of process parameters on the mechanical strength properties of the bioabsorbable fiber.

May 2016 – August 2016

Investigated the effect of grinding & sieving a pharmaceutical antimicrobial drug, on its final particle size distribution, other physicochemical characteristics, and drug elution profiles from a medical device.

Research Intern, Western Research Institute, Laramie, WY May 2010 – August 2010

Simulated a liquid desiccant dehumidification (LDDS) model, and a condensation model on ***ASPEN***® to determine the effect of flue gas moisture contents, desiccant concentration, flow rates of flue gas, inlet conditions, and desiccant-flue gas contact methods on the water vapor recovery efficiency from flue gases.

SELECTED ACADEMIC PROJECTS/FELLOWSHIP PROPOSALS

Synthesis of a Multilayered, Biocompatible Hydrogel and an in-vivo Drug Delivery Model to Prevent Bacterial Infections in Tissue surrounding Implanted Medical Devices. A design proposal for synthesizing a novel onion-structured chitosan-antimicrobial peptide hydrogel, for sequential drug delivery to tissues surrounding an implanted medical device.

Localized Surface Plasmon Resonance (LSPR) based Nanosensors. A review paper on the most recent methodologies used to develop, modify and enhance the performance of LSPR, which is a higher sensitivity technique used detect a variety of biochemical compounds.

Combining Miniaturized Ion Exchange Chromatography with Fluorescence Polarization Immunoassay to Detect Amphetamine Levels. A design proposal for developing a biosensor with higher sensitivity to detect amphetamine in human saliva. Fluorescence Polarization Immunoassay coupled to a miniaturized ion exchange column was proposed for rapid and accurate detection of a labeled-antibody, with diminished background noises caused by large enzymes.

A Quantitative Analysis to Model Arabidopsis Thaliana ROP Signaling. A computational analysis to study the relationship between ROP-RIC signaling pathways in two adjacent plant cells.

Mathcad and MATLAB tools were used to carry out mass balances, equation derivation, and ODE discretization, in order to establish the predicted antagonistic relationship.

Howard Hughes Medical Institute International Student Fellowship 2015, Purdue Nominee. A research project proposal for synthesizing a novel bioconjugate using DNA and antimicrobial peptides (AMPs), without surface immobilization techniques, mediated by precipitation via DNA hybridization.

Emerging Leaders In Science and Society, AAAS Fellowship 2015, Purdue Semi-finalist. An educational workshop proposal outlining the logistics, an optimized budget, and organizational milestones. The goal of the workshop was to disseminate knowledge among the community on how to respond to a (hypothetical) H7N9 outbreak in Lafayette.

SKILLS

Laboratory Techniques

Good laboratory practice (GLP), good documentation practices (GDP), aseptic technique, Gas chromatography (GC), Reversed phase High Performance Liquid Chromatography (HPLC), Size Exclusion Chromatography (SEC), Fluorescence spectroscopy, UV-Vis spectrometry, Fourier Transform Infrared Spectroscopy (FTIR), Optical microscopy, Polymer extrusion, Tensile testing.

Working Knowledge

Scanning Electron Microscopy *(SEM)*, Transmission Electron Microscopy *(TEM)*, Atomic Force Microscopy *(AFM)*, Nuclear Magnetic Resonance *(NMR)*, Matrix Assisted Laser Desorption/Ionization-Time of Flight *(MALDI-TOF)*, Differential Scanning Calorimetry *(DSC)*, Fabrication of Micro-Integrated Systems and MEMS, Energy Dispersive X-Ray *(EDS)*, Electron Spectroscopy for Chemical Analysis *(ESCA)*, Secondary Ion Mass Spectroscopy *(SIMS)*, X-Ray Diffraction *(XRD)*, Porosimetry, *Raman* Spectrometry.

Software

Mathcad, ASPEN®, JMP, MS Excel statistical quality control (SQC) & design of experiments (DOE), MATLAB.

TEACHING ASSISTANTSHIPS & MENTORING

- Purdue University, TA, *Modeling & Computational Tools in Biological Engineering.* *S*pring 2016, 2018
- Purdue University, TA, *Chemical Reaction Engineering*. January 2014 – May 2014
- Purdue ABE Graduate Student Mentoring Program, *Mentor*. 2015 – 2018
- University of Missouri, TA, *Chemical Engineering Thermodynamics I & II.* August 2012 – May 2013
- University of Wyoming, TA, *Process Controls and Dynamics*. August 2010 – December 2010
- University of Wyoming, TA, *General Molecular Biology*. May – August, 2011, 2012, 2013
- University of Wyoming, Tutor and Mentor, *Athletics Department*. August 2010 – May 2011
- University of Wyoming, Student Mentor, *Multicultural Leadership Initiative*. 2009 – 2010

PUBLICATIONS

- **Wickramathilaka, M.**, William, A. J. Electronic dissertation, University of Missouri: "*Supercritical water gasification of waste residues."* May 2013.
- Ketnawa, S., **Wickramathilaka, M.**, Liceaga, A. "*Changes on antioxidant activity of microwave-treated protein hydrolysates after simulated gastrointestinal digestion: Purification and identification*". Accepted in Food Chemistry, 2018.
- **Wickramathilaka, M.**, Tao, Bernard. Y. "*Characterization and evaluation of zero-length covalent crosslinking strategies for DNA based applications*." Submitted to Biomacromolecules, 2018.
- Wilkinson N, **Wickramathilaka M.**, Hendry D., and Jacoby "*Rate determination of supercritical water gasification of primary sewage sludge as a replacement for anaerobic digestion."* Bioresource Technology 124: 269-275 (2012).
- Hendry, D., Miller, A., Wilkinson, N., **Wickramathilaka, M.**, Espanani, R., Jacoby, W. A. "*Exploration of High Pressure Separations of Supercritical Nitrogen and Carbon Dioxide."* Journal of CO_2 Utilization 3: 37-43 (2013).

PRESENTATIONS

- Purdue ABE Graduate Symposium. "Investigating bioconjugation techniques to construct spontaneously assembling DNA-Enzyme macromolecules." – 1st place in Biological Engineering oral presentations. February, 2018
- AIChE, Annual Meeting, Minneapolis. "Characterization of Covalent Crosslinking Strategies for synthesizing DNA-based Bioconjugates.' November, 2017
- Purdue ABE Graduate Symposium. "Synthesizing DNA-protein bioconjugates." 2014, 2015
- Purdue Sigma Xi Graduate student and Post-doctoral Fellow's Research Competition. "Investigation of crosslinking strategies to synthesize DNA-peptide conjugates." 2015, 2018
- MU, Graduate Professional Council's Research and Creative Activities Forum "Supercritical water gasification of waste residues: Parameterization of rate expressions" – 3rd place. 2013
- UW, Senior Design Symposium. "Thermochemical conversion of biomass into biofuel" – 1st place. 2010
- AIChE Rocky Mountain Regional Car Design Competition, Arizona – 3rd place & most creative car design. 2007

LEADERSHIP ROLES/AWARDS

- Purdue, College of Agriculture, *Outstanding Graduate Teaching Assistant Award.* 2017
- Purdue, College of Engineering, *Magoon Teaching Award*. 2016
- Purdue, Center for Instructional Excellence, *Teaching Academy Graduate Teaching Award.* 2016
- Purdue, College of Engineering. *Ross Fellowship recipient*. 2013 – 2014
- Purdue, Club Sports. *Treasurer, Badminton Club*. 2015 – 2016

- Purdue nominee, *HHMI International Student Research Fellowship.* 2014
- Purdue semi-finalist. *ELISS Fellowship (AAAS).* 2015
- Purdue, Women in Engineering Program. *Women of Color in STEM*. 2015
- UM, *Curators Grant in Aid*. 2012
- UM, *Student Auxiliary Services Scholarship*. 2012
- UM, Dept. of Biological Engineering. *Treasurer, Graduate Club of Biological Engineering.* 2012
- UW, Dept. of Chemical Engineering. *AIChE UW Chapter. Chemical Car Design Team, Secretary.* 2008, 2009
- AIChE Rocky Mountain Regional conferences (Arizona, New Mexico, Tennessee), National conferences (Utah, Pennsylvania). 2007 – 2011
- UW, College of Engineering. *Freshman Honors Roll*. Fall 2006
- UW, *Vice President's List.* Summer 2008, Fall 2010
- UW, *Western Heritage Scholarship*. Fall 2006 – Spring 2009
- UW, *International Students Scholarship*. 2007 – 2010
- UW, Office of Multicultural Affairs. *Multicultural Students Scholarship*. May 2010 – August 2010
- UW, Half-Acre Recreational Center. *Supervisor, and Cashier*. 2009 – 2010
- UW, *Public Relations Office, International Students Association.* 2007 – 2008
- UW, Office of Admissions. *Orientation Leader*. May 2008 – August 2008
- UW, Office of Admissions. *Student Ambassador, Tele-counselor, Prospector.* 2007 – 2011
- UW, Office of Multicultural Students. *National Conference for Women Student Leaders.* 2007

PROFESSIONAL AFFILIATIONS/CERTIFICATIONS

- Purdue University, *Graduate Instructional Development Certificate.* 2017
- American Institute of Chemical Engineers (AIChE). 2007 – 2011, 2017
- Society for Biological Engineers (SBE). 2008 – 2009
- Society for Petroleum Engineers (SPE). 2008 – 2009
- American Association for the Advancement of Science (AAAS). 2015, 2016
- Fundamentals of Engineering License, National Council of Examiners for Engineering and Surveying. 2010

VOLUNTEER ACTIVITIES

- Peer reviewer, *Journal of Biological Engineers*, and *Biotechnology Progress*. 2017 – Present
- Purdue "Introduce a Girl to Engineering Education" program, *Mentor.* 2015
- Purdue ABE Senior Design Symposium, *Graduate student judge.* 2014 – 2018
- Purdue Summer Undergraduate Research Forum (SURF), *Graduate student judge.* 2015, 2017
- Lafayette middle school Math Counts mathletes competition, *Proctor*. 2015
- Purdue International Center Summer Suppers series, *"Food Preparer."* 2015
- UW Safe Ride, Radio presenter, Up Until Dawn for St. Jude's Hospital. 2007 – 2011
- UM, Walking School Bus, Dance Marathon fundraiser for Riley Children's Hospital. 2012, 2013